UNCLASSIFIED

AD NUMBER

AD845599

LIMITATION CHANGES

TO:

Approved for public release; distribution is unlimited.

FROM:

Distribution authorized to U.S. Gov't. agencies and their contractors; Critical Technology; NOV 1968. Other requests shall be referred to Air Force Technical Applications Center, Washington, DC. This document contains export-controlled technical data.

AUTHORITY

usaf, ltr, 25 jan 1972

THIS PAGE IS UNCLASSIFIED

AD845599

TR 68-47

TECHNICAL REPORT NO. 68-47

PRELIMINARY EVALUATION OF BEAM-STEERING CAPABILITIES OF THE TFSO 37-ELEMENT ARRAY

NOTICE

THIS DOCUMENT IS SUBJECT TO SPECIAL EXPORT CONTROLS AND EACH TRANSMITTAL TO FOREIGN GOVERNMENTS OR FOREIGN NATIONALS MAY BE MADE ONLY WITH PRIOR APPROVAL OF CHIEF, AFTAC.

DDC
JAN 7 1969
A

GEOTECH
A TELEDYNE COMPANY

16

BEST
AVAILABLE COPY

TECHNICAL REPORT NO. 68-47

PRELIMINARY EVALUATION OF BEAM-STEERING CAPABILITIES OF THE TFSO 37-ELEMENT ARRAY

by

Don R. Phillips and Dale S. Kelley

Sponsored by

Advanced Research Projects Agency
Nuclear Test Detection Office
ARPA Order No. 624

NOTICE

THIS DOCUMENT IS SUBJECT TO SPECIAL EXPORT CONTROLS AND EACH TRANSMITTAL TO FOREIGN GOVERNMENTS OR FOREIGN NATIONALS MAY BE MADE ONLY WITH PRIOR APPROVAL OF CHIEF, AFTAC.

attn: VSC
Wash DC 20333

GEOTECH
A TELEDYNE COMPANY
3401 Shiloh Road
Garland, Texas

27 November 1968

IDENTIFICATION

AFTAC Project No.	VELA T/8702
Project Title:	Operation of TFSO
ARPA Order No:	624
ARPA Program Code No:	8F10
Name of Contractor:	Teledyne Industries, Incorporated Geotech Division Garland, Texas
Date of Contract:	1 January 1968
Amount of Contract:	$493,500
Contract Number:	AF 33657-68-C-0766
Contract Expiration Date:	31 December 1968
Program Manager:	B. B. Leichliter, BR1-2561, ext. 222

CONTENTS

ILLUSTRATIONS

TABLES

ABSTRACT

The evaluation of the beam steering capabilities of the 37-element short-period seismograph array at TFSO indicates that the array provides a signal-to-noise ratio improvement over a single detector of approximately 12 dB at frequencies near 1.0 cps. The phased summed output of the array suppresses the noise by a factor of $\sqrt{N}$ (15.6 dB) for frequencies greater than about 1.5 cps. At 1.0 cps, the average noise reduction relative to an individual output is 13.7 dB. The signal amplitude loss in a 30-second P-wave coda is between 1.0 and 2.0 dB in the frequency range of greatest signal power (0.5-1.0 cps).

PRELIMINARY EVALUATION OF BEAM-STEERING CAPABILITIES OF THE TFSO 37-ELEMENT ARRAY

1. INTRODUCTION

In November 1967, construction and instrumentation were completed on a medium aperture 37-element short-period seismograph array at the Tonto Forest Seismological Observatory (TFSO). The design of the array was directed toward providing the capability for velocity filtering of teleseismic signals and, more specifically, to increasing the signal-to-noise ratio (S/N) of processed outputs in the frequency range of 0.5 to 2.0 cps. The results of noise studies conducted on data recorded by the cross-linear and 31-element arrays, used in conjunction with theoretical array response studies, indicated that significant S/N improvement could be provided by velocity filtering of a hexagonal array in which the distance between sensors is 5 kilometers and the overall diameter of the hexagon is 30 kilometers. The array was designed on this basis; however, due to considerable topographic relief in the area and problems of legal access, the actual locations of the elements, shown in figure 1, were slightly perturbed from the ideal theoretical locations.

This report deals with the evaluation of the beam steering capabilities exhibited by the 37-element short-period array during the first months of its operation.

2. DATA SELECTION AND PREPARATION

2.1 METHOD OF EVALUATION

The evaluation consisted basically of the comparison of the S/N of the phased summed outputs of the 37-element array and of two subarrays to the S/N of the average of the outputs of the individual seismographs and to the unphased summation and the unphased filtered summation of the cross-linear array. Figure 2 shows the locations of the seismographs which were contributing elements to the unphased summation and to the unphased filtered summation of the cross-linear array. One of the subarrays chosen for evaluation consisted of the center seismograph and the seismographs of the inner ring; the other subarray was composed of the center element and the elements of the inner and middle ring. Twenty earthquakes occurring at teleseismic distances from TFSO were used.

The S/N for each of the various outputs was computed by two methods. The first method utilized the ratio of the power density spectrum of the signal to that of the noise; the second used the ratio of an amplitude measurement from a dominant half-cycle of the signal and the rms of the noise. Noise reduction and signal loss were computed in addition to the S/N.

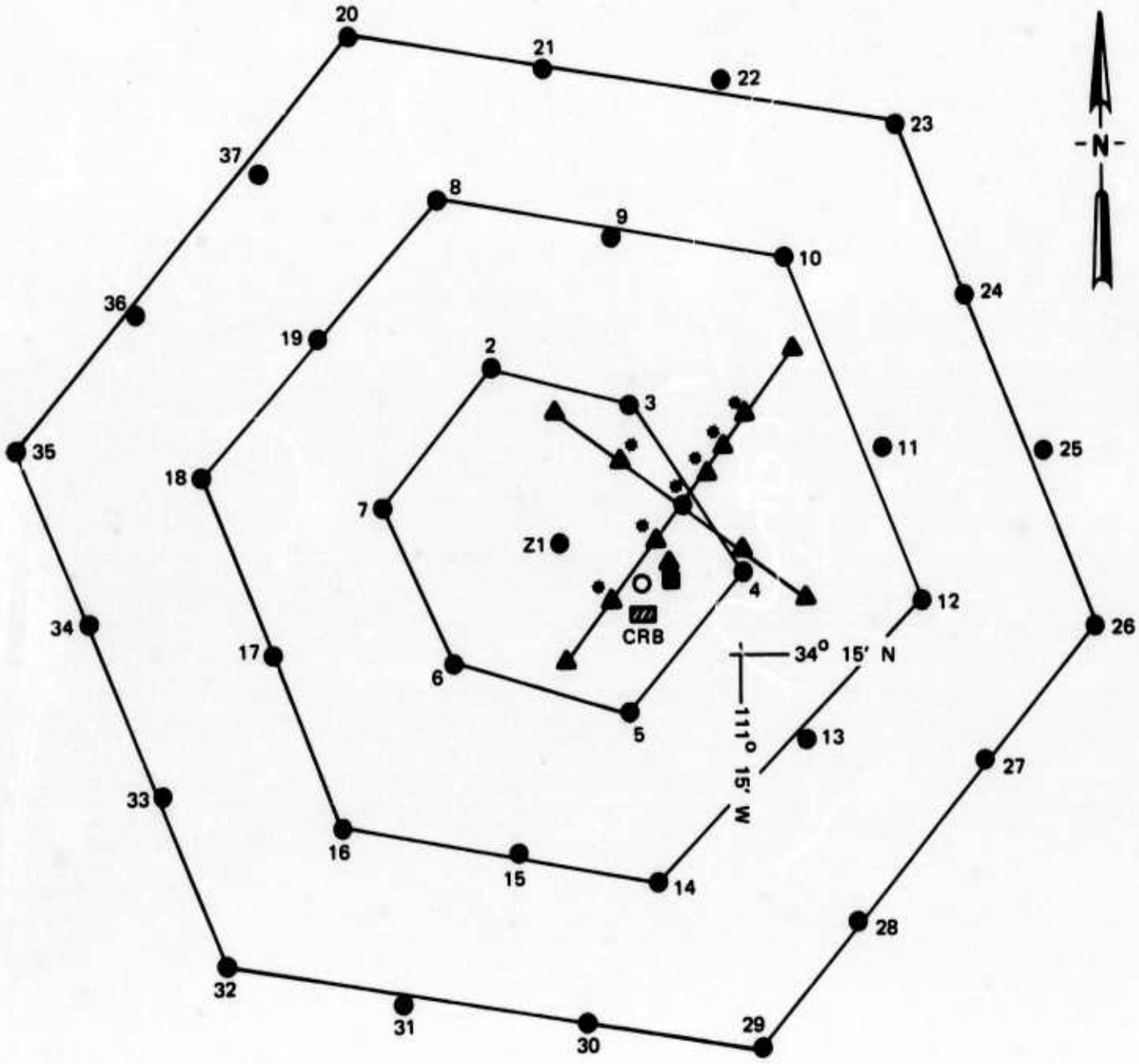

SCALE

0 5 10 15 20 25 30 35 FEET (K)

0 1 2 3 4 5 6 7 8 9 10 KILOMETERS

- SHORT-PERIOD VERTICAL SEISMOGRAPH
- THREE COMPONENT SHORT-PERIOD SEISMOGRAPH
- EXPERIMENTAL VAULT
- LONG-PERIOD VAULT
- CENTRAL RECORDING BUILDING
- CONTRIBUTING ELEMENT TO CROSS-LINEAR SUMMATION (FILTERED)

Figure 1. Tonto Forest Seismological Observatory 37-element and cross-linear arrays

G 4432

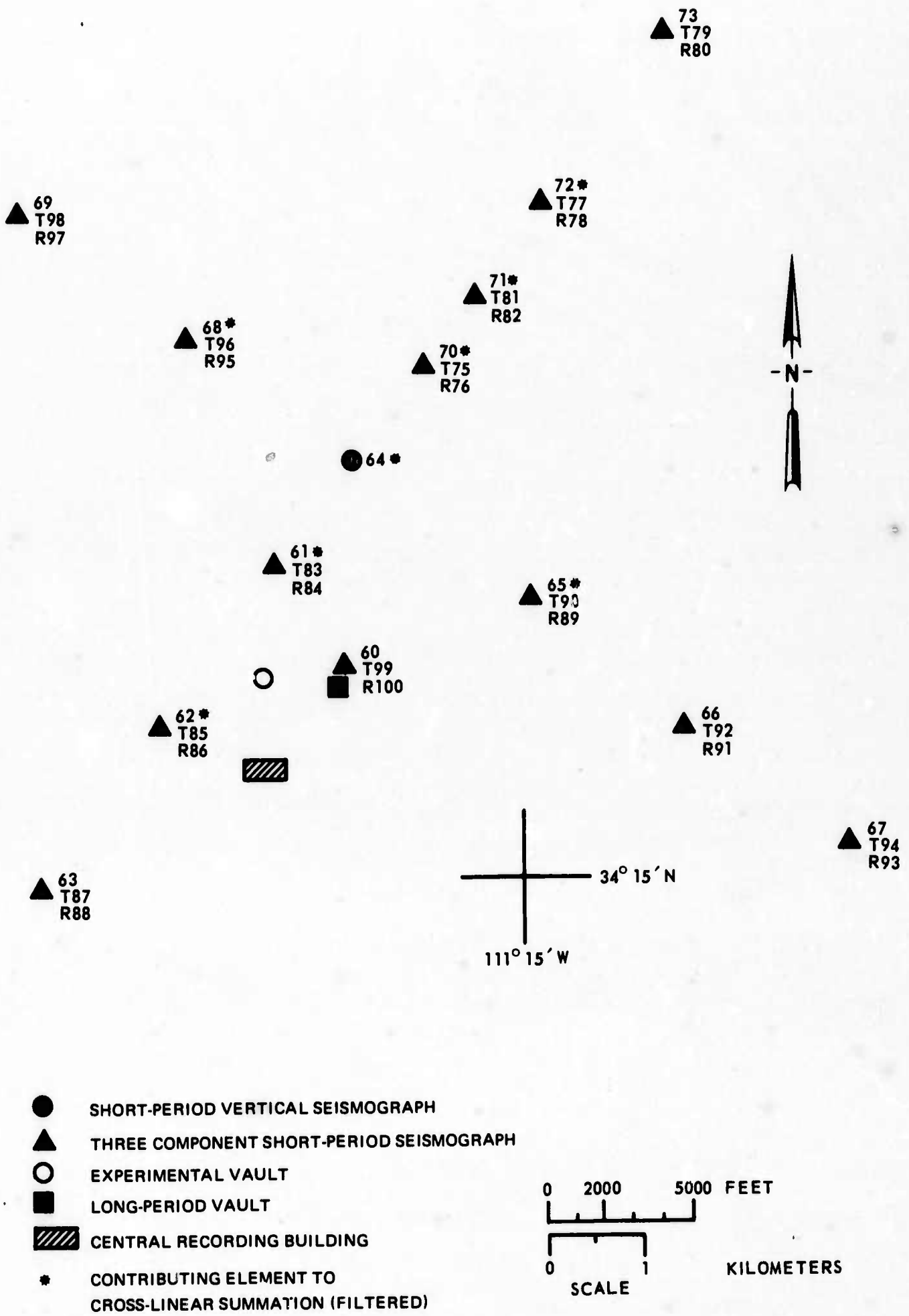

Figure 2. Cross-linear array, Tonto Forest Seismological Observatory

G 4433

2.2 DATA SELECTION

The data samples were selected from 16-millimeter film seismograms of the individual elements of the 37-element array. The daily TFSO station message to the Coast and Geodetic Survey (C&GS) and the daily LASA bulletin were used as guides in the search for suitable data samples. Each sample selected satisfied the following requirements:

a. At least 5 elements from the inner ring, 10 elements from the middle ring, and 15 elements from the outer ring were operational and not excessively noisy at the time the signal was recorded. Also, it was required that each of the 8 elements of the cross-linear array was operating properly.

b. Each data sample was 3 minutes and 20 seconds long, consisting of 2 minutes and 50 seconds of noise followed by 30 seconds of signal coda.

c. Each signal originated within the epicentral distance range of 30 to 90 degrees from TFSO.

Many samples which satisfied these requirements were later rejected when digital-to-analog plots of the Astrodata digital magnetic tapes indicated that an acceptable number of channels had not been suitably recorded. Excessive spiking and parity errors on the digital recordings caused many samples to be rejected. The spiking was due primarily to lightning and to the fact that both data and power were transmitted over the same spiral-4 cable. The parity errors resulted from a defective tape transport. Ultimately, 20 data samples satisfying the selection criteria were obtained and processed. Table 1 gives the epicentral data for each signal and lists the unusable channels for each sample. The epicentral data were obtained from the "Preliminary Determination of Epicenter" cards published by the C&GS. Figure 3 shows the distance and azimuth of each epicenter relative to TFSO.

The calibration constants for each of the individual outputs and for the unphased filtered and unfiltered summations were determined from 1.0 cps sinusoidal calibrations. Prior to 24 May 1968, the individual elements were calibrated both separately and simultaneously in groups of about 10 elements. After 24 May, the simultaneous calibrations were discontinued because of some doubt as to their validity. The calibration constants for data samples 1 through 11 were computed from the simultaneous calibrations, while the calibration constants for the remaining data samples were necessarily computed from individual calibrations. As a check on the two types of calibrations, 3 data samples were processed with calibration constants computed from both individual and simultaneous calibrations. The output data showed that the two methods of calibration gave essentially the same results.

Digital-to-analog plots of the calibrations were obtained to determine whether any of the Astrodata channels were overloaded. In some cases, overloading caused the calibrations for some elements to be recorded improperly. The problem was essentially eliminated by the installation of an automatic overload reset circuit in the Astrodata system on 16 April 1968.

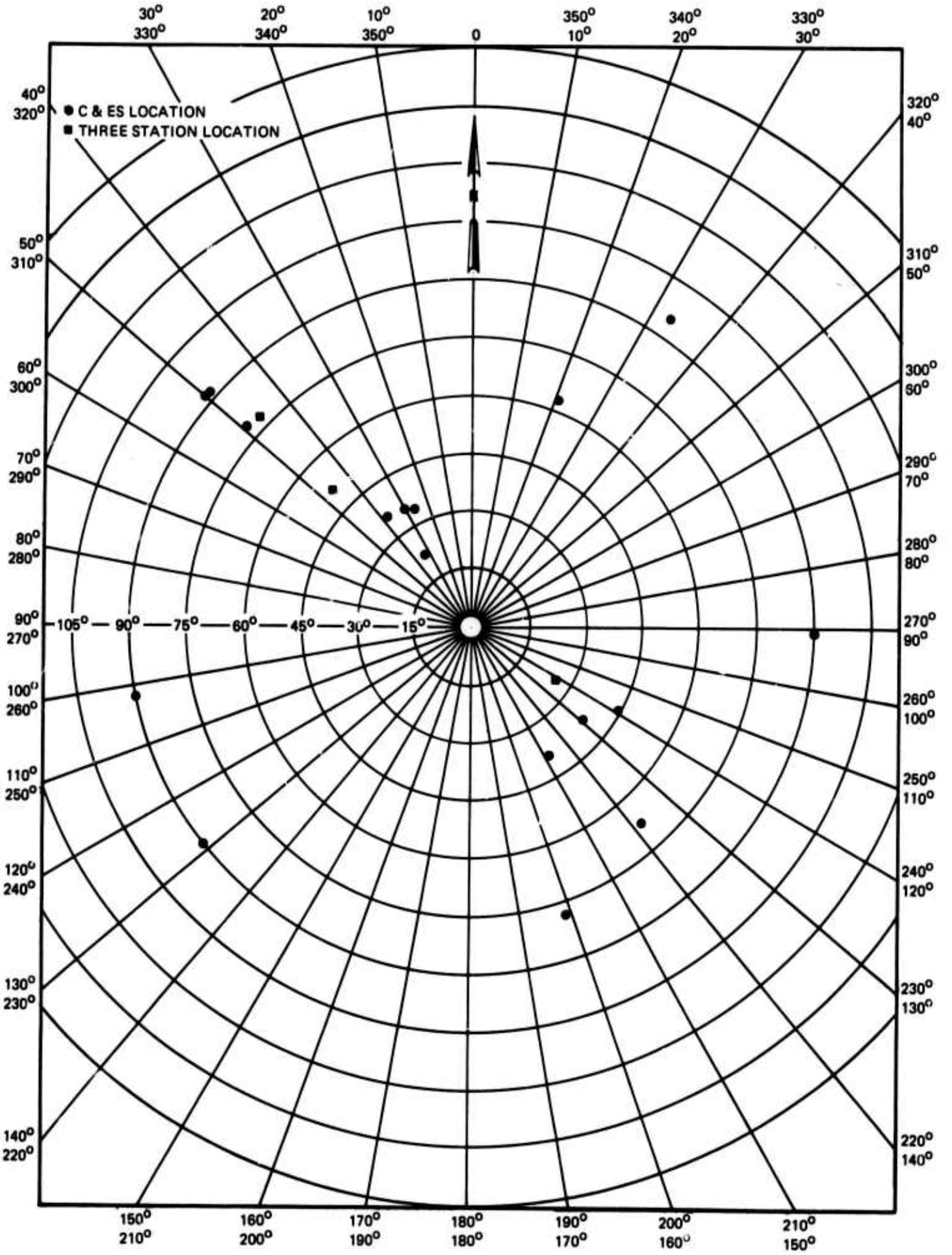

Figure 3. Location of signal epicenters relative to TFSO

G 4434

Because of parity errors, the calibration constants for data samples 1 through 8, excluding sample 6, were computed from calibrations recorded on a day different from the day on which the data sample was recorded. In almost all of the samples there were a few elements for which calibration constants were estimated. Estimates were based either on previous calibrations or on the basis of calibration levels of other systems.

Calibrations were demultiplexed from the Astrodata field tape and analyzed by computer to obtain the calibration constant.

3. DATA PROCESSING

After the calibration constants were computed, each data sample was demultiplexed from the Astrodata digital field tape, and an X-Y plot of each output was generated. Figures 4 through 8 show a portion of the plots for each individual element and for the unphased filtered summation output of the cross-linear array from data sample 6 (see table 1). Each trace has been normalized by the plot routine on the basis of the maximum amplitude for that particular element; consequently, no relationship between relative trace amplitudes can be obtained from the plots. The plots were used to determine the relative delay times necessary to form the phased sums. The element with the earliest signal arrival was used as the reference element.

Formation of the phased sums, determination of signal amplitude and calculation of noise rms, calculation of the average output of the individuals, and comparison of the average output with the phased sums were accomplished by a computer program (TFOSAN). Because three phased sums were desired for each sample, that is, the 7-element subarray (PS1), the 19-element subarray (PS2), and the 37-element subarray (PS3); the sample was processed three times by program TFOSAN. On each pass, only those elements contributing to the particular phased sum under consideration were used. Besides the subset tape containing the data sample, program TFOSAN required as input the delay times, calibration constants, filter coefficients, label of any element to be deleted from consideration, time window length, and a reference start time for the time window. The filter coefficients used were for the standard SDL bandpass filter. Figure 9 shows the amplitude response of the SDL filter and the analog filter used in the cross-linear filtered summation (CLSF). The SDL filter was applied both forward and backward in time in order to achieve zero phase-shift; thus, the effective bandpass applied to the data is the square of the SDL filter amplitude response. Each element was filtered prior to the analysis of the data sample. The phased sum was formed from the filtered elements. Figure 10 shows a portion of the plot of the filtered and aligned traces for Z1 through Z10 for data sample 6. The relative amplitudes between traces are correct. Comparison of the filtered data with the raw traces shows that the signal is enhanced considerably by the bandpass filter.

Program TFOSAN allowed any element in the data sample to be deleted from the analysis procedures and the phased sum. This option was used in forming PS1 and PS2.

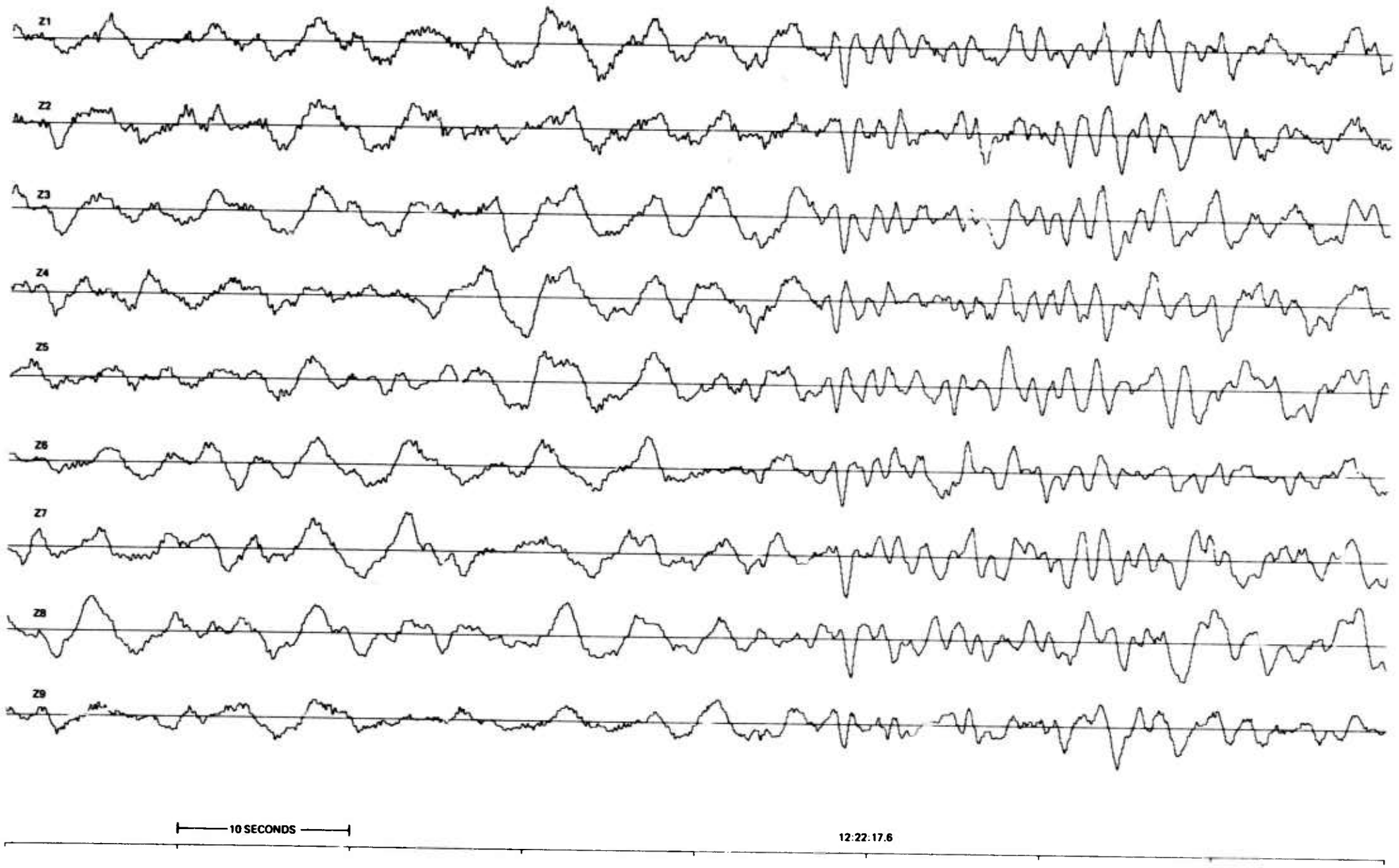

Figure 4. Calcomp plot of Astrodata recording of a portion of data sample 6

G 4435

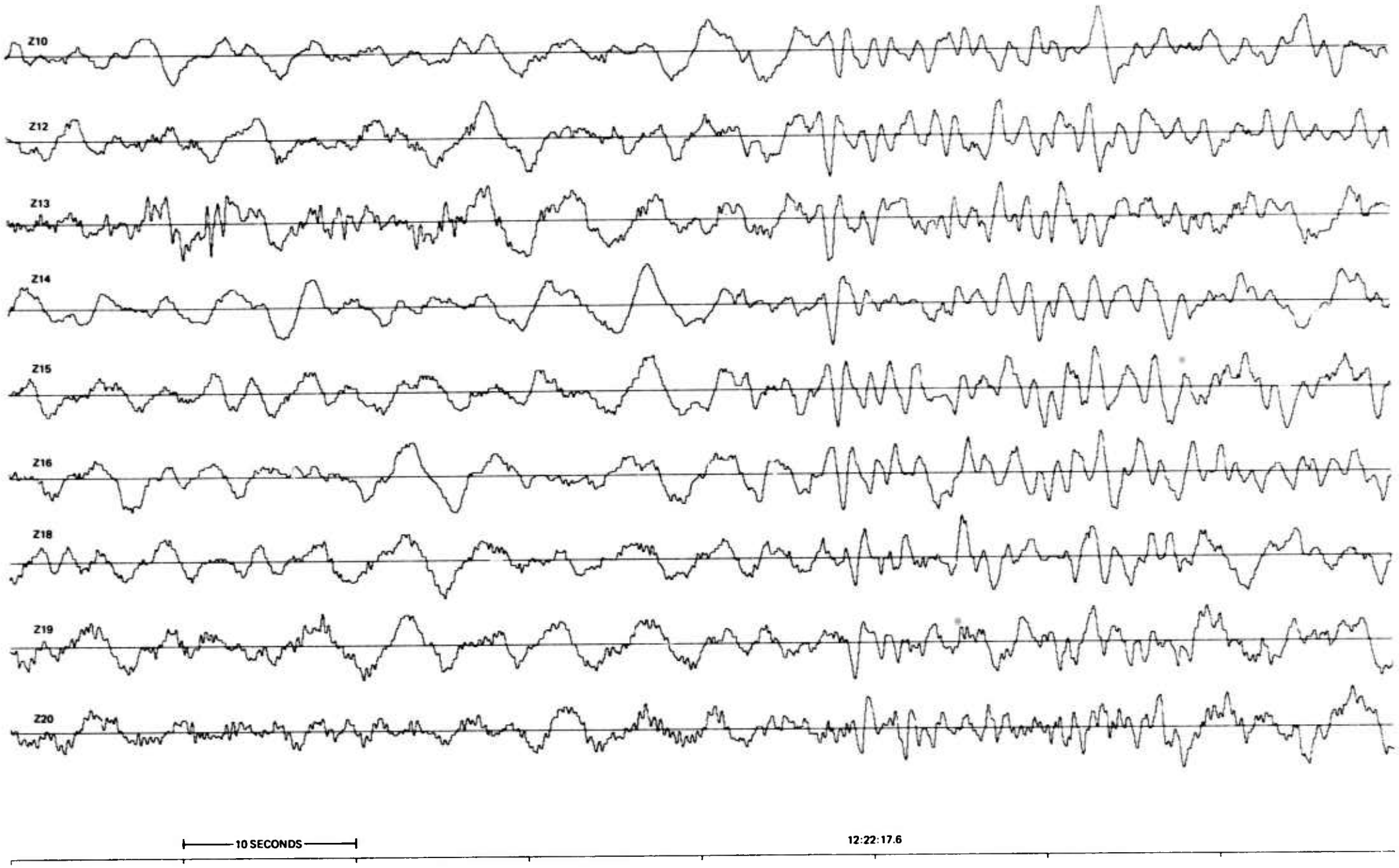

Figure 5. Calcomp plot of Astrodata recording of a portion of data sample 6

G 4436

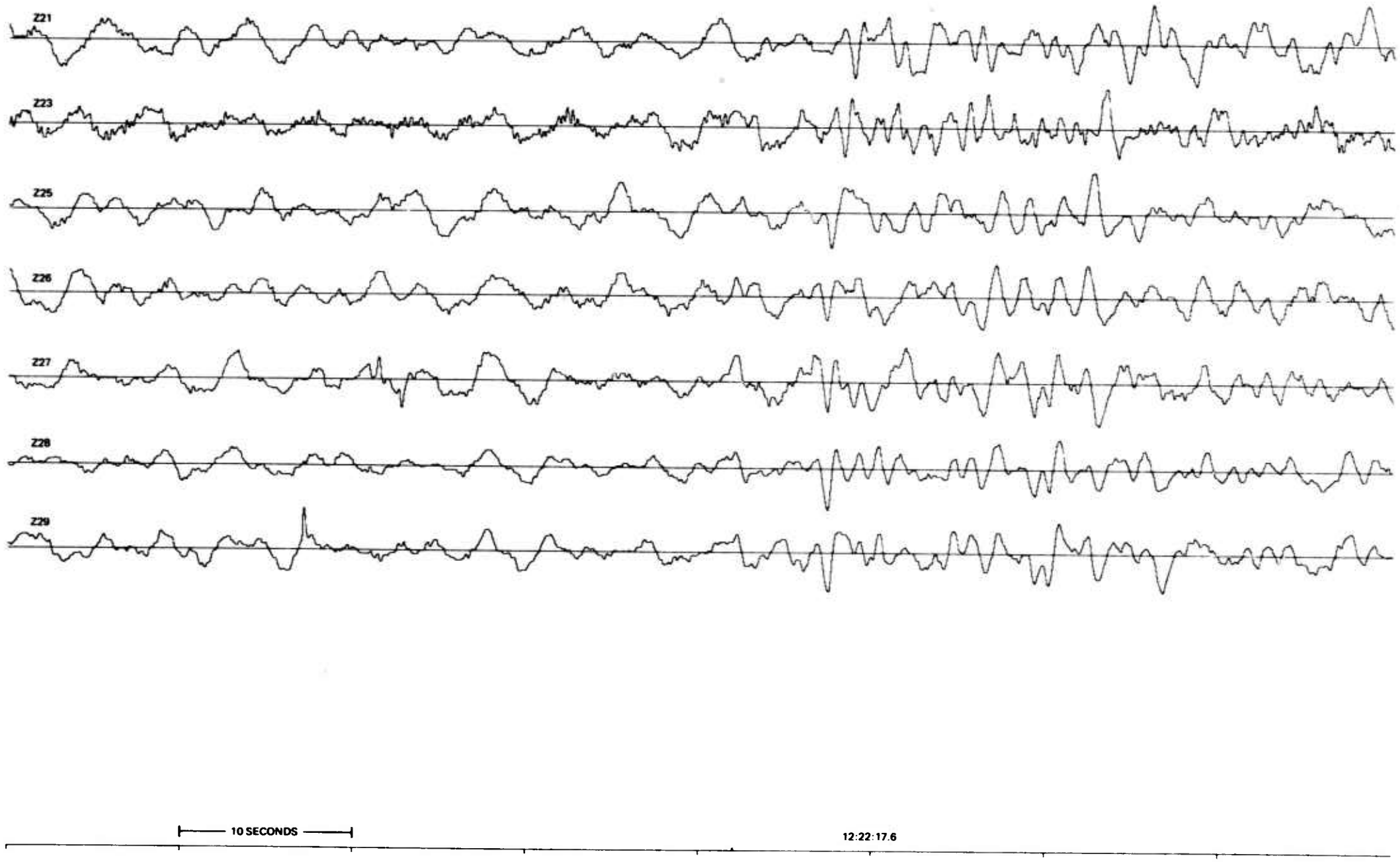

Figure 6. Calcomp plot of Astrodata recording of a portion of data sample 6

G 4437

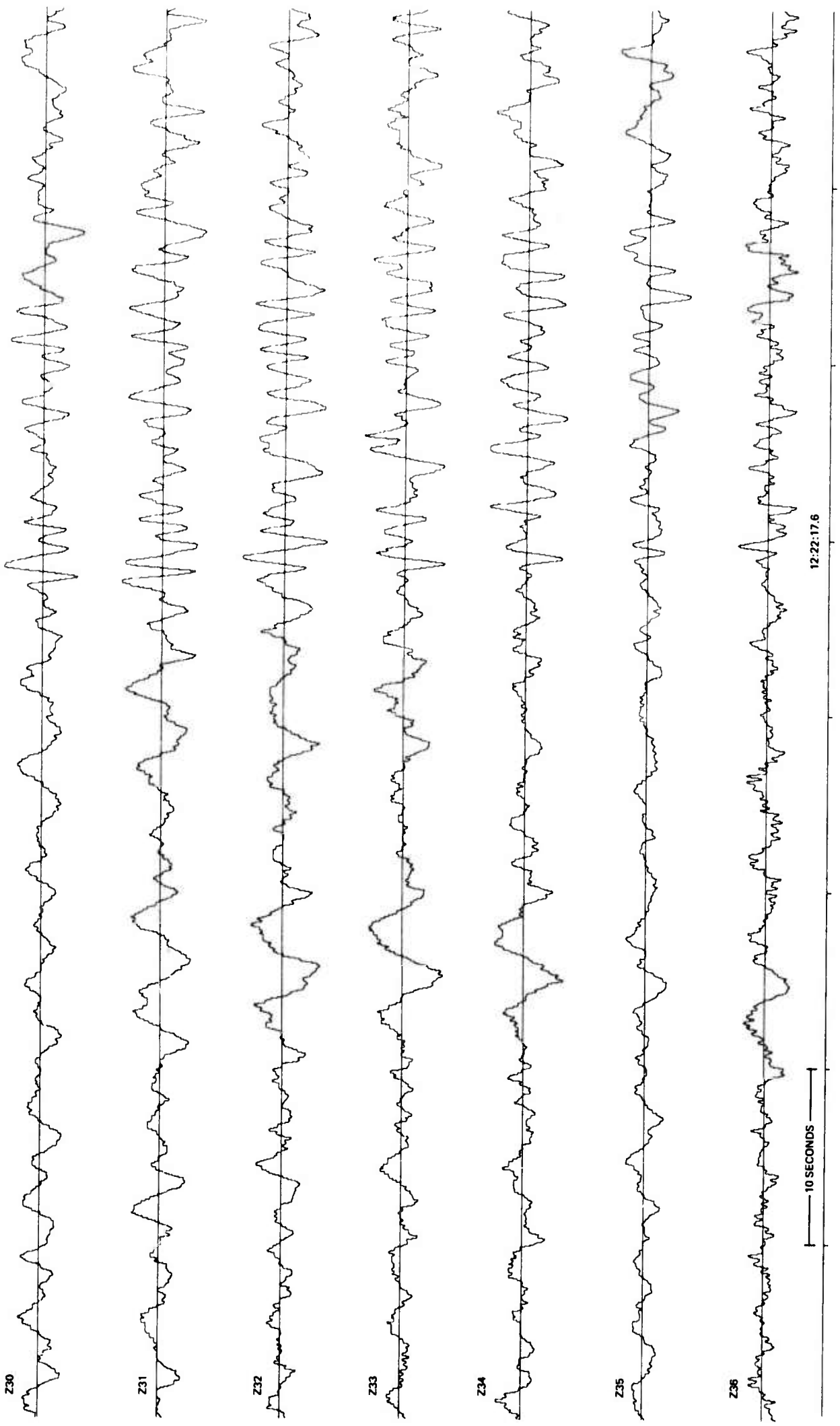

Figure 7. Calcomp plot of Astrodata recording of a portion of data sample 6

G 4438

Figure 8. Calcomp plot of Astrodata recording of a portion of data sample 6

G 4439

Table 1. Epicentral data and unusable elements for each data samples

Data sample	Date	Signal origin time	Latitude	Longitude	General area of epicenter	Depth (km)	Mag. (mb)	Dist. from TFSO	AZI from TFSO	Unusable elements
1	23 Mar	16:49:09.8	6.82N	72.98W	Northern Colombia	160	4.4	44.6°	119°	Z12, Z17, Z32, Z33, Z37
2	24 Mar	15:58:49.0	32.11N	130.60E	Kyushu, Japan	4	4.9	92.0°	312°	Z12, Z20, Z23, Z24,
3	24 Mar	16:21:04.7	32.11N	130.66E	Kyushu, Japan	33	4.9	92.0°	311°	Z1, Z9, Z12, Z20, Z23, Z32
4	26 Mar	04:19:11.2	0.95S	22.15W	Mid-Atlantic Ridge	Normal	4.9	89.8°	91°	Z11
5	28 Mar	07:39:57.1	37.90N	20.88E	Ionian Sea	6	5.4	95.5°	36°	Z11, Z17, Z22, Z27
6*	30 Mar	12:16:27.6	18.02N	87.95W	Yucatan Peninsula	-	-	26.3°	122°	Z11, Z17, Z22, Z24, Z37
7	05 Apr	11:41:49.0	64.17N	148.91W	Central Alaska	128	4.1	37.7°	334°	Z6, Z11, Z17, Z22, Z24, Z30
8*	07 Apr	07:33:31.7	53.40N	179.99E	Rat Island, Aleutian Is.	-	-	51.1°	314°	Z6, Z11, Z24, Z30
9	15 Apr	13:15:48.8	6.69N	82.20W	South of Panama	39	4.4	38.4°	129°	Z6, Z24, Z30, Z33
10	21 Apr	06:10:19.1	31.64S	177.67W	Kermadec Is.	57	4.7	90.6°	231°	Z16, Z19, Z22, Z34, Z37
11	27 Apr	10:58:21.5	10.48S	165.12E	Santa Cruz Is.	75	5.1	90.6°	258°	Z17, Z23, Z25, Z37,
12	11 Jun	11:38:50.0	21.2S	69.6W	Northern Chile	22	4.7	67.8°	138°	Z6, Z11, Z18, Z20, Z36, Z37
13	11 Jun	11:45:15	41.5S	85.4W	West Chile Rise	33R	4.9	79.0°	161°	Z6, Z11, Z18, Z20, Z37
14	13 Jun	03:58:11	71.2N	5.6W	Jan Mayen Is. Region	33R	4.6	62.8°	21°	Z15, Z17, Z23, Z32, Z37
15	13 Jun	04:56:22	0.6S	91.5W	Galapagos Is.	33R	4.5	39.2°	148°	Z29, Z37
16	13 Jun	08:51:29	51.5N	129.8W	Queen Charlotte Is. Region	33R	4.1	21.9°	328°	Z25, Z37
17	15 Jun	13:38:06.5	61.0N	146.9W	Southern Alaska	19	4.9	35.3°	330°	Z17, Z23, Z27, Z33
18*	16 Jun	11:37:56.0	42.57N	142.54E	Hokkaido	-	-	78.1°	314°	Z6, Z9, Z20, Z23
19	16 Jun	16:56:36.4	40.3N	143.8E	Off Coast of Honshu, Japan	11	4.7	78.7°	311°	Z1, Z5, Z12, Z20, Z23, Z30
20	23 Jun	15:01:56.0	56.8N	152.2W	Kodiak Is. Region	35	4.4	35.8°	322°	Z6, Z17

*Three station location using arrival times at TFSO, UBSO, WMSO.

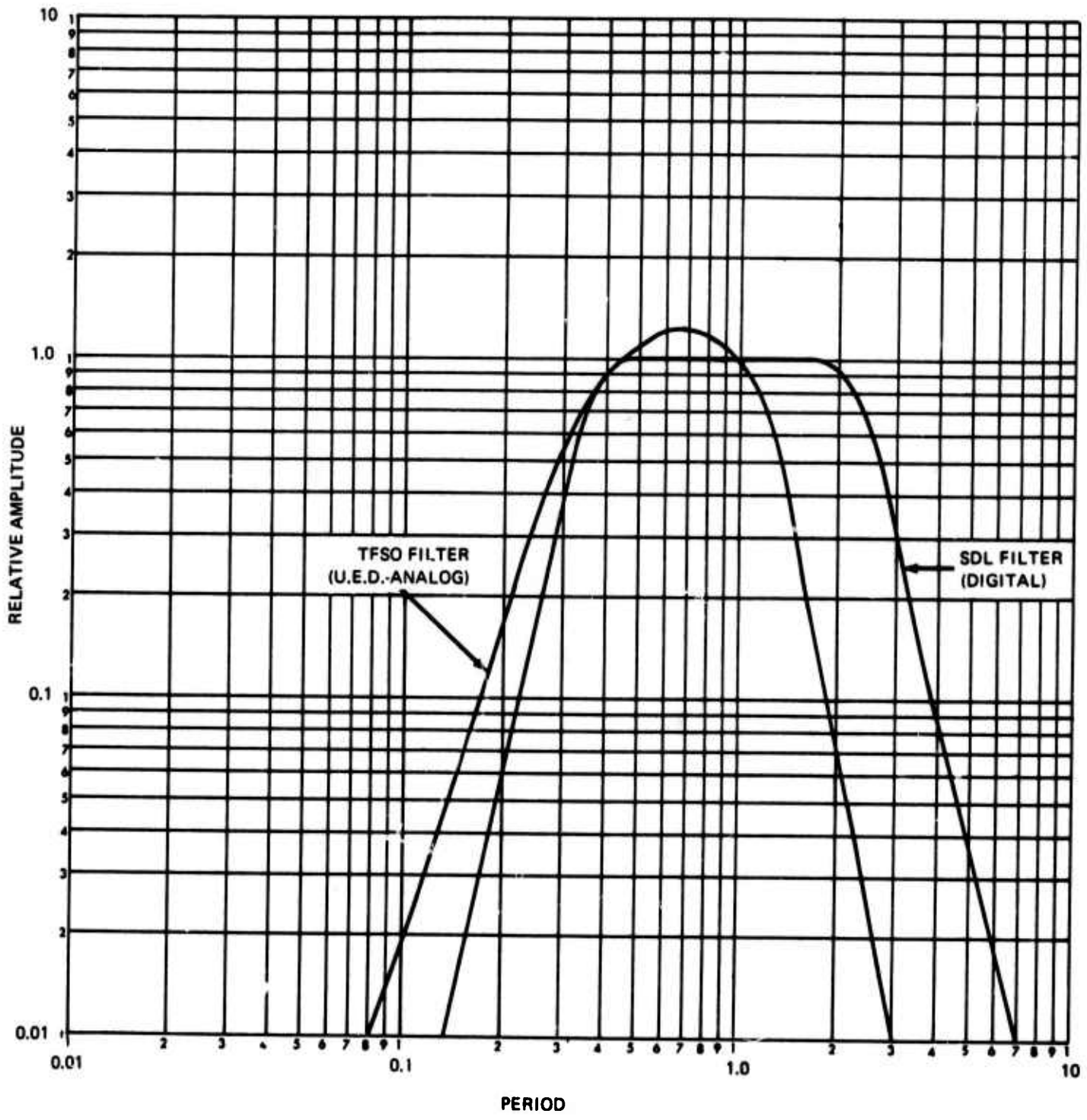

Figure 9. Filter amplitude responses

G 4440

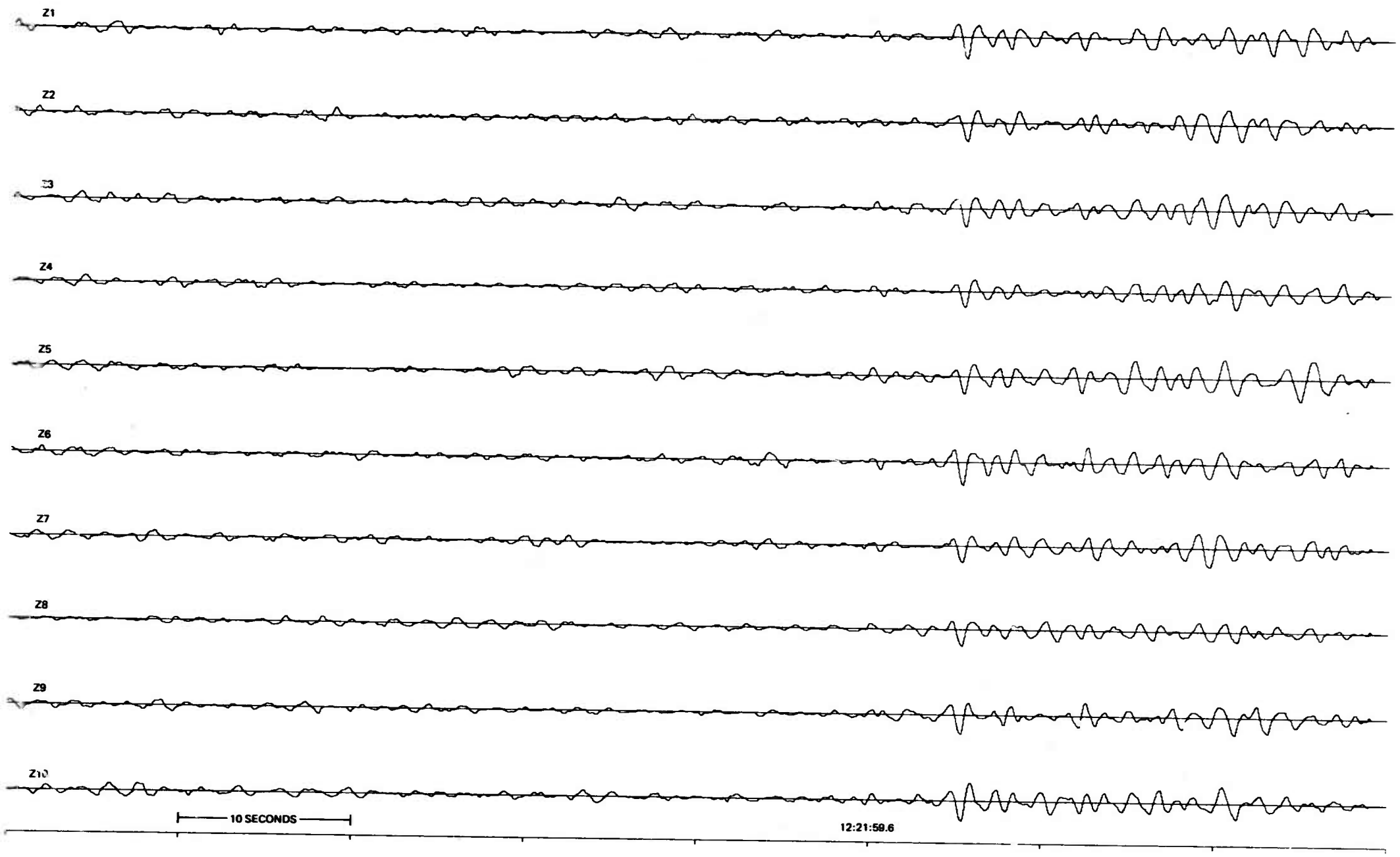

Figure 10. Calcomp plot of the filtered and aligned traces for Z1 through Z10 from data sample 6

G 4441

An arbitary time-window (generally no more than 8 seconds) was established and a reference time selected so that the time window spanned the start of the signal. In this window the largest (peak-to-peak)/2 signal amplitude was determined for each individual element and the phased sum. In general, this measurement was made on the same half-cycle of the signal on each trace.

The noise analysis was accomplished by computing the rms and the center-to-peak range of the noise for the 100 seconds preceding the start of the signal.

Figure 11 shows the major portion of the TFOSAN printer output for PS3 of data sample 6. The trace amplitude values in columns 2, 3, and 4 are given in millimicrons. Columns 5 and 6 are signal-to-noise ratios and column 8 contains the delay times, in seconds, used to form the phased sum. For each statistic computed in the analysis of the individual elements, the mean, the variance, and the standard deviation of that statistic is computed. Program TFOSAN analyzes the phased sum in the same manner as an individual element is analyzed and compares the analysis to the average analysis of the individual elements. The comparison of PS3 to the average individual element for data sample 6 shows 0.19 dB signal loss, 13.02 dB rms noise reduction, and 12.81 dB signal-to-rms noise ratio improvement.

A high-magnification plot of each phased sum was obtained. Figure 12 shows a portion of PS3 for data sample 6. The magnification of the plot of PS3 is approximately eight times that of the individual traces in figure 10. It is interesting to note that PS3 shows clearly the first cycle of the signal, which is completely obscured on the unprocessed seismograms and only faintly visible on the filtered individual seismograms. Figure 12 also shows the high-magnification plots of PS1 and PS2 for data sample 6. The noise reduction provided by PS2 over PS1 and PS3 over PS2 can be seen clearly from these data.

The spectra of the signal and the noise were computed for each of the elements and averaged over the data sample. A maximum lag of 3 seconds was used in calculating both the signal spectra and the noise spectra, resulting in estimates of signal power and noise power at the same frequencies. The spectra for the three phased sums were computed in the same manner, except for the averaging. The spectra for the average individual element (IND), the three phased sums, and the filtered summation of the cross-linear array (CLSF) are shown in appendix 5. The secondary peak in the noise spectra at about 2.0 cps was a common feature of all of the noise spectra. Another common characteristic of the noise was that the average peak power for the individual elements was generally about 0.1 $m\mu^2$/cps. For the 20 signals in the data ensemble, the signal power peaked below 1.0 cps on 18 signals, with the majority peaking at 0.67 cps. It should be noted that the frequency resolution of the spectra was about 0.16 cps, which allows only a rough estimation of peak frequencies.

The complete processing scheme for a data sample is summarized in figure 13.

VENEZUELA A 30 MAR 68 1219 TFO 14910

CH	S(P-P/2)	RMS	RANGE	S/RANGE	S/RMS	RANGE/RMS	DELTA T	SDL	FILTER
+Z0	2.42	.357	1.01	2.40	6.79	2.82	1.05		
Z2	2.14	.322	1.01	2.11	6.64	3.14	1.25		
Z3	2.06	.352	1.01	2.05	5.86	2.86	1.05		
Z4	1.98	.312	.88	2.26	6.35	2.80	.65		
Z5	2.02	.318	1.07	1.89	6.37	3.36	.70		
Z6	2.50	.327	1.30	1.92	7.63	3.97	1.10		
Z7	1.91	.347	1.27	1.50	5.50	3.67	1.35		
Z8	1.80	.330	.99	1.82	5.45	3.00	1.65		
Z9	2.18	.324	.97	2.26	6.73	2.98	1.35		
Z10	2.62	.357	1.02	2.58	7.36	2.85	.95		
Z12	2.66	.400	1.32	2.16	7.14	3.30	.35		
Z13	3.30	.563	2.20	1.50	5.87	3.92	.35		
Z14	2.76	.343	1.05	2.62	8.03	3.06	.45		
Z15	2.47	.318	.98	2.53	7.78	3.07	.70		
Z16	2.53	.318	.88	2.88	7.97	2.77	.95		
Z18	2.02	.356	1.16	1.74	5.68	3.26	1.60		
Z19	1.57	.377	1.36	1.15	4.16	3.61	1.55		
Z20	2.10	.446	1.32	1.59	4.71	2.96	1.90		
Z21	2.46	.316	.83	2.97	7.80	2.63	1.55		
Z23	3.47	.385	1.31	2.66	9.03	3.40	.95		
Z25	2.16	.359	1.07	2.01	6.02	2.99	.25		
Z26	1.77	.368	.99	1.78	4.79	2.69	0		
Z27	3.05	.385	1.37	2.23	7.93	3.56	.05		
Z28	4.20	.455	1.27	3.30	9.23	2.79	.05		
Z29	4.40	.572	2.41	1.83	7.69	4.21	.15		
Z30	3.70	.397	1.12	3.31	9.32	2.81	.35		
Z31	2.84	.335	.89	3.19	8.48	2.66	.70		
Z32	3.10	.427	1.57	1.97	7.25	3.68	.90		
Z33	1.84	.298	1.07	1.73	6.19	3.58	1.20		
Z34	1.90	.325	.98	1.42	4.30	3.03	1.55		
Z35	2.01	.437	1.20	1.68	4.61	2.75	1.95		
Z36	1.24	.450	1.43	.87	2.75	3.17	2.00		
SUM	78.90	11.98	38.30	67.93	211.40	101.36			
MEAN	2.47	.37	1.20	2.12	6.61	3.17			
VAR	.57	.00	.12	.36	2.51	.18			
STD	.75	.07	.34	.60	1.58	.42			
U-SUM	.26	.133	.45	.59	1.99	3.35			
P-SUM	2.41	.084	.29	8.28	28.86	3.49			
RU-SUM	.25	.129	.42	.59	1.93	3.25			
RP-SUM	2.38	.085	.26	9.14	27.93	3.06			

	SIGNAL (DB)	RMS (DB)	NOISE (DB)	S/N (DB)	S/RMS (DB)
U-SUM	-19.39	-8.97	-8.57	-11.08	-10.44
P-SUM	-.19	-13.02	-12.27	11.82	12.81
RU-SUM	-19.90	-9.25	-9.11	-11.05	-10.67
RP-SUM	-.31	-12.86	-13.25	12.68	12.52

Figure 11. TFOSAN printer output for PS3 for data sample 6

G 4442

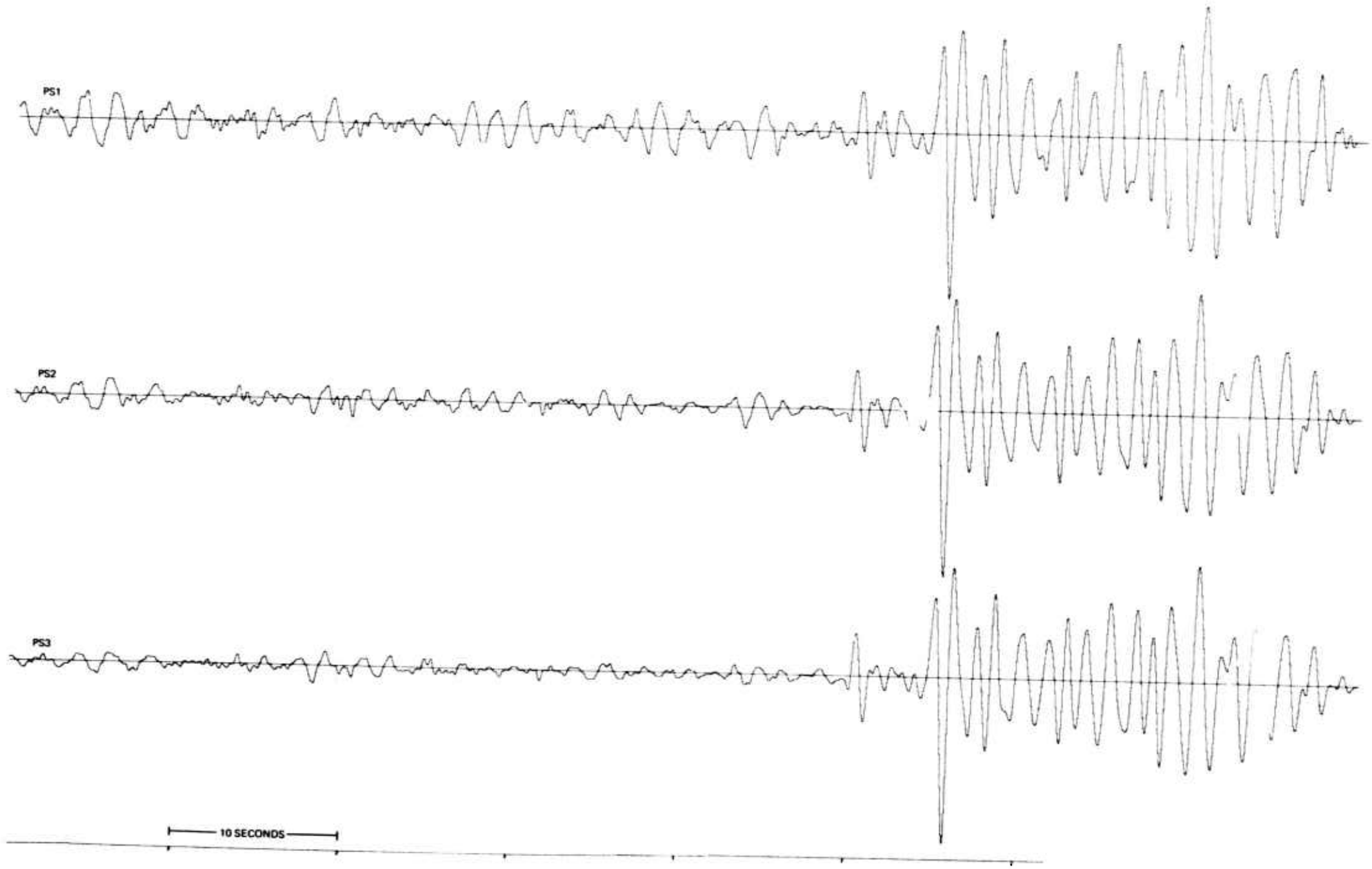

Figure 12. High-gain X-Y plots of PS1, PS2, and PS3 from data sample 6

G 4443

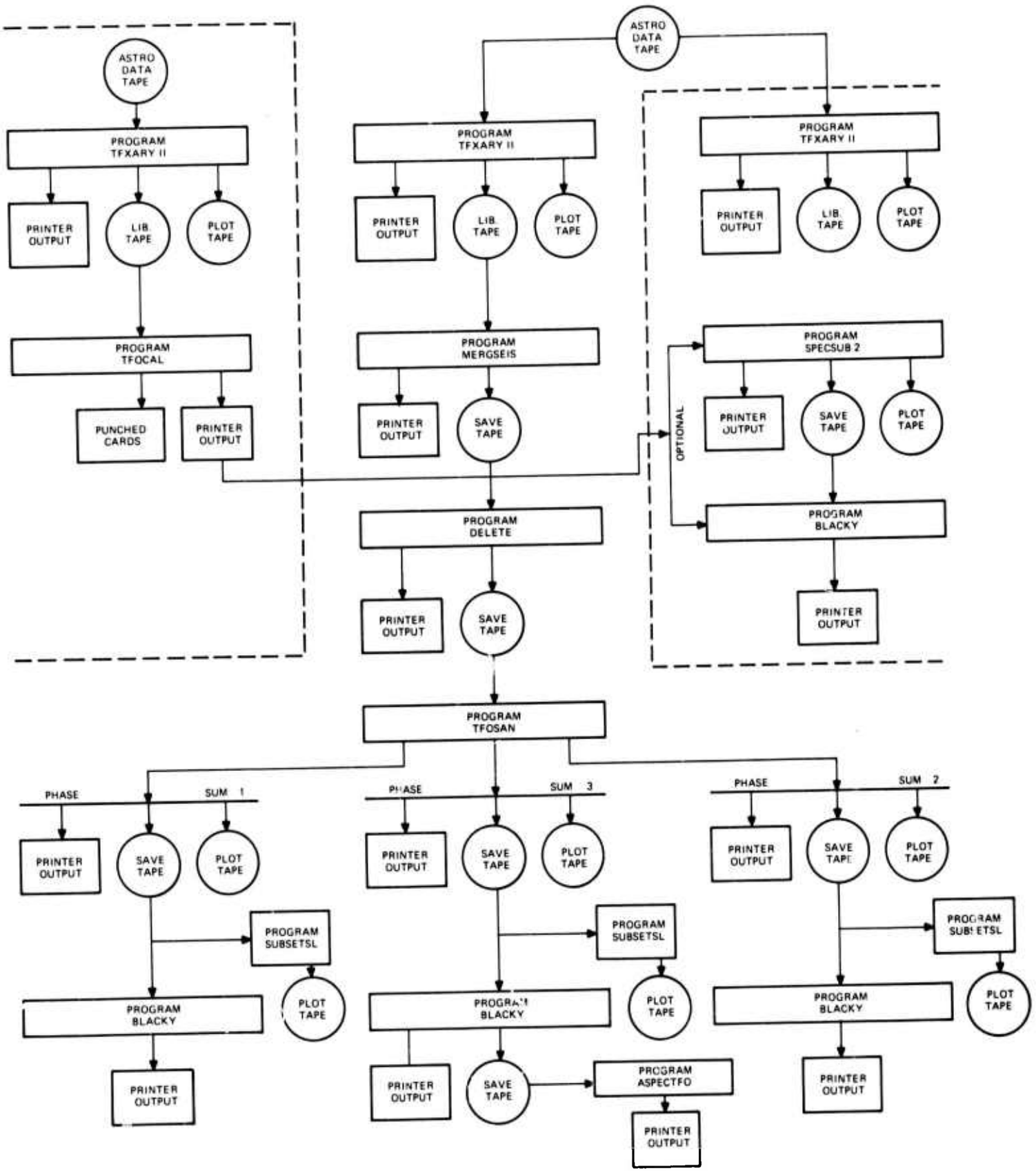

Figure 13. Outline of data sample processing sequence

G 4444

4. DATA ANALYSIS

4.1 NOISE REDUCTION

For each data sample, the noise power spectra were used to form the following ratios: PS1/IND, PS2/IND, PS3/IND, and CLSF/IND. These ratios indicate, as a function of frequency, the amount of noise reduction achieved by each system. The noise reduction ratios for each data sample are shown in appendix 1. It is evident that the three phased sums provide essentially the $\sqrt{N}$ noise reduction at the higher frequencies. The result of the combination of the analog and the digital filtering is evident in the noise ratio CLSF/IND, especially at the higher frequencies.

The noise ratios for a given system were averaged over the data ensemble and figure 14 shows the results. From the average noise reduction ratios, we conclude:

a. Below about 1.2 cps, PS1 provides about 3 dB more noise reduction that does the unfiltered summation of the cross-linear array (CLS). Above 1.2 cps, the two systems are about equal.

b. PS2 provides about 4 dB more noise reduction than PS1 at every frequency.

c. PS3 provides about 2 dB more noise reduction than PS2 at every frequency.

d. The noise reduction provided by the CLSF varies considerably due to the analog filtering. At the lowest frequency considered, 0.33 cps, the noise reduction achieved by the CLSF is equivalent to that of PS2, but the effectiveness of the CLSF decreases with increasing frequency until at 1.0 cps it is equivalent to the CLS. For frequencies above 1.0 cps, the CLSF provides increasing noise reduction with increasing frequency. At the highest frequency considered, 3.0 cps, the CLSF is about 4 dB more effective than PS3. Table 2 summarizes the average noise reduction provided by each system relative to the average individual element.

Table 2. Average noise reduction at 3 frequencies

Sys \ Freq	0.5 cps	1.0 cps	2.0 cps
PS1	5.1 dB	7.0 dB	9.7 dB
PS2	8.7 dB	11.1 dB	13.3 dB
PS3	11.3 dB	13.7 dB	15.0 dB
CLS	2.0 dB	3.7 dB	10.6 dB
CLSF	6.8 dB	4.6 dB	14.9 dB

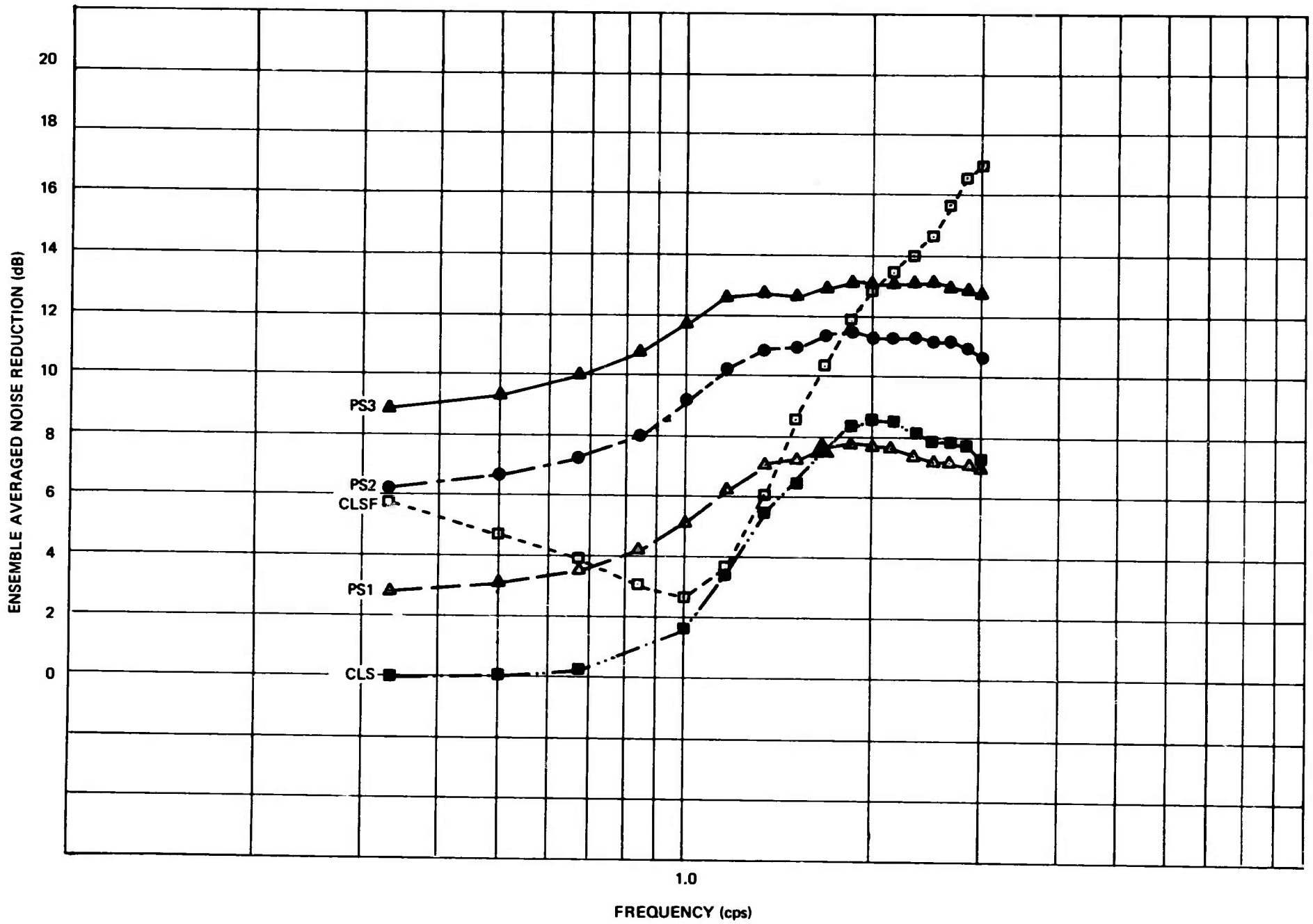

Figure 14. Ensemble averaged noise reduction ratios

G 4445

The rms measurements of the noise on the individual elements, the phased sums, CLS, and CLSF were used to obtain an rms noise reduction ratio for each system relative to the average individual element. Table 3 gives the value of the rms noise reduction for each system.

Table 3. Rms noise reduction ratios

System	Rms noise reduction
PS1	5.64 dB
PS2	9.15 dB
PS3	11.84 dB
CLS	2.04 dB
CLSF	6.36 dB

It should be noted that the rms measure of the noise is dominated by the noise power at the lower frequencies (~0.5 cps). Thus, the rms noise reduction is a lower bound for each system except CLSF. The rms noise reduction is in complete agreement with the noise reduction ratios obtained from the spectra.

4.2 SIGNAL LOSS

In a manner analogous to the formation of the noise reduction ratios, the signal power spectra were used to determine signal loss ratios as a function of frequency. Figure 15 shows the ratios that were computed for data sample 6. These curves show that for data sample 6, the signal loss at the frequency of peak power was 1.4 dB for PS1, 2.0 dB for PS2, 1.9 dB for PS3, and 3.6 dB for CLSF. From figure 10, it is evident that slight differences in the signal coda on the individual elements are the primary reason for the signal loss on the phased sums. The larger signal loss on the CLSF is due to the response of the analog filter. The signal loss ratios for each data sample are shown in appendix 2.

The signal loss ratios for a given system were averaged over the data ensemble (see figure 16). The average signal loss ratios indicate that the three phased sums and the CLS have a signal loss of between 1.0 and 2.0 dB in the frequency range of large signal power. The difference between the signal loss ratios of CLS and CLSF is the result of the efforts of analog filter in the CLSF system.

From a signal detection standpoint, the signal loss is not as great as that indicated by the signal-loss ratios. Program TFOSAN computed the signal loss for the phase sums from the amplitude measurements made from the dominant half-cycle in the time window. For each phased sum, the signal loss was averaged over the data sample ensemble. The results are given in table 4.

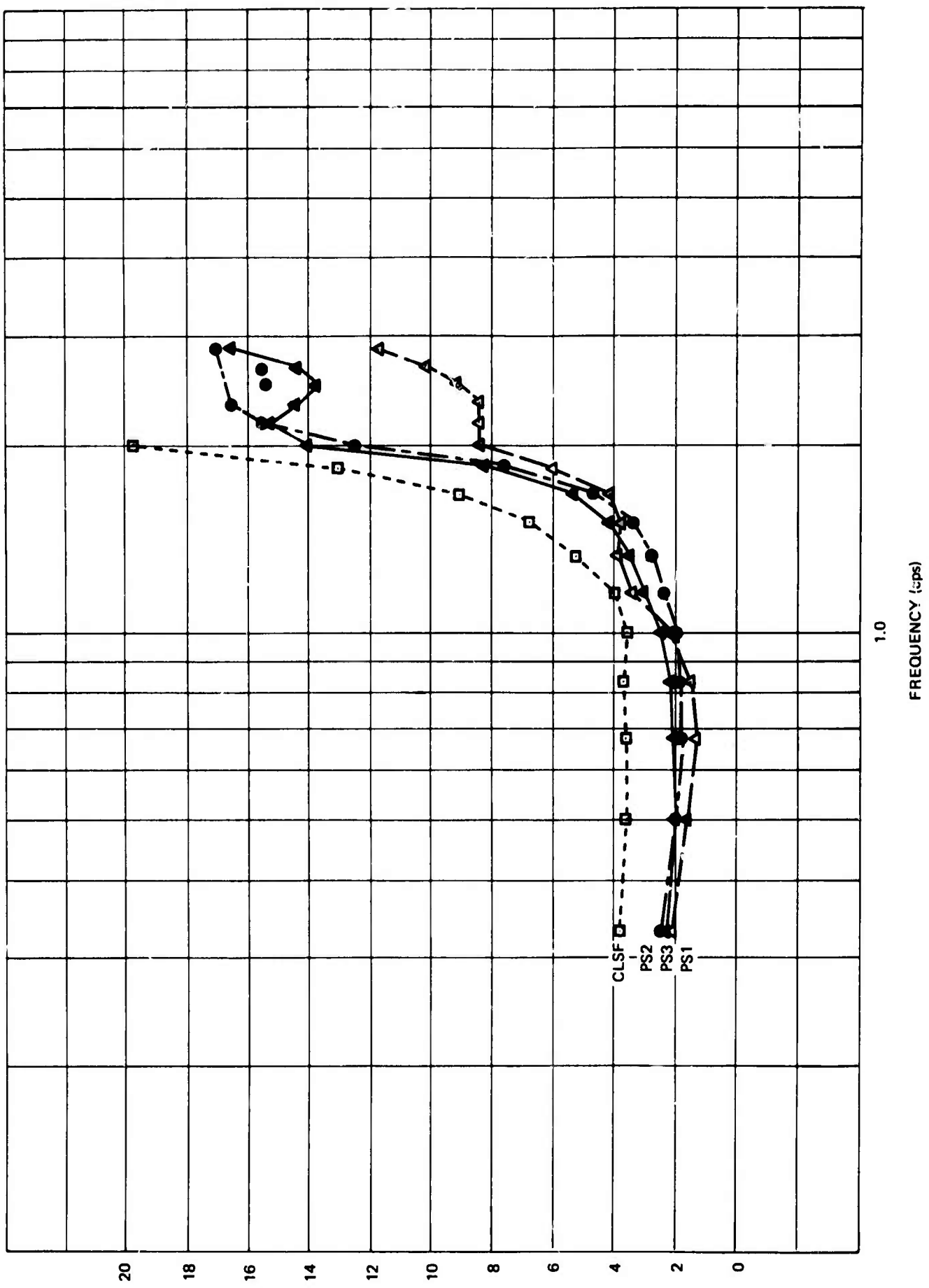

Figure 15. Signal loss ratios for data sample 6

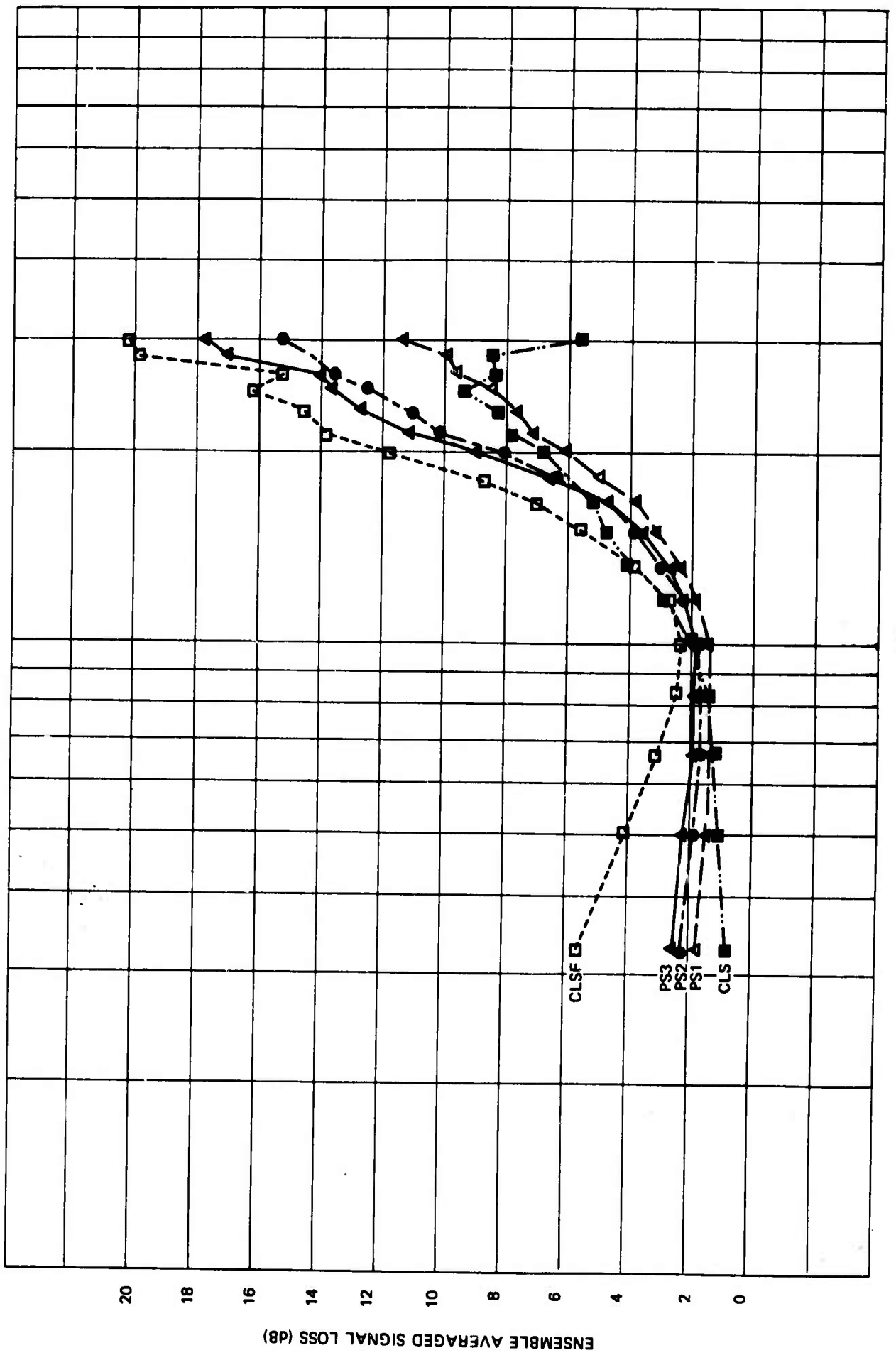

G 4447

Figure 16. Ensemble averaged signal loss ratios

Table 4. Average signal loss

System	Signal loss
PS1	0.37 dB
PS2	0.55 dB
PS3	0.62 dB

The CLS and CLSF were not included in table 4 because the amplitude measurements of the signal for these systems were calculated using Program SPECSUB2 which calculates the maximum center-to-peak amplitude in the signal coda; whereas, TFOSAN calculates the maximum peak-to-peak amplitude within a restricted window. Because of this, comparison of CLS and CLSF signal amplitudes with the average amplitude recorded by the individual elements was not necessarily meaningful in all instances.

4.3 SIGNAL-TO-NOISE RATIOS

The signal and the noise power spectra for each system were used to obtain S/N as a function of frequency. The curves for data sample 6 are shown in figure 17. It should be noted that the maximum S/N does not occur at the same frequency as the maximum signal power. In general, the S/N curves peaked at about 1.17 or 1.33 cps. The S/N curves for a given system were not averaged over the ensemble because they do not have a common reference point, and thus vary from data sample to data sample. The signal-to-noise ratios for each data sample are shown in appendix 3.

Program TFOSAN computed a signal-to-noise ratio for the individual elements and the phased sums by taking the ratio of the (peak-to-peak)/2 signal amplitude to the rms noise value. Table 5 gives the S/N for data sample 6.

Table 5. S/N from Program TFOSAN for data sample 6

System	S/N
IND	16.4 dB
PS1	21.2 dB
PS2	26.2 dB
PS3	29.2 dB

4.4 S/N IMPROVEMENT

S/N improvement for the phased sums and CLSF was computed as a function of frequency by taking the ratio of the S/N of the system under consideration to the S/N of an average individual element (IND). Figure 6 in appendix 4 shows the results for data sample 6. At 0.67 cps, the frequency of maximum signal power, the S/N improvement is 4.0 dB for PS1, 7.8 dB for PS2, 10.8 dB for PS3, and 2.0 dB for CLSF. At the frequency where the maximum S/N occurs,

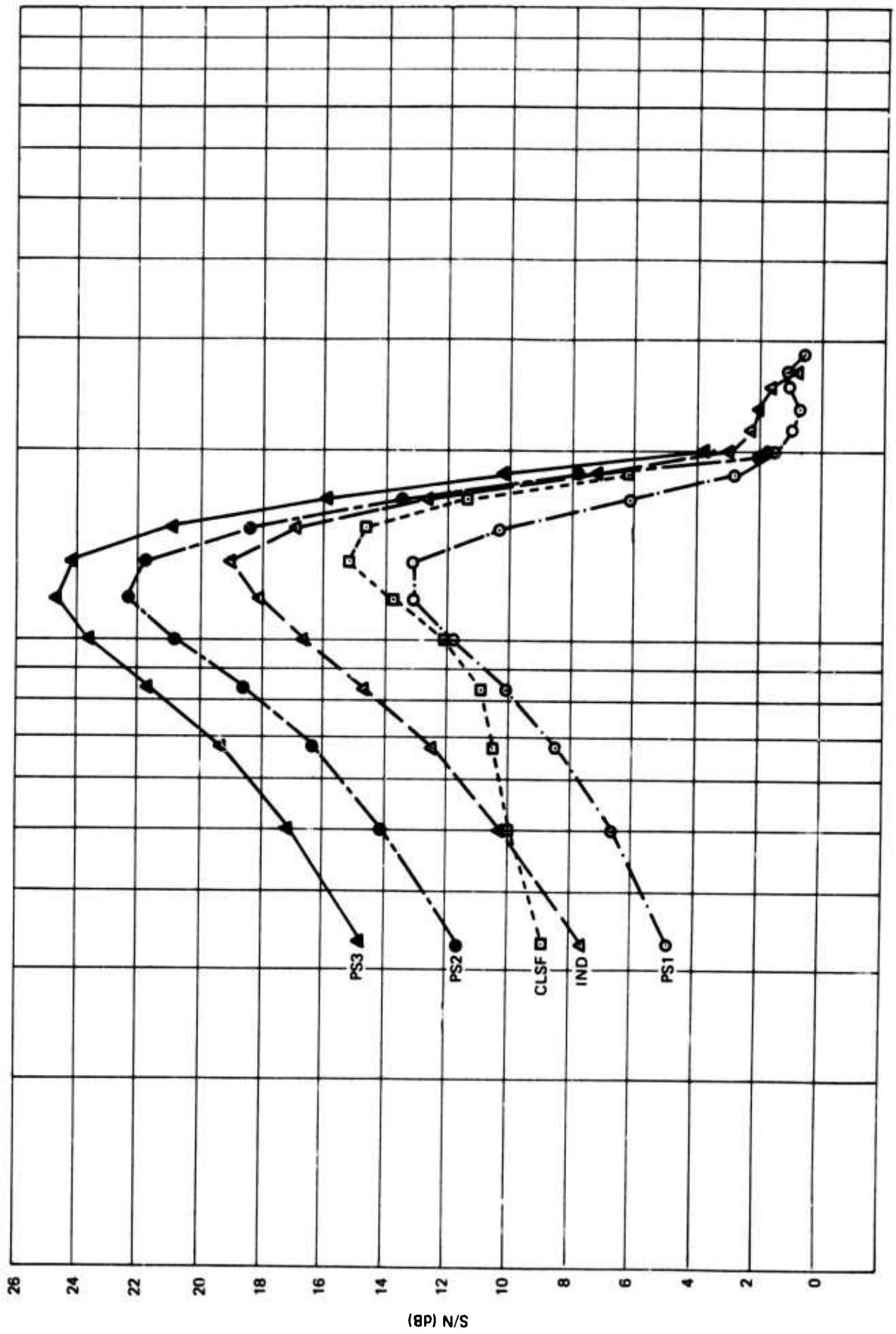

G 4448

Figure 17. Signal-to-noise ratios for data sample 6

the improvement is 5.9 dB for PS1, 9.1 dB for PS2, 11.5 dB for PS3, and 2.0 dB for CLSF.

The S/N improvement ratios for each system were averaged over the data sample ensemble, and the results are shown in figure 18. The ratios show that the systems rank in the following order, from poorest to best: CLS, CLSF, PS1, PS2, and PS3. Table 6 summarizes the S/N improvement provided by each system relative to the average individual.

Table 6. S/N improvement at 3 frequencies

System	0.67 cps	1.0 cps	1.17 cps
PS1	4.1 dB	5.6 dB	6.4 dB
PS2	7.5 dB	9.3 dB	10.0 dB
PS3	10.0 dB	11.9 dB	12.4 dB
CLS	1.1 dB	1.7 dB	2.7 dB
CLSF	2.8 dB	2.3 dB	2.9 dB

It should be noted that the drop in the S/N improvement at the higher frequencies (≥2.0 cps) is due to the general absence of signal power at these frequencies.

Average S/N improvement was also computed from the S/N improvement factors output by program TFOSAN for the three phased sums. Phased-Sum 1 shows an average S/N improvement factor of 5.26 dB, PS2 shows 8.58 dB improvement, and PS3 shows an improvement of 11.25 dB. These values compare favorably with the S/N improvement ratios at 1.0 cps (table 6).

4.5 CONCLUSIONS

The following conclusions can be made from the data analysis:

1. The three phased sums and CLS suppress the noise by a factor of $\sqrt{N}$ for frequencies greater than about 1.5 cps. At 1.0 cps, the average noise reduction relative to an average individual element is 7.0 dB for PS1, 11.1 dB for PS2, 13.7 dB for PS3, 3.7 dB for CLS, and 4.6 dB for CLSF. For the pass band of 0.4 to 3.0 cps, the average rms noise reduction is 5.64 dB for PS1, 9.15 dB for PS2, 11.84 dB for PS3, 2.04 dB for CLS, and 6.36 dB for CLSF.

2. The signal amplitude loss in the 30-second P-wave coda is between 1.0 and 2.0 dB in the frequency range of greatest signal power (0.5 to 1.0 cps) for the three phased sums and the CLS. Due to the response of the analog filter, CLSF suffers about 3.0 dB signal loss in the same frequency band. Using (peak-to-peak)/2 signal amplitude values measured on a dominant half-cycle in a time window, the average signal loss relative to an average individual is 0.37 dB for PS1, 0.55 dB for PS2, and 0.62 dB for PS3.

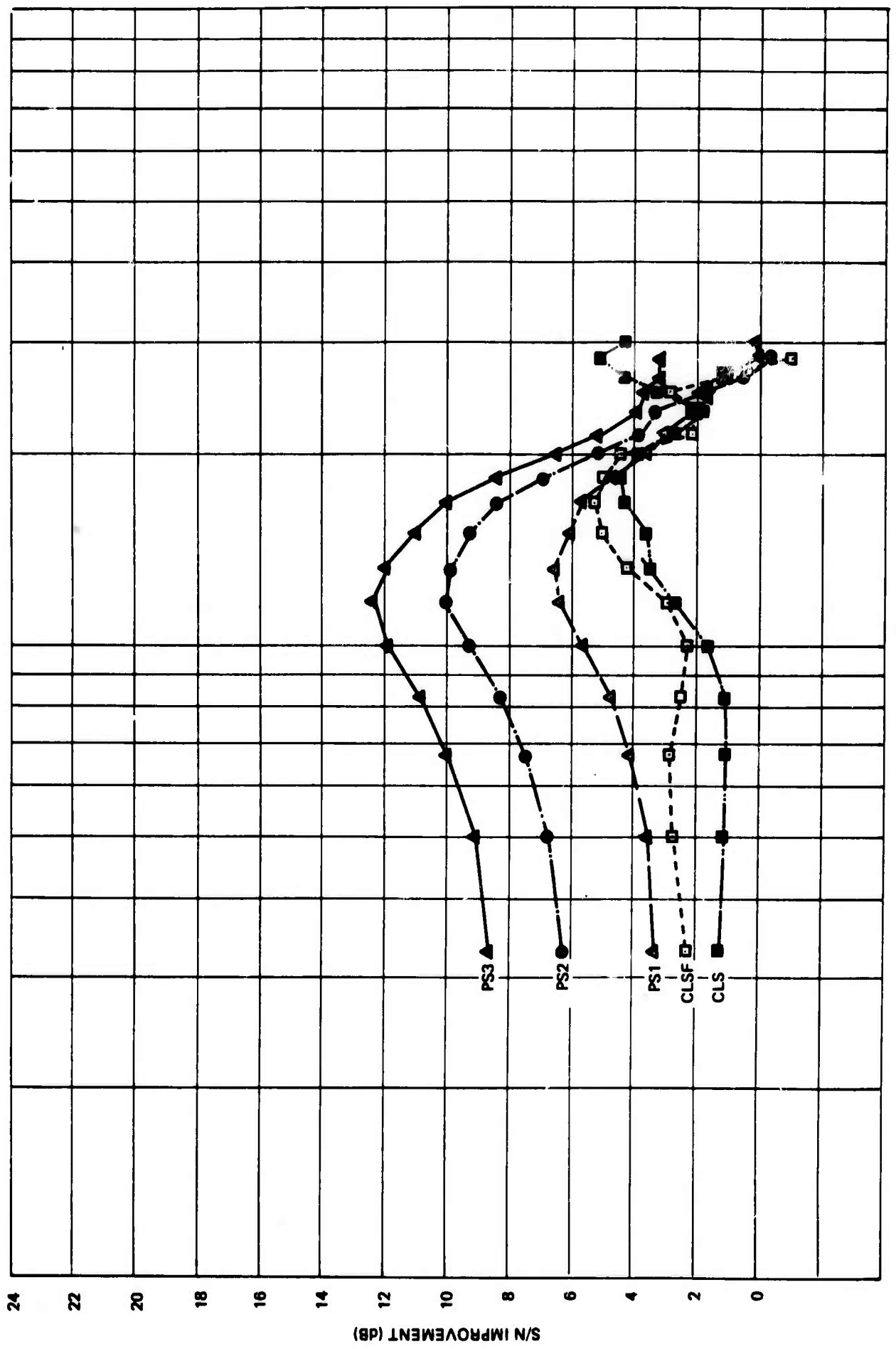

G 4449

Figure 18. Ensemble averaged S/N improvement ratios

3. From a S/N improvement standpoint, the five systems that were studied rank as follows, from poorest to best: CLS, CLSF, PS1, PS2, PS3. The maximum S/N improvement generally occurred at about 1.17 or 1.33 cps on the three phased sums. At 1.17 cps, the average S/N improvement relative to an average individual is 6.4 dB for PS1, 10.0 dB for PS2, 12.4 dB for PS3, 2.7 dB for CLS, and 2.9 dB for CLSF. For S/N computed with (peak-to-peak)/2 signal amplitudes and rms noise values, the average S/N improvement is 5.26 dB for PS1, 8.58 dB for PS2, and 11.25 dB for PS3.

APPENDIX 1 to TECHNICAL REPORT NO. 68-47

NOISE REDUCTION RATIOS FOR EACH DATA SAMPLE
RELATIVE TO AN AVERAGE INDIVIDUAL ELEMENT

BLANK PAGE

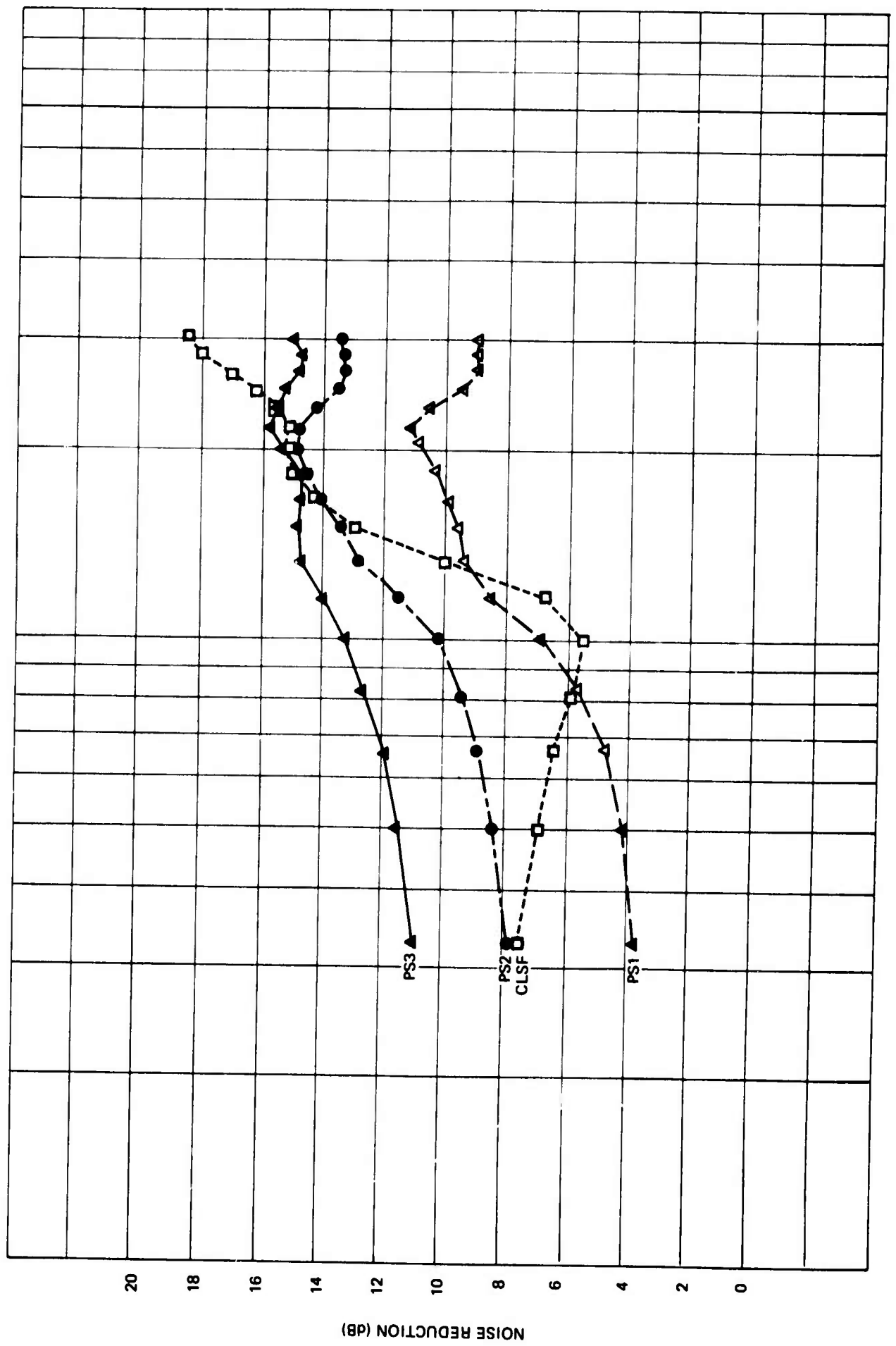

G 4450

Figure 1. Noise reduction ratios for data sample 1

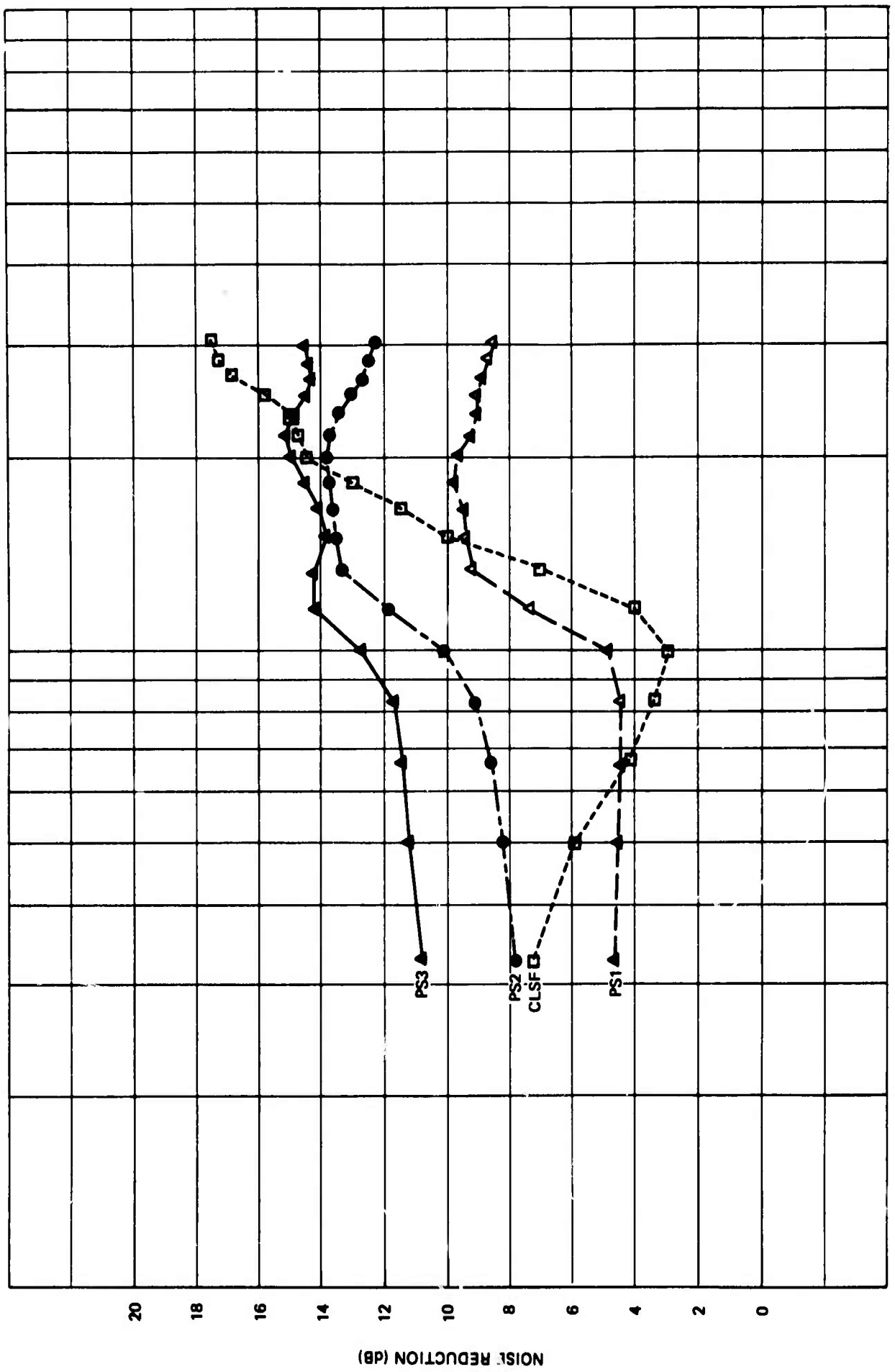

G 4451

Figure 2. Noise reduction ratios for data sample 2

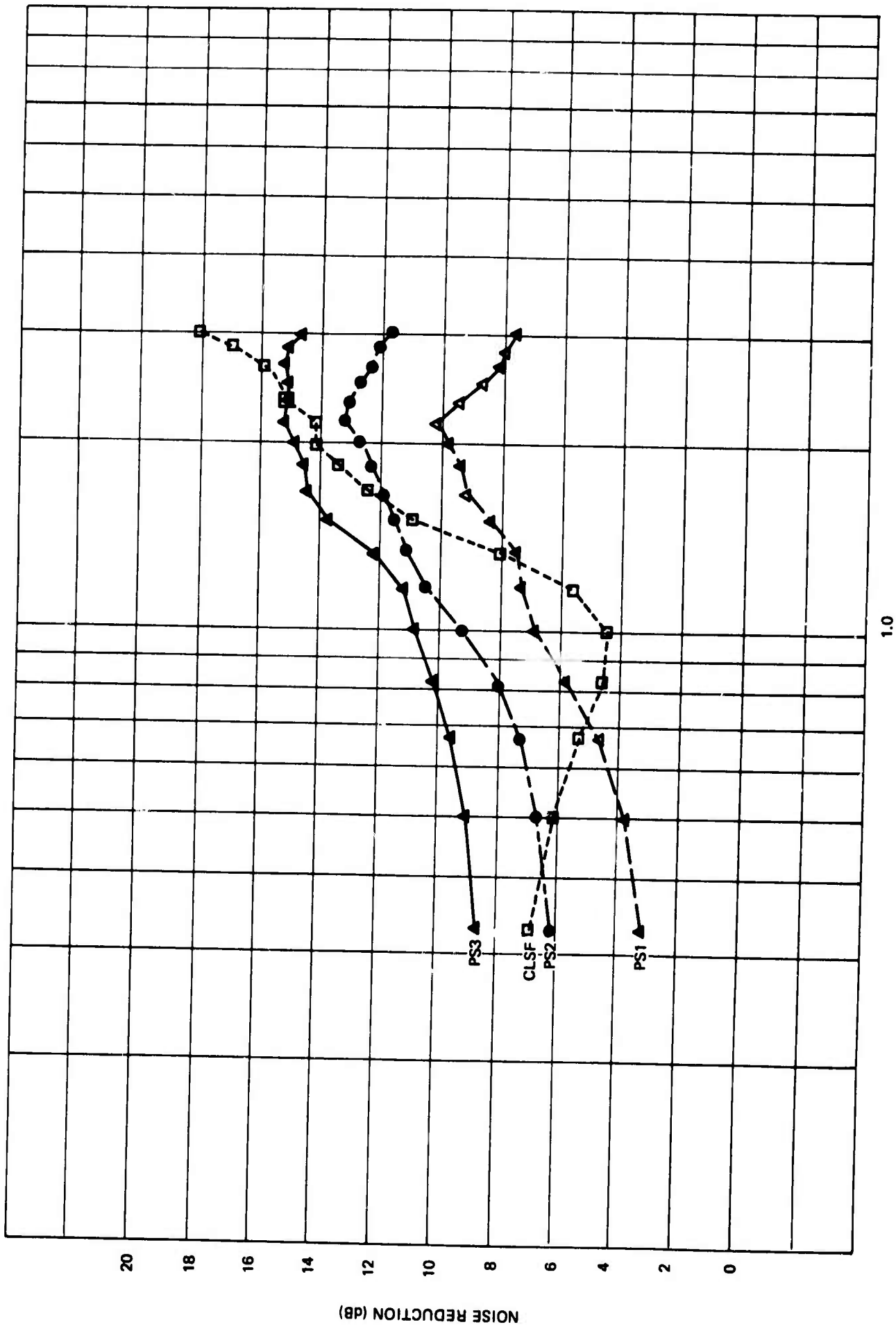

G 4452

Figure 3. Noise reduction ratios for data sample 3

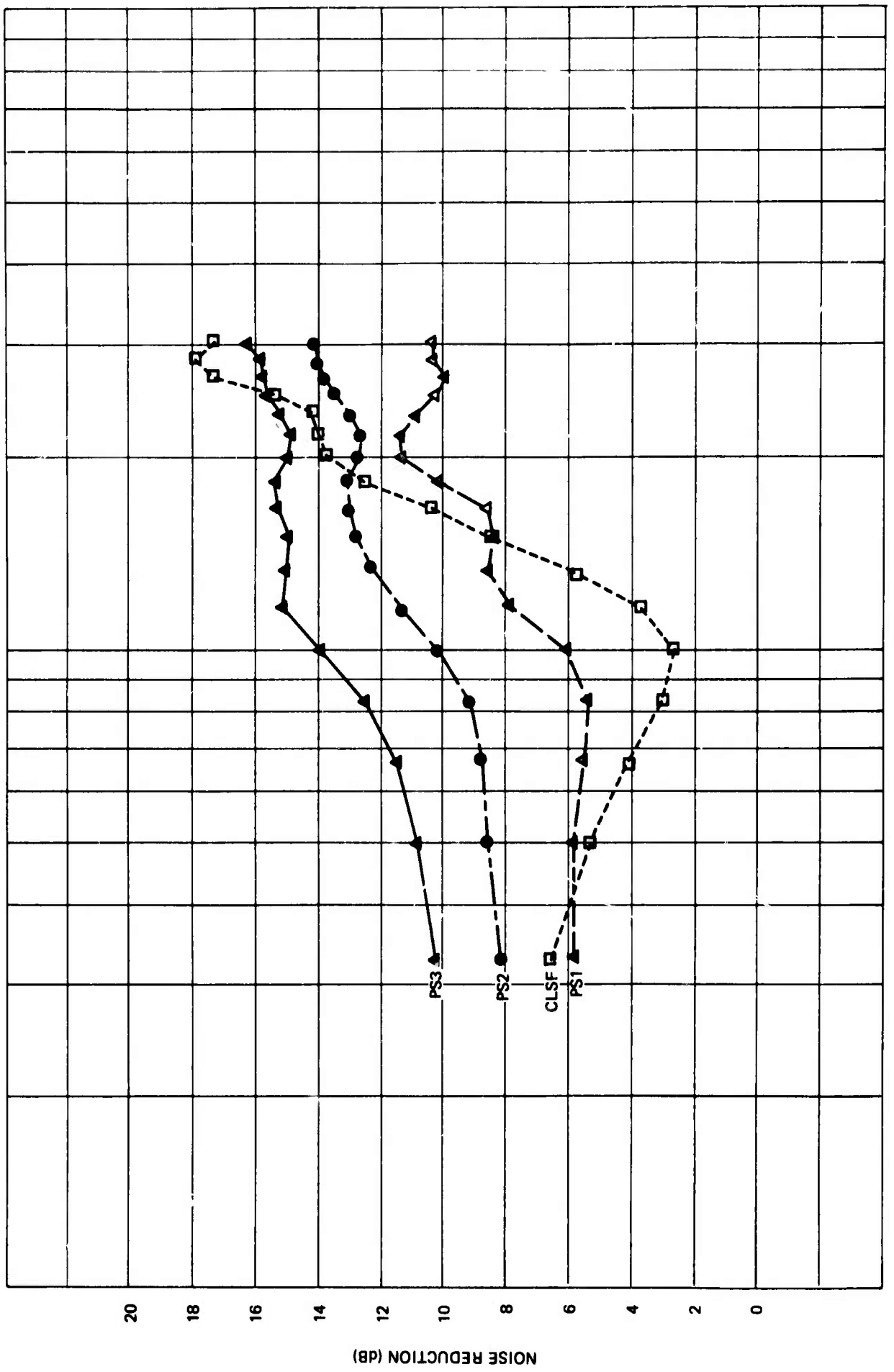

G 4453

Figure 4. Noise reduction ratios for data sample 4

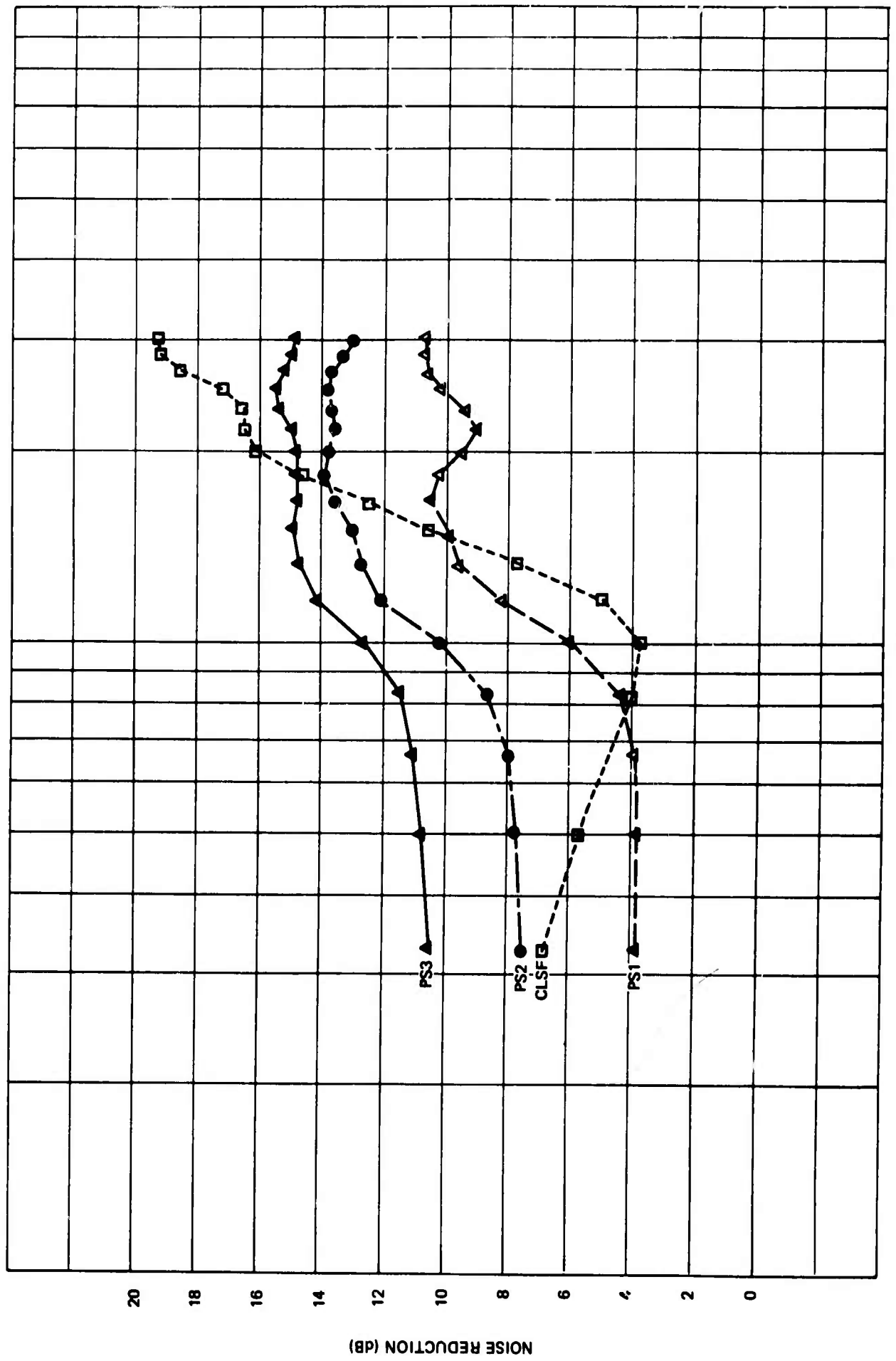

G 4454

Figure 5. Noise reduction ratios for data sample 5

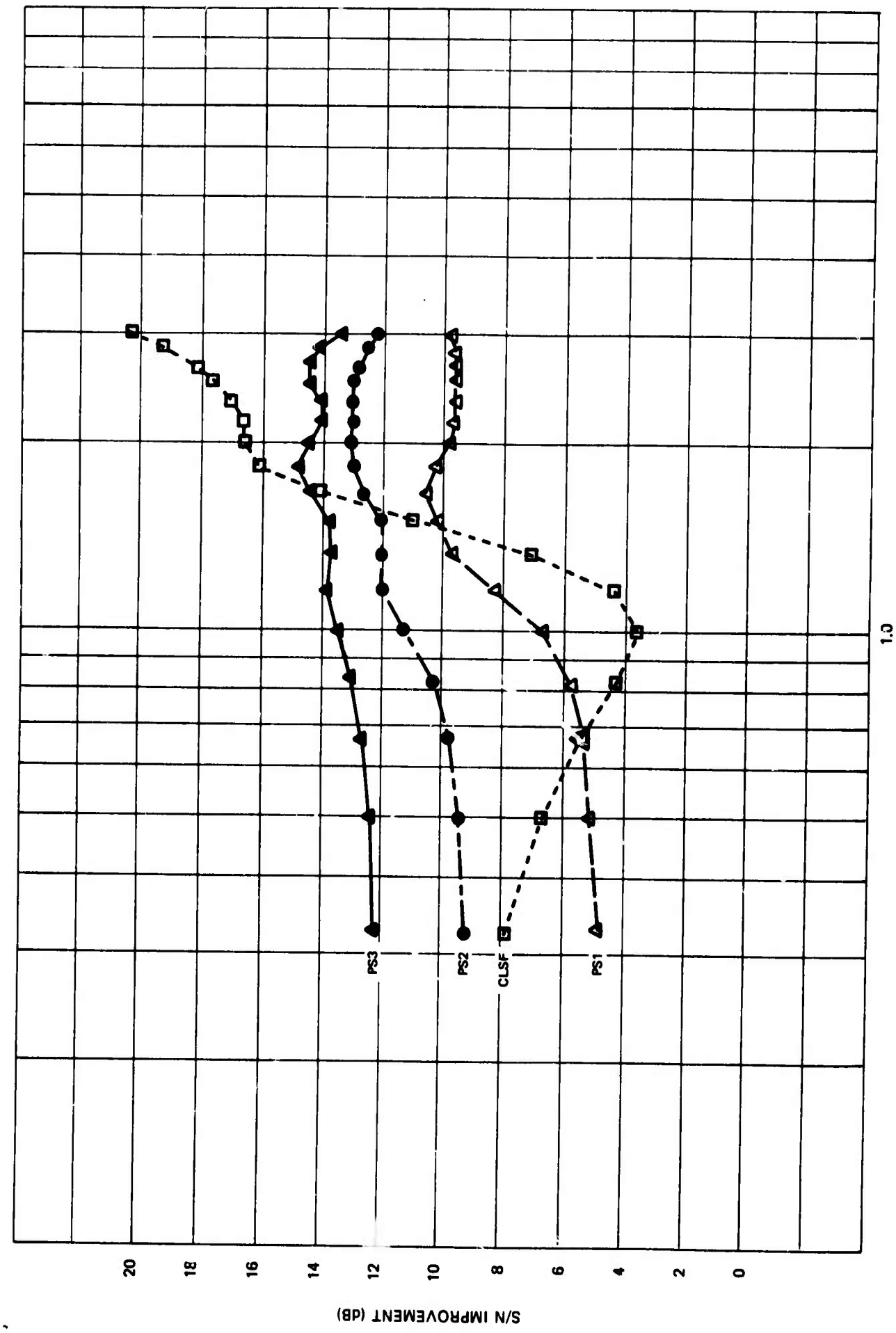

G 4455

Figure 6. Noise reduction ratios for data sample ó

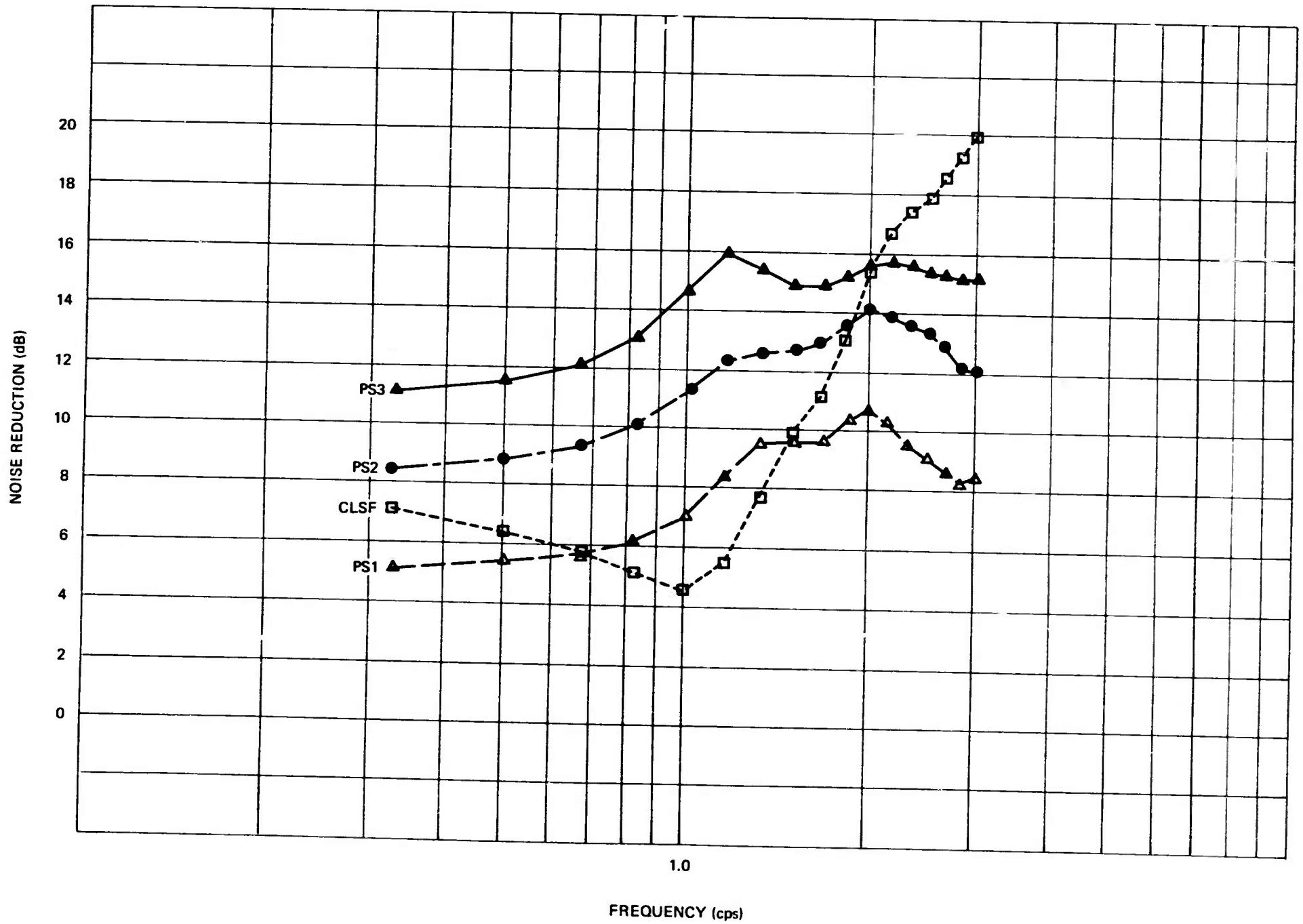

Figure 7. Noise reduction ratios for data sample 7

G 4456

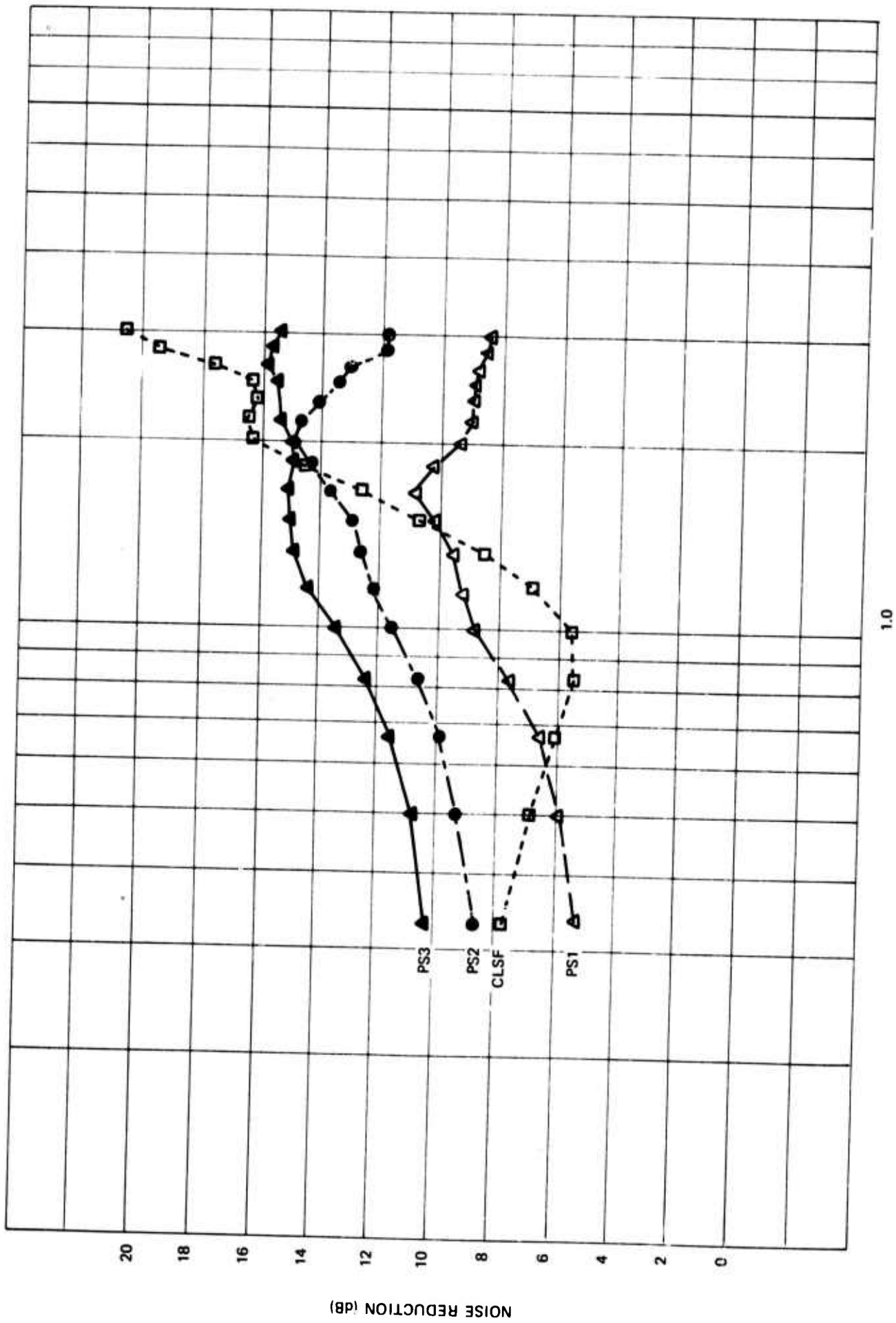

G 4457

Figure 8. Noise reduction ratios for data sample 8

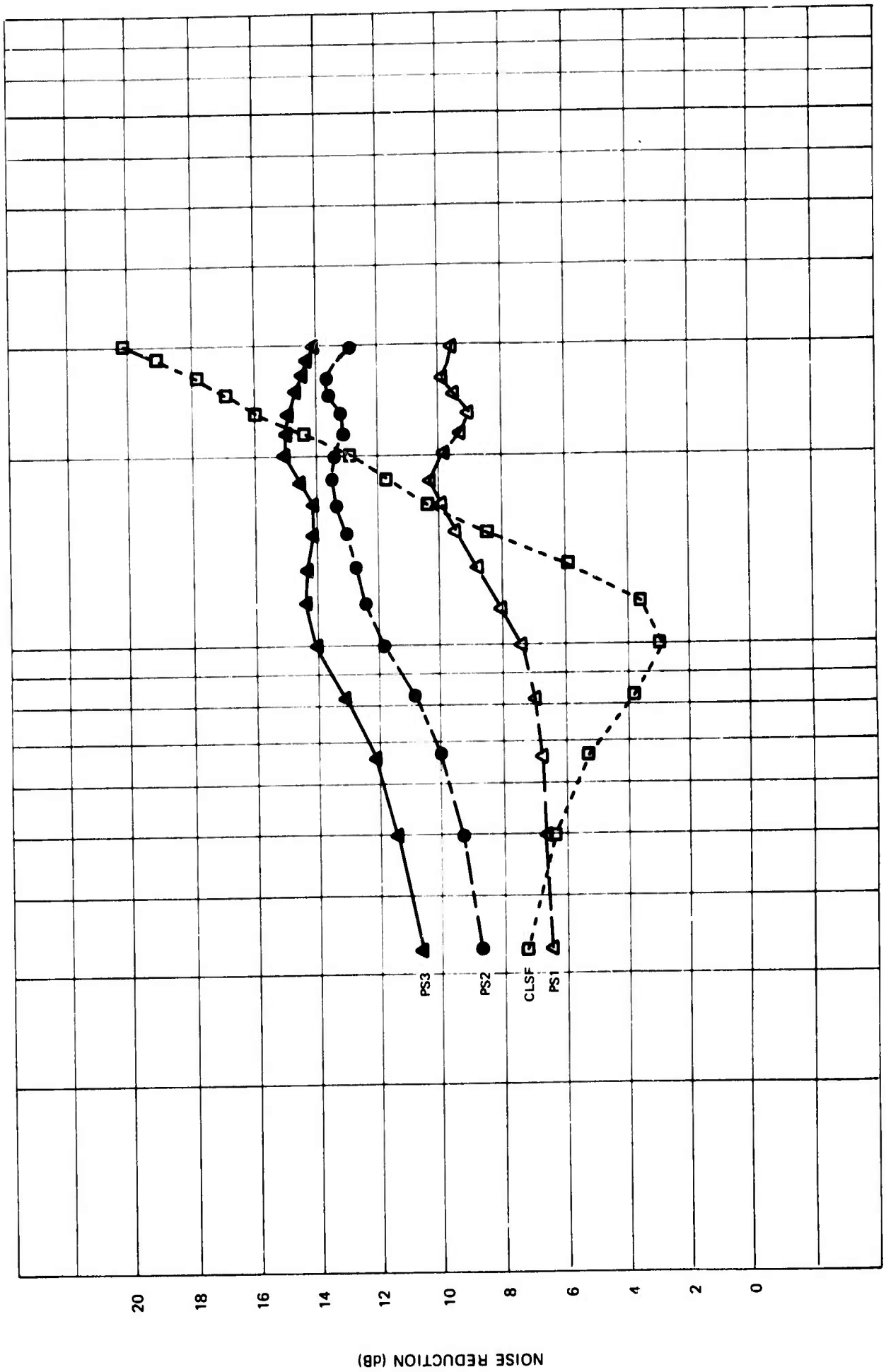

G 4458

Figure 9. Noise reduction ratios for data sample 9

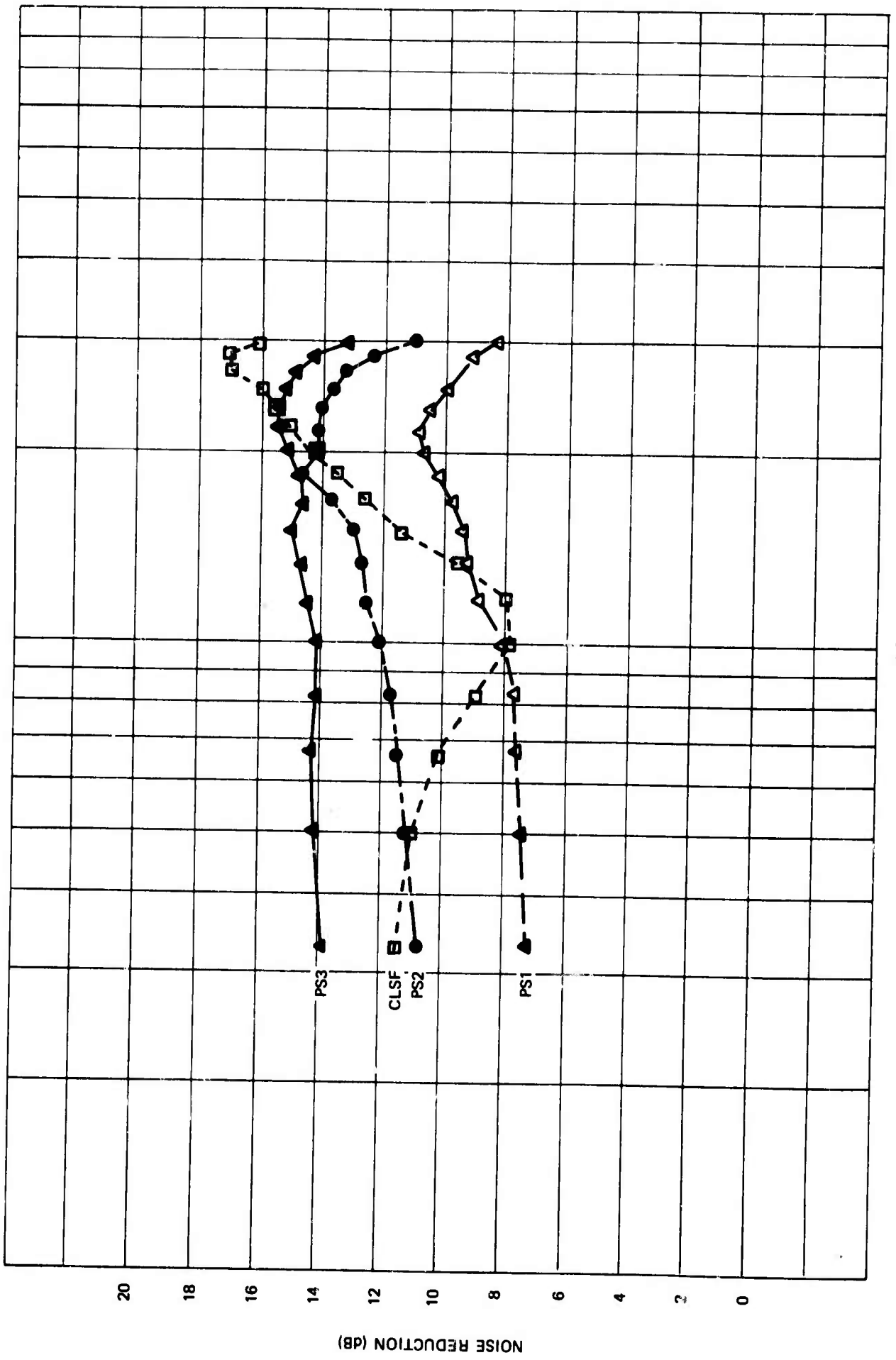

G 4459

Figure 10. Noise reduction ratios for data sample 10

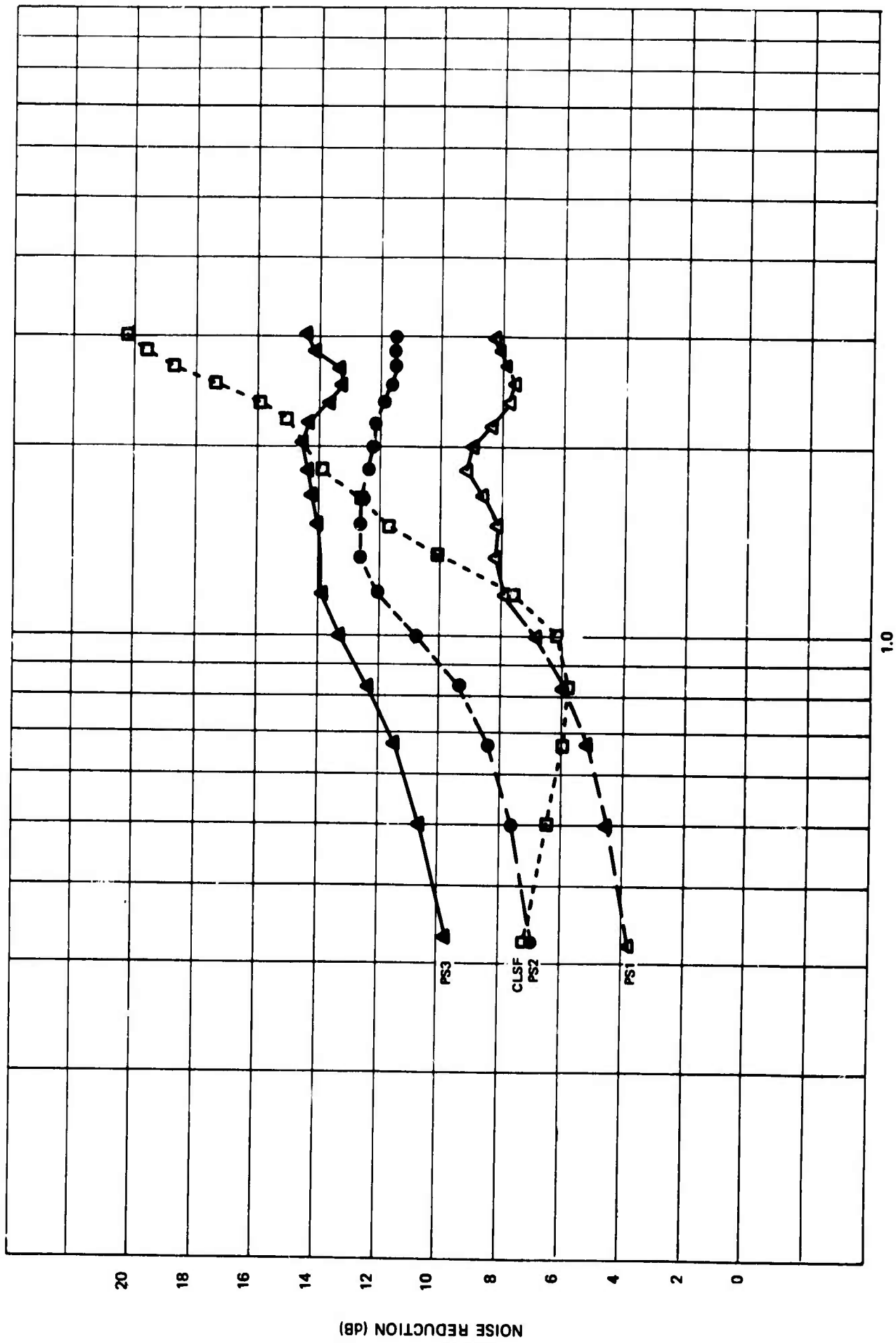

G 4460

Figure 11. Noise reduction ratios for data sample 11

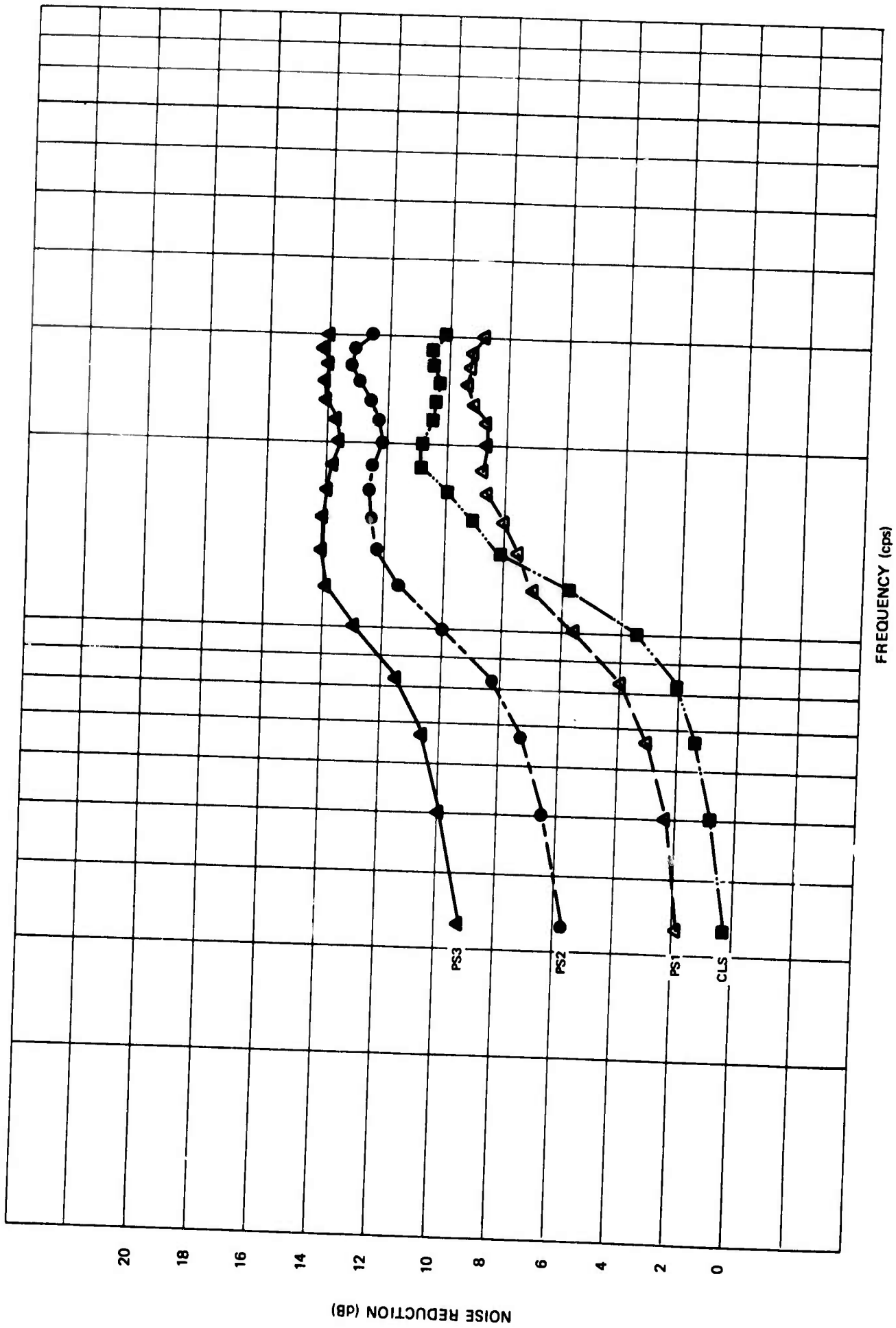

G 4461

Figure 12. Noise reduction ratios for data sample 12

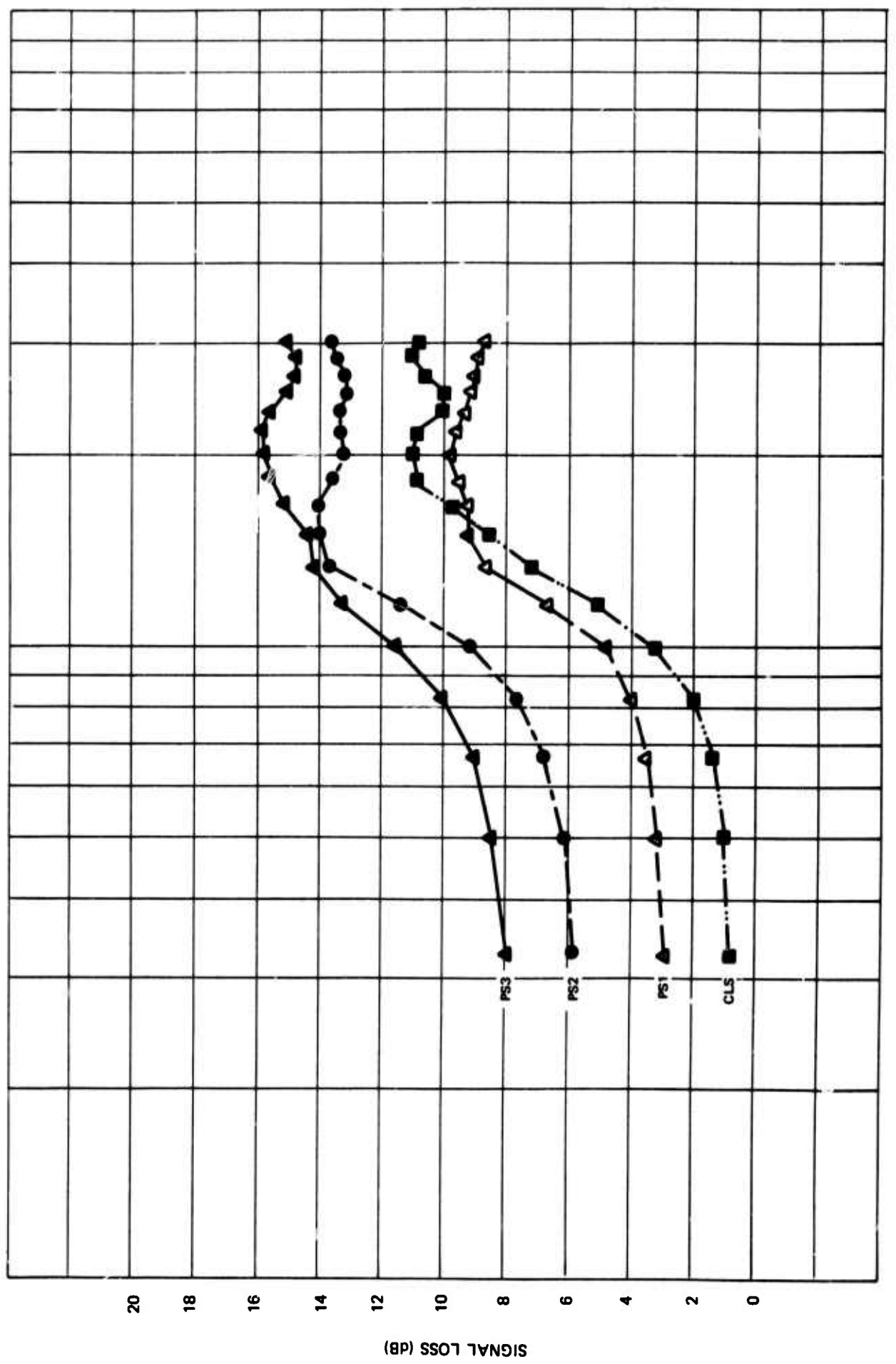

G 4462

Figure 13. Noise reduction ratios for data samples 13

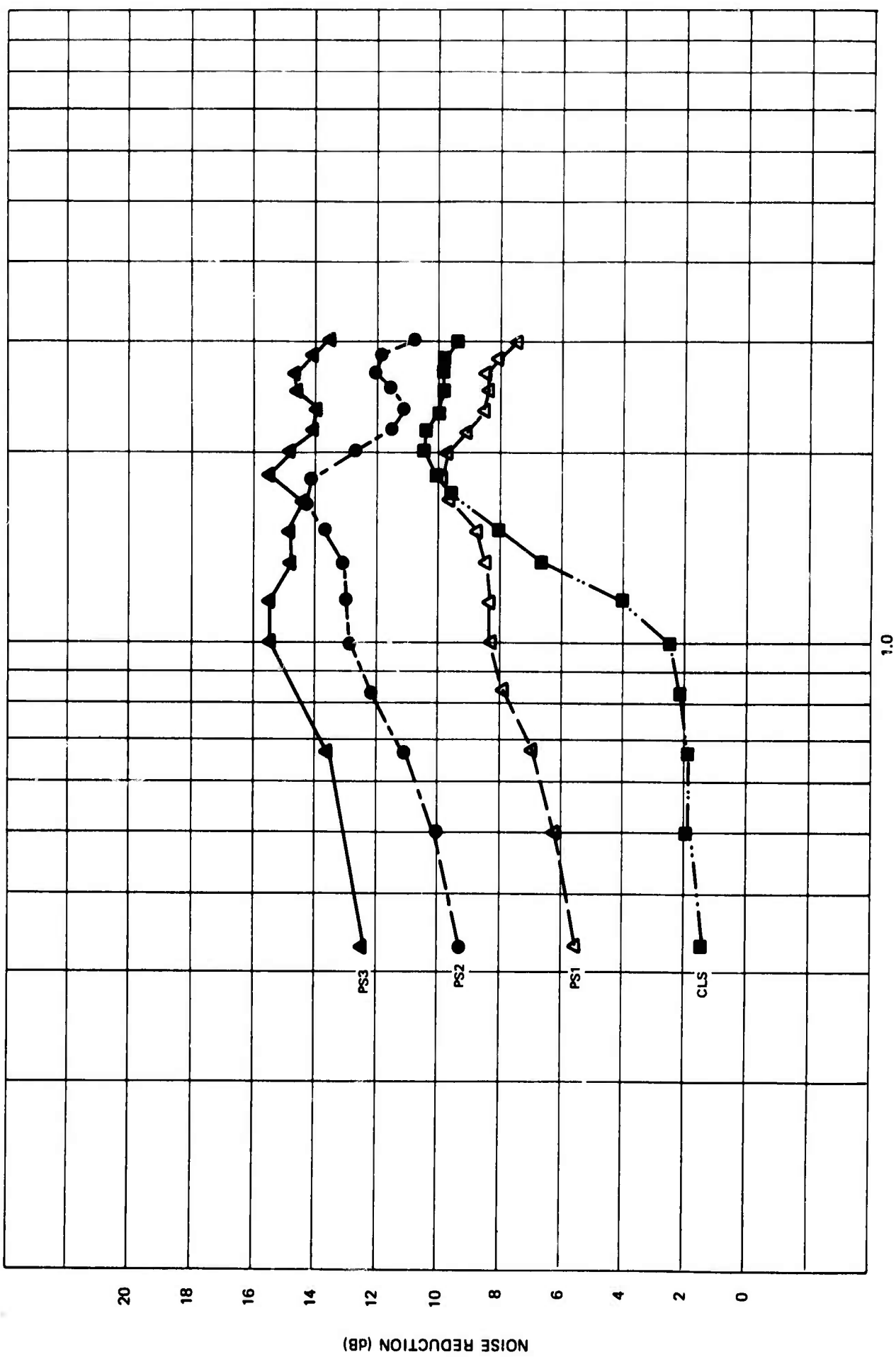

G 4463

Figure 14. Noise reduction ratios for data sample 14

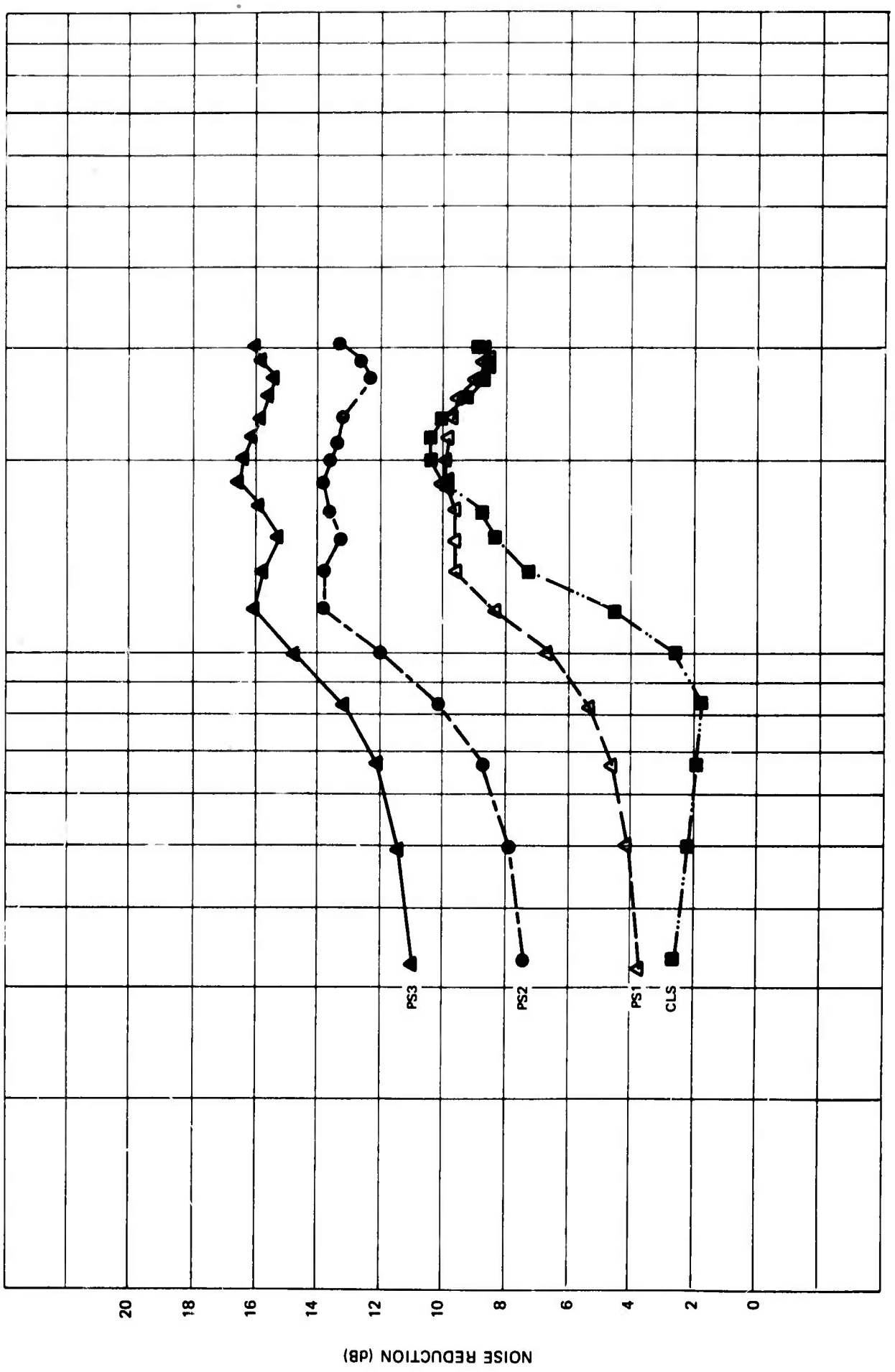

G 4464

Figure 15. Noise reduction ratios for data sample 15

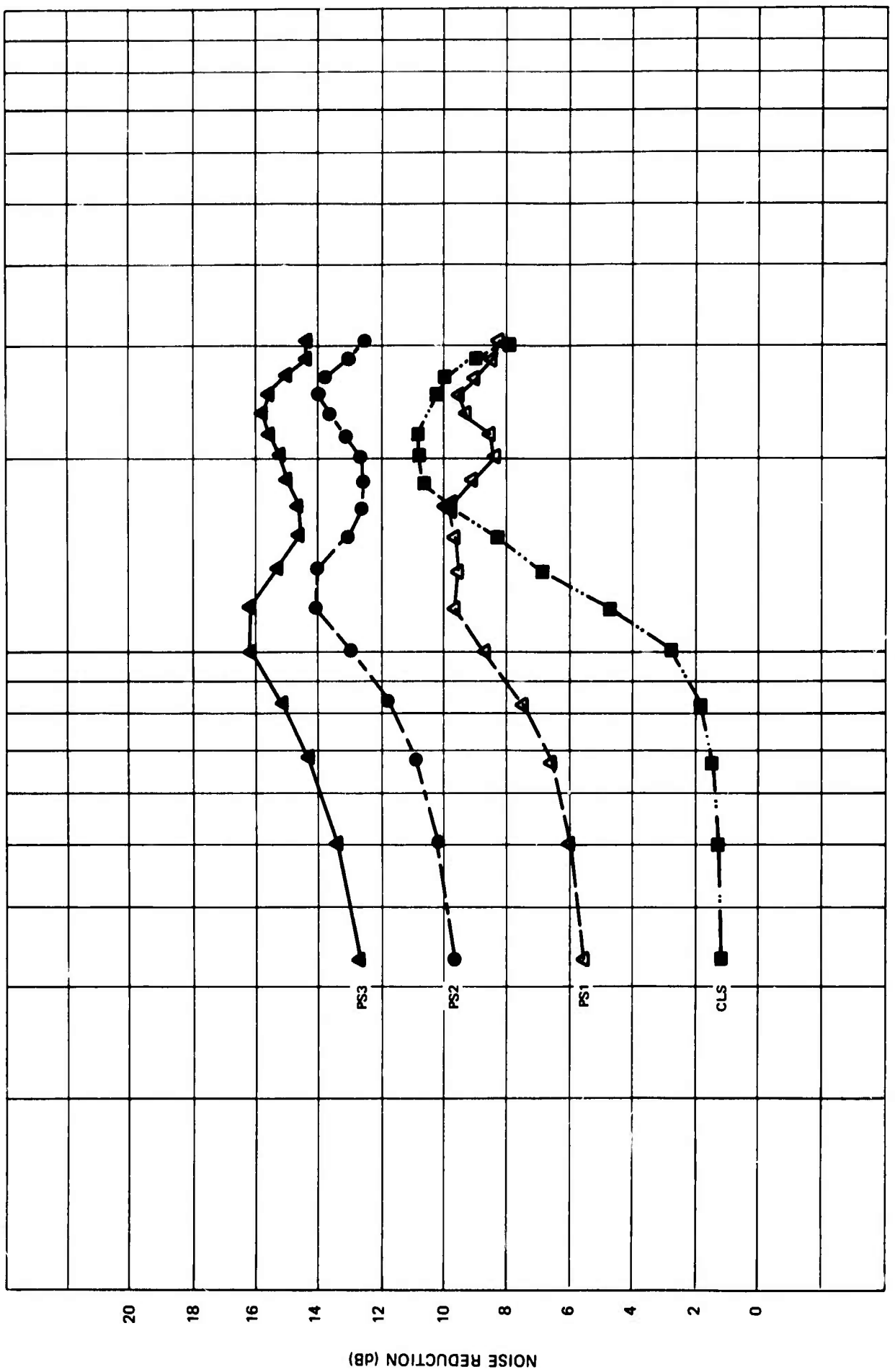

G 4465

Figure 16. Noise reduction ratios for data sample 16

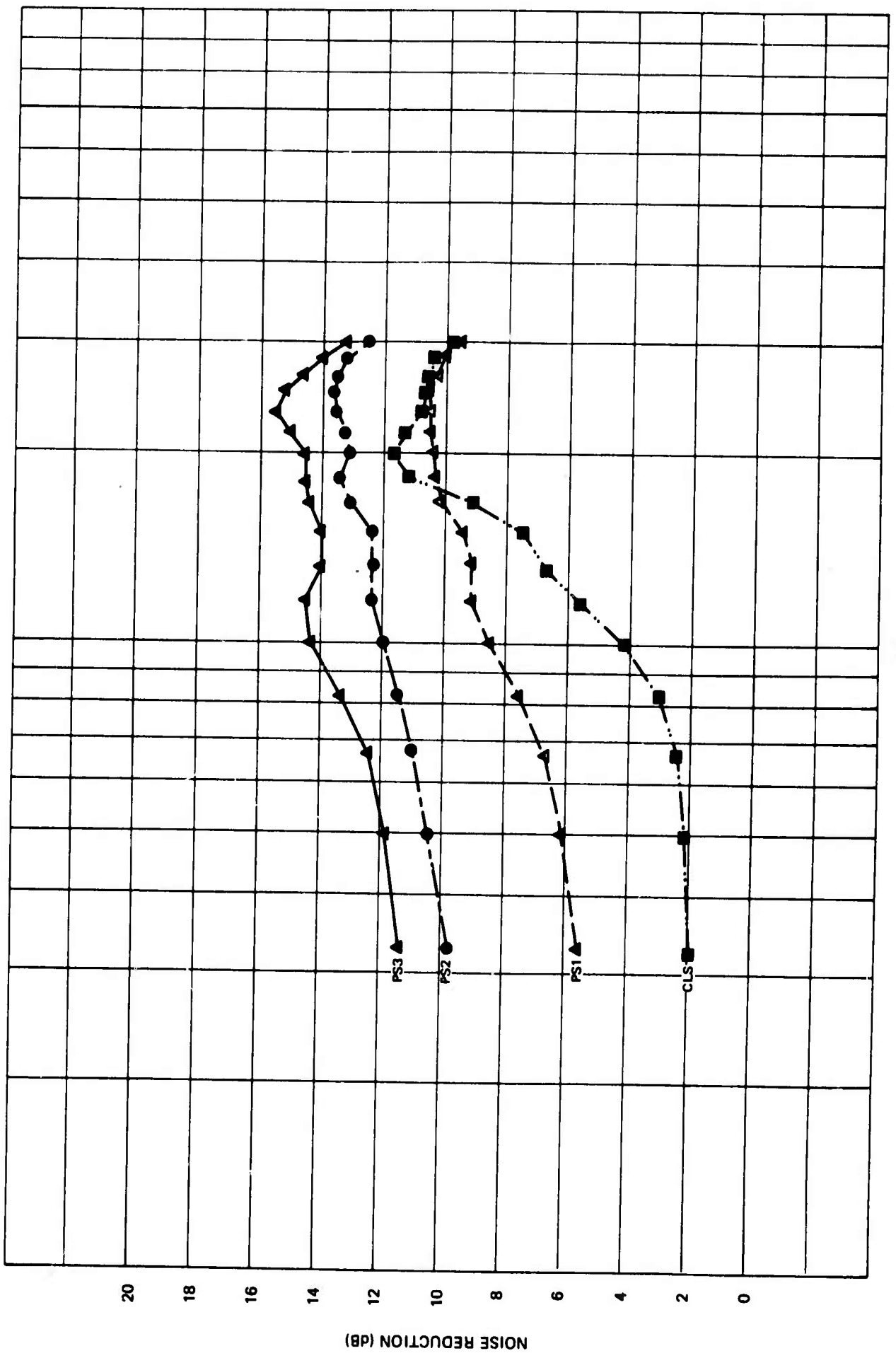

G 4466

Figure 17. Noise reduction ratios for data sample 17

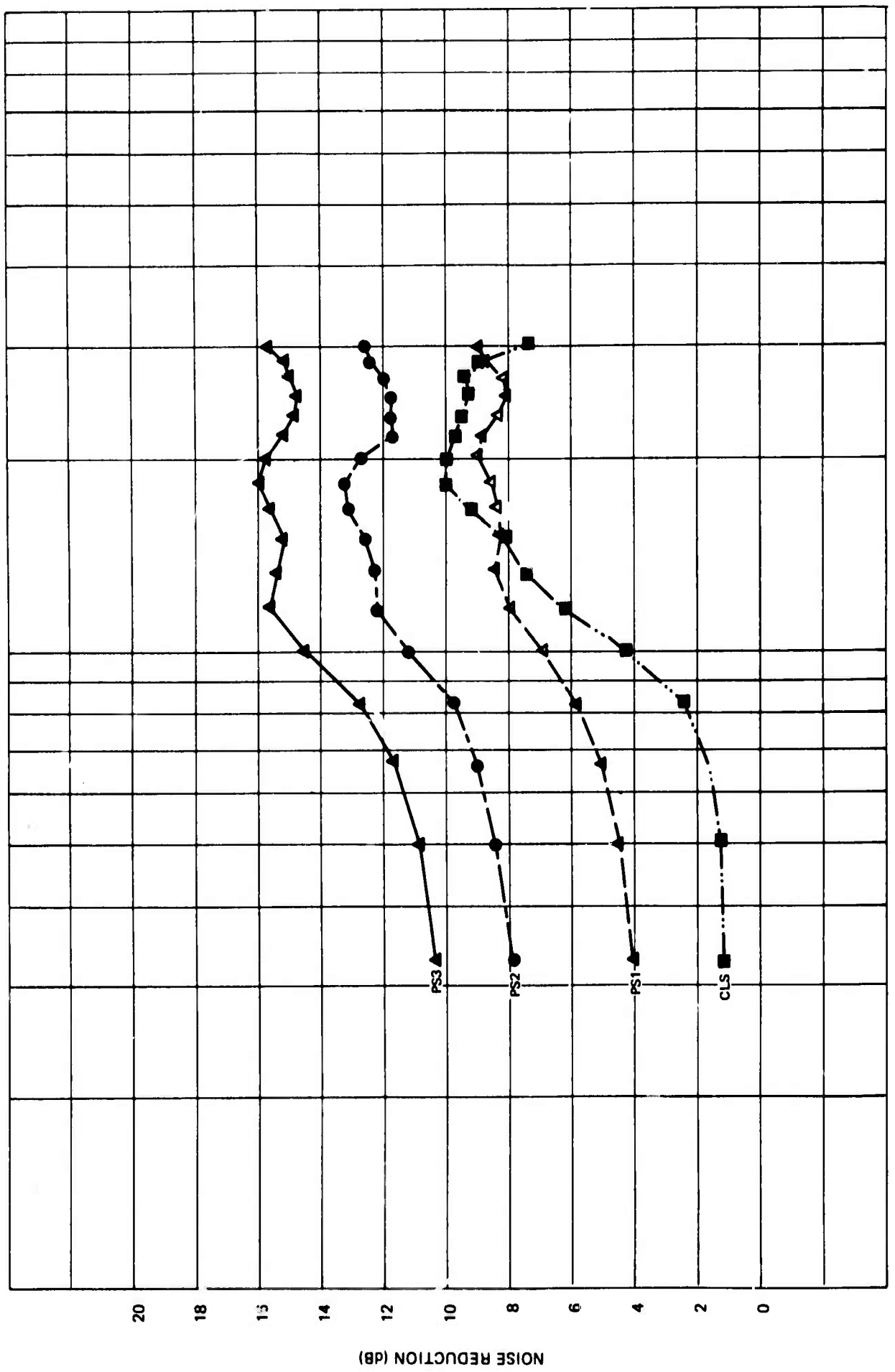

G 4467

Figure 18. Noise reduction ratios for data sample 18

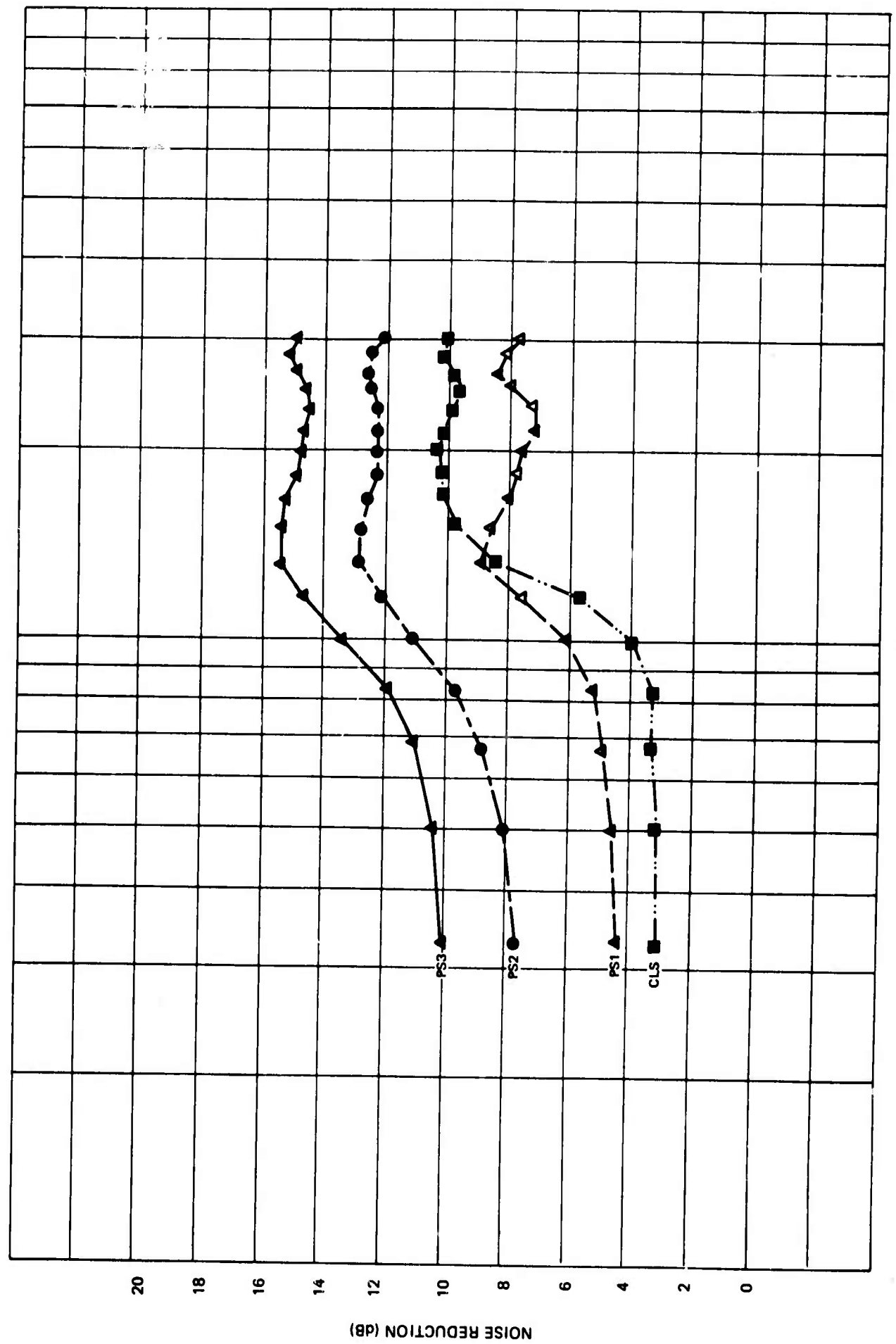

G 4468

Figure 19. Noise reduction ratios for data sample 19

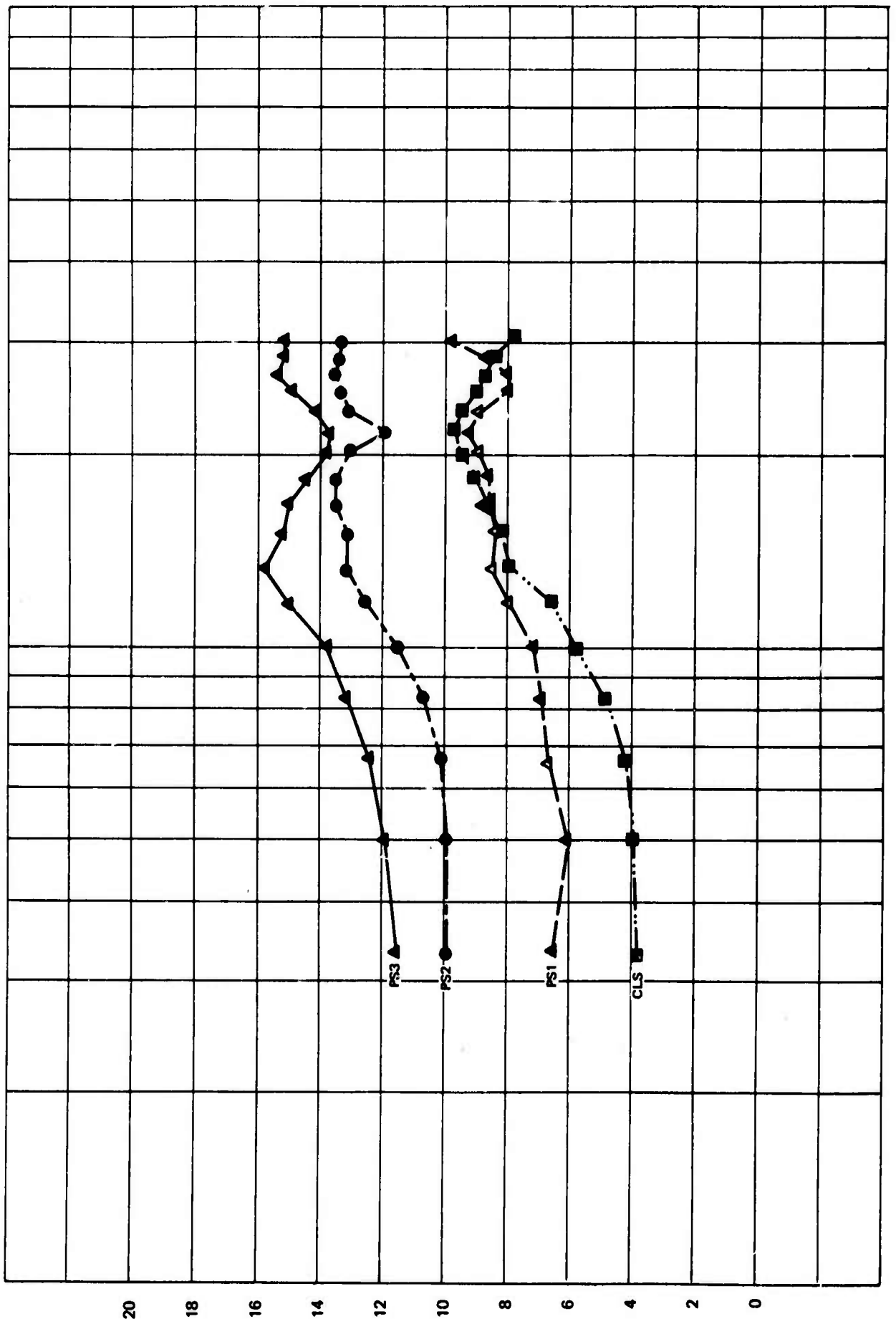

G 4469

Figure 20. Noise reduction ratios for data sample 20

APPENDIX 2 to TECHNICAL REPORT NO. 68-47

SIGNAL LOSS RATIOS FOR EACH DATA SAMPLE
RELATIVE TO AN AVERAGE INDIVIDUAL ELEMENT

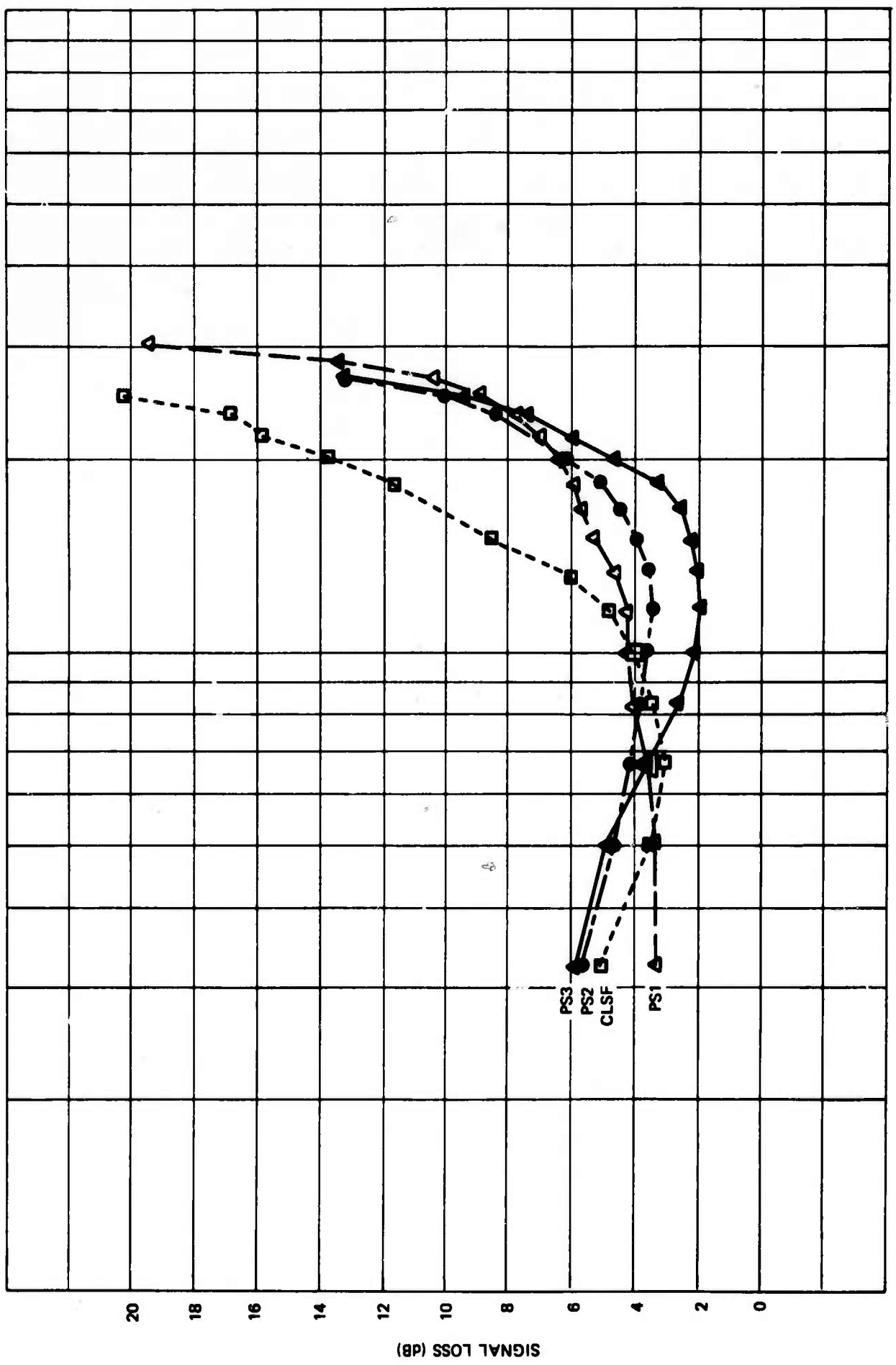

G 4470

Figure 1. Signal loss ratios for data sample 1

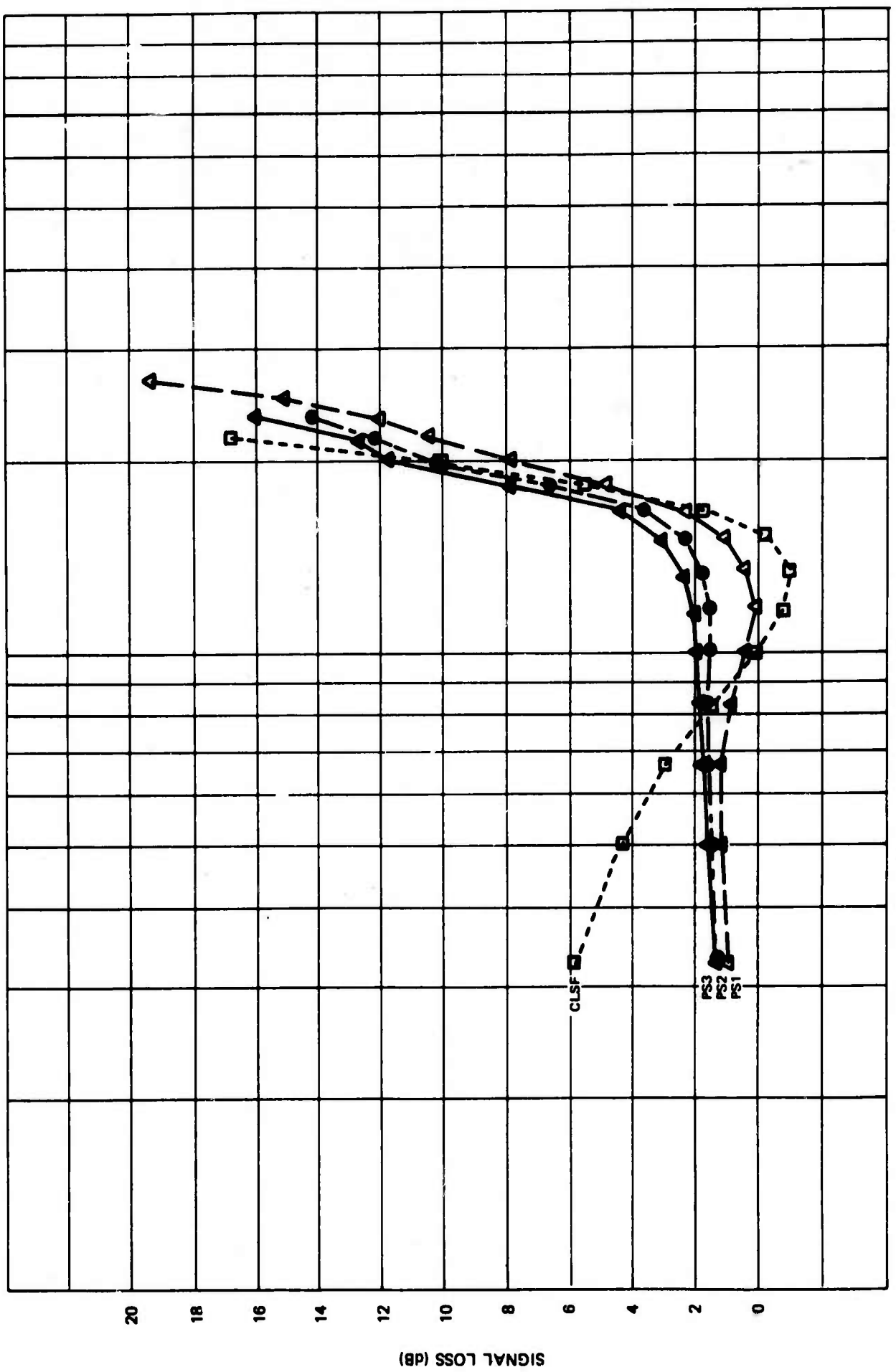

G 4471

Figure 2. Signal loss ratios for data sample 2

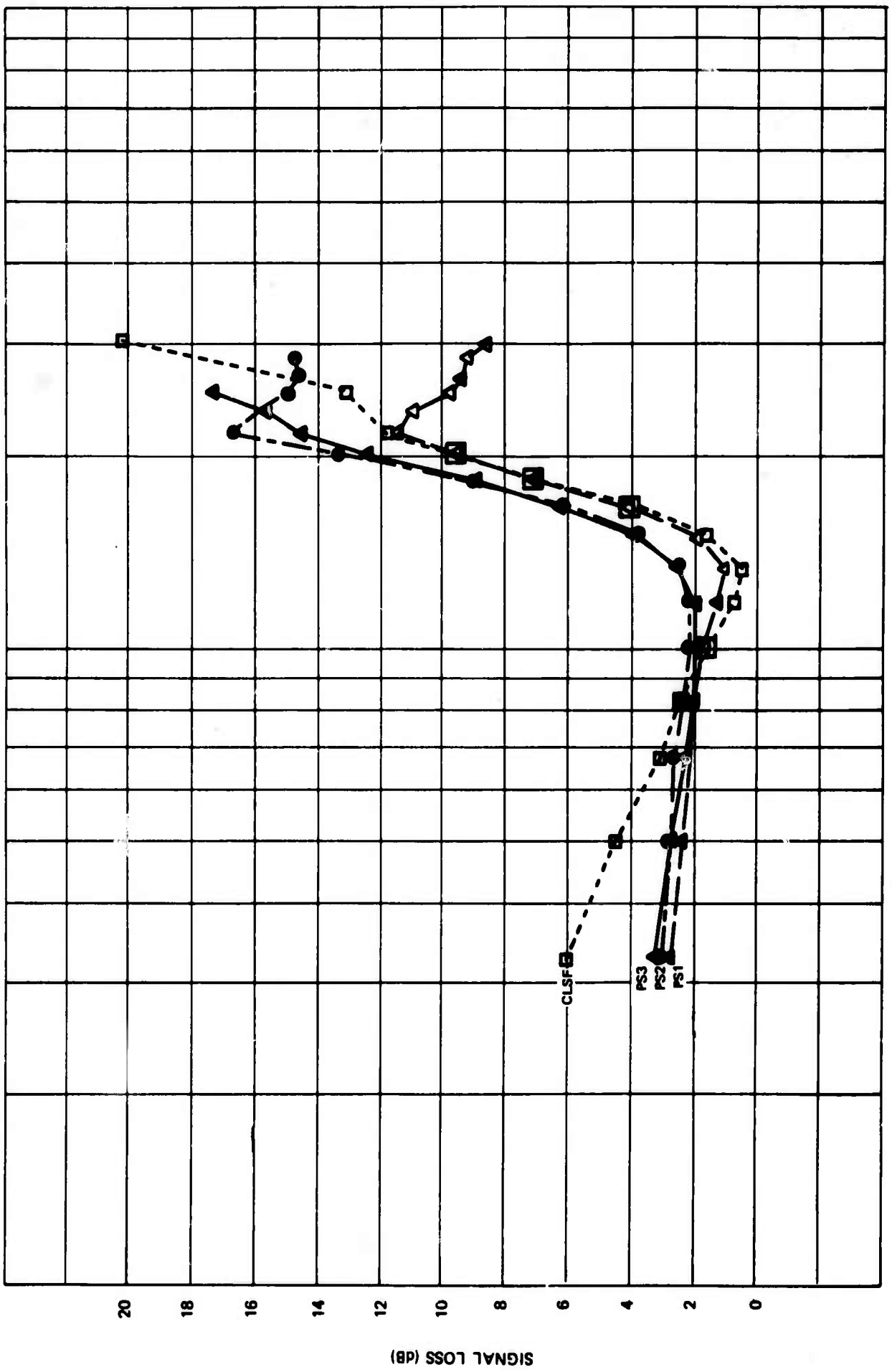

G 4472

Figure 3. Signal loss ratios for data sample 3

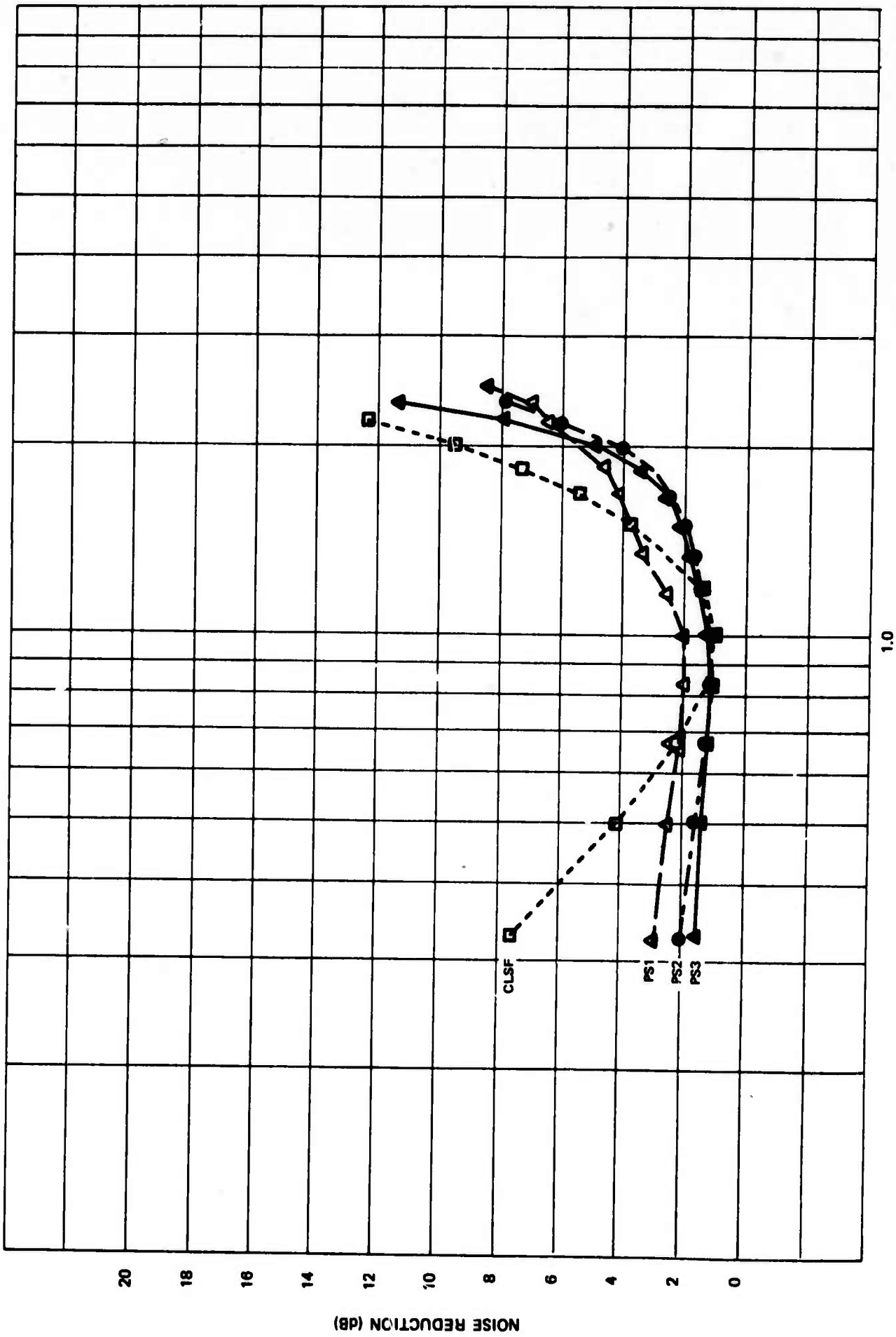

G 4473

Figure 4. Signal loss ratios for data sample 4

BLANK PAGE

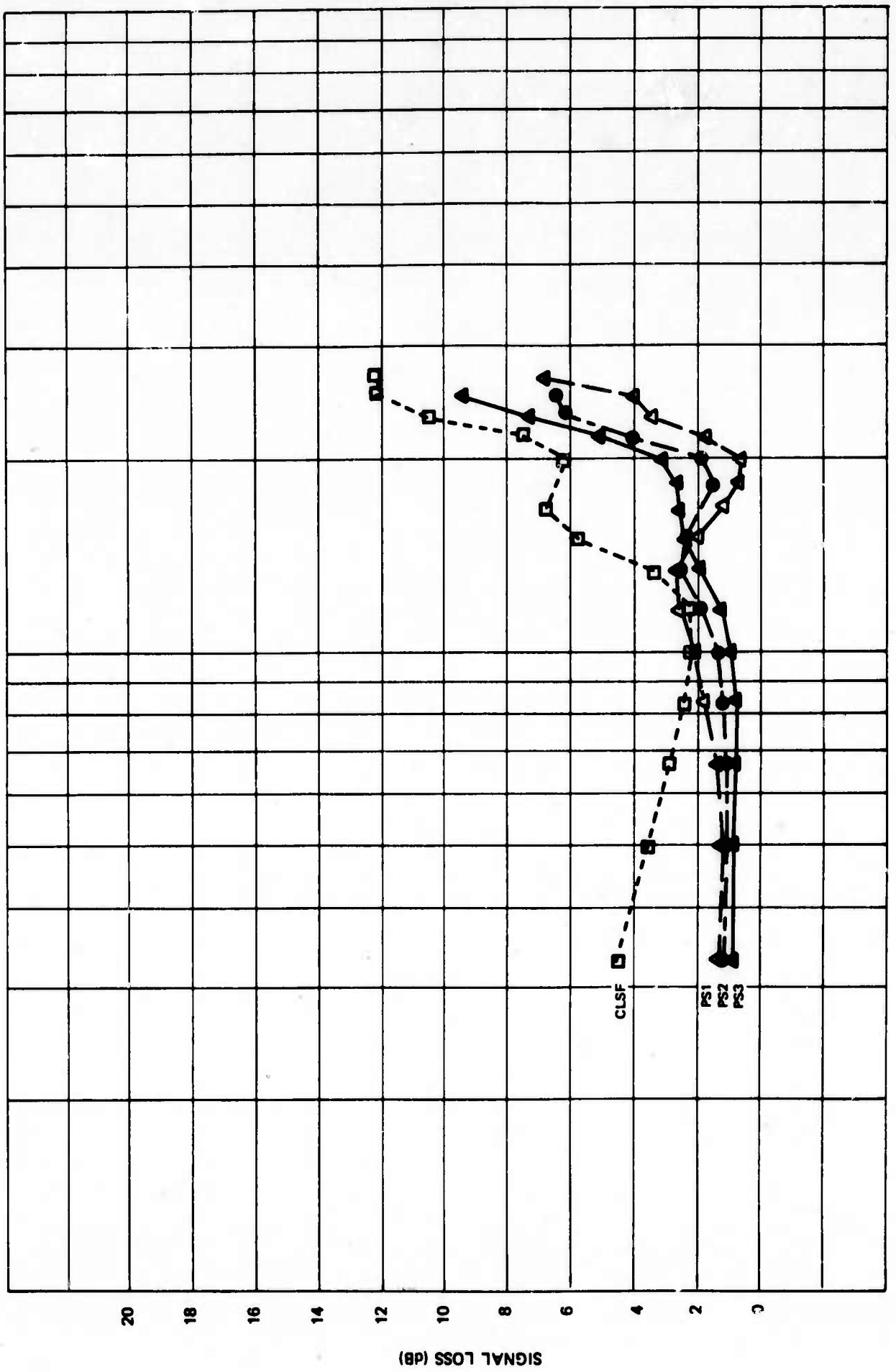

G 4474

Figure 5. Signal loss ratios for data sample 5

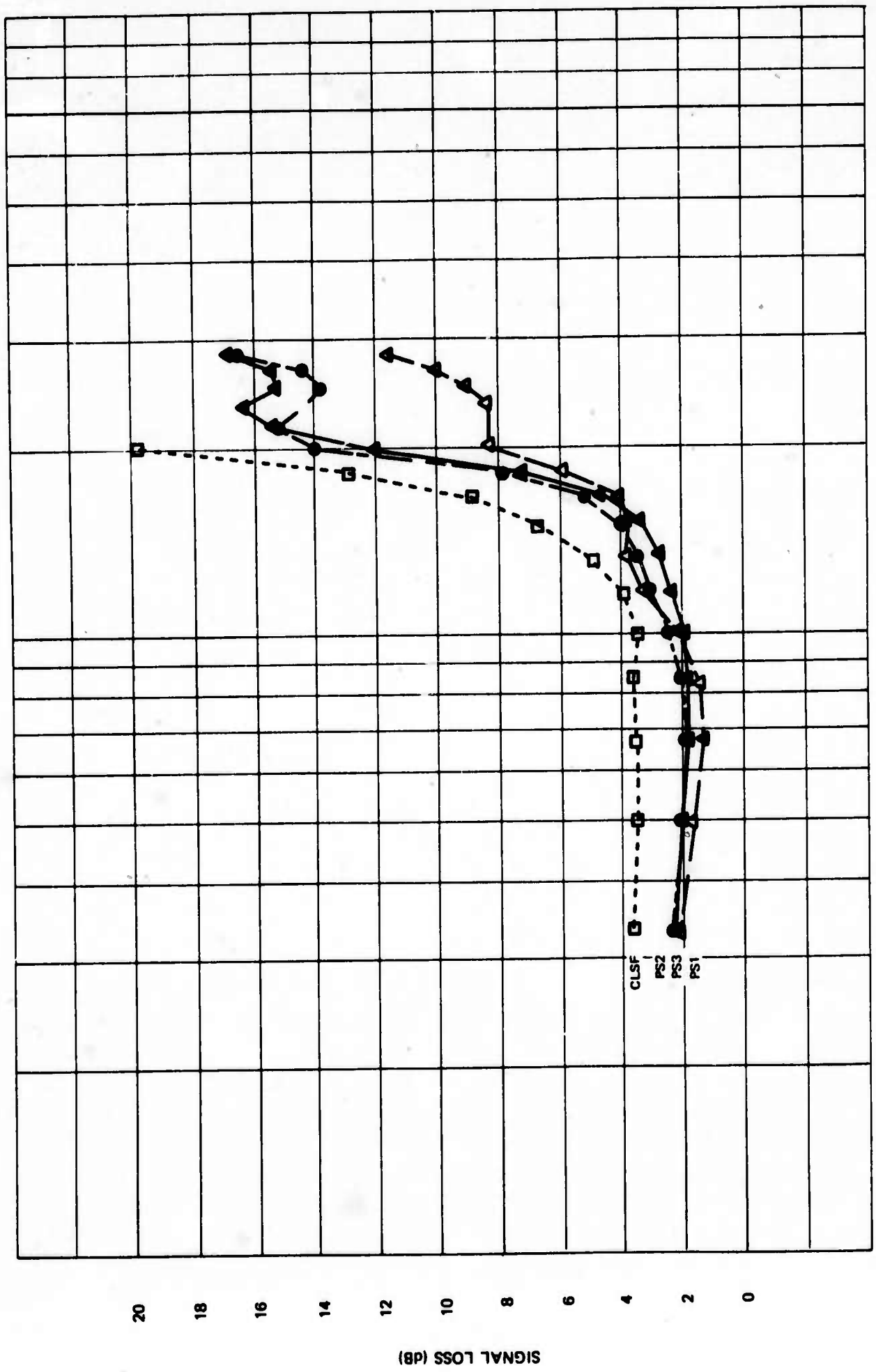

G 4475

Figure 6. Signal loss ratios for data sample 6

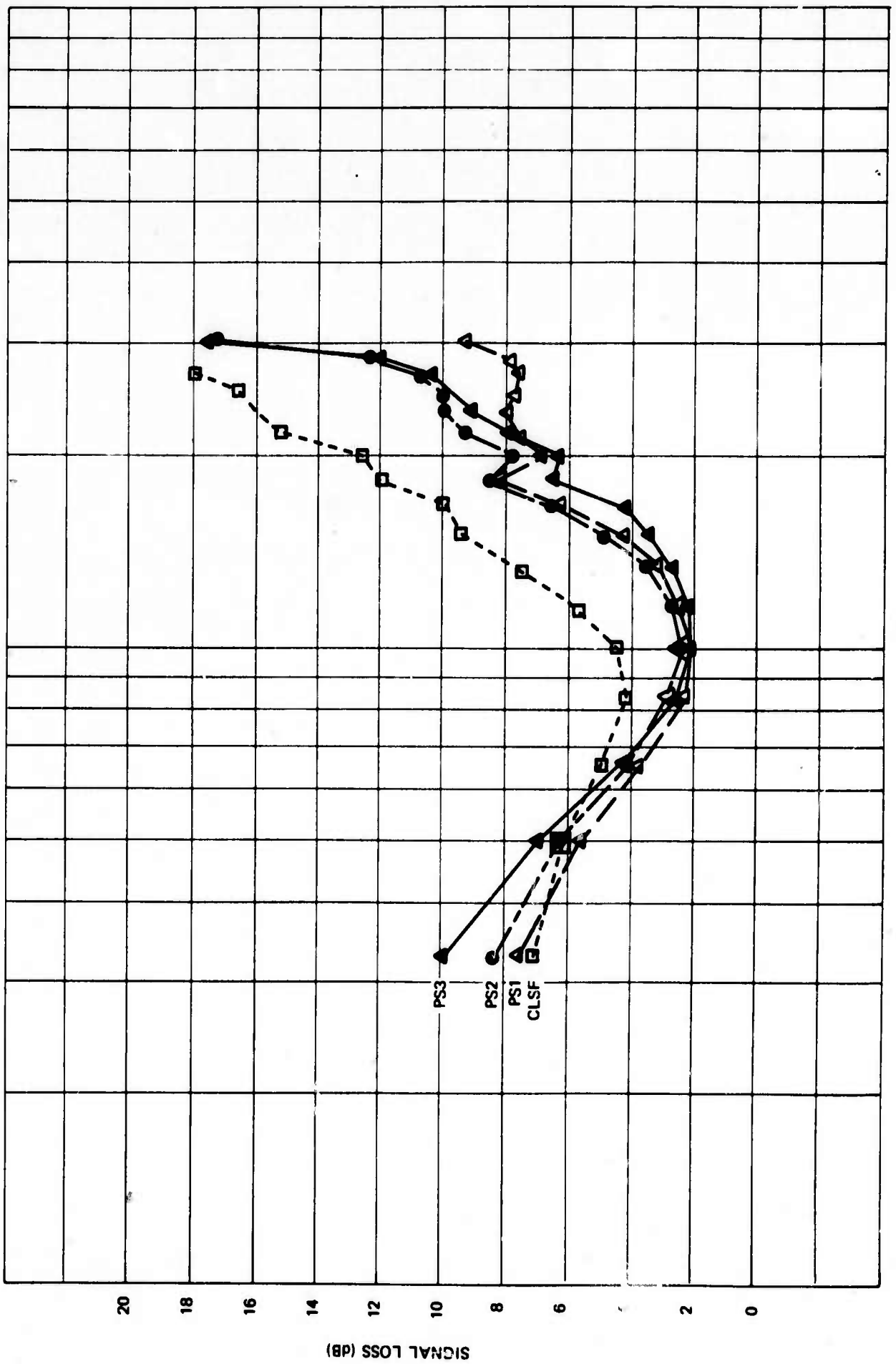

Figure 7. Signal loss ratios for data sample 7

G 4476

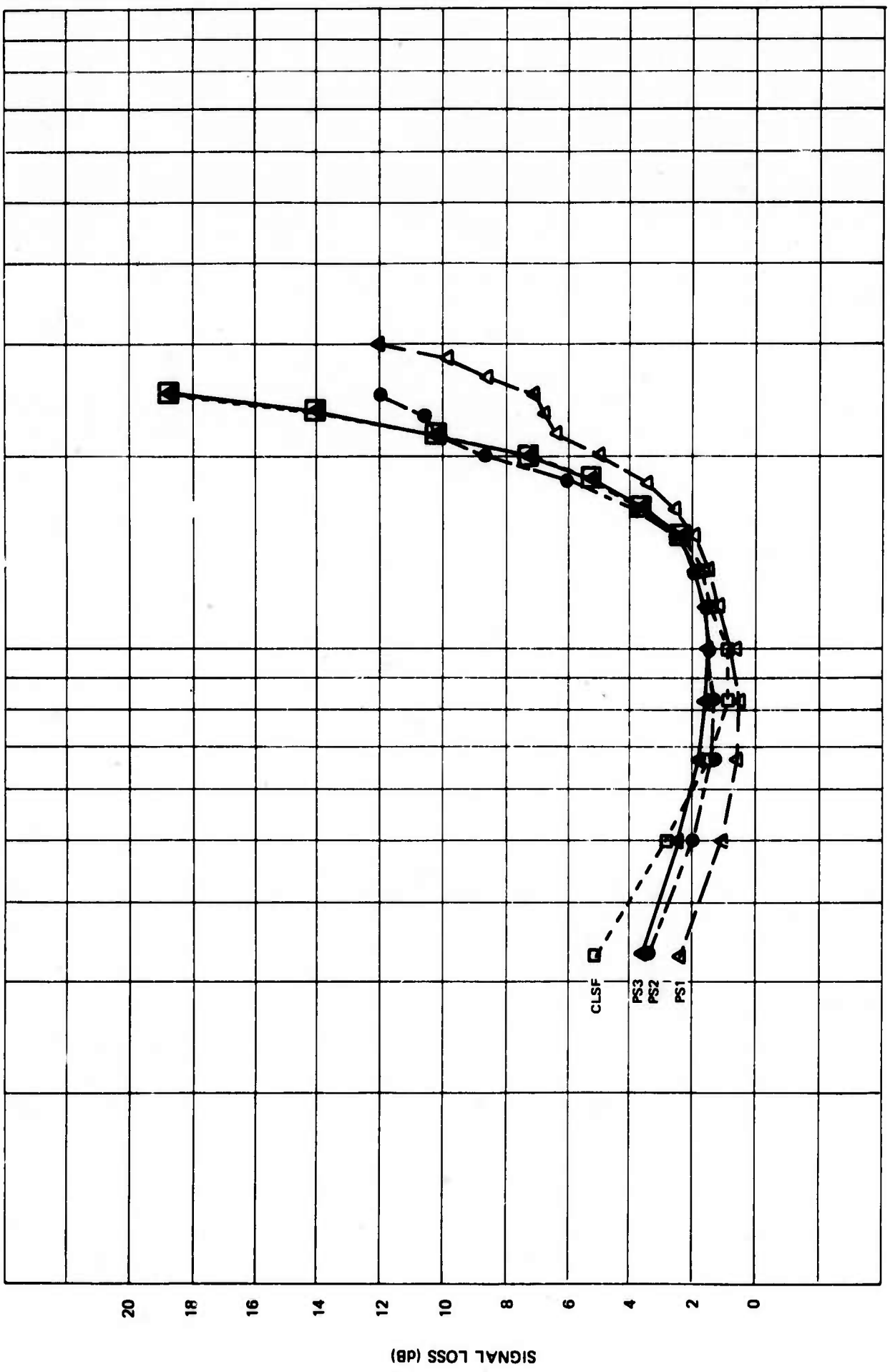

G 4477

Figure 8. Signal loss ratios for data sample 8

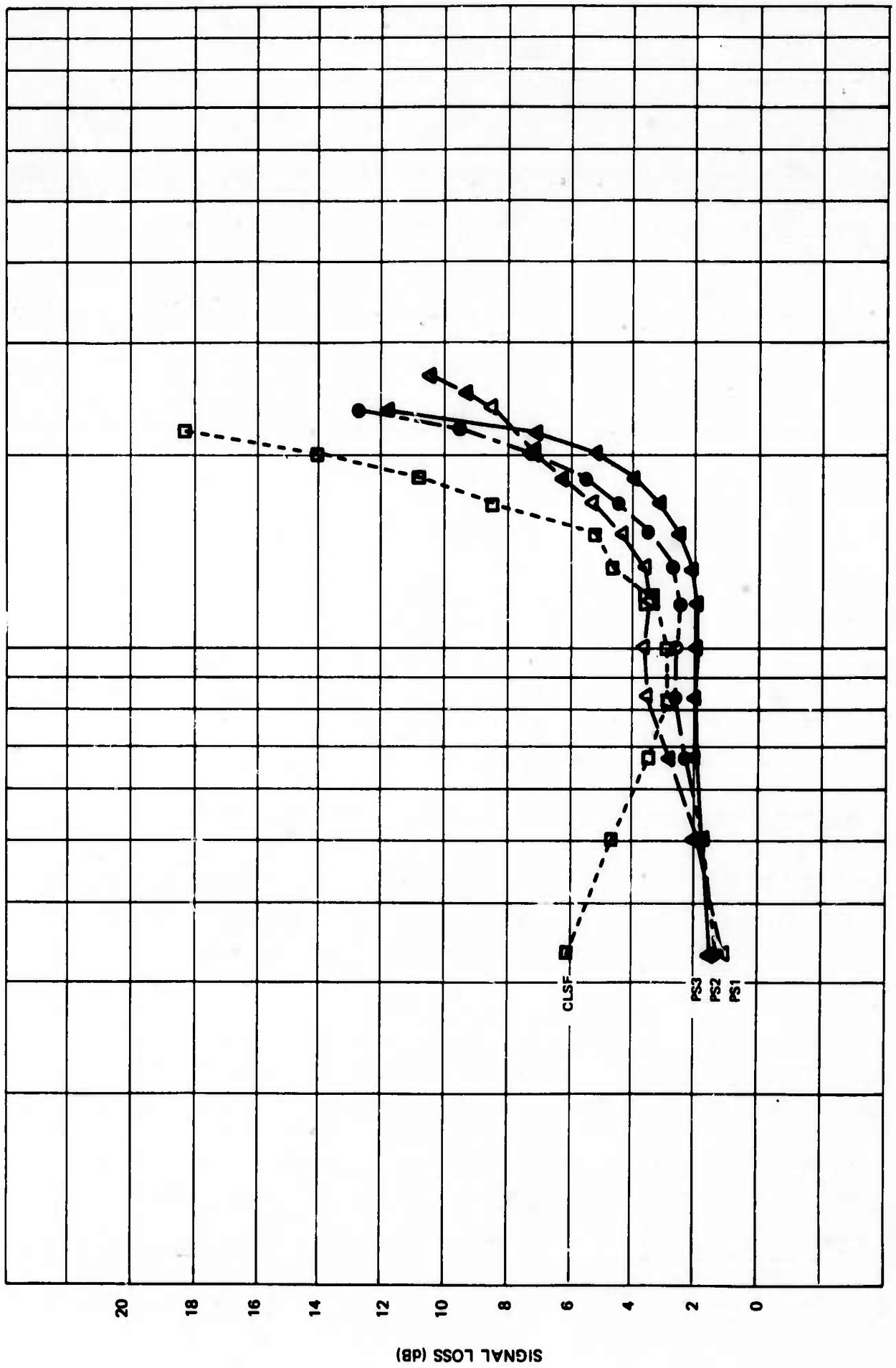

G 4478

Figure 9. Signal loss ratios for data sample 9

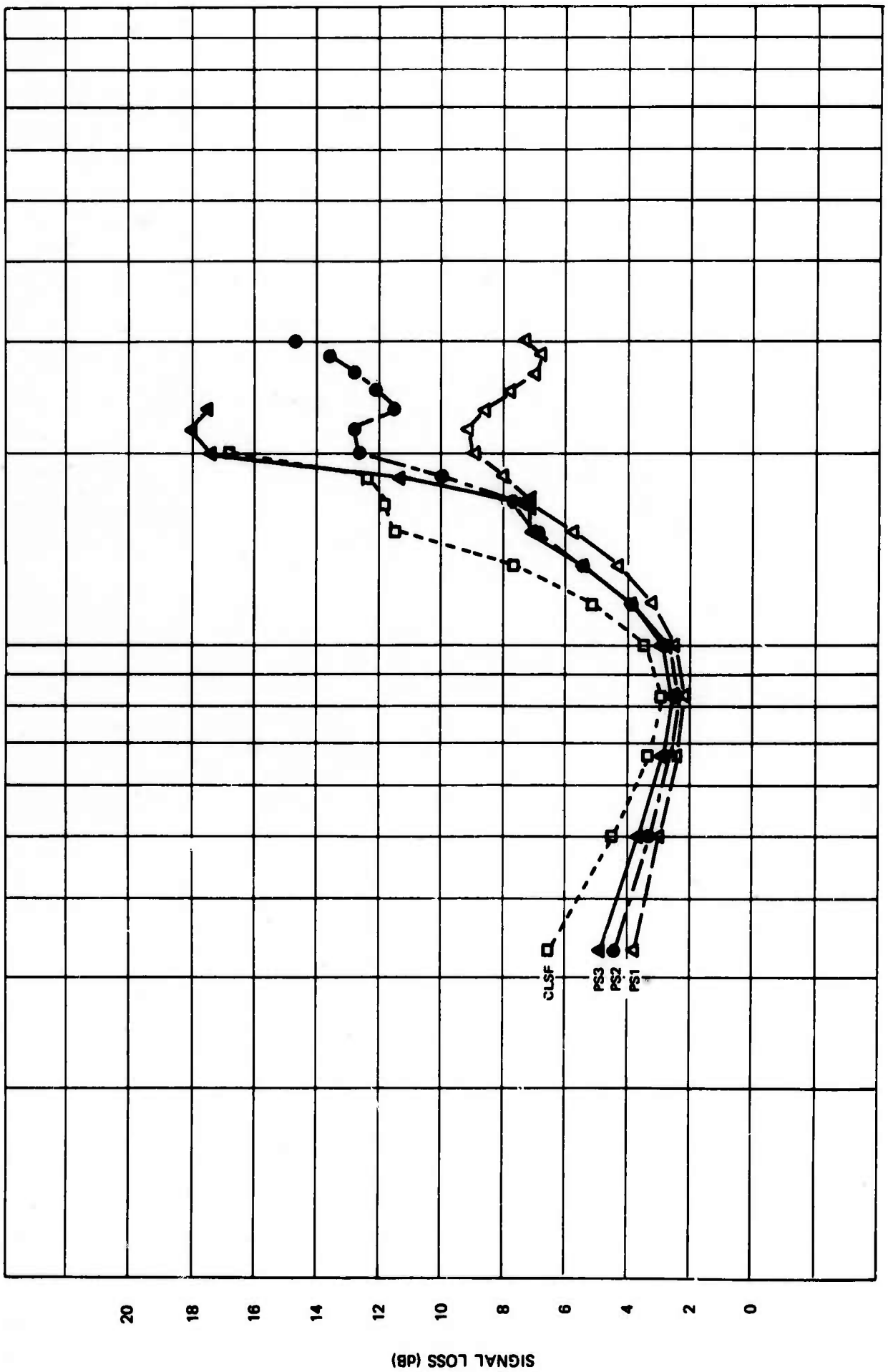

G 4479

Figure 10. Signal loss ratios for data sample 10

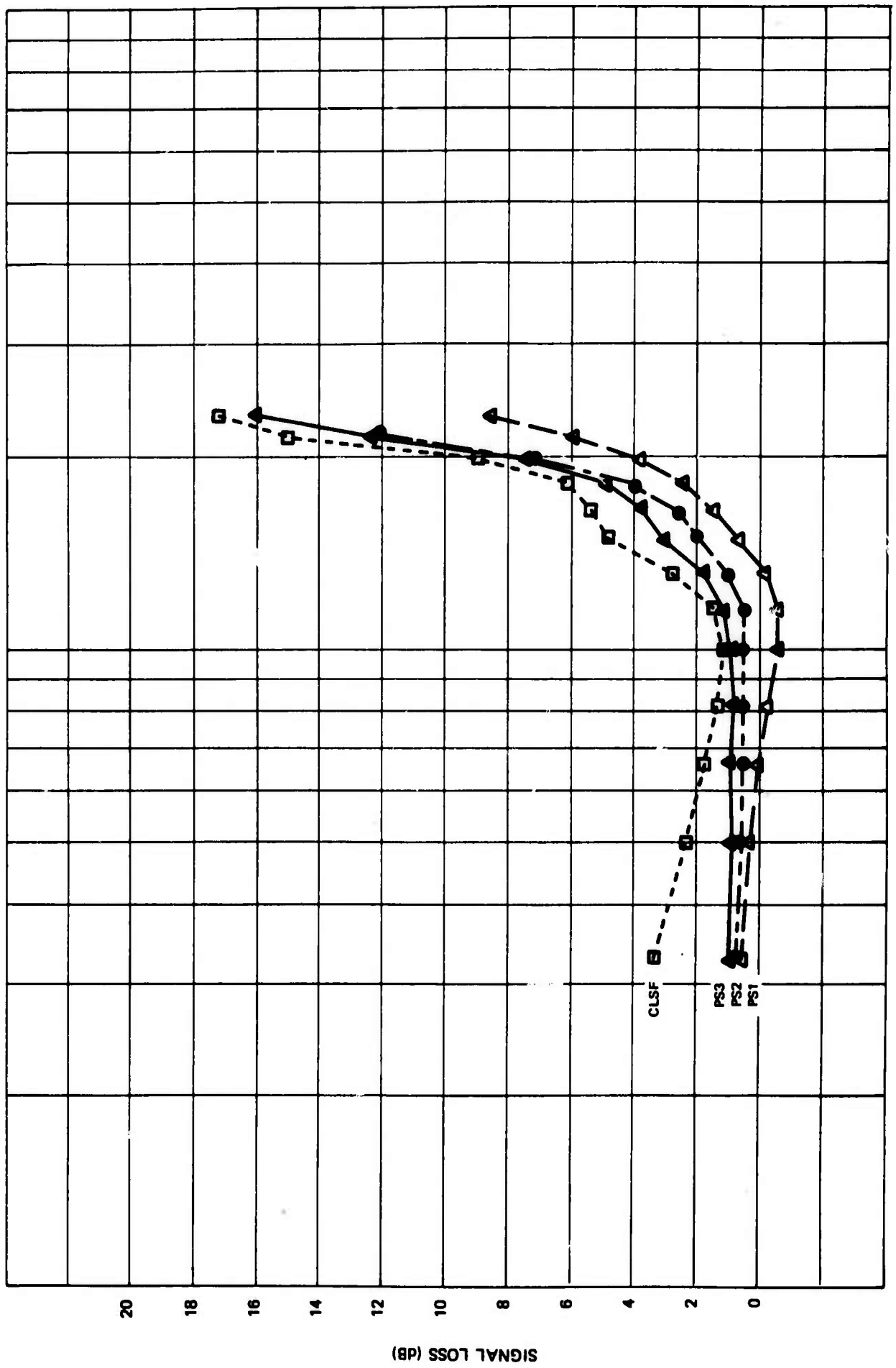

G 4480

Figure 11. Signal loss ratios for data sample 11

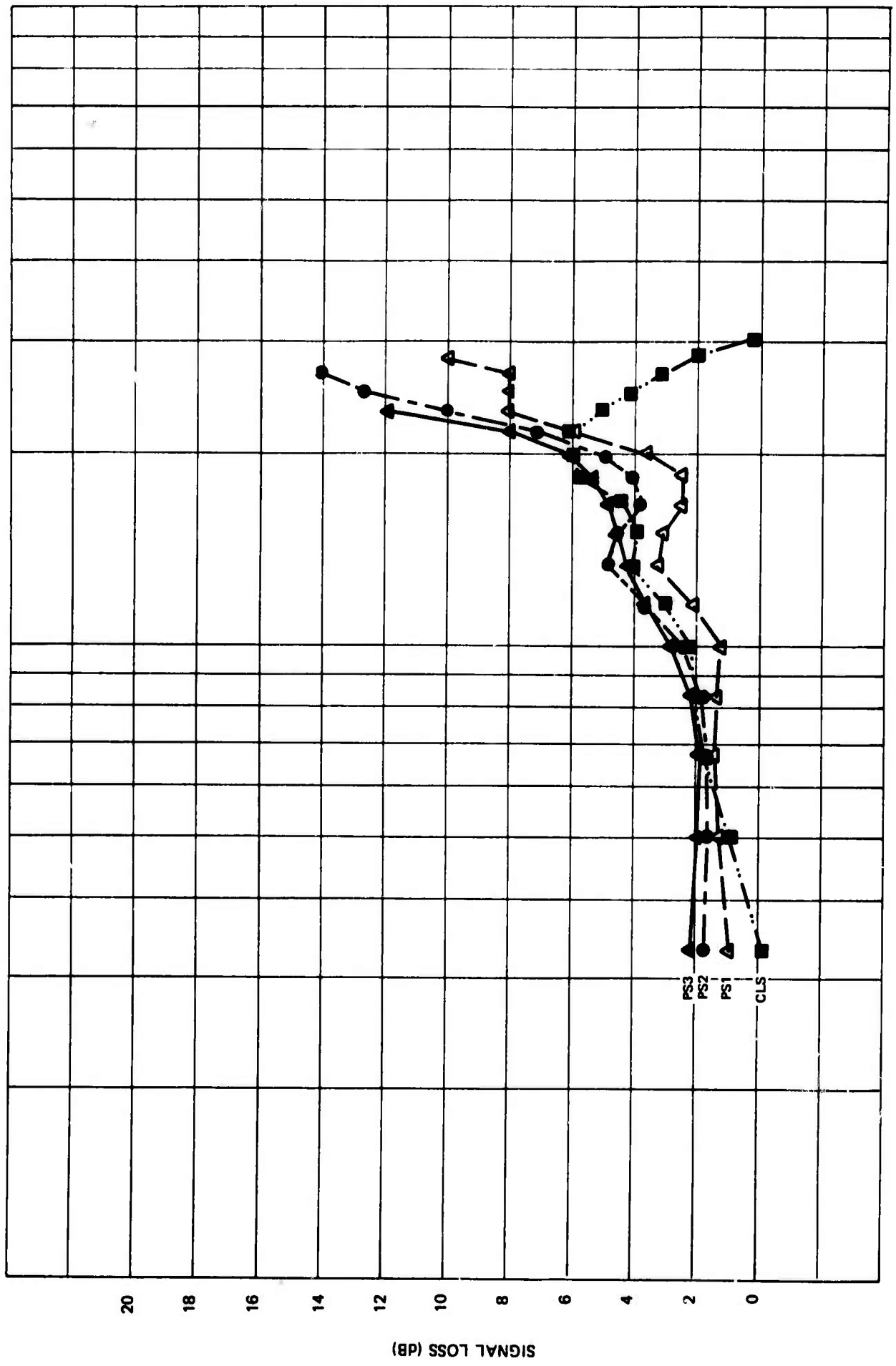

G 4481

Figure 12. Signal loss ratios for data sample 12

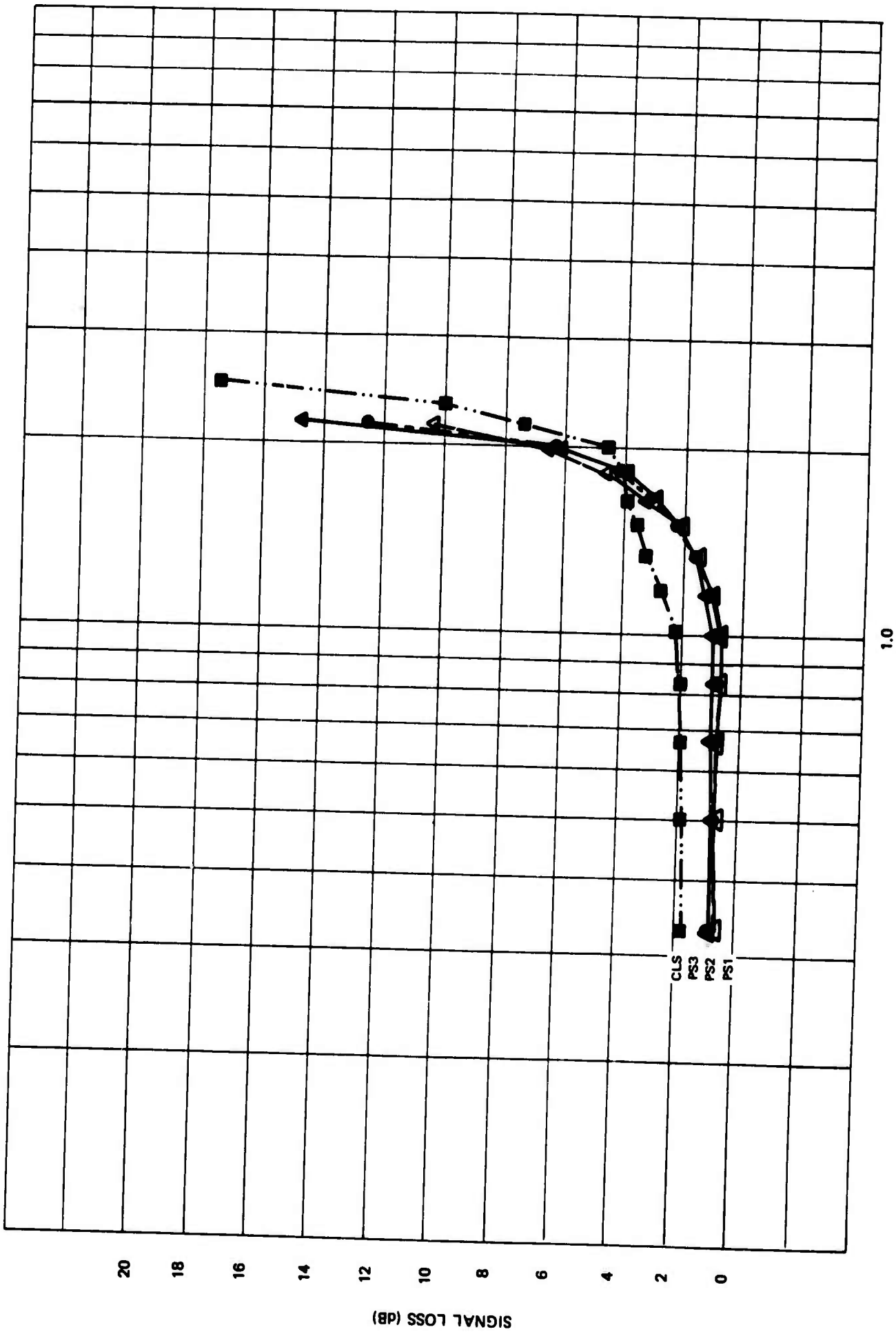

G 4482

Figure 13. Signal loss ratios for data sample 13

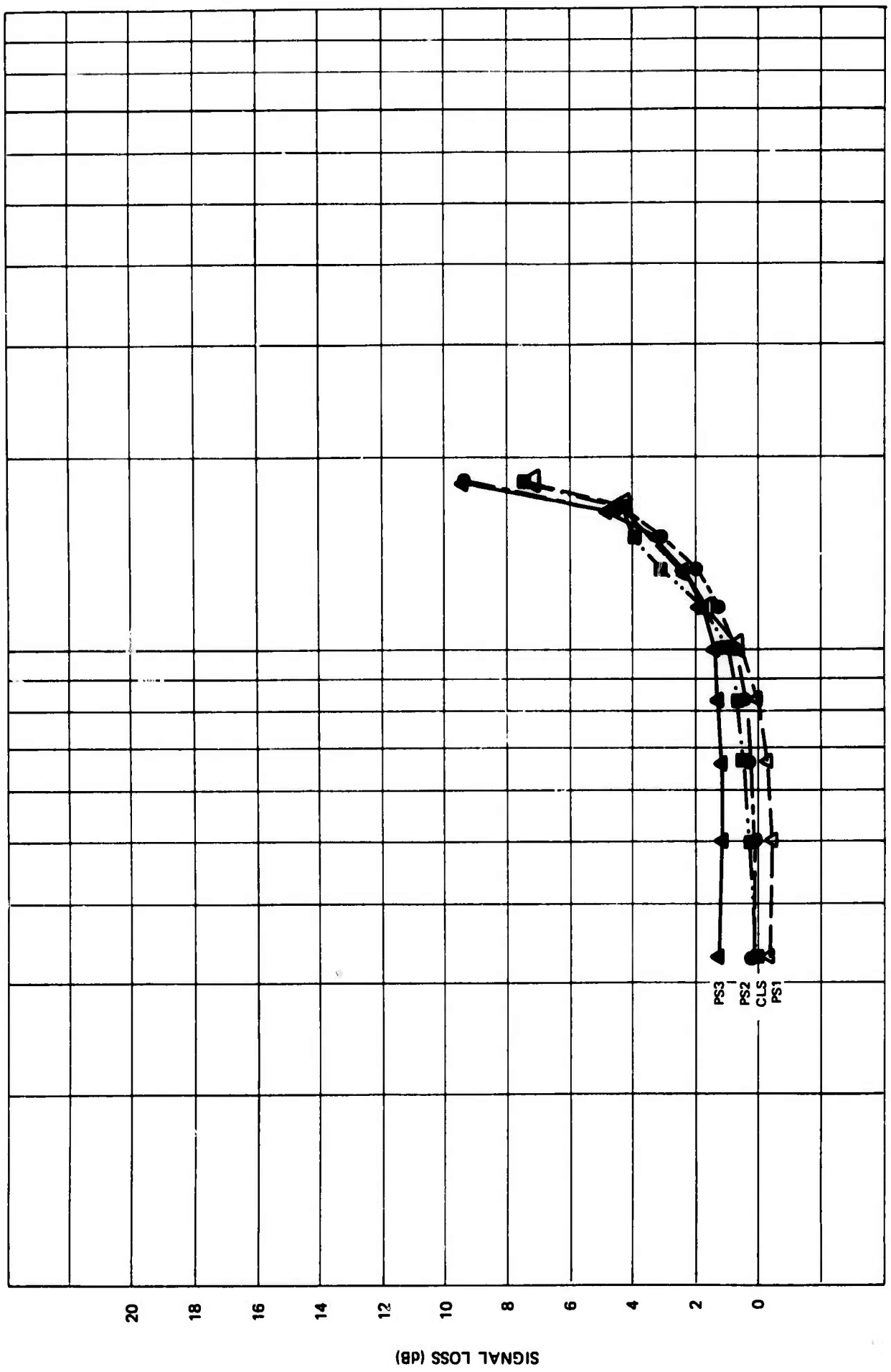

G 4483

Figure 14. Signal loss ratios for data sample 14

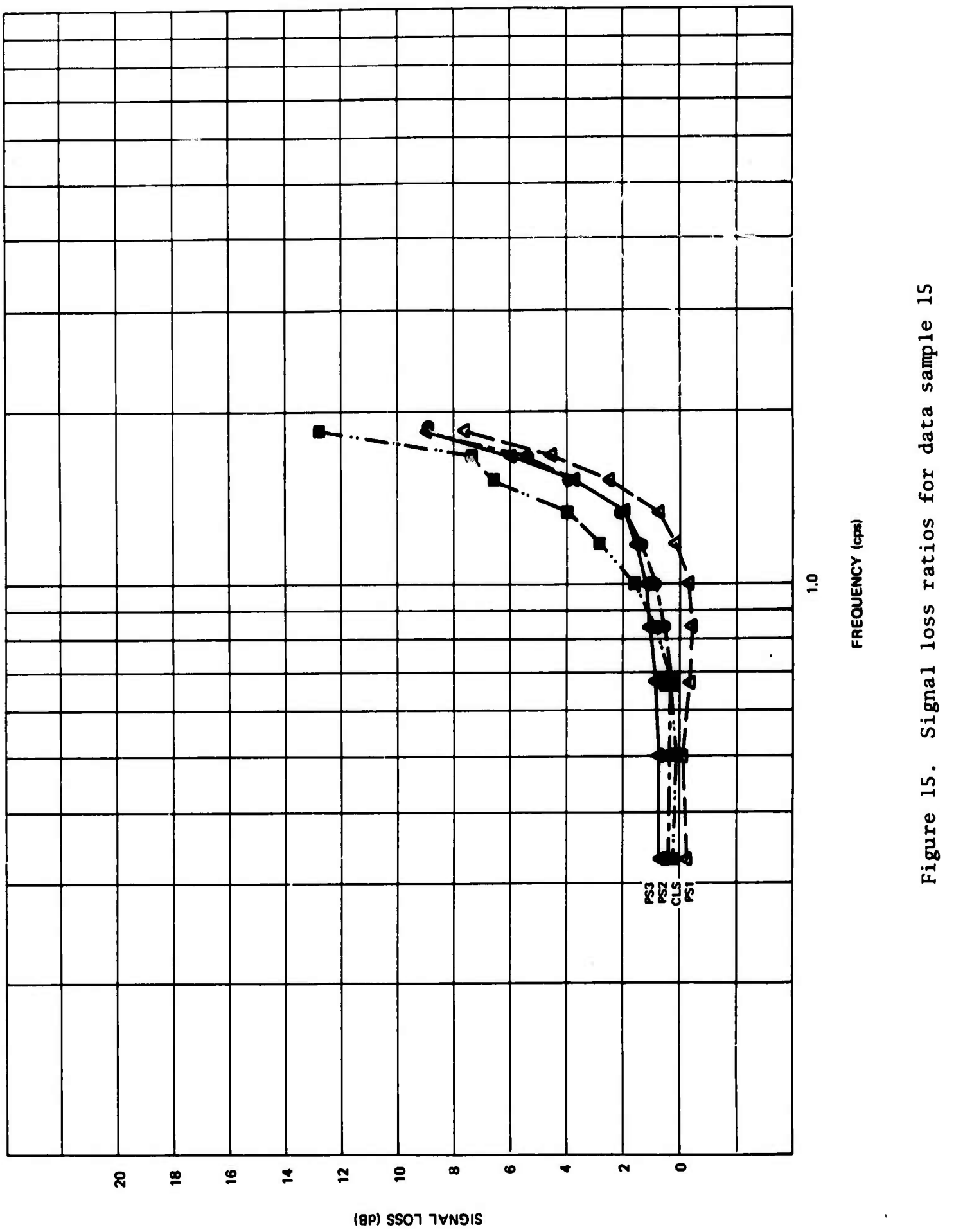

G 4484

Figure 15. Signal loss ratios for data sample 15

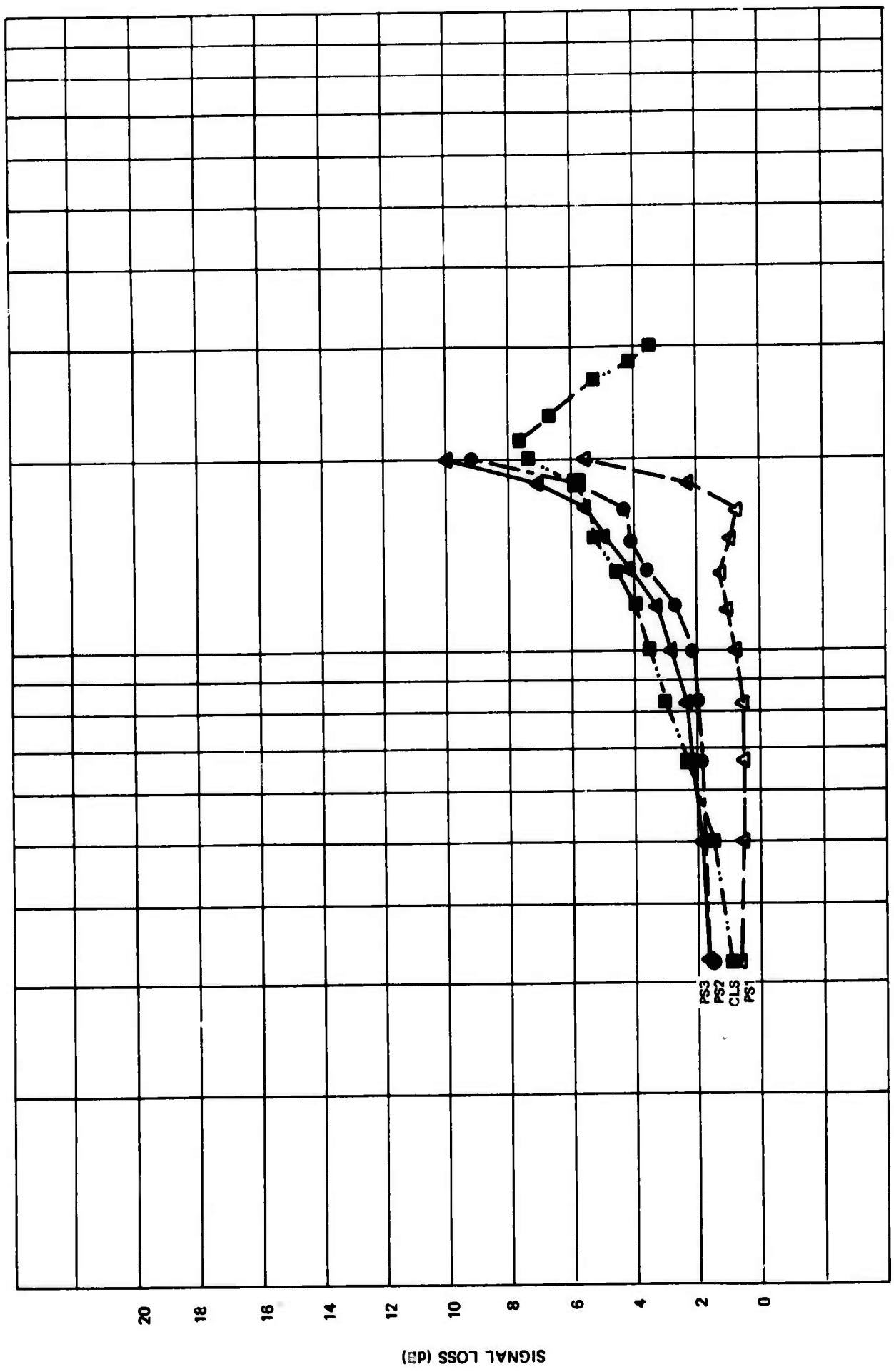

G 4485

Figure 16. Signal loss ratios for data sample 16

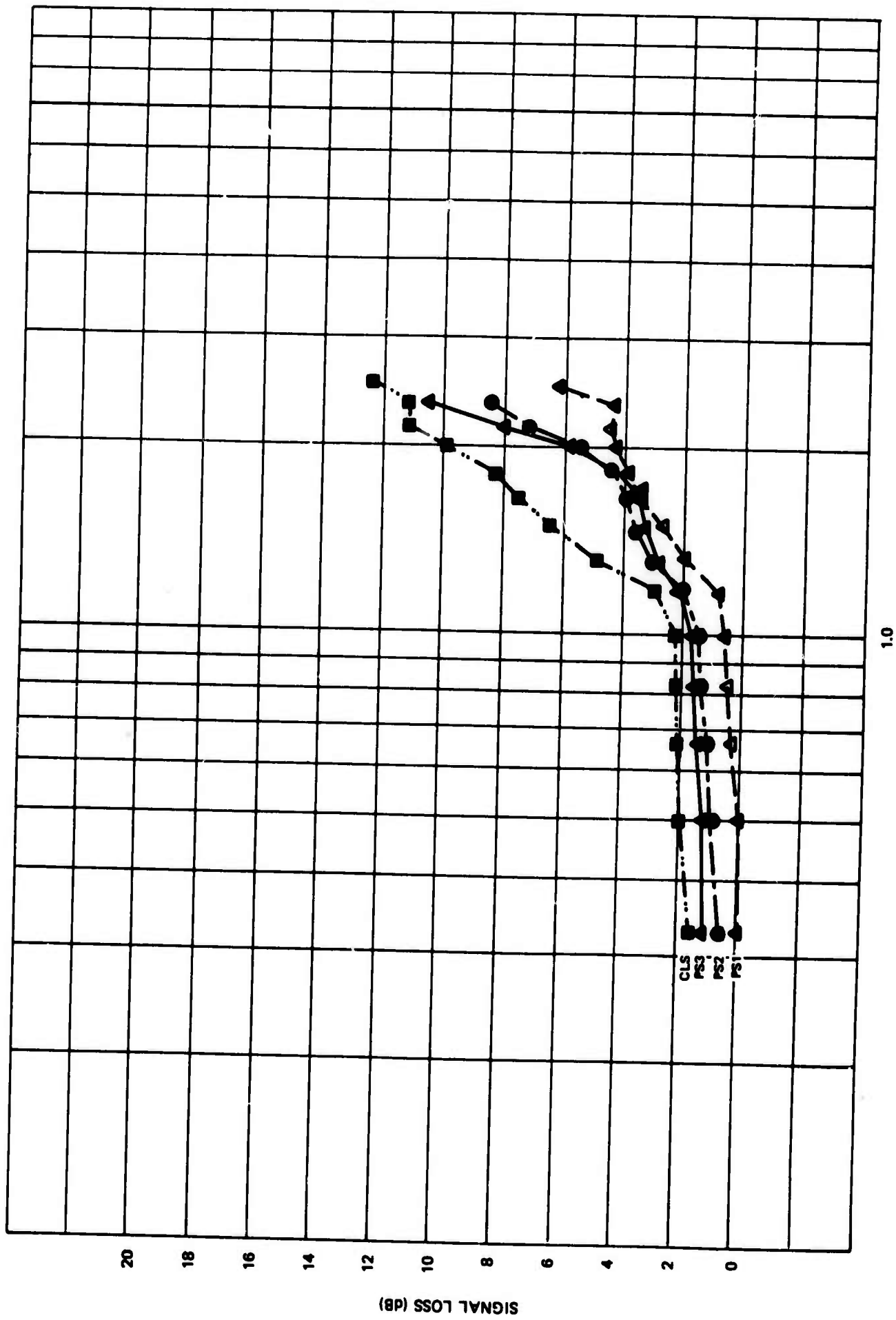

G 4486

Figure 17. Signal loss ratios for data sample 17

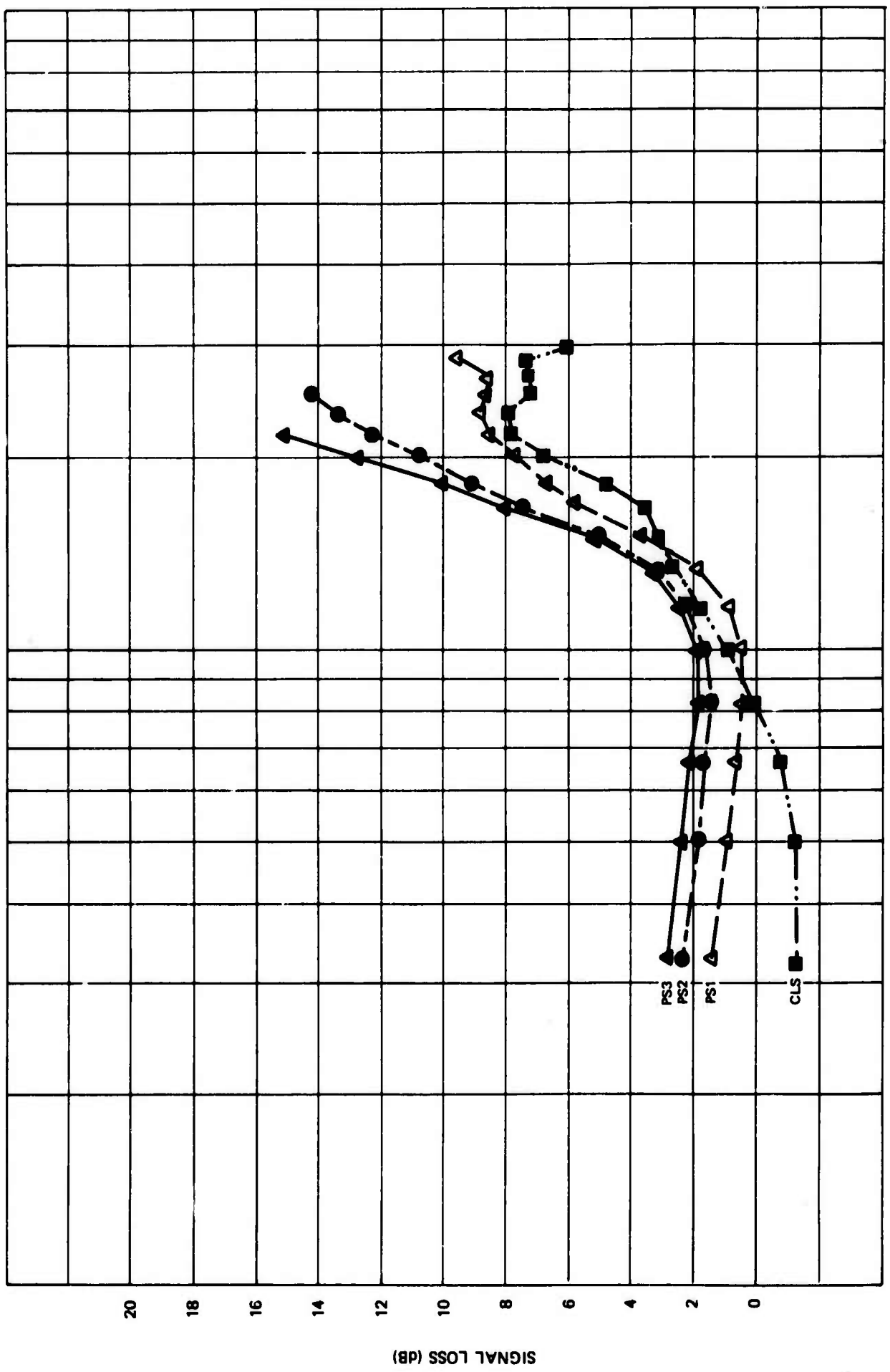

Figure 18. Signal loss ratios for data sample 18

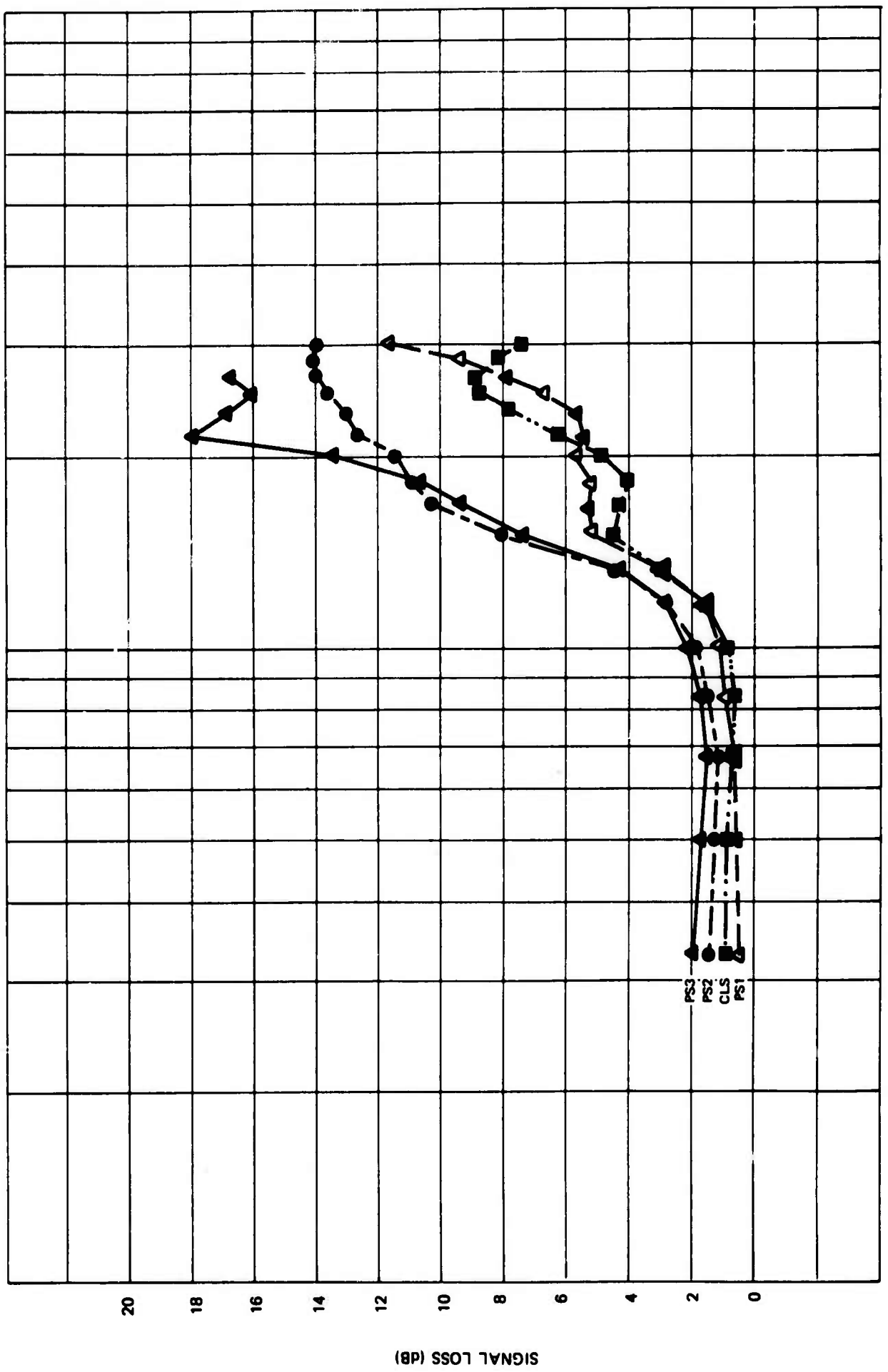

G 4488

Figure 19. Signal loss ratios for data sample 19

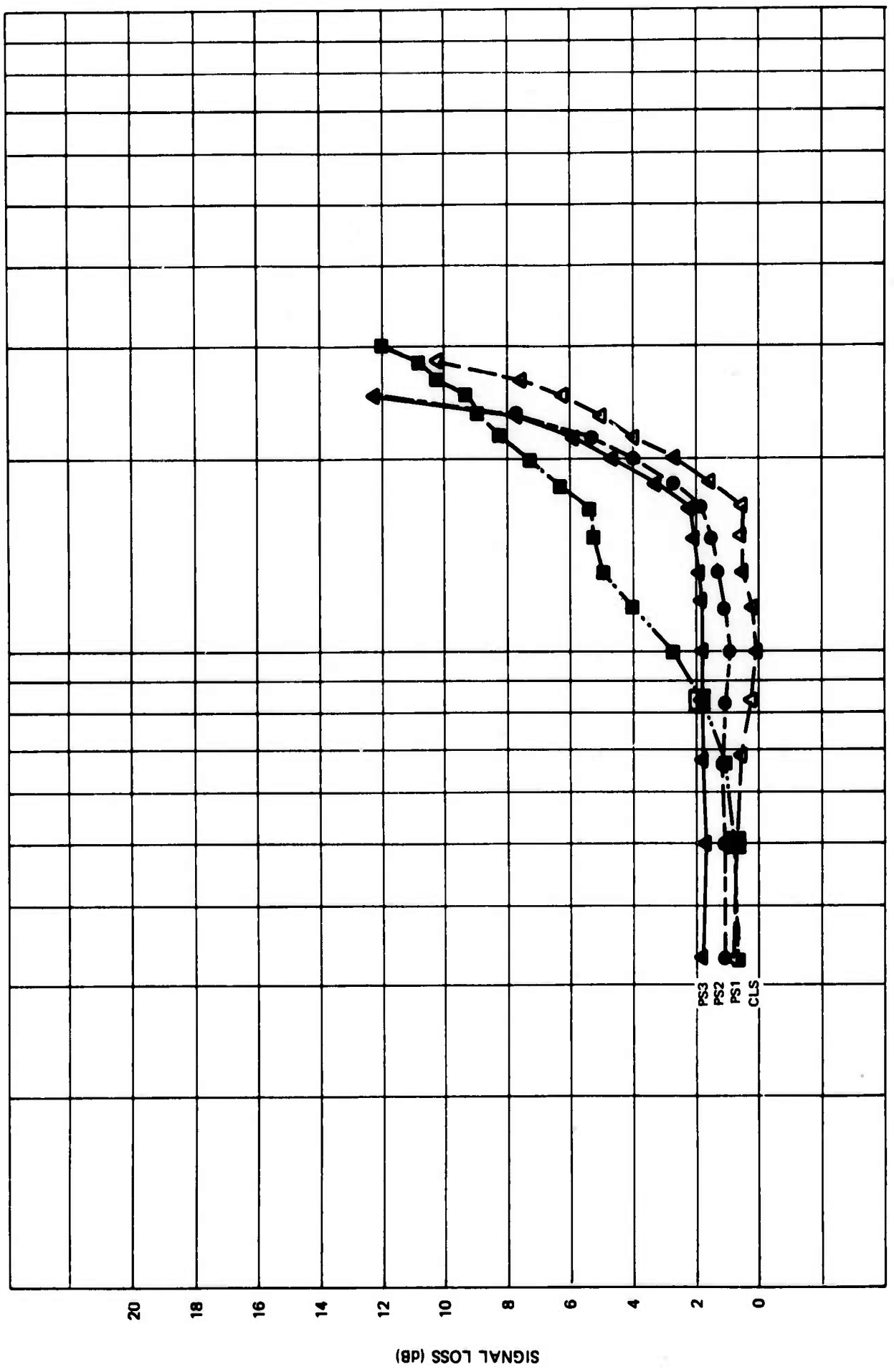

G 4489

Figure 20. Signal loss ratios for data sample 20

APPENDIX 3 to TECHNICAL REPORT NO. 68-47

SIGNAL-TO-NOISE RATIOS FOR EACH DATA SAMPLE

BLANK PAGE

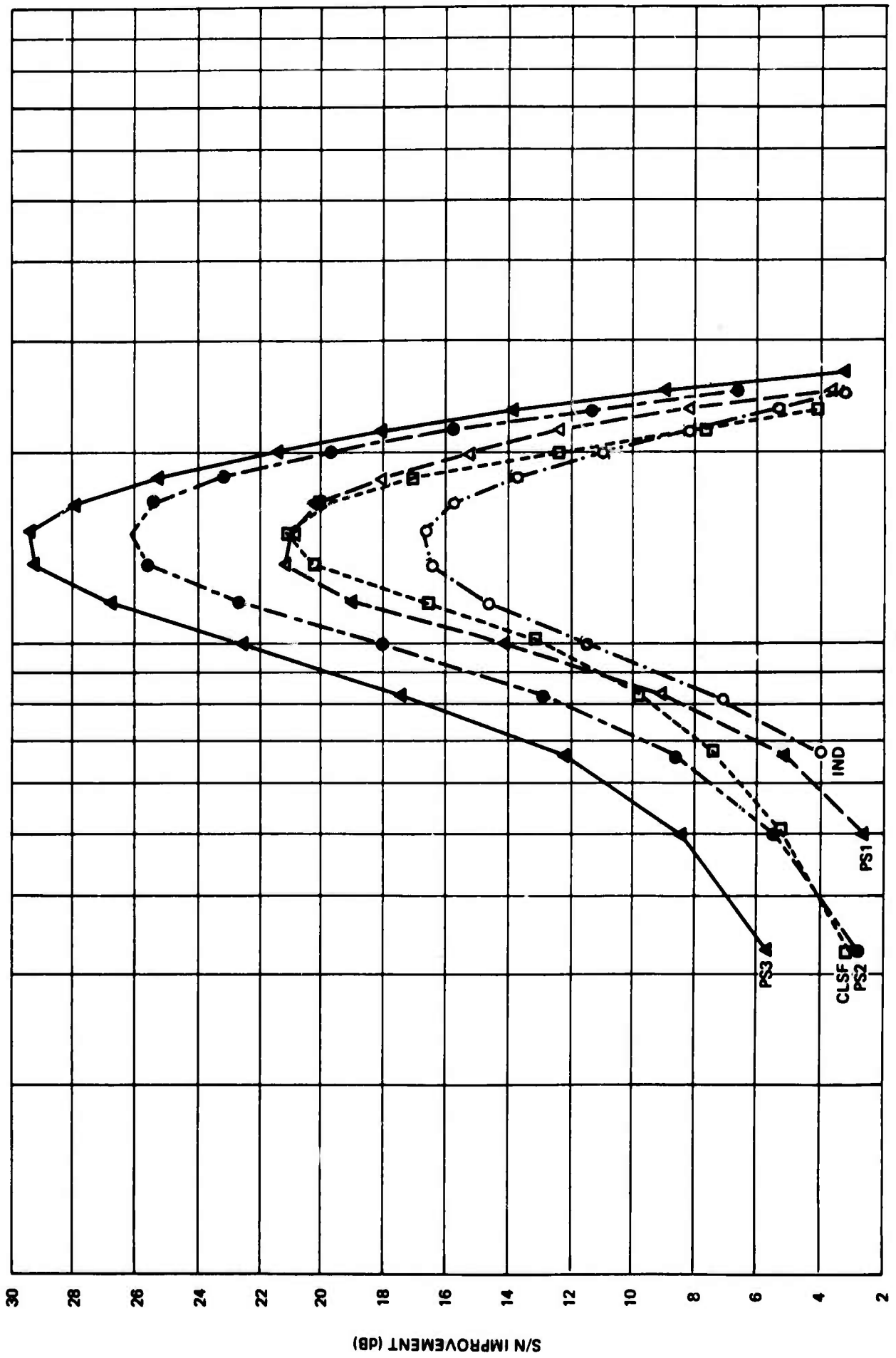

G 4490

Figure 1. Signal-to-noise ratios for data sample 1

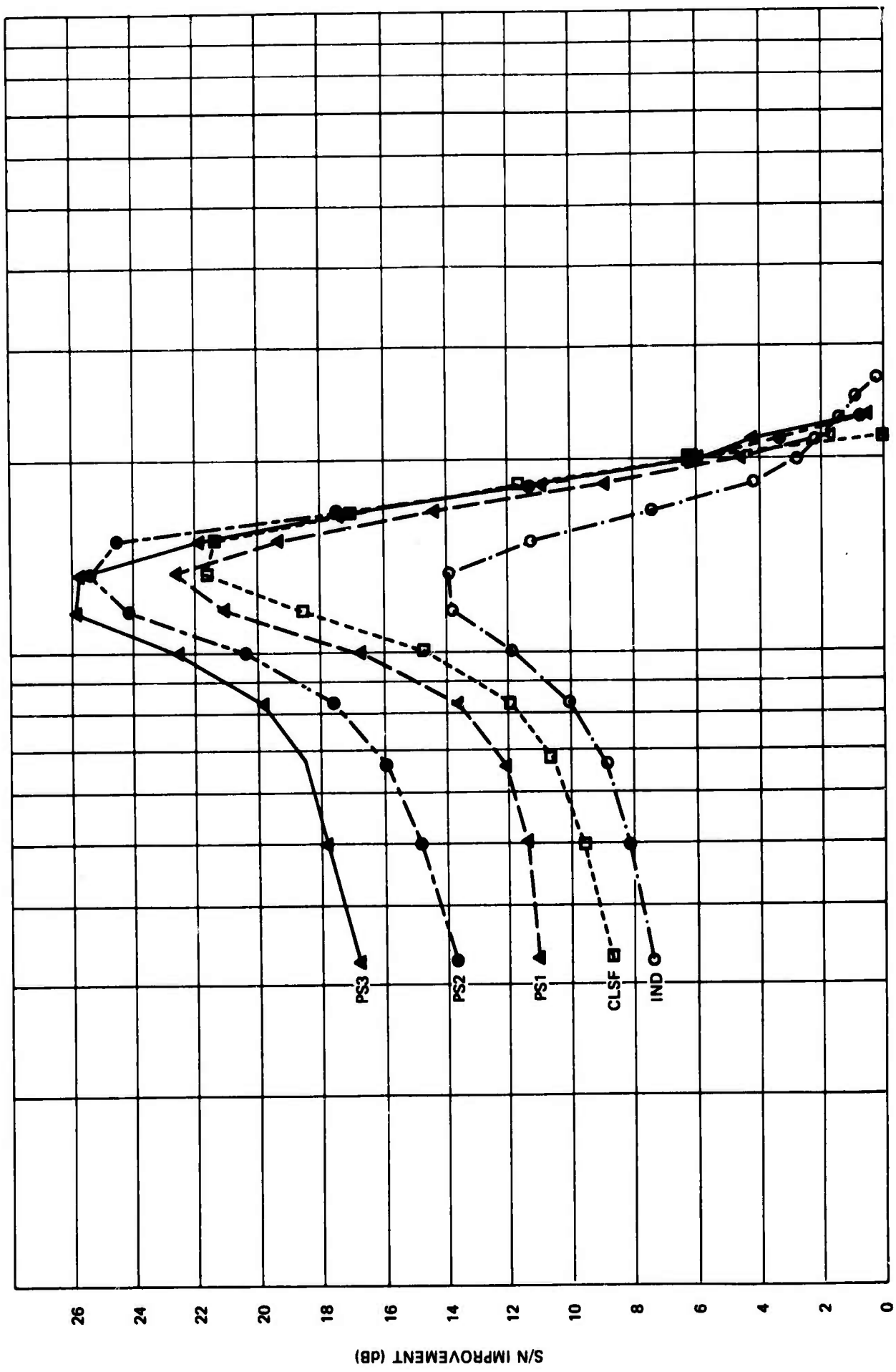

G 4491

Figure 2. Signal-to-noise ratios for data sample 2

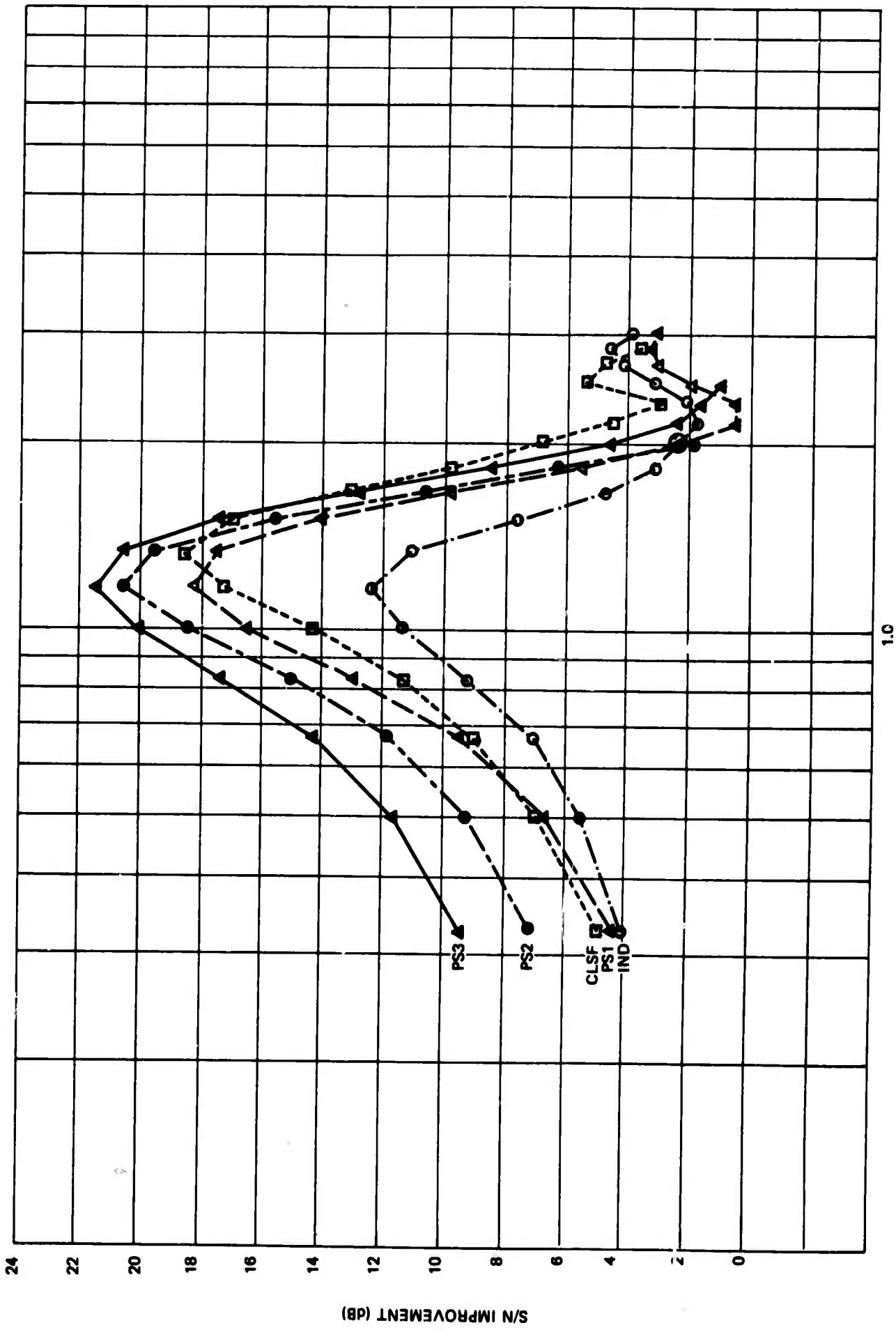

G 4492

Figure 3. Signal-to-noise ratios for data sample 3

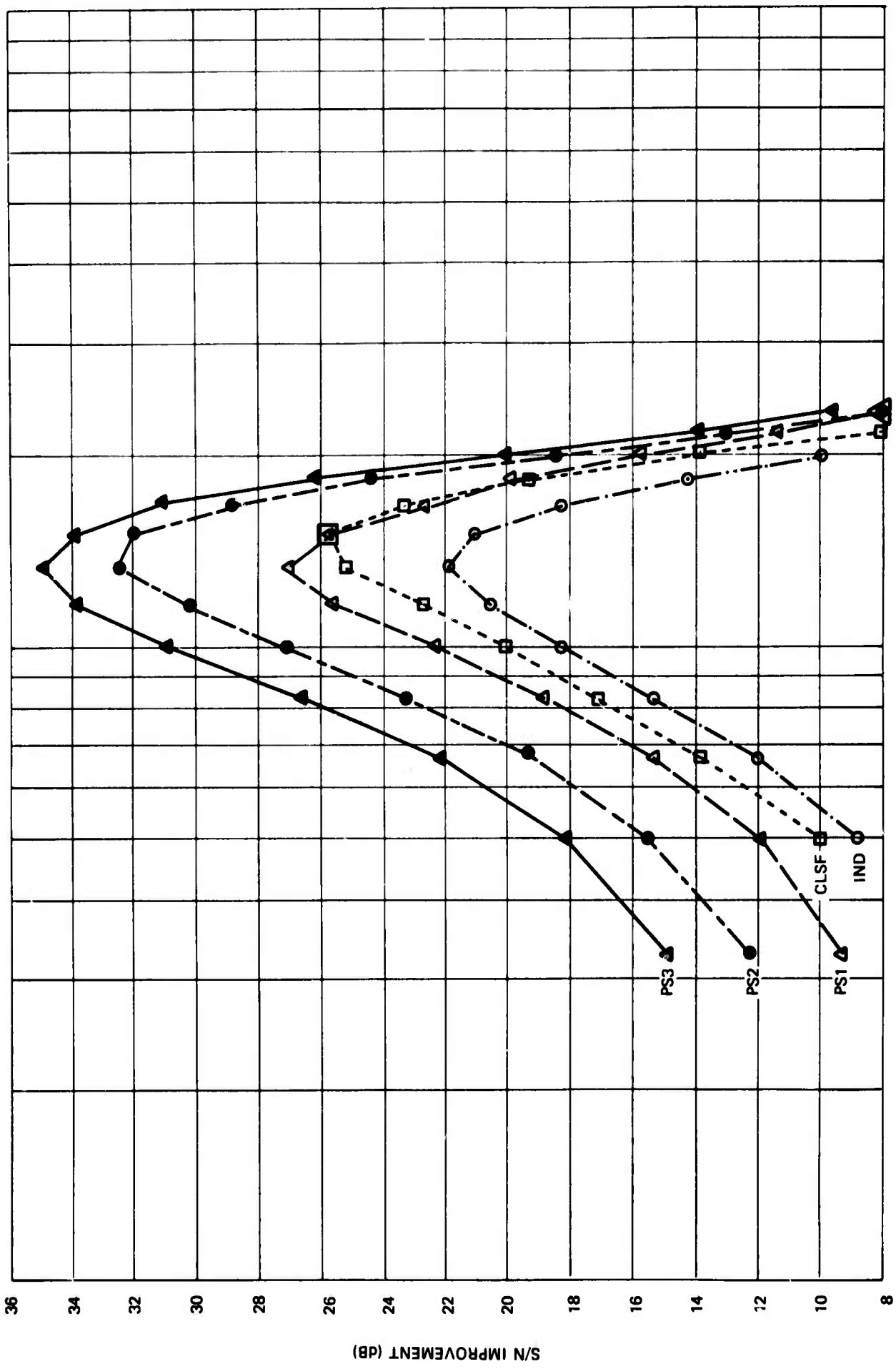

G 4493

Figure 4. Signal-to-noise ratios for data sample 4

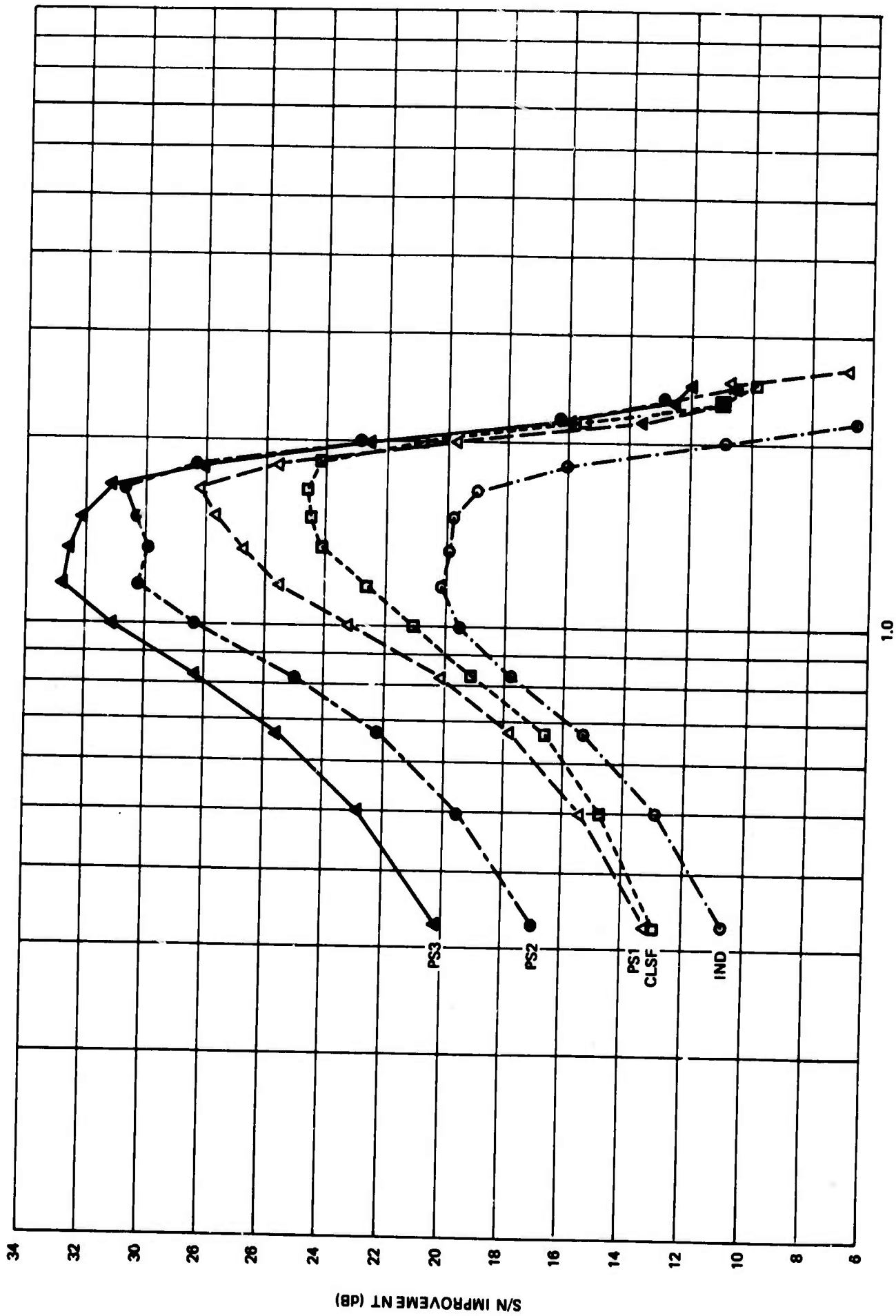

G 4494

Figure 5. Signal-to-noise ratios for data sample 5

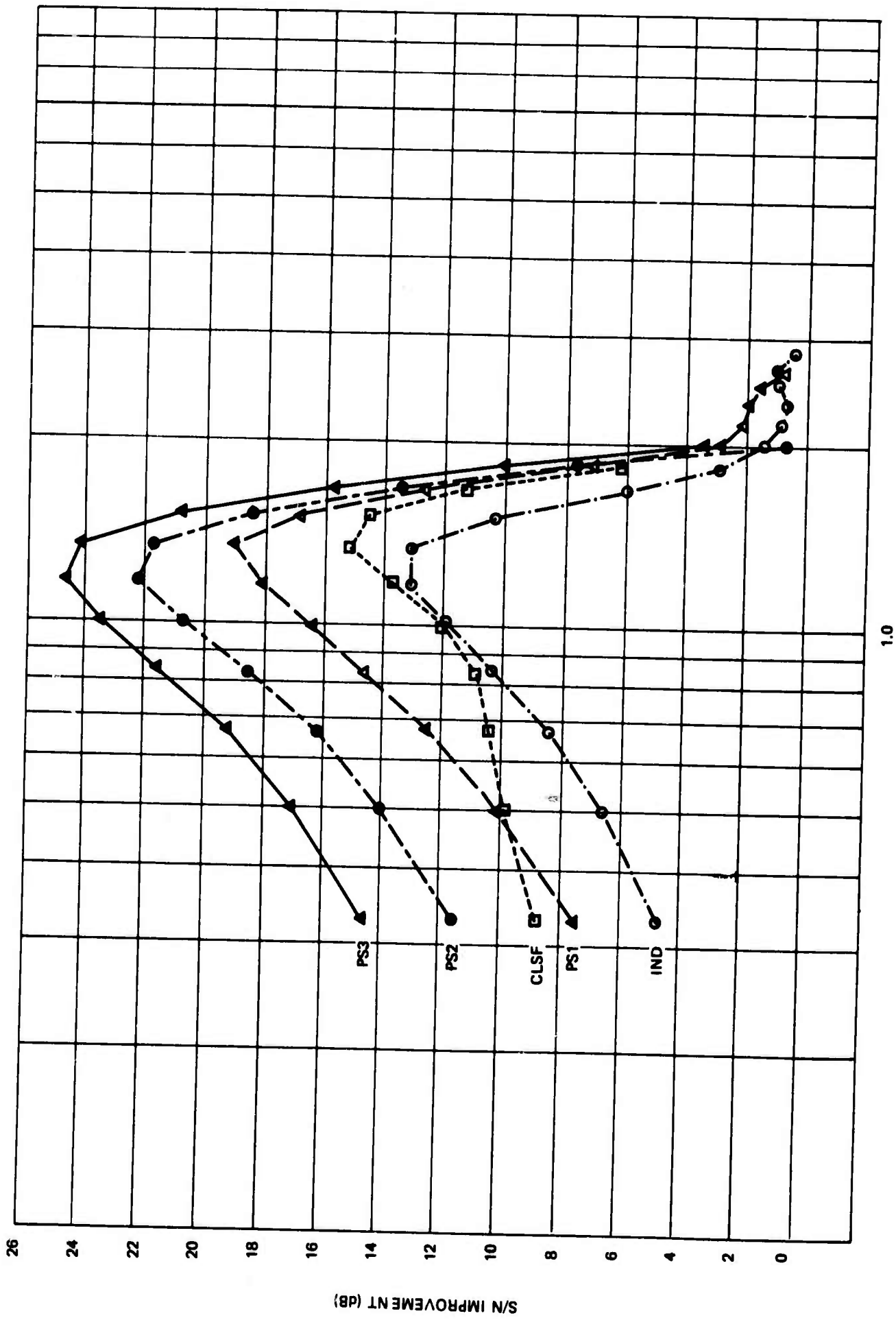

G 4495

Figure 6. Signal-to-noise ratios for data sample 6

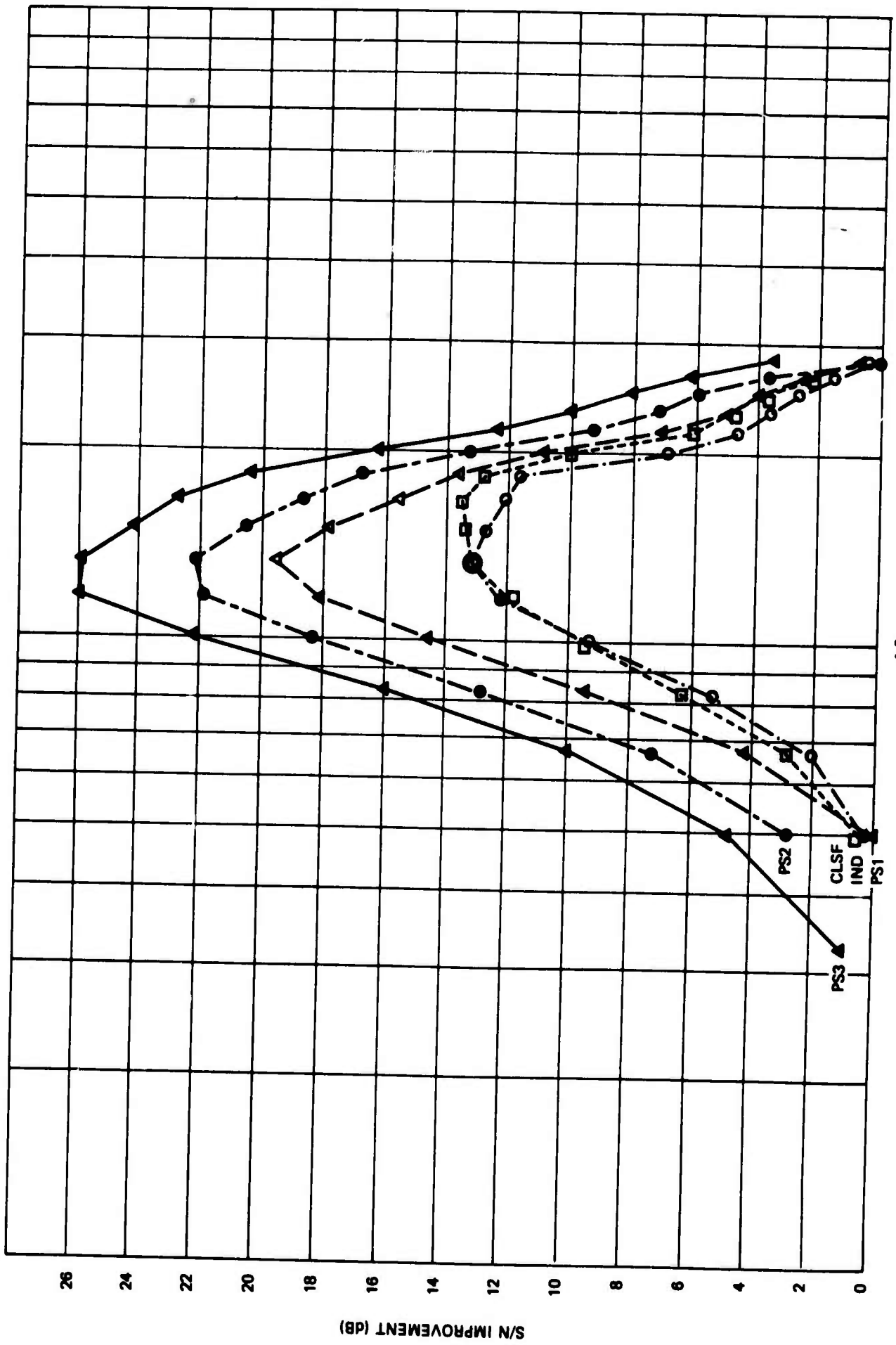

G 4496

Figure 7. Signal-to-noise ratios for data sample 7

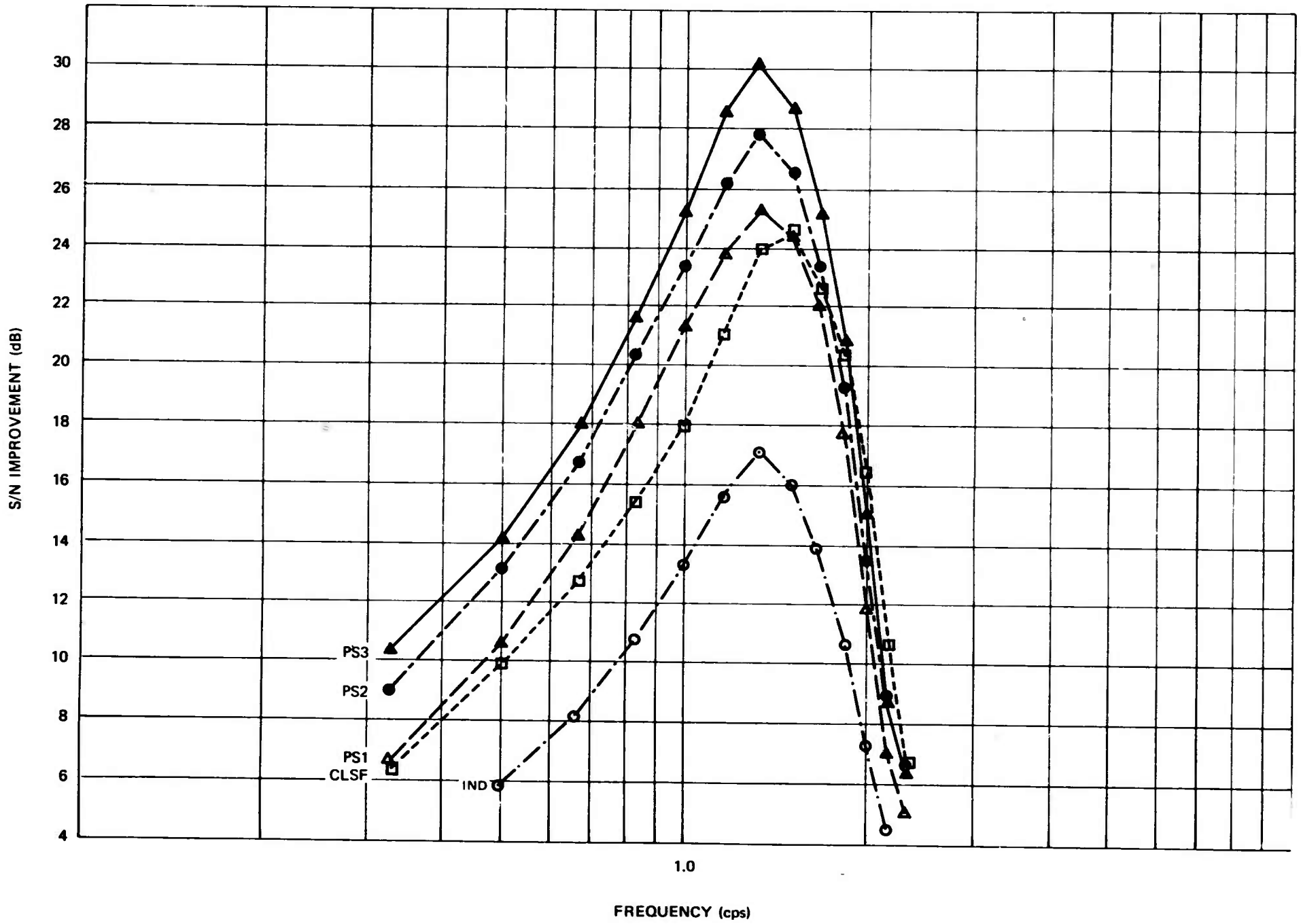

Figure 8. Signal-to-noise ratios for data sample 8

G 4497

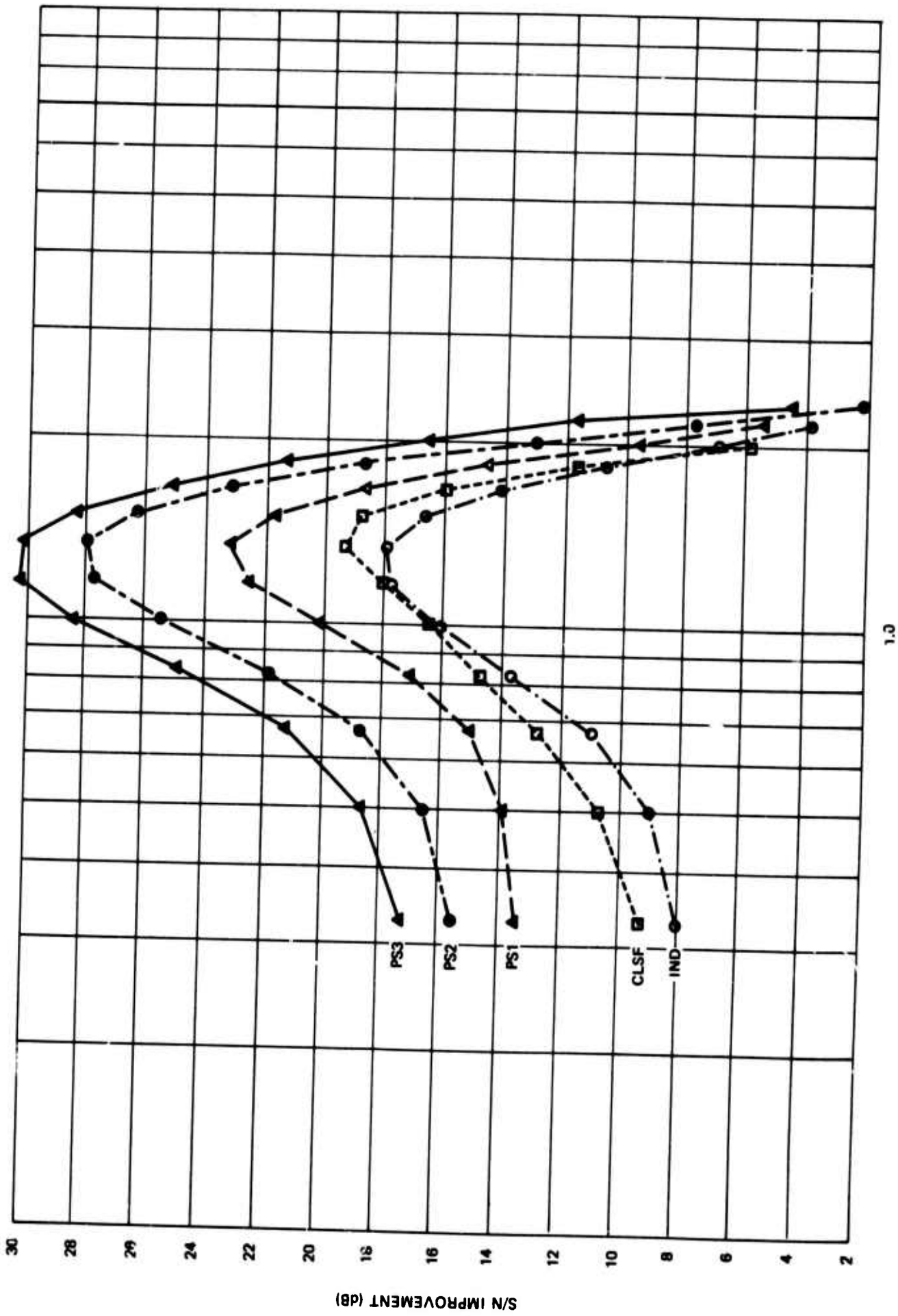

G 4498

Figure 9. Signal-to-noise ratios for data sample 9

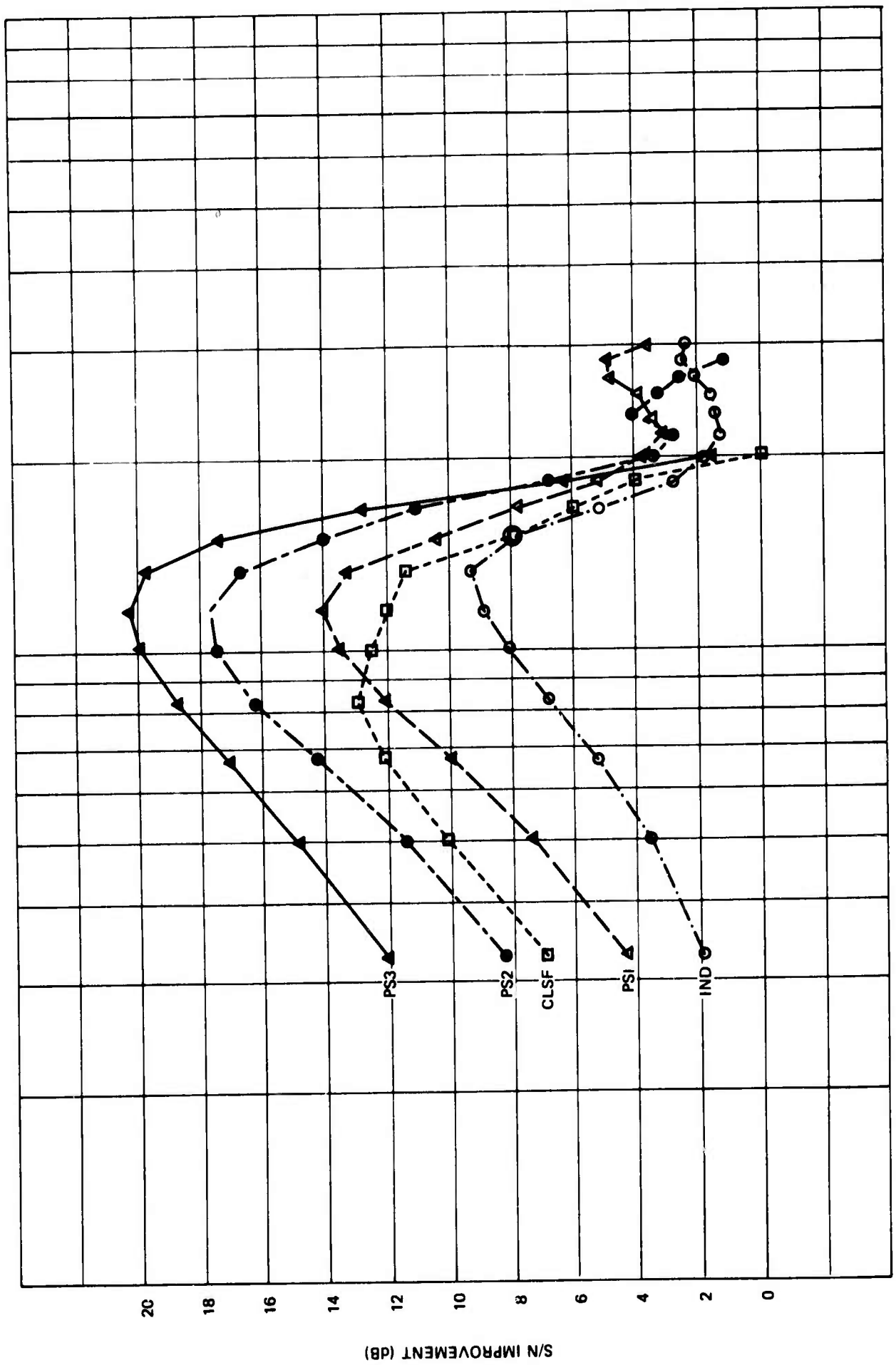

G 4499

Figure 10. Signal-to-noise ratios for data sample 10

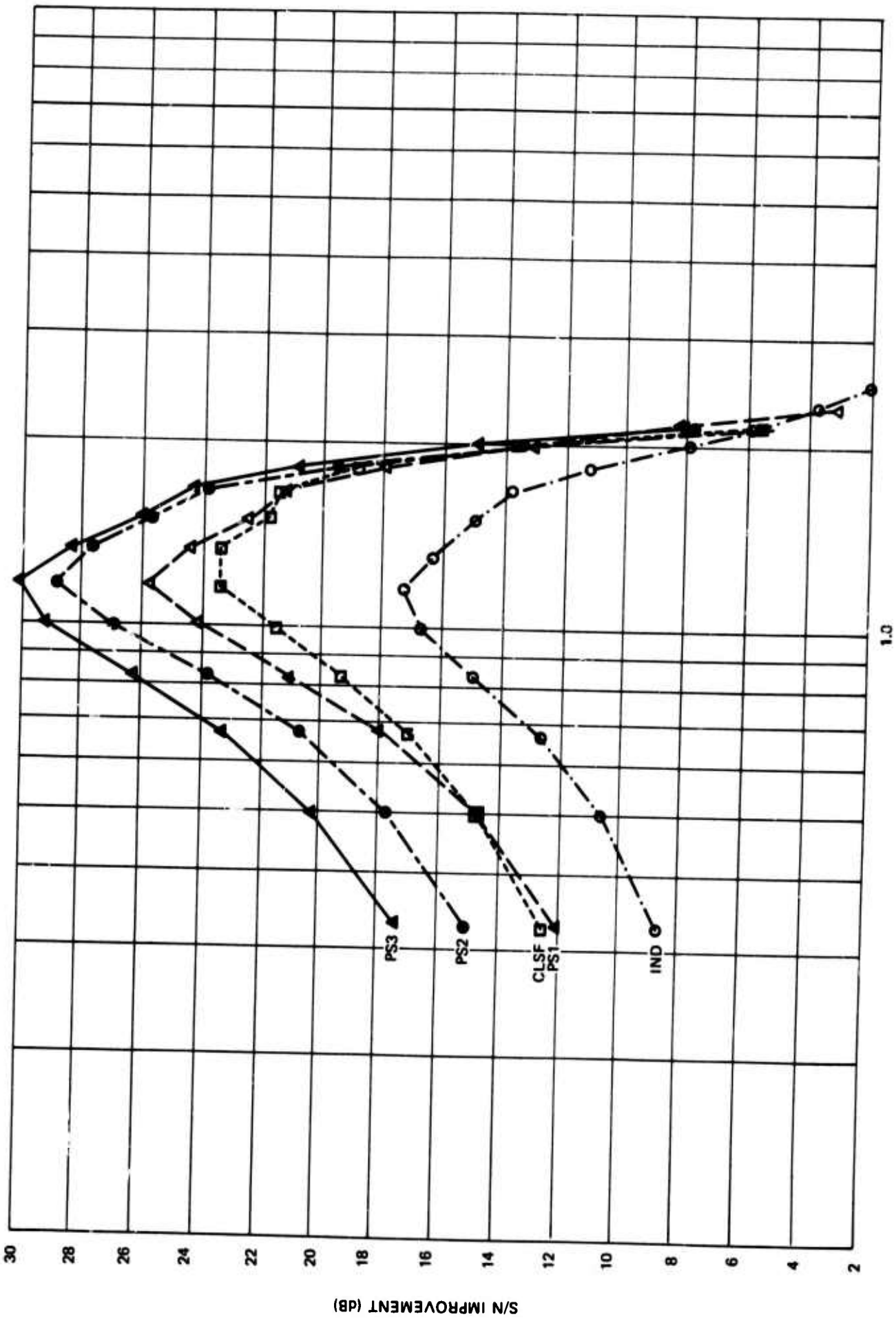

G 4500

Figure 11. Signal-to-noise ratios for data sample 11

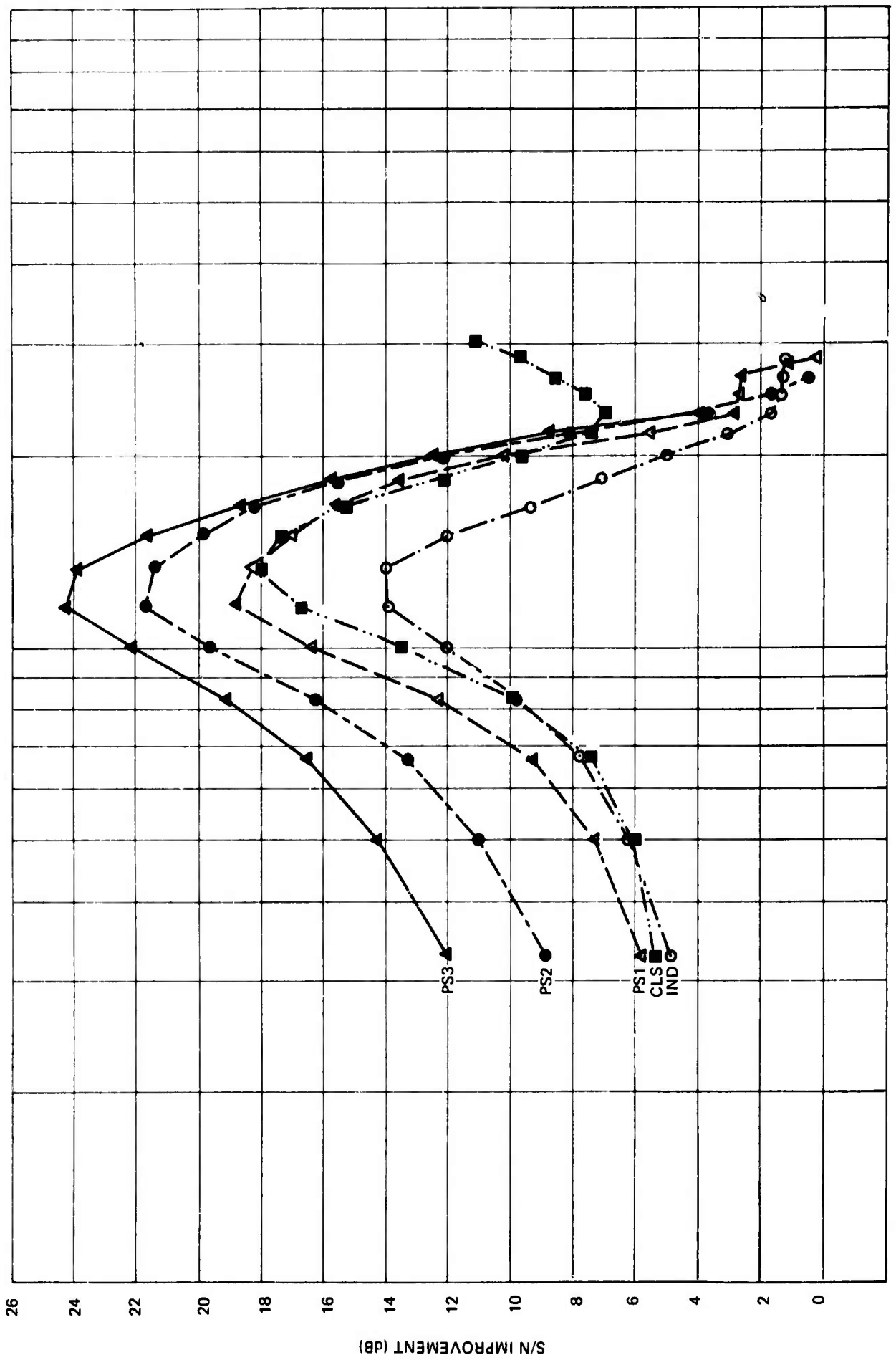

G 4501

Figure 12. Signal-to-noise ratios for data sample 12

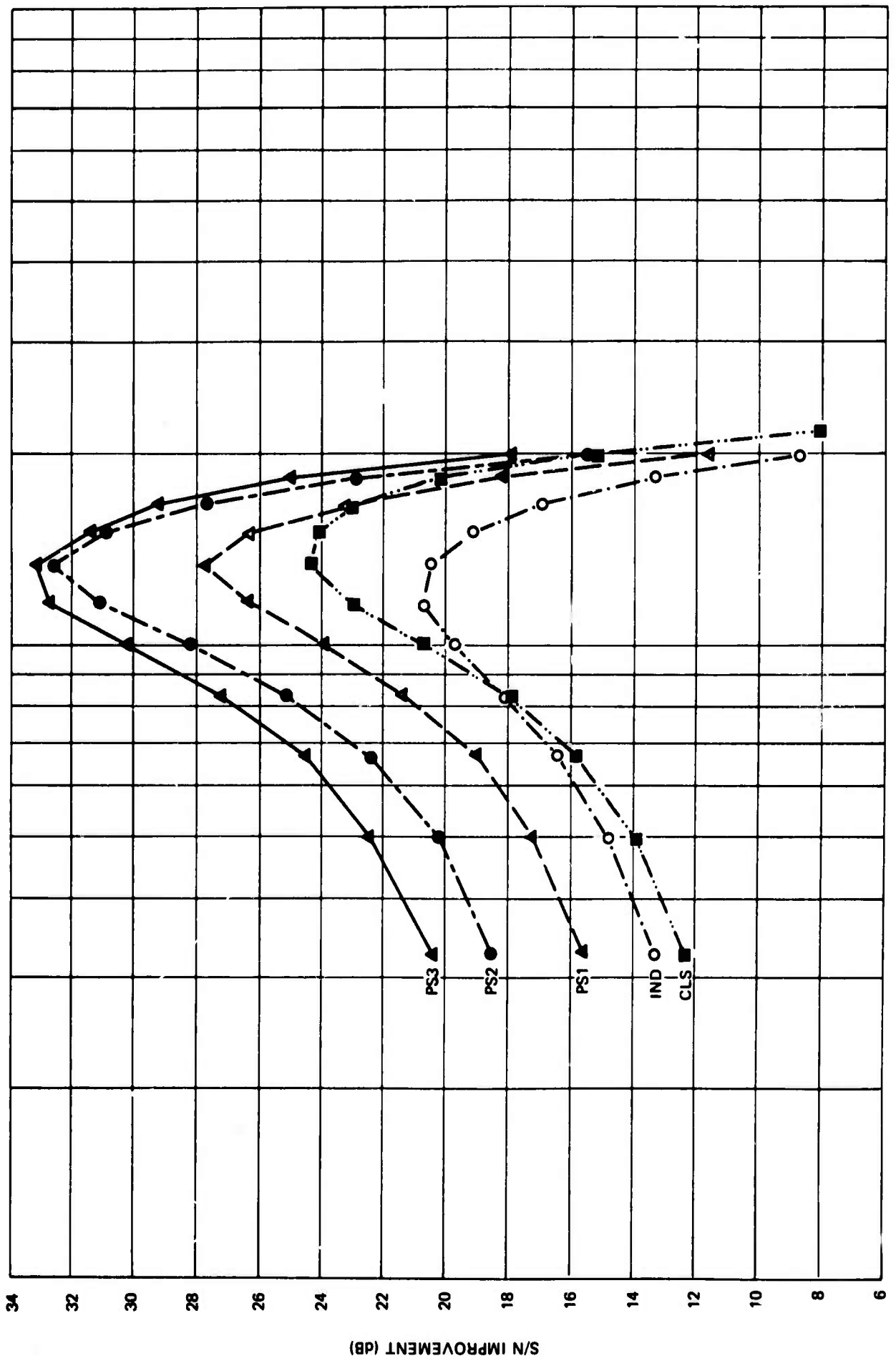

G 4502

Figure 13. Signal-to-noise ratios for data sample 13

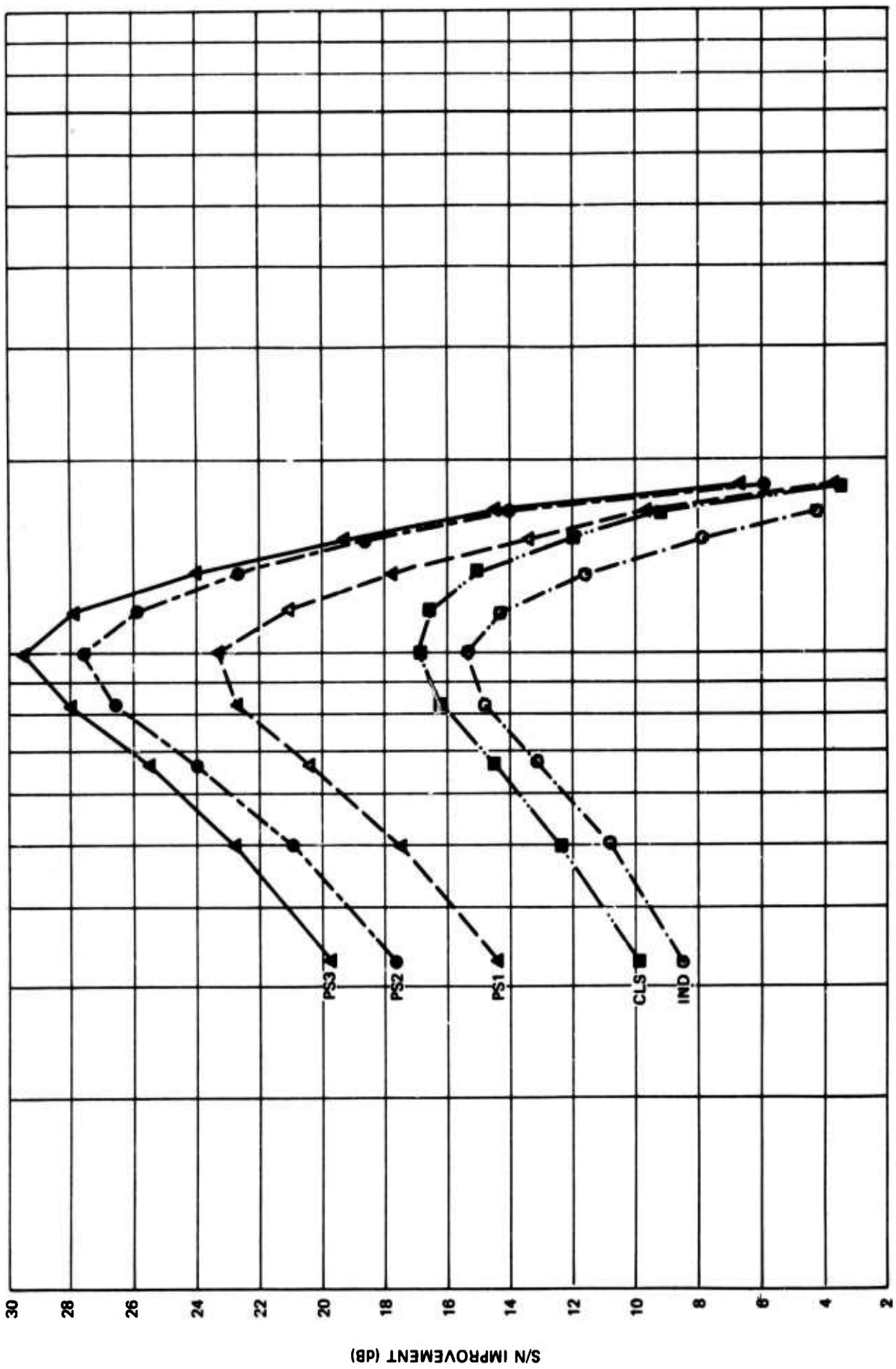

G 4503

Figure 14. Signal-to-noise ratios for data sample 14

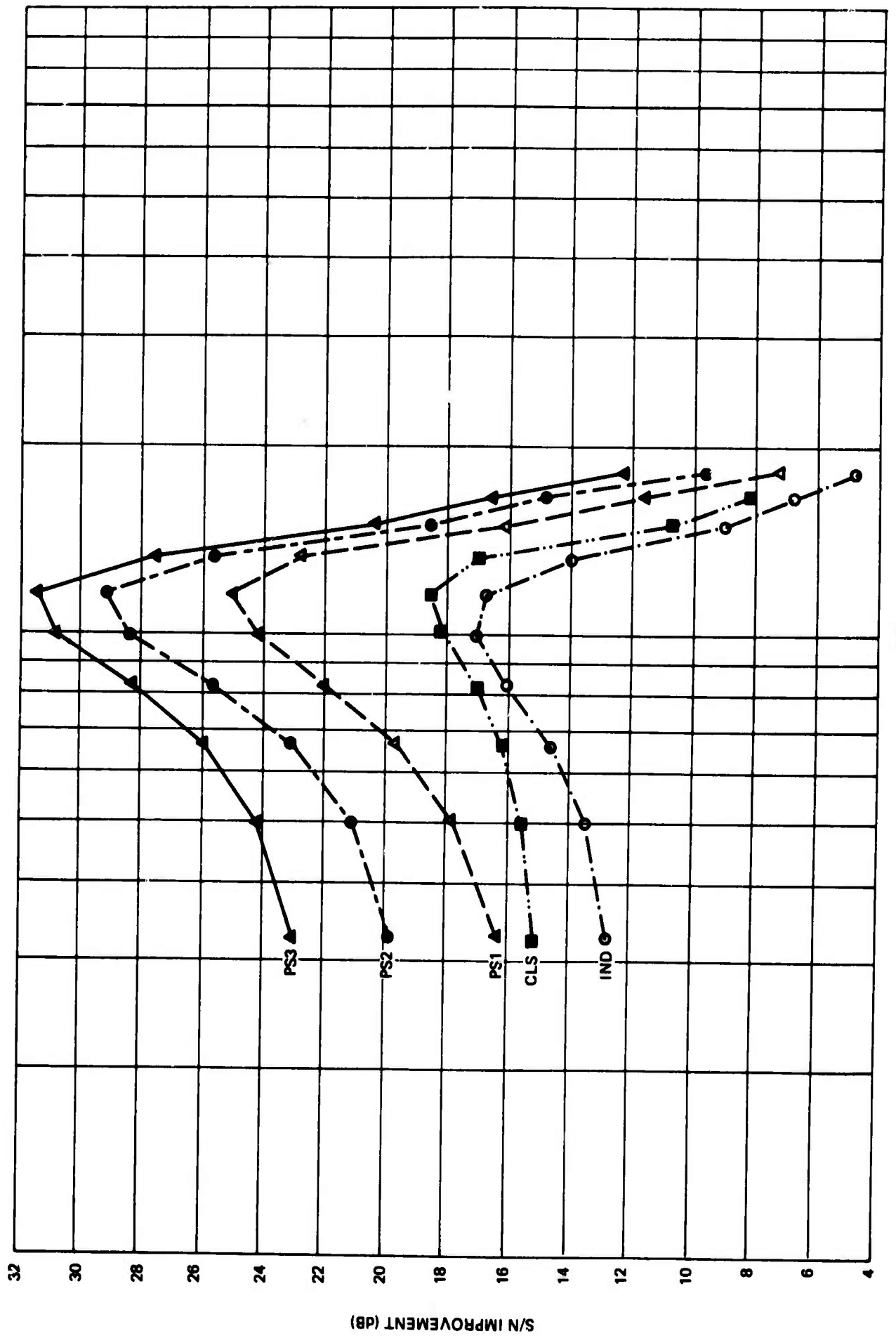

G 4504

Figure 15. Signal-to-noise ratios for data sample 15

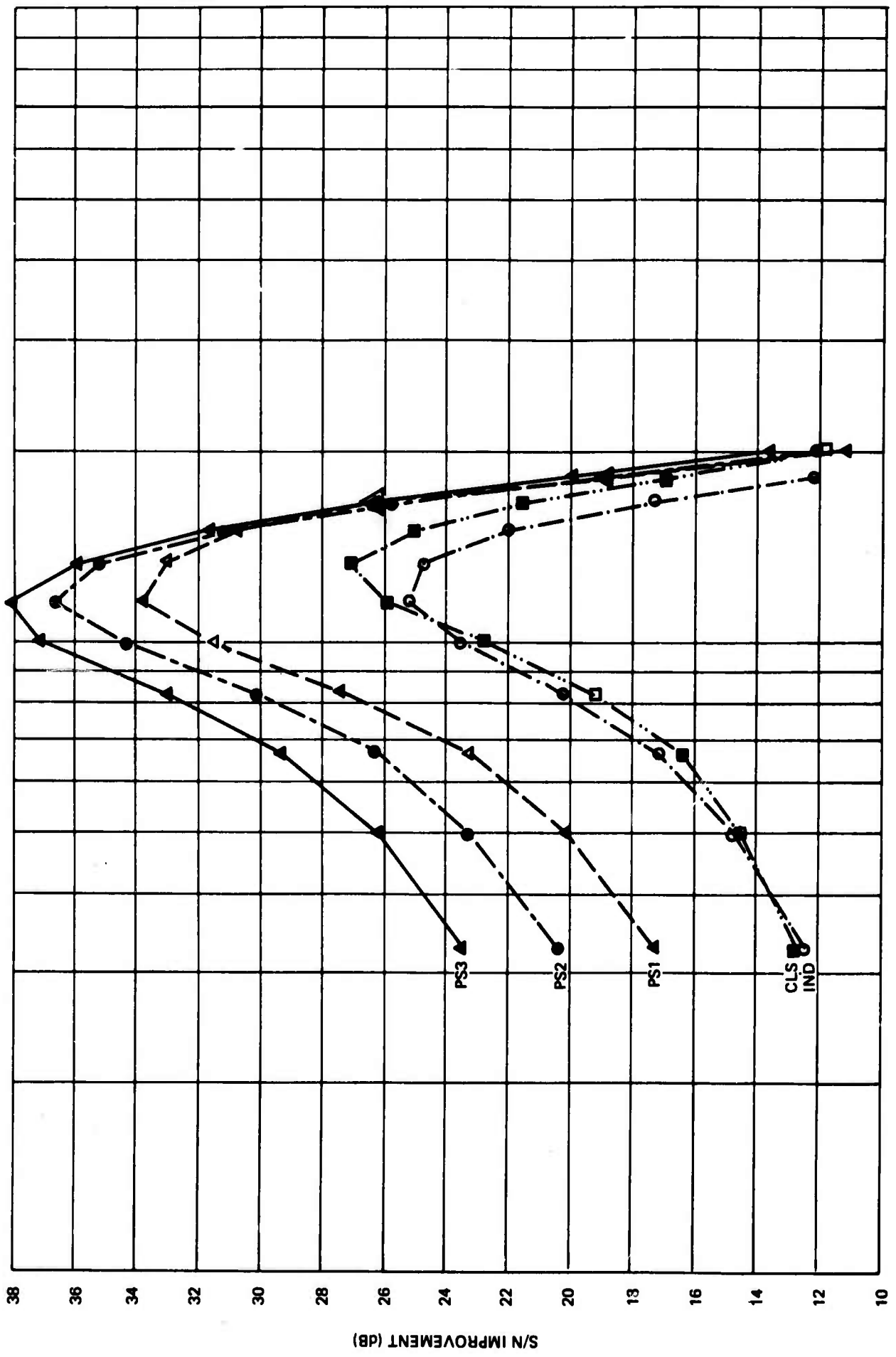

G 4505

Figure 16. Signal-to-noise ratios for data sample 16

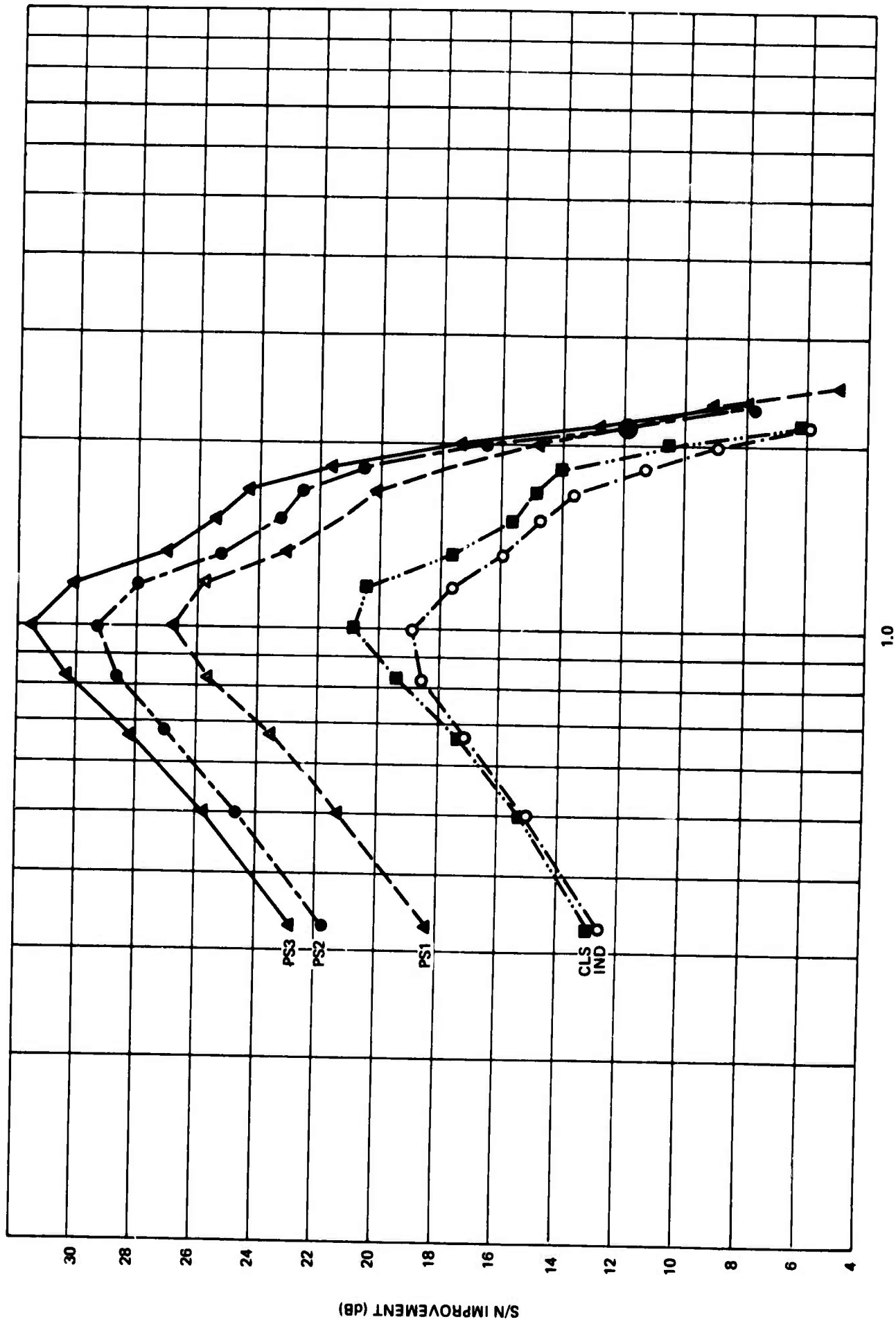

G 4506

Figure 17. Signal-to-noise ratios for data sample 17

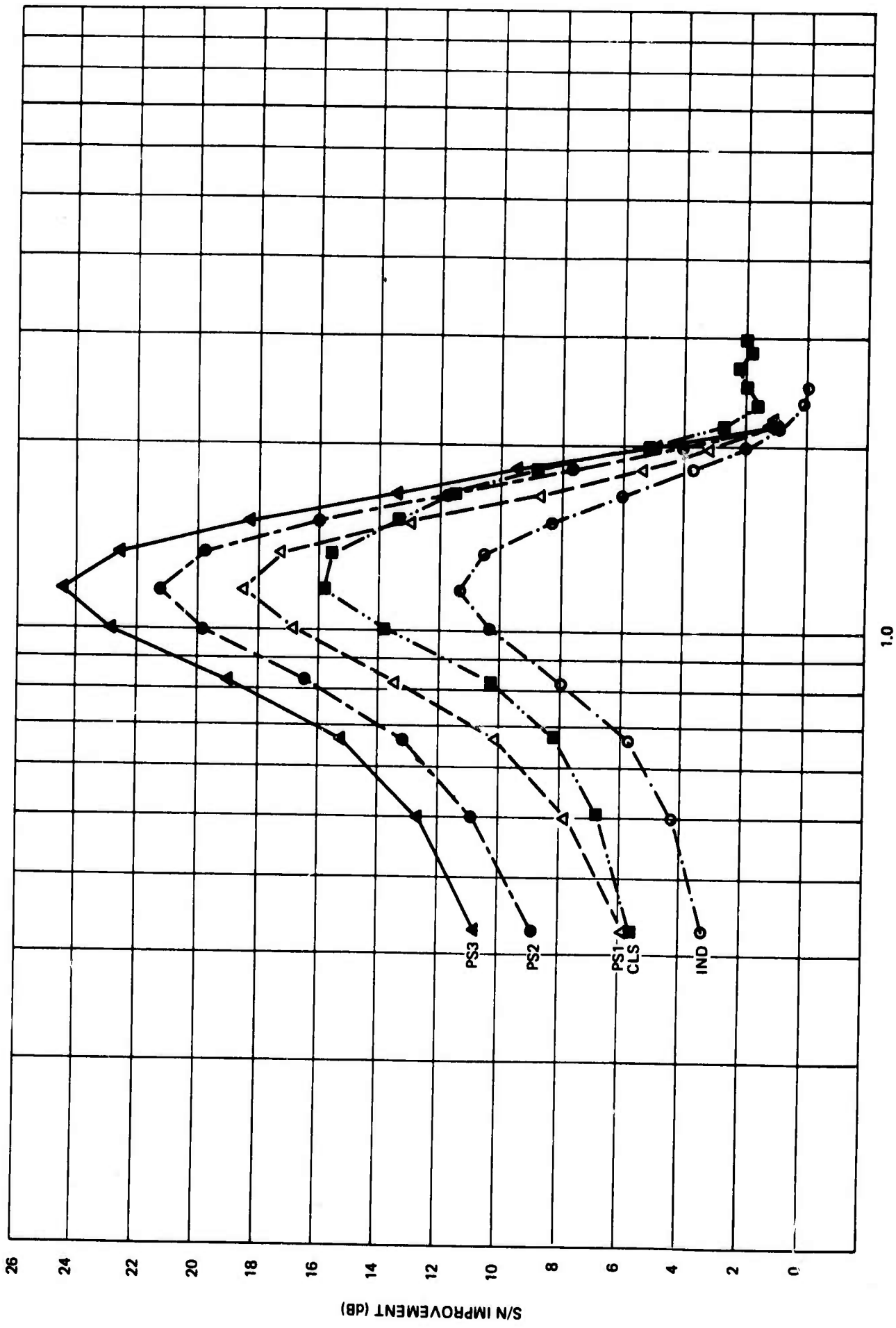

G 4507

Figure 18. Signal-to-noise ratios for data sample 18

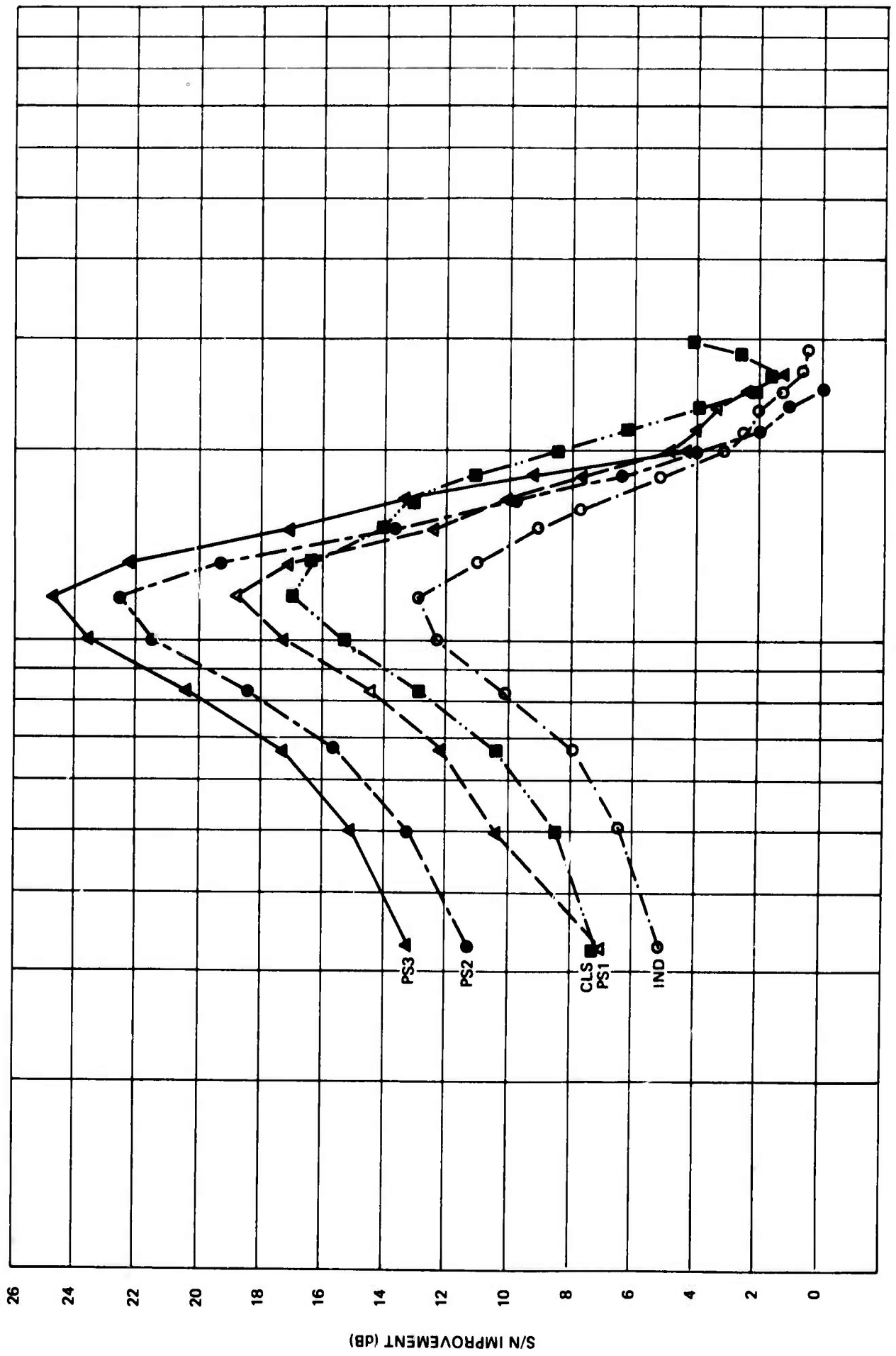

G 4508

Figure 19. Signal-to-noise ratios for data sample 19

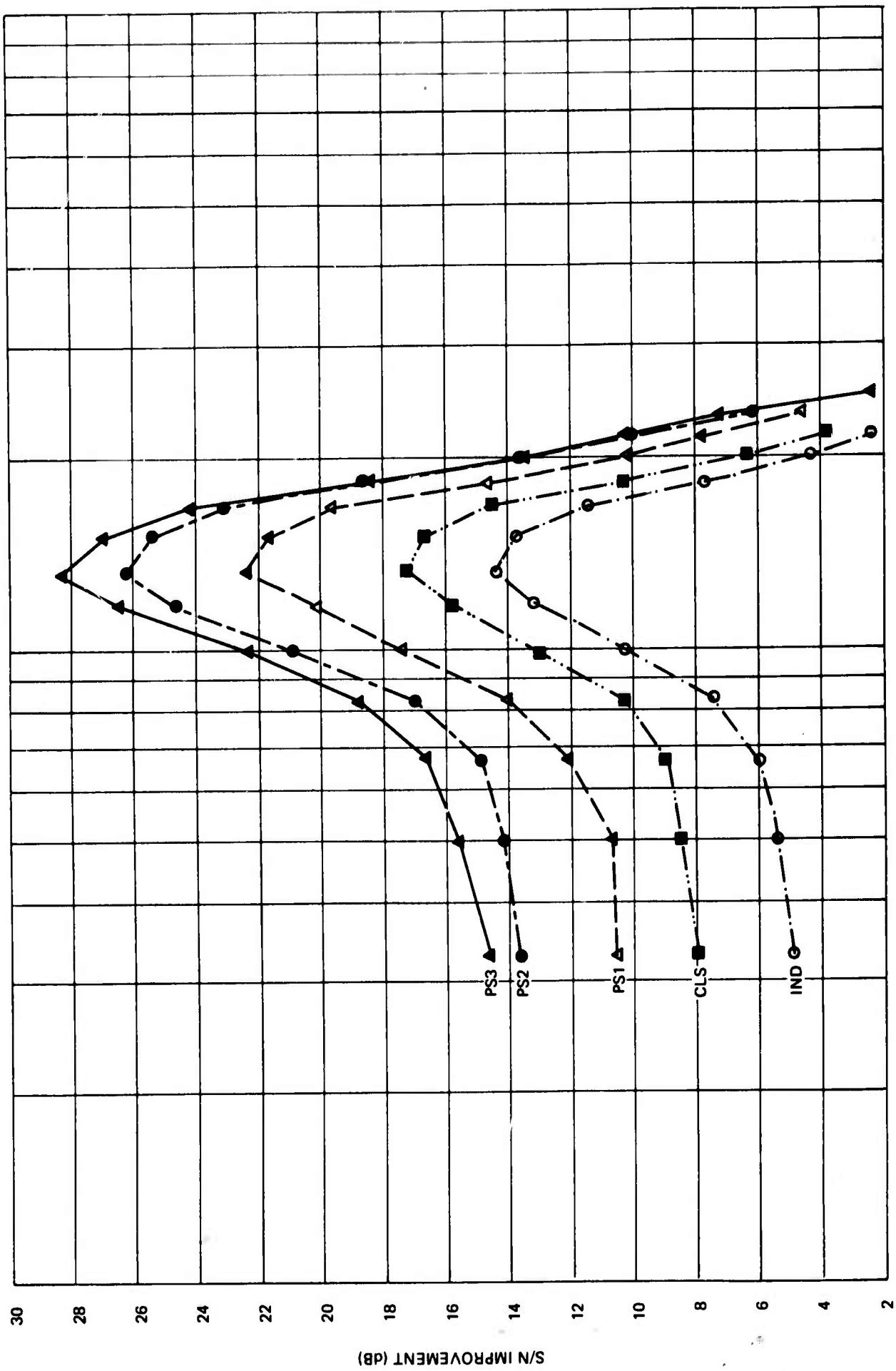

Figure 20. Signal-to-noise ratios for data sample 20

APPENDIX 4 to TECHNICAL REPORT NO. 68-47

SIGNAL-TO-NOISE IMPROVEMENT FOR EACH DATA SAMPLE RELATIVE TO THE SIGNAL-TO-NOISE RATIO FOR THE AVERAGE OF THE INDIVIDUAL ELEMENTS

BLANK PAGE

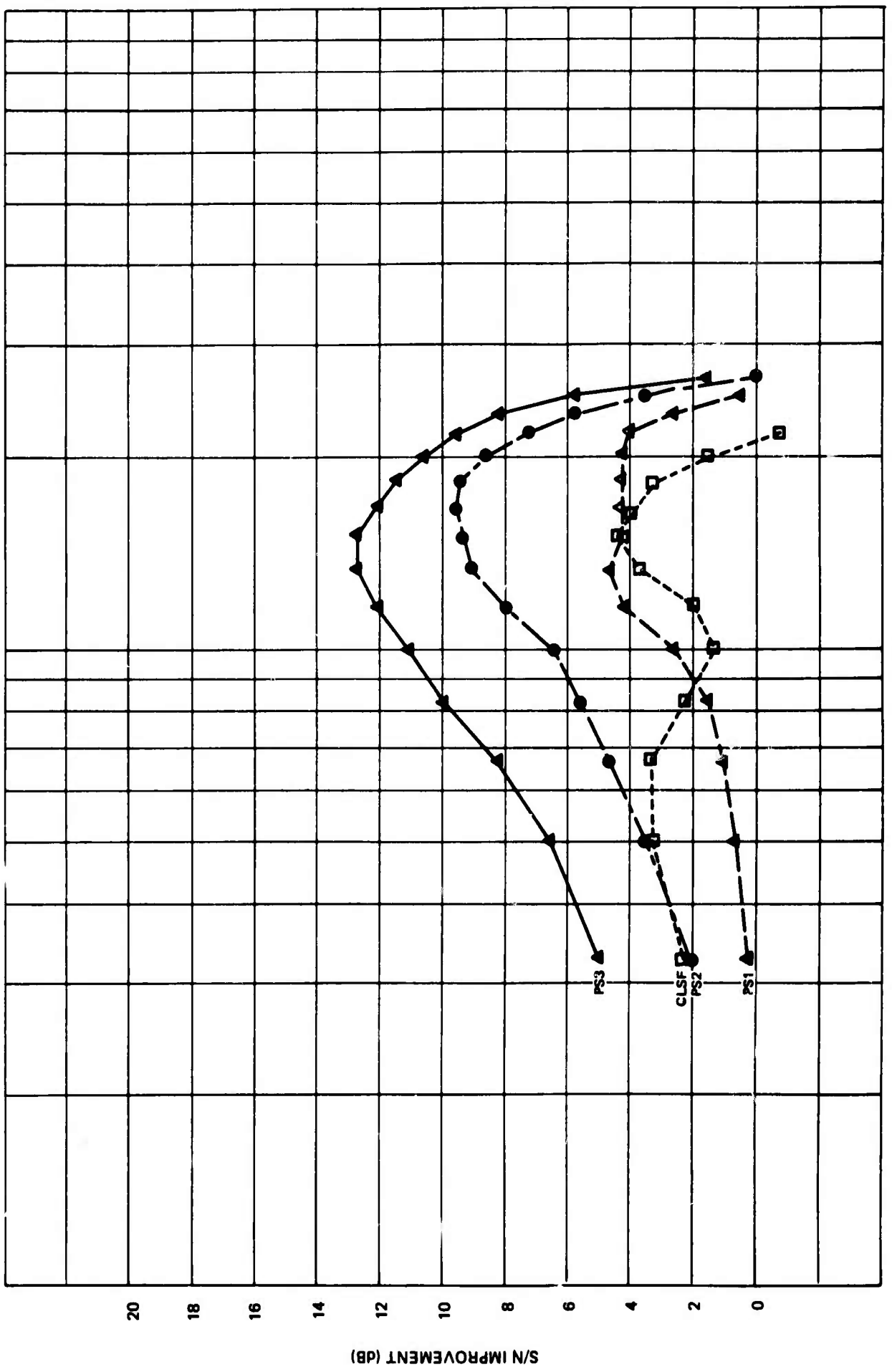

G 4510

Figure 1. Signal-to-noise improvement for data sample 1

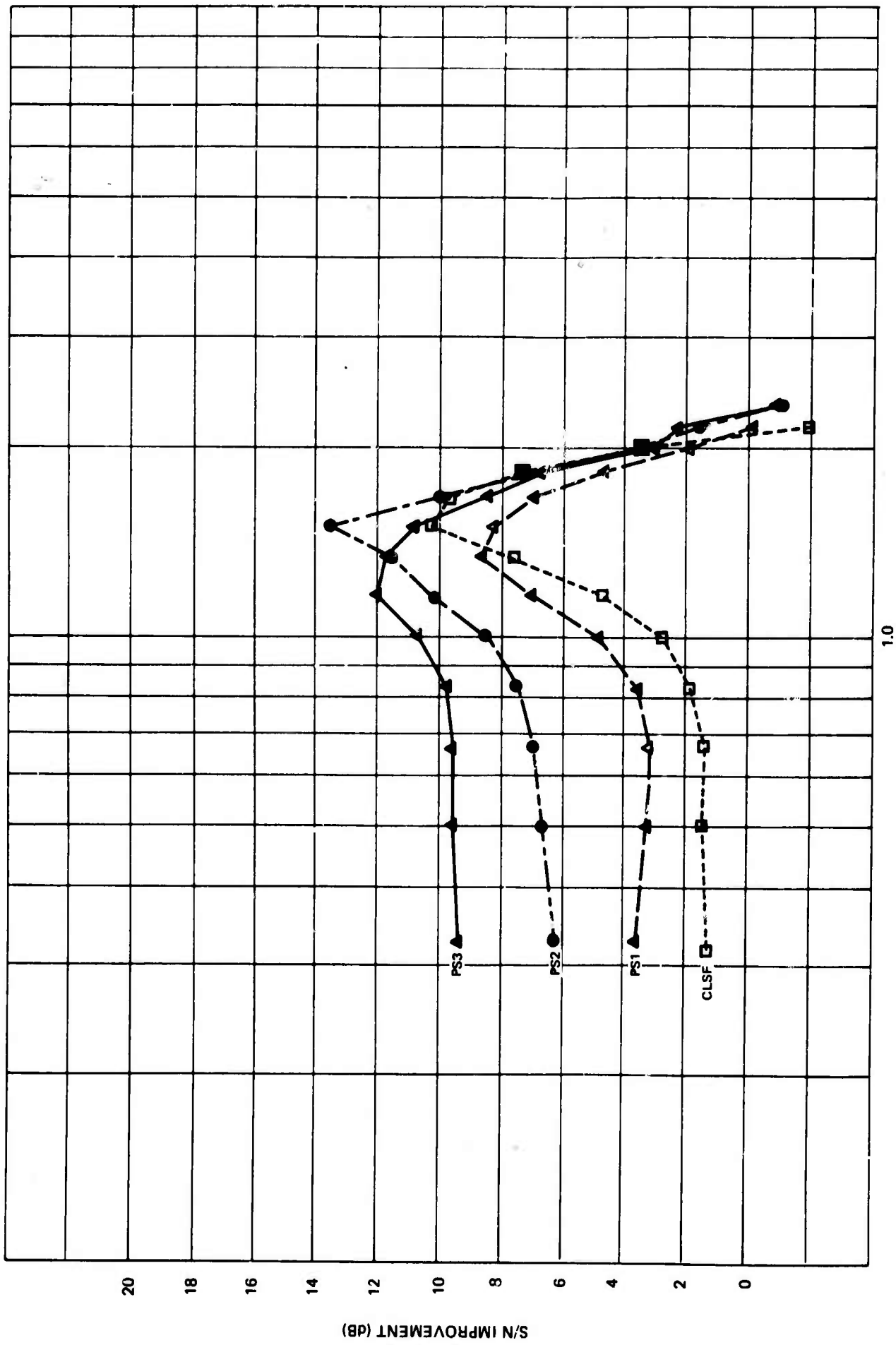

G 4511

Figure 2. Signal-to-noise improvement for data sample 2

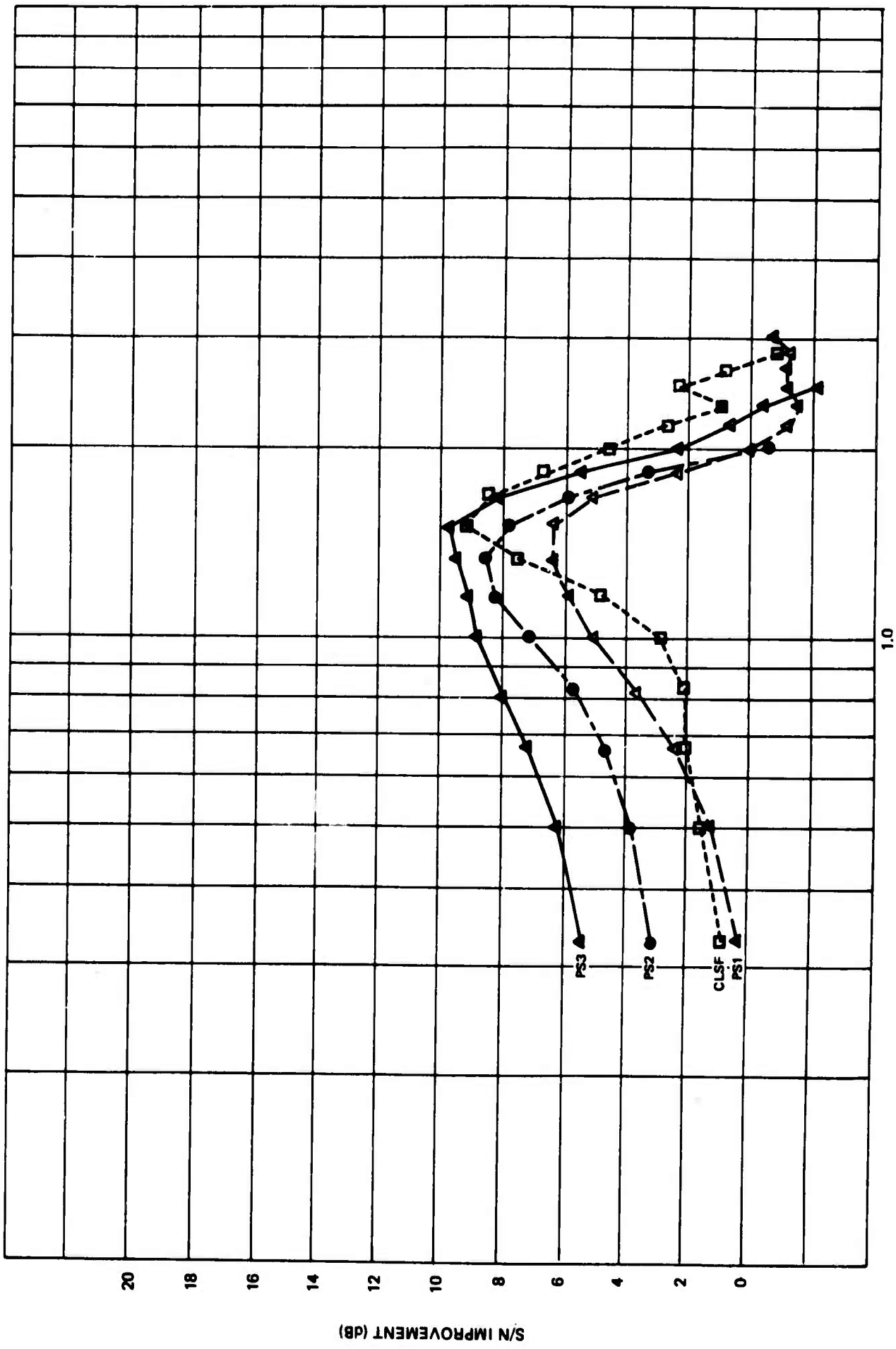

Figure 3. Signal-to-noise improvement for data sample 3

G 4512

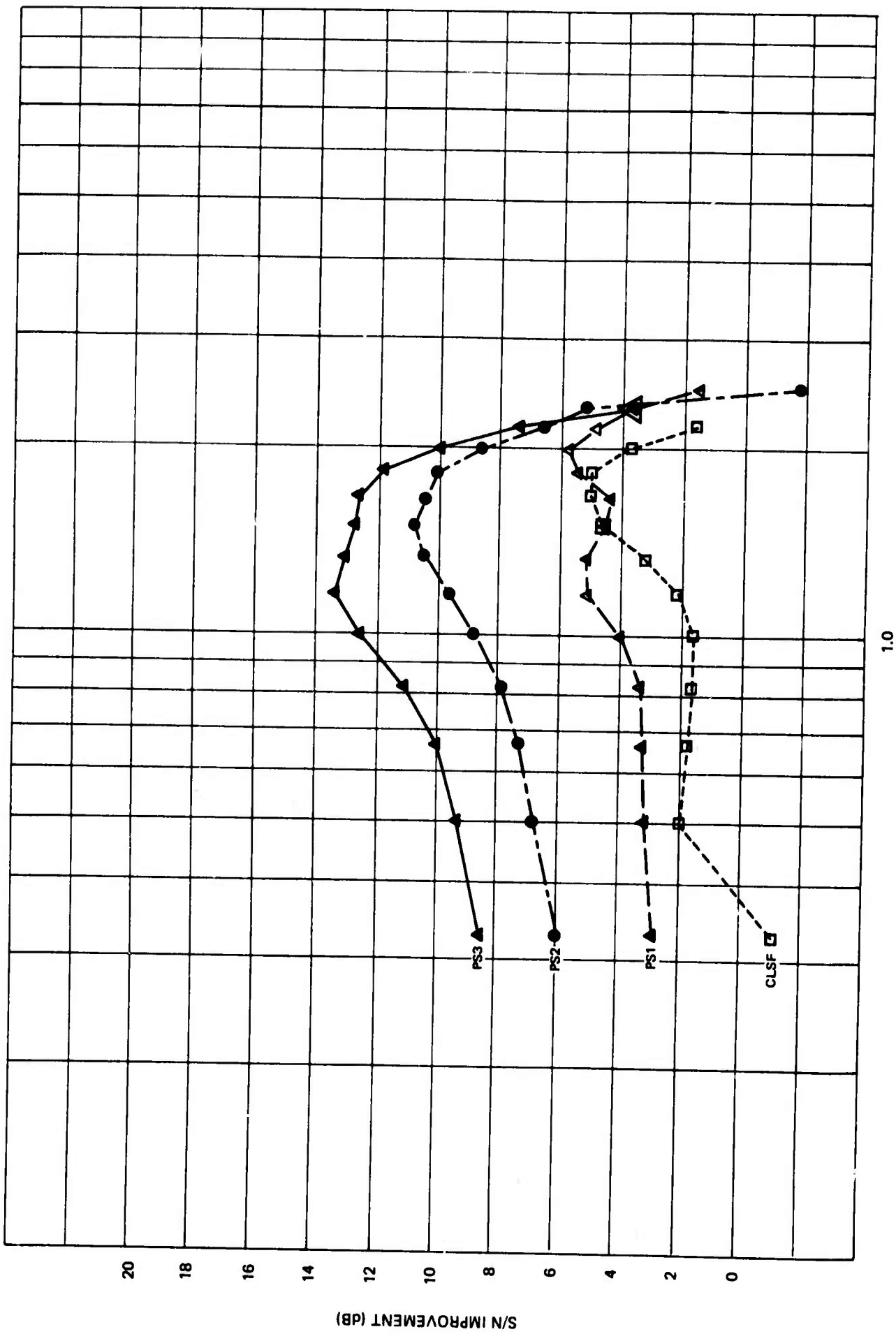

G 4513

Figure 4. Signal-to-noise improvement for data sample 4

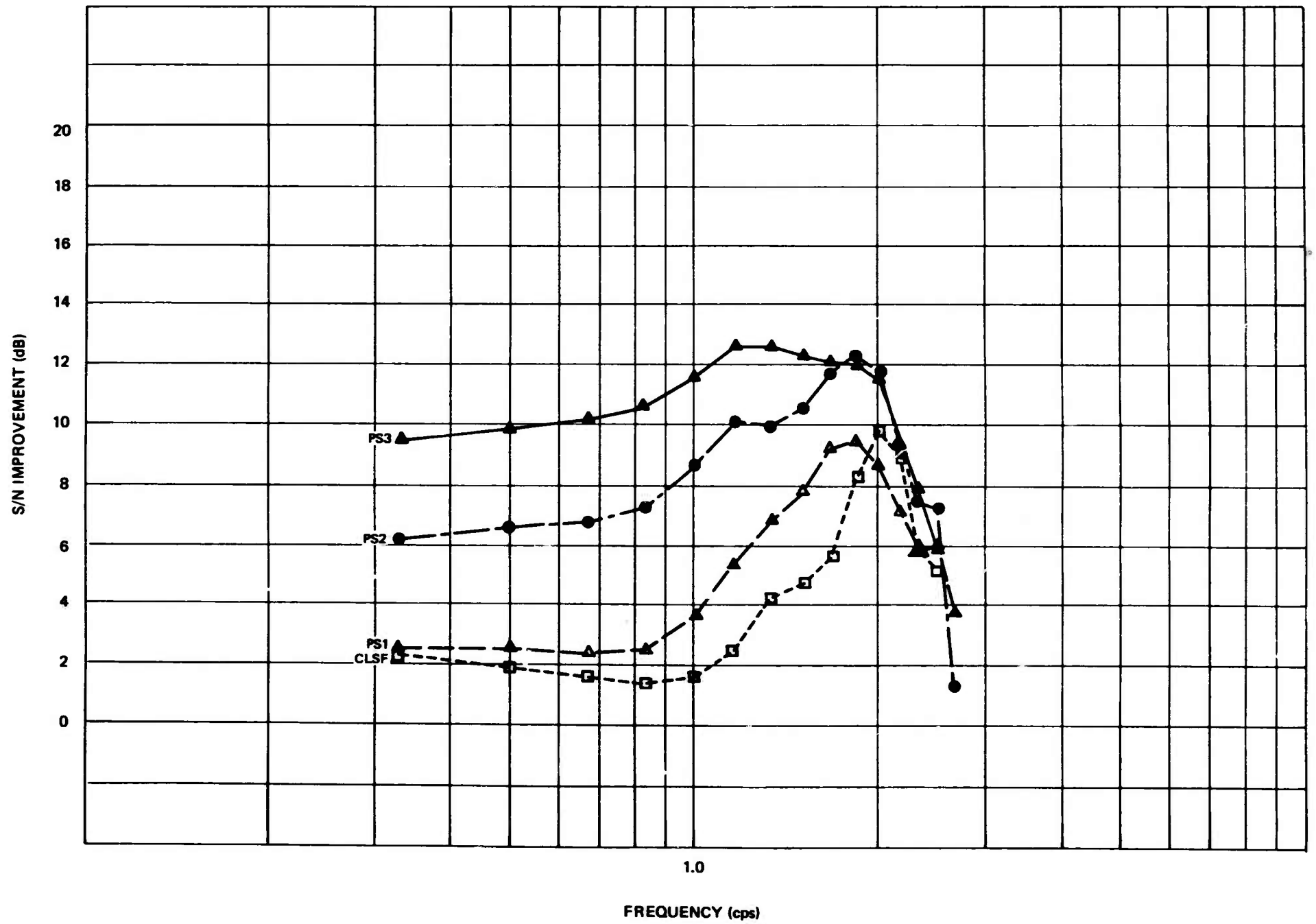

Figure 5. Signal-to-noise improvement for data sample 5

G 4514

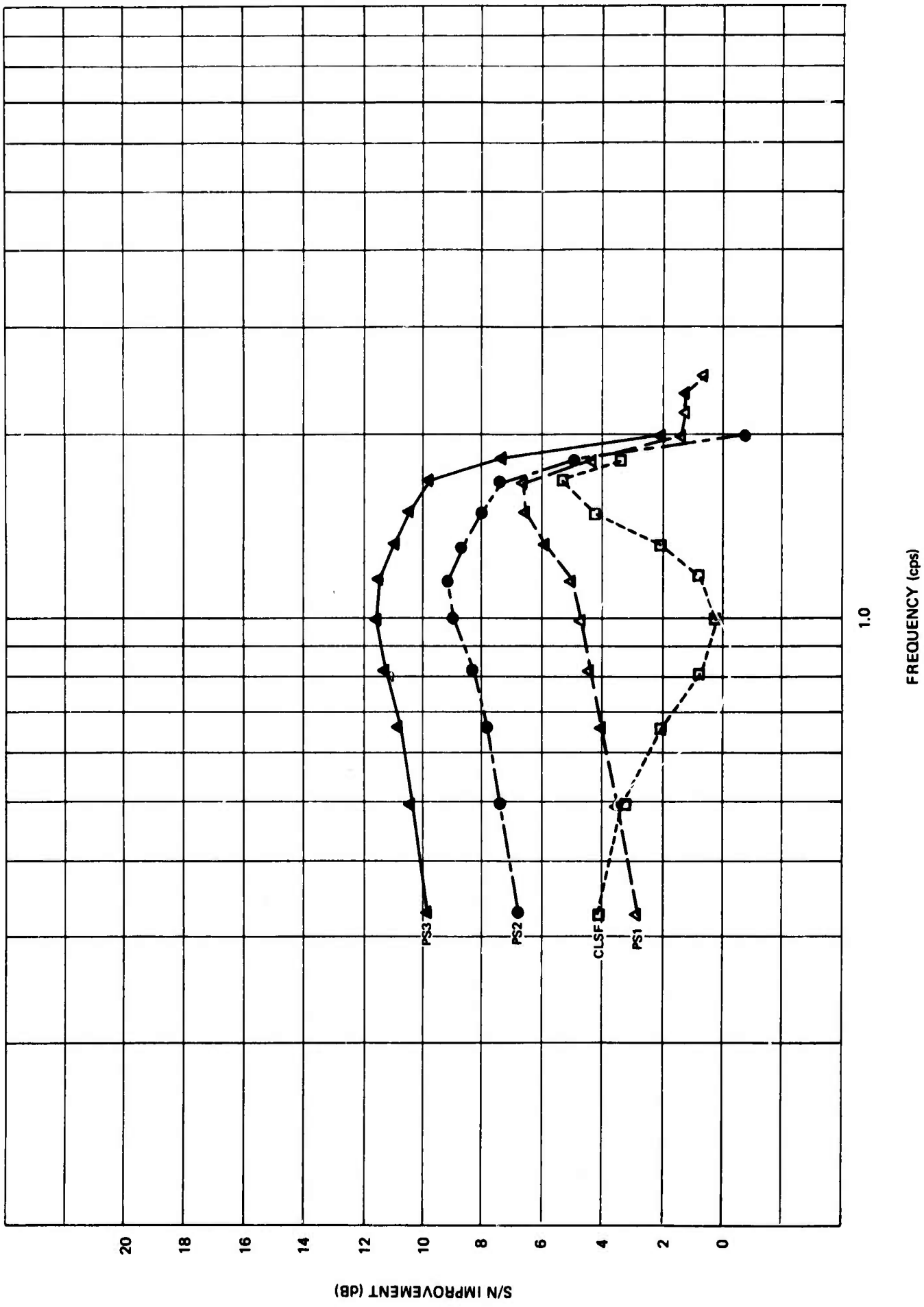

G 4515

Figure 6. Signal-to-noise improvement for data sample 6

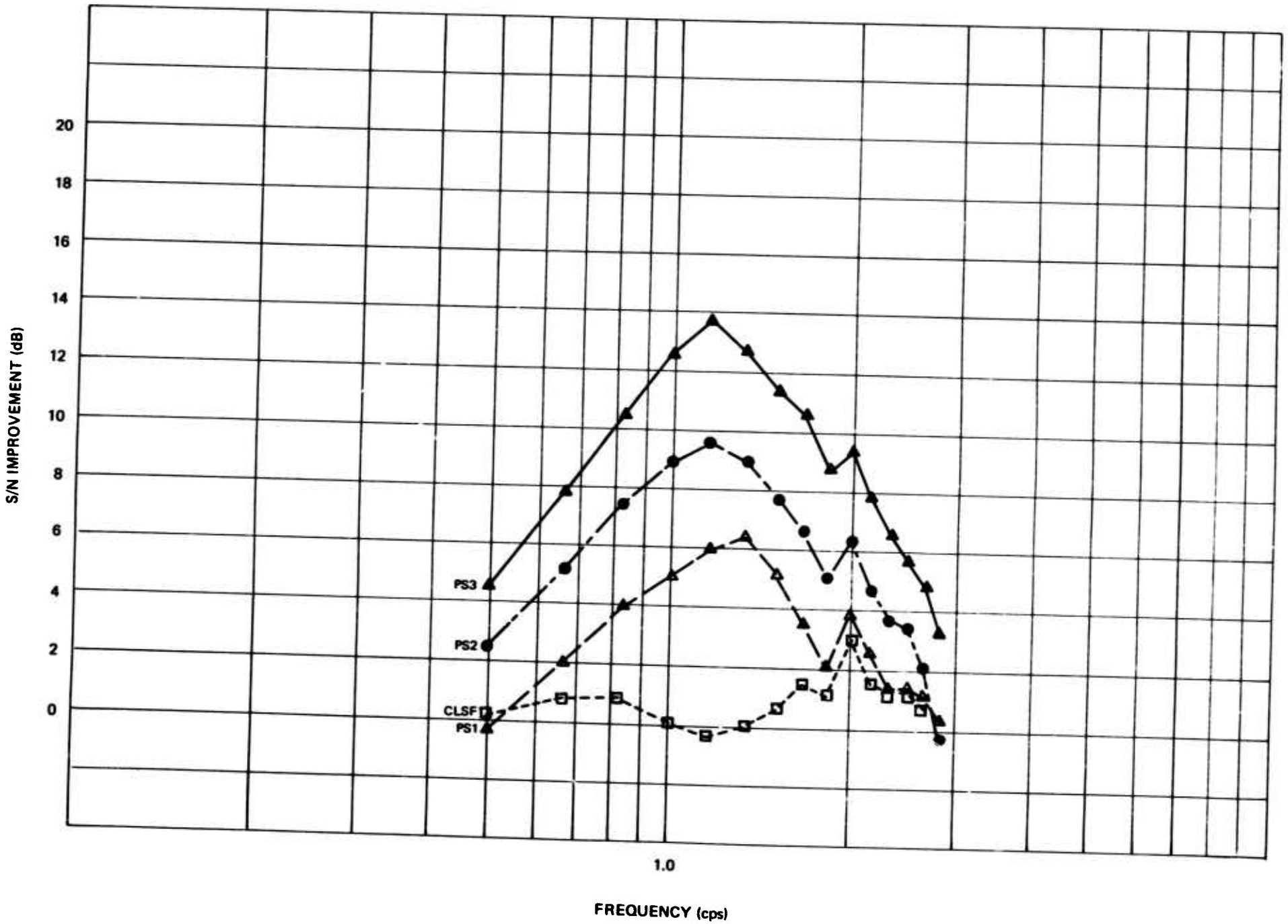

Figure 7. Signal-to-noise improvement for data sample 7

G 4516

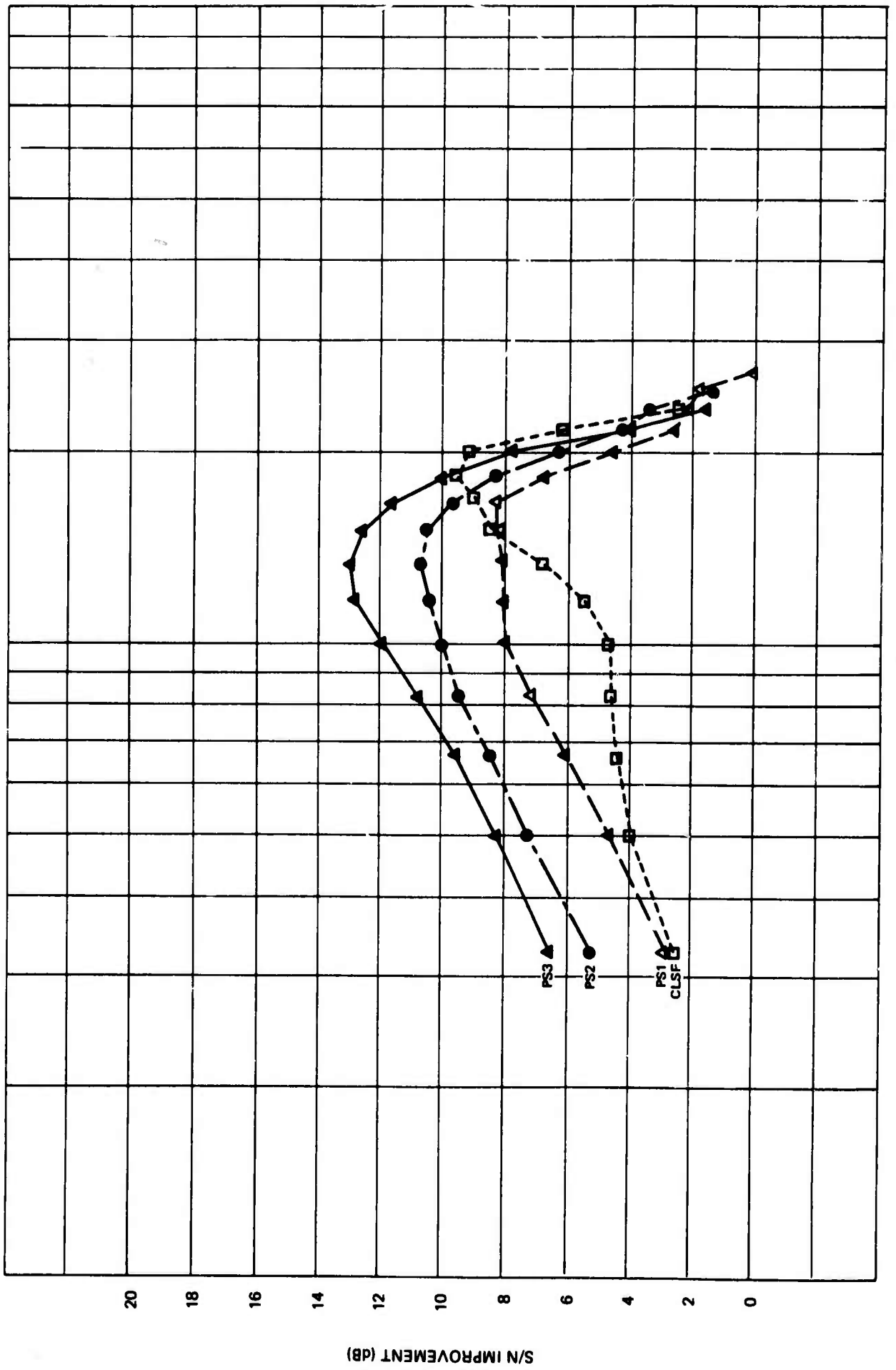

G 4517

Figure 8. Signal-to-noise improvement for data sample 8

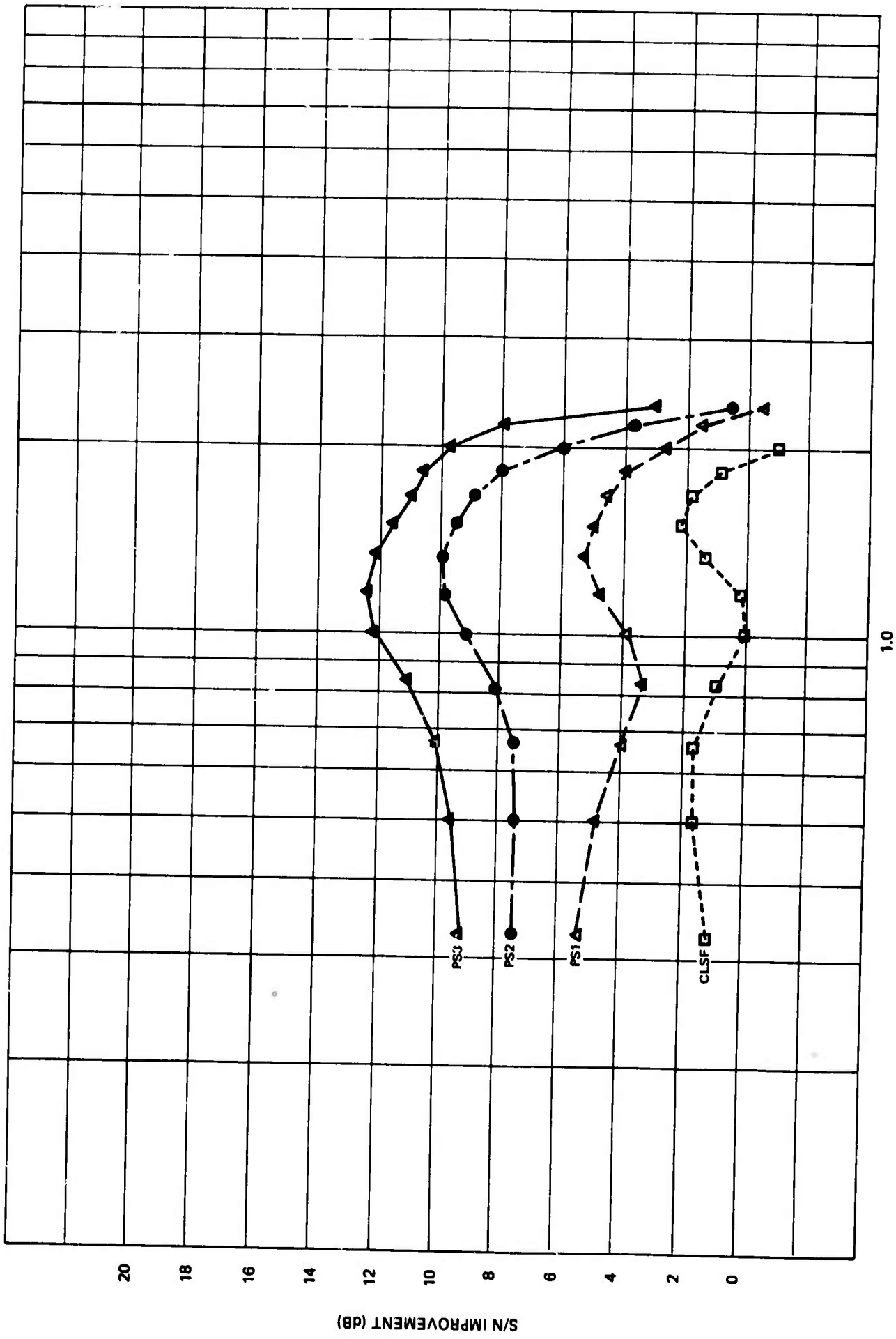

G 4518

Figure 9. Signal-to-noise improvement for data sample 9

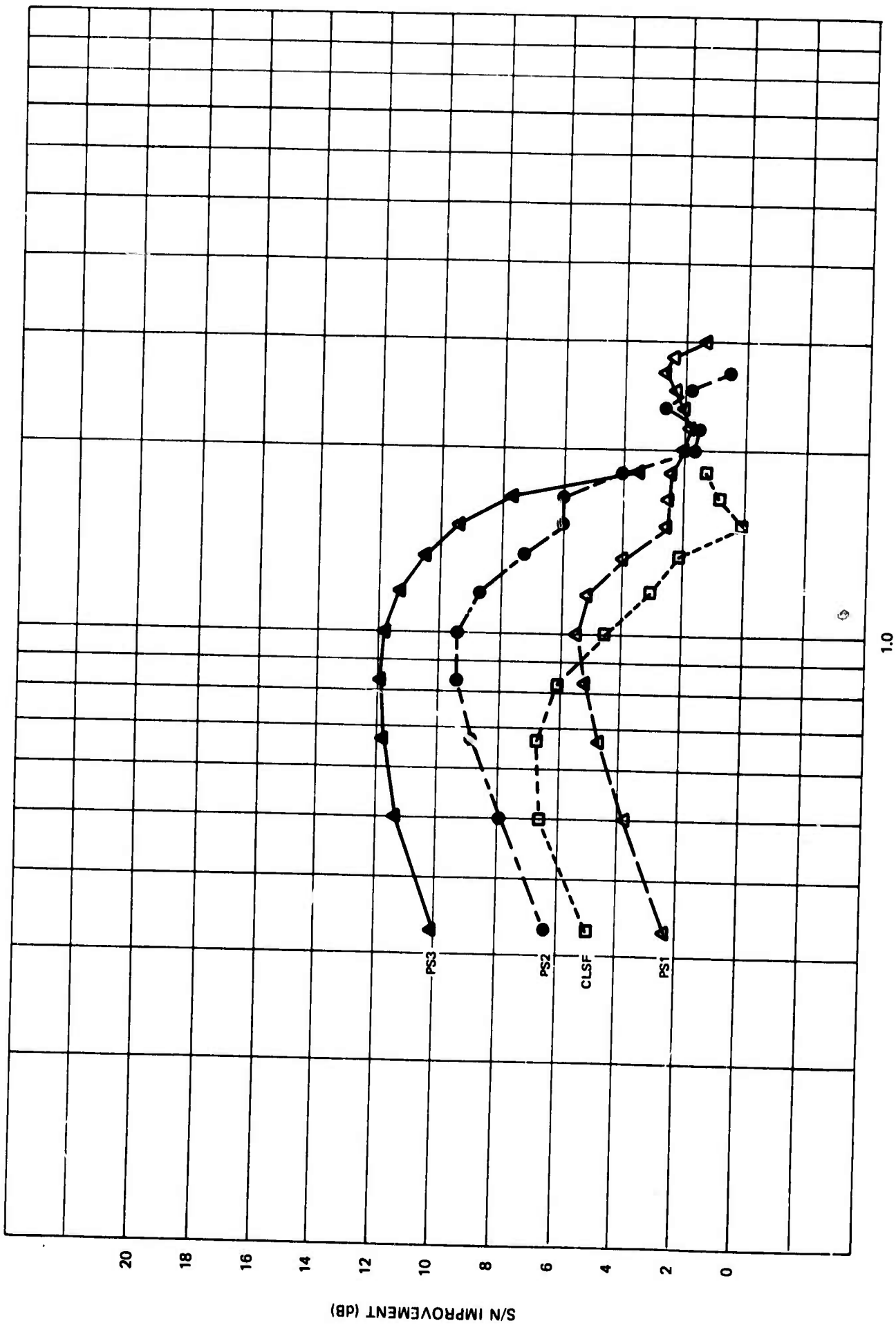

G 4519

Figure 10. Signal-to-noise improvement for data sample 10

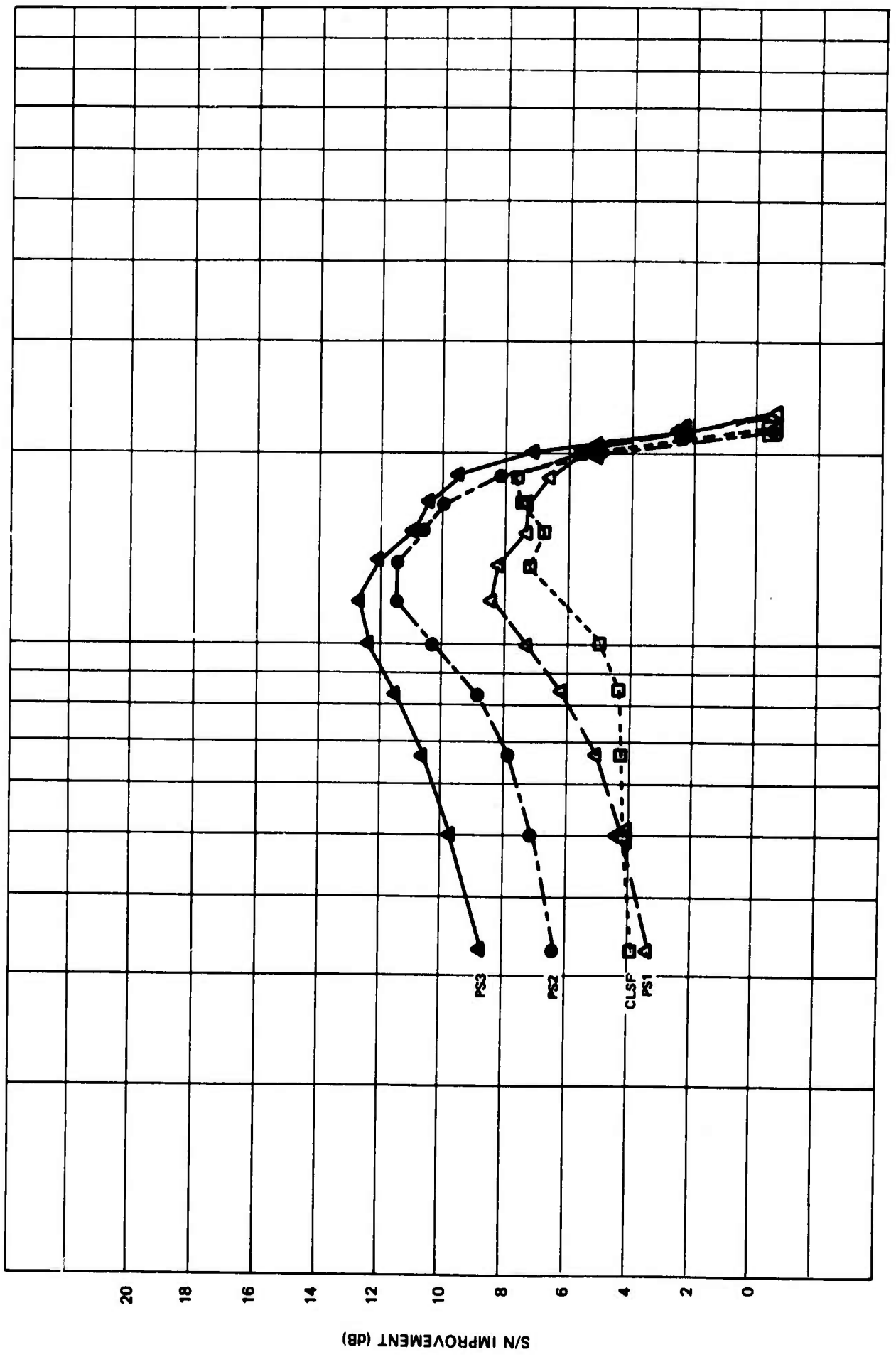

G 4520

Figure 11. Signal-to-noise improvement for data sample 11

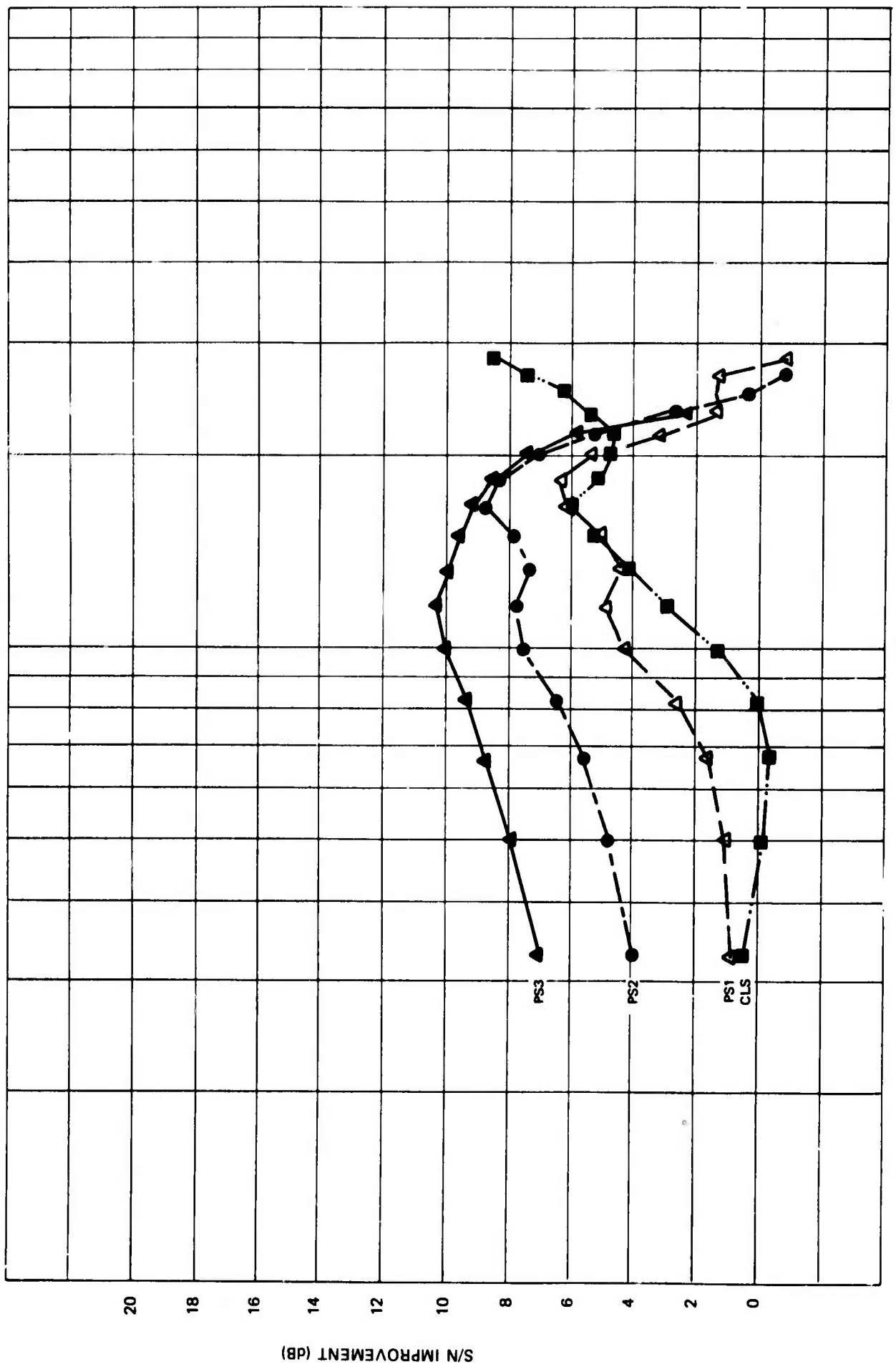

Figure 12. Signal-to-noise improvement for data sample 12

G 4521

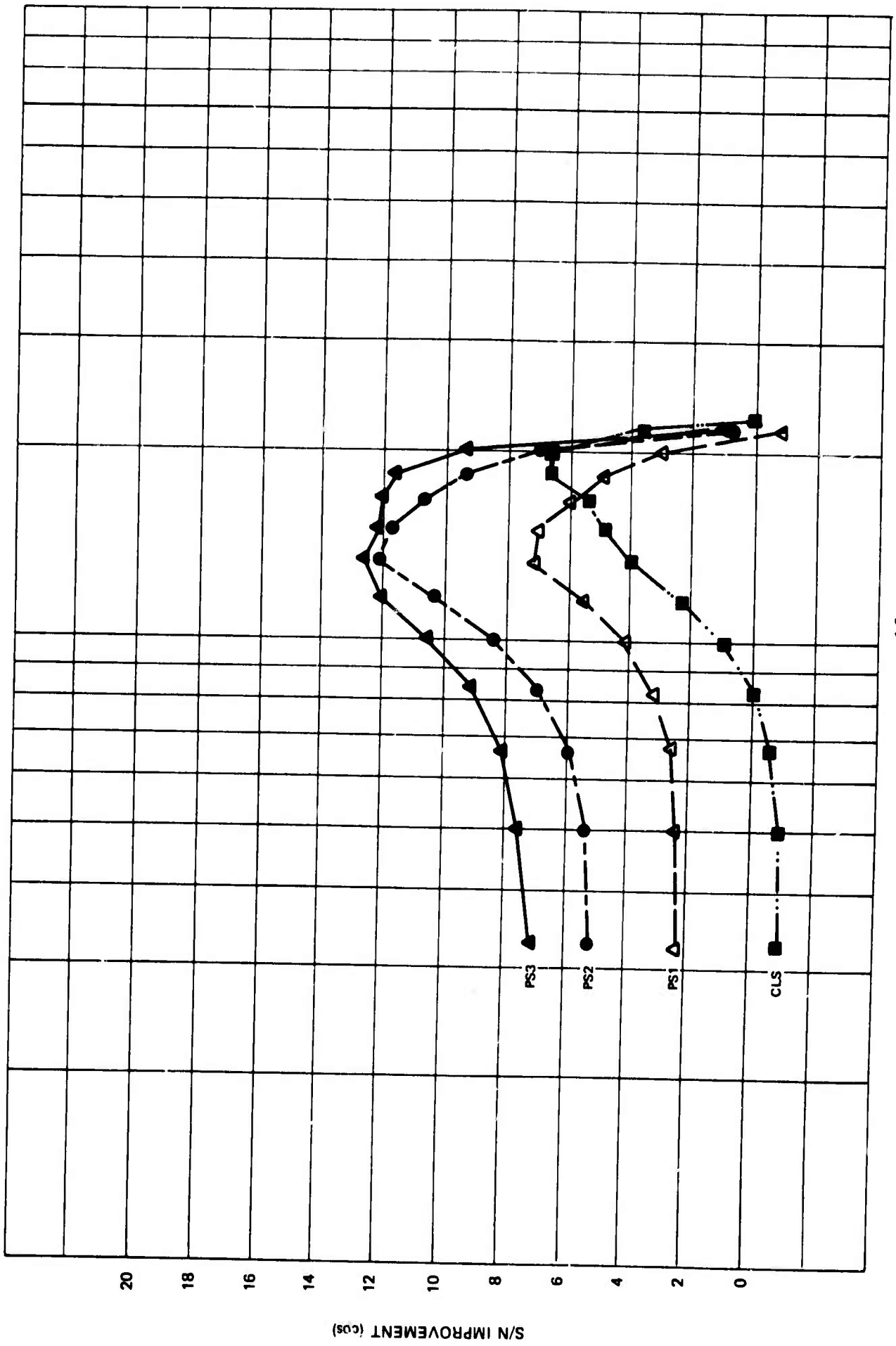

G 4522

Figure 13. Signal-to-noise improvement for data sample 13

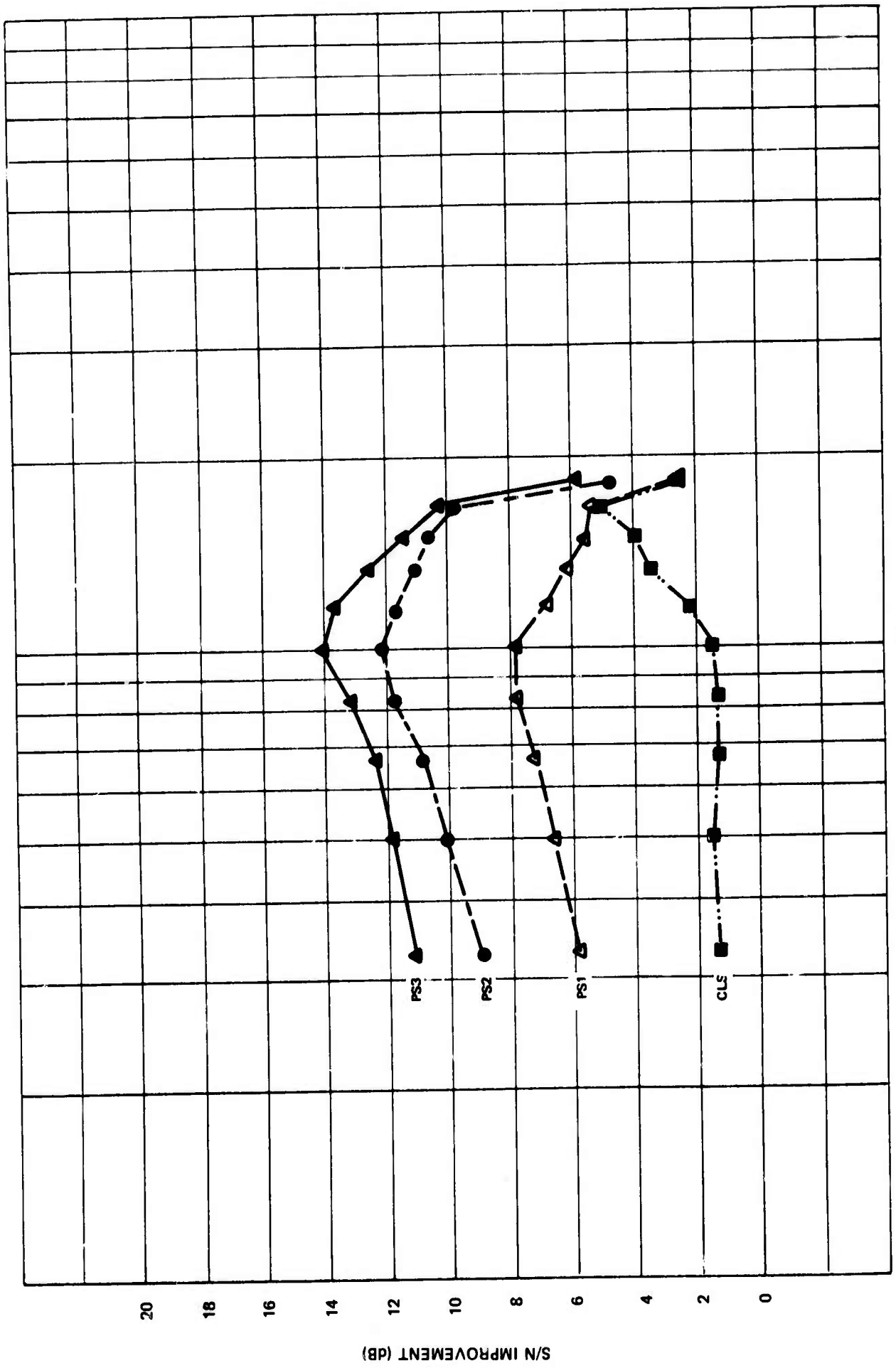

Figure 14. Signal-to-noise improvement for data sample 14

G 4523

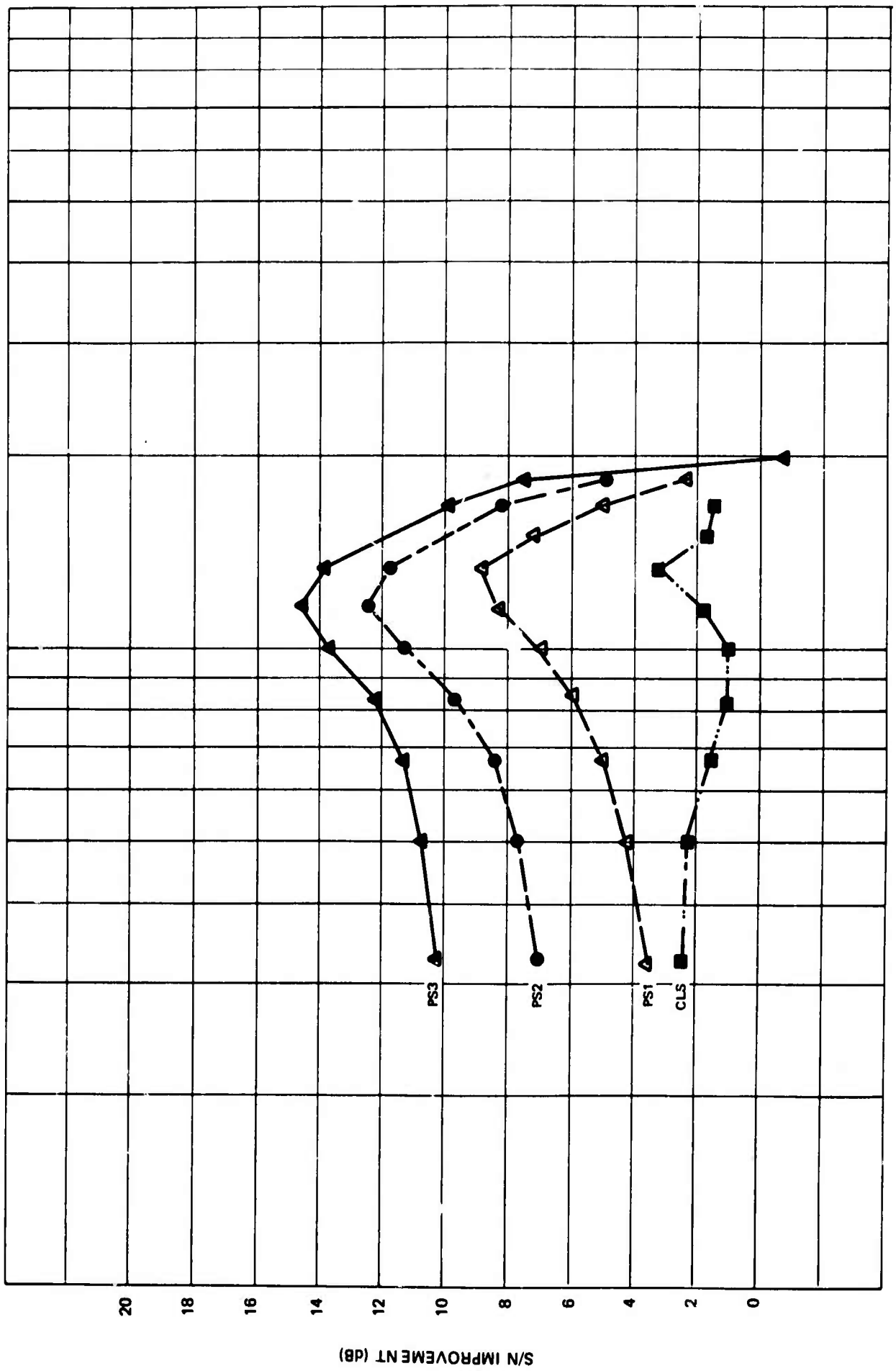

G 4524

Figure 15. Signal-to-noise improvement for data sample 15

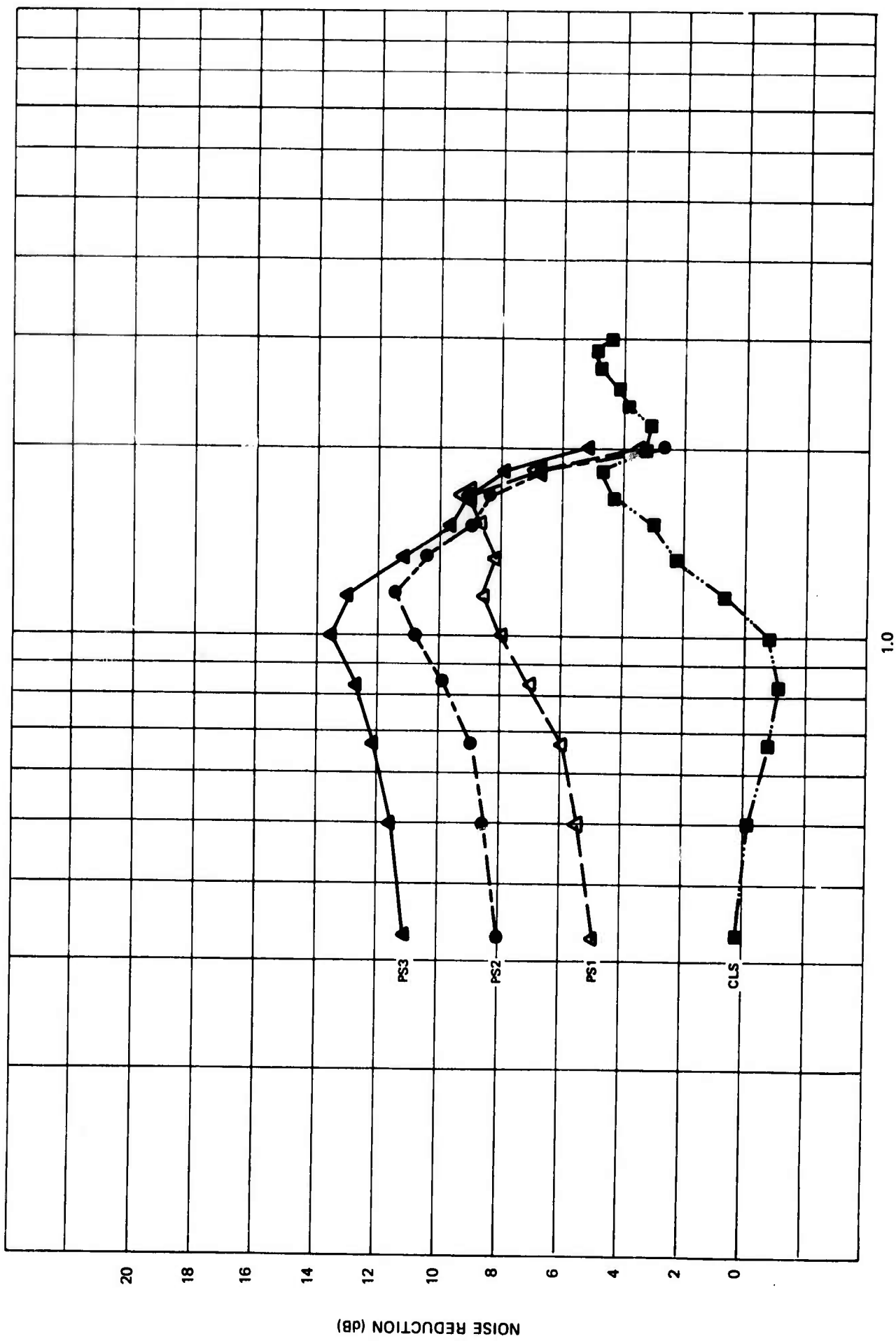

G 4525

Figure 16. Signal-to-noise improvement for data sample 16

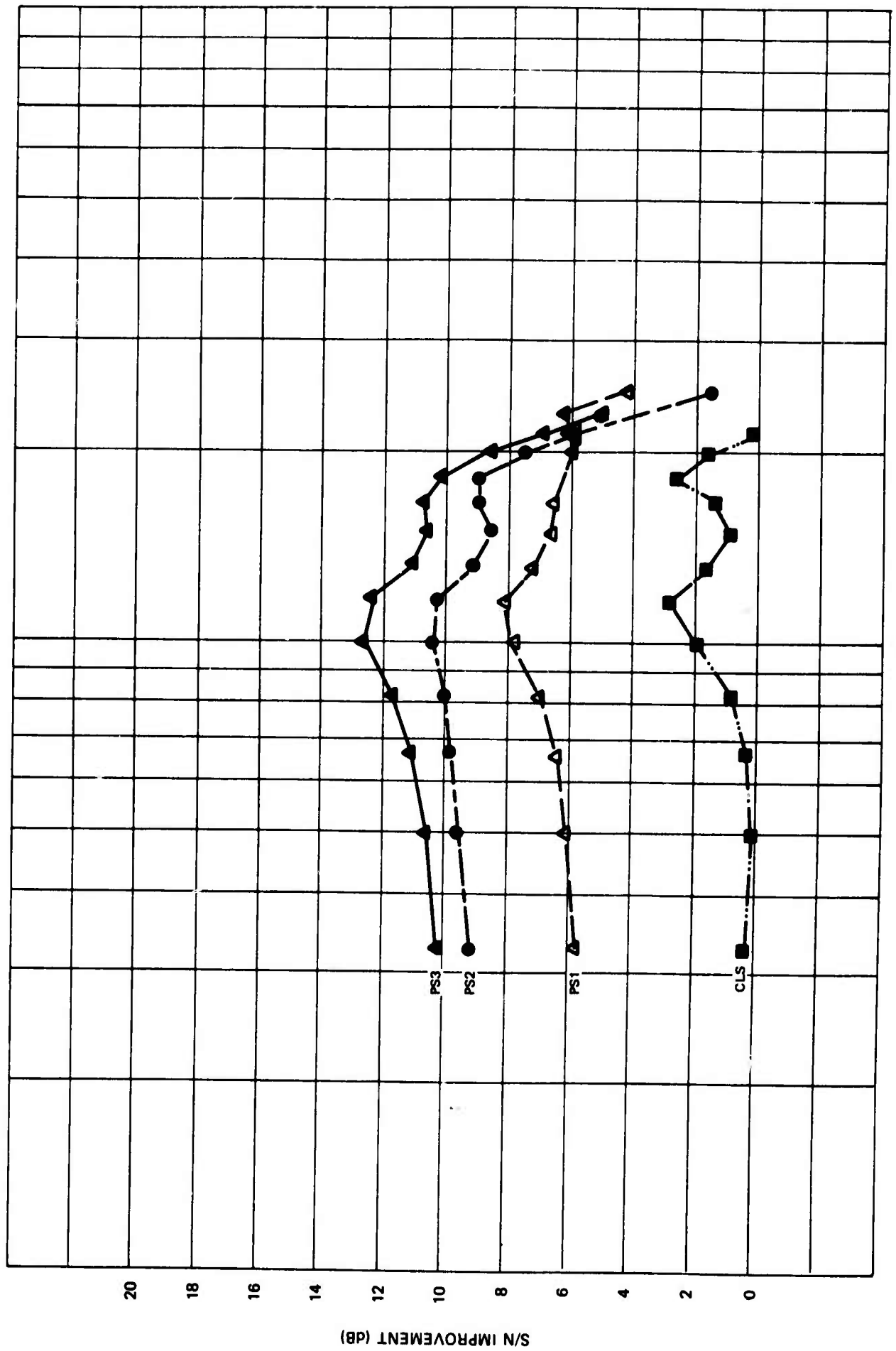

G 4526

Figure 17. Signal-to-noise improvement for data sample 17

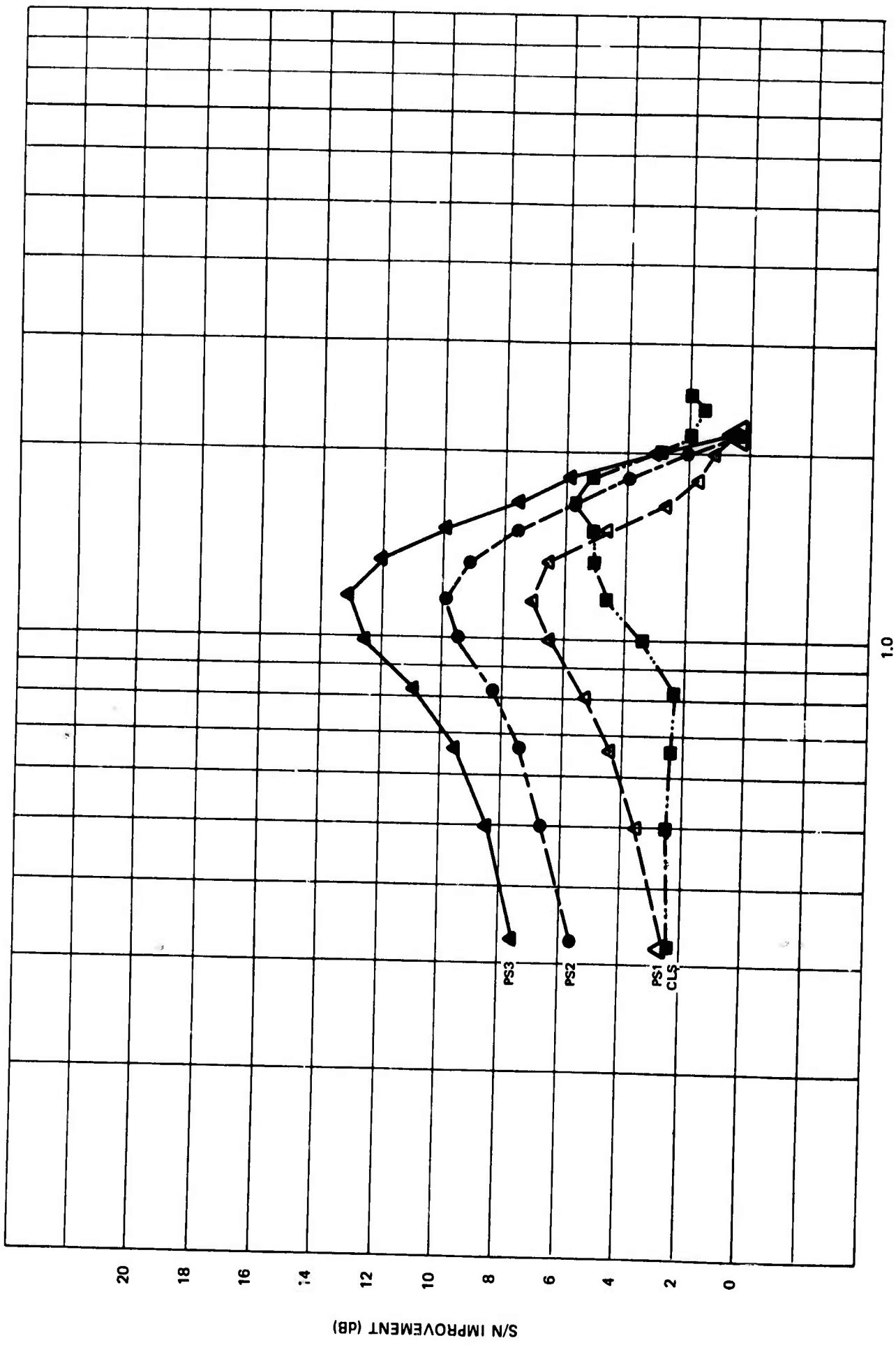

G 4527

Figure 18. Signal-to-noise improvement for data sample 18

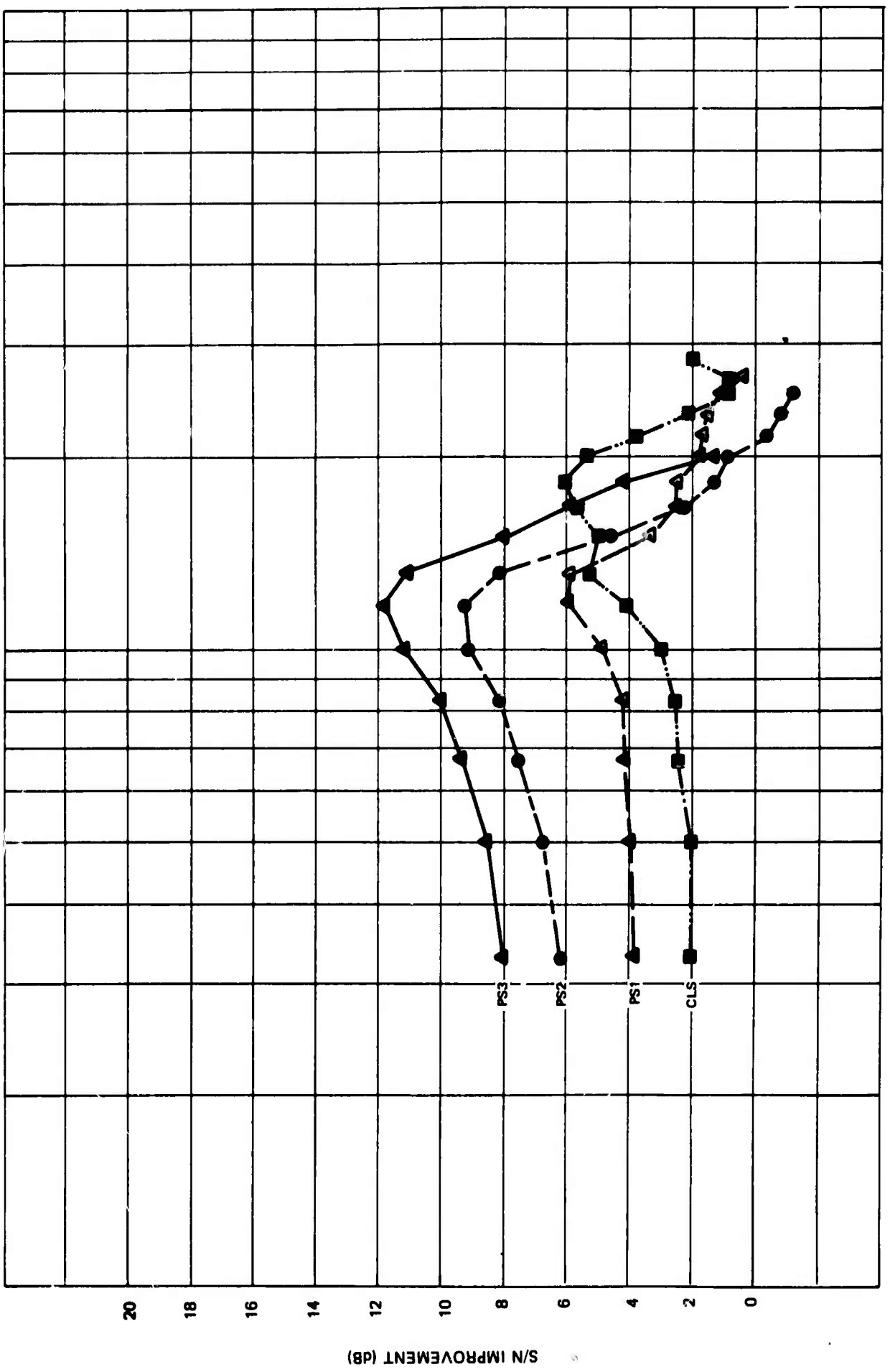

G 4528

Figure 19. Signal-to-noise improvement for data sample 19

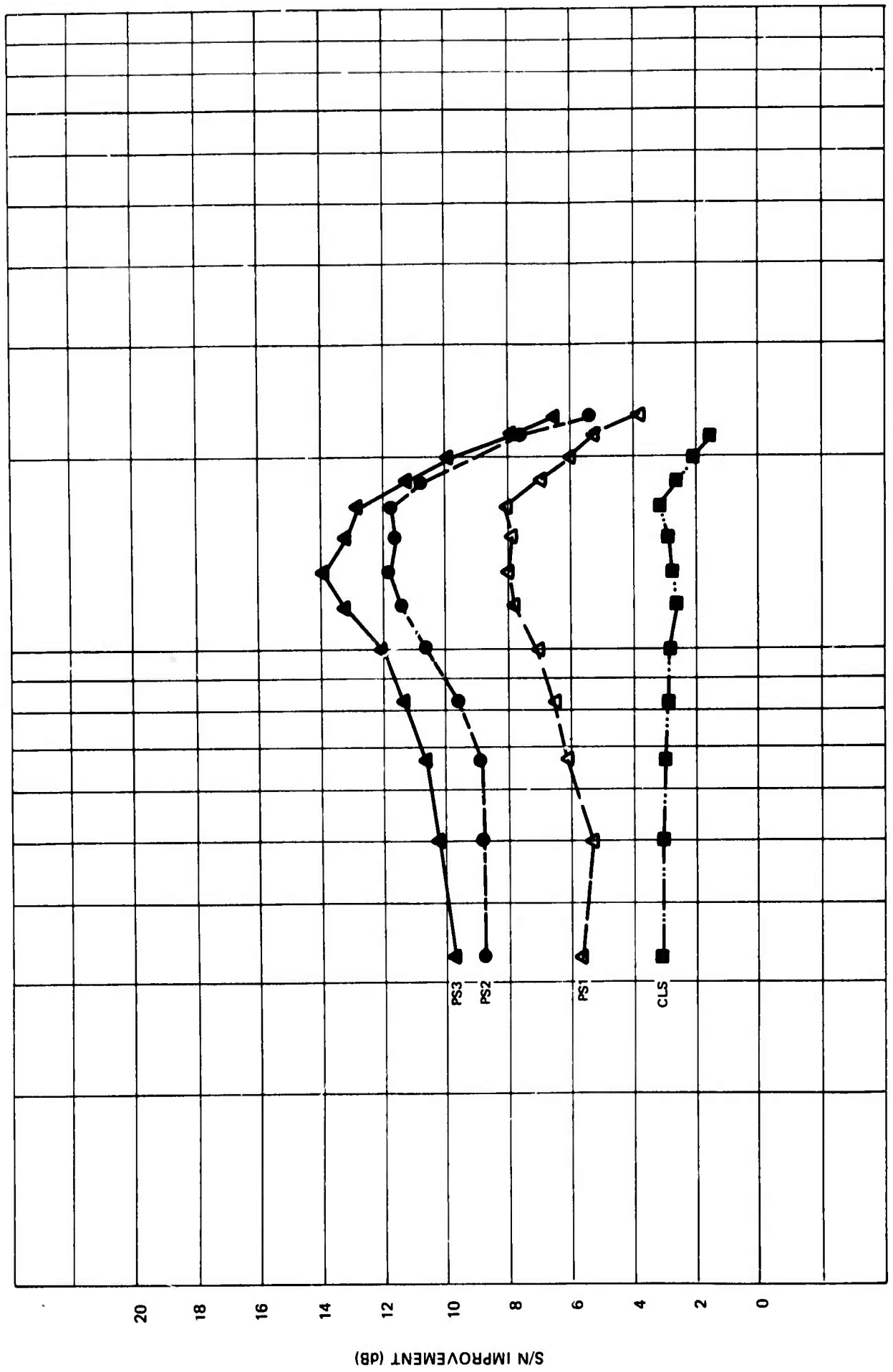

G 4529

Figure 20. Signal-to-noise improvement for data sample 20

APPENDIX 5 to TECHNICAL REPORT NO. 68-47

NOISE AND SIGNAL POWER SPECTRA FOR EACH DATA SAMPLE

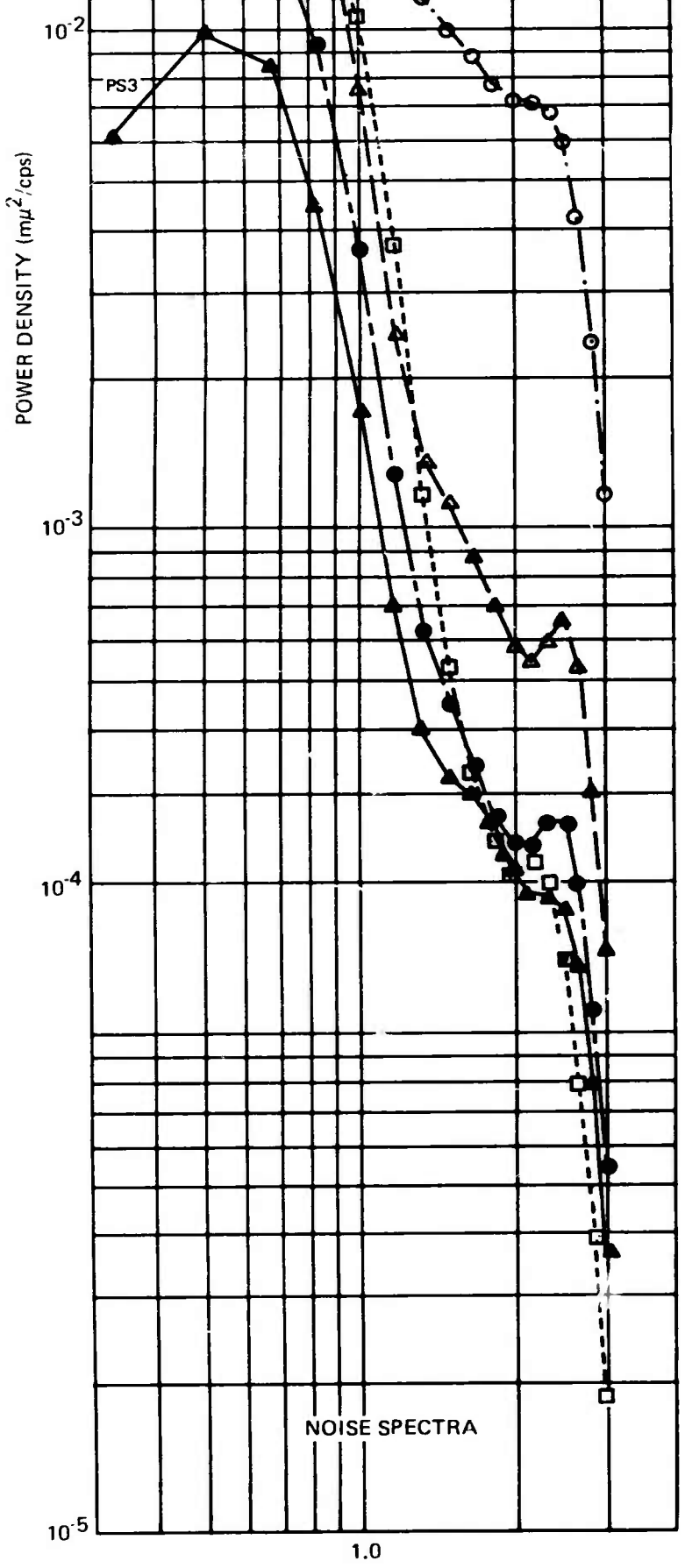
POWER DENSITY (mμ²/cps)
10⁻²
10⁻³
10⁻⁴
10⁻⁵
PS3
NOISE SPECTRA
1.0
FREQUENCY (cps)

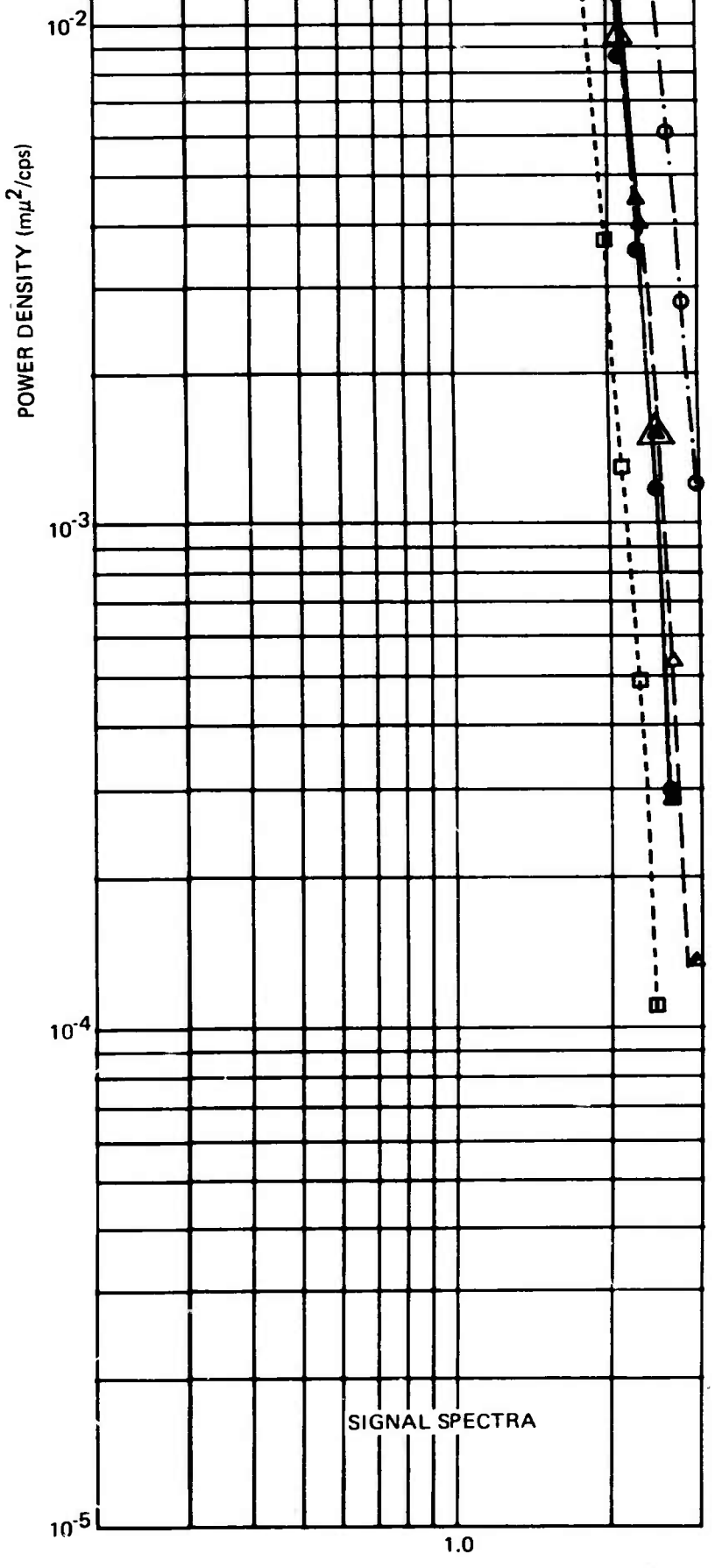
POWER DENSITY (mμ²/cps)
10⁻²
10⁻³
10⁻⁴
10⁻⁵
SIGNAL SPECTRA
1.0
FREQUENCY (cps)

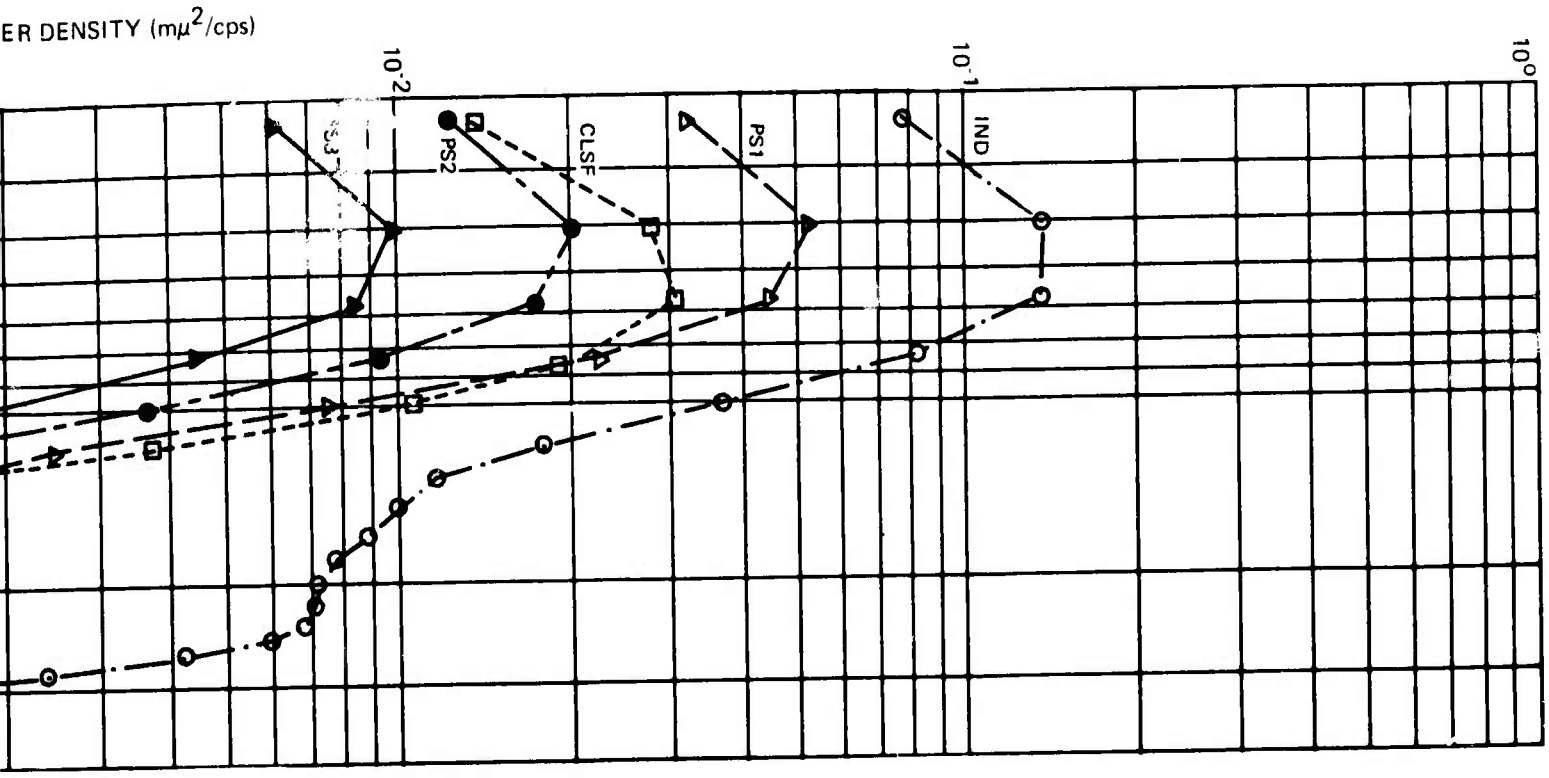

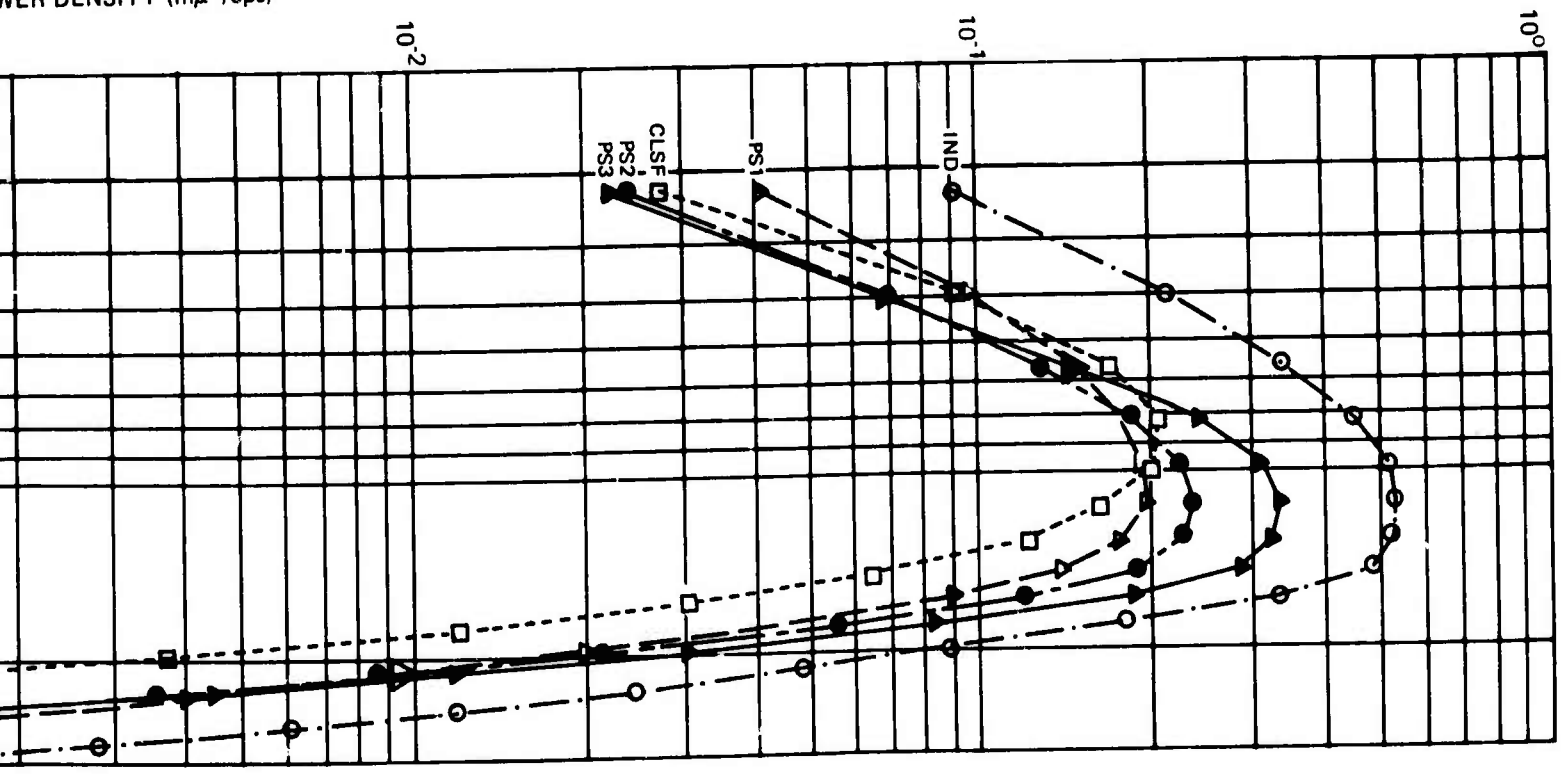

Figure 1. Noise reduction ratios for data sample 1

G 4530

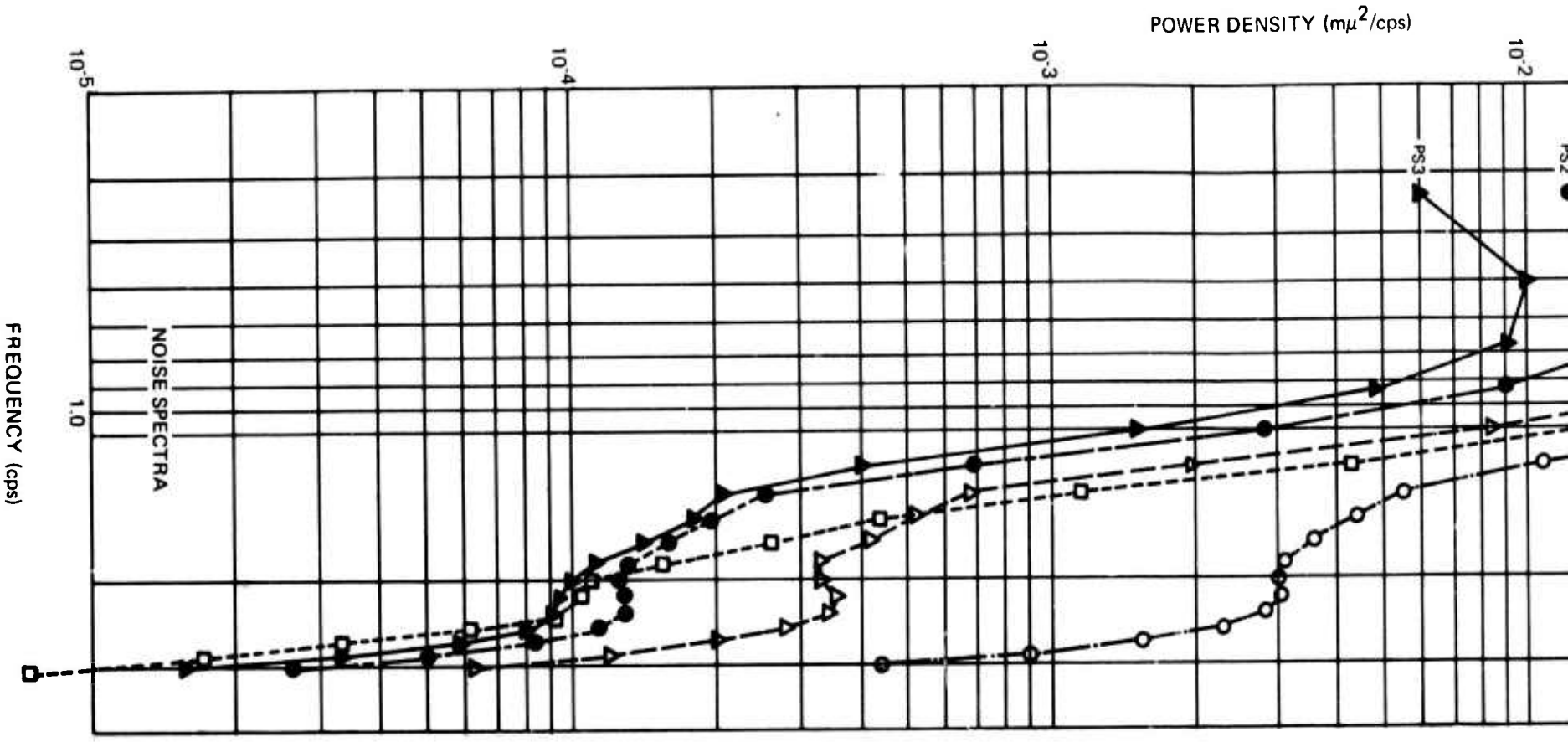
POWER DENSITY (mμ²/cps)
10⁻⁵
10⁻⁴
10⁻³
10⁻²
PS3
NOISE SPECTRA
1.0
FREQUENCY (cps)

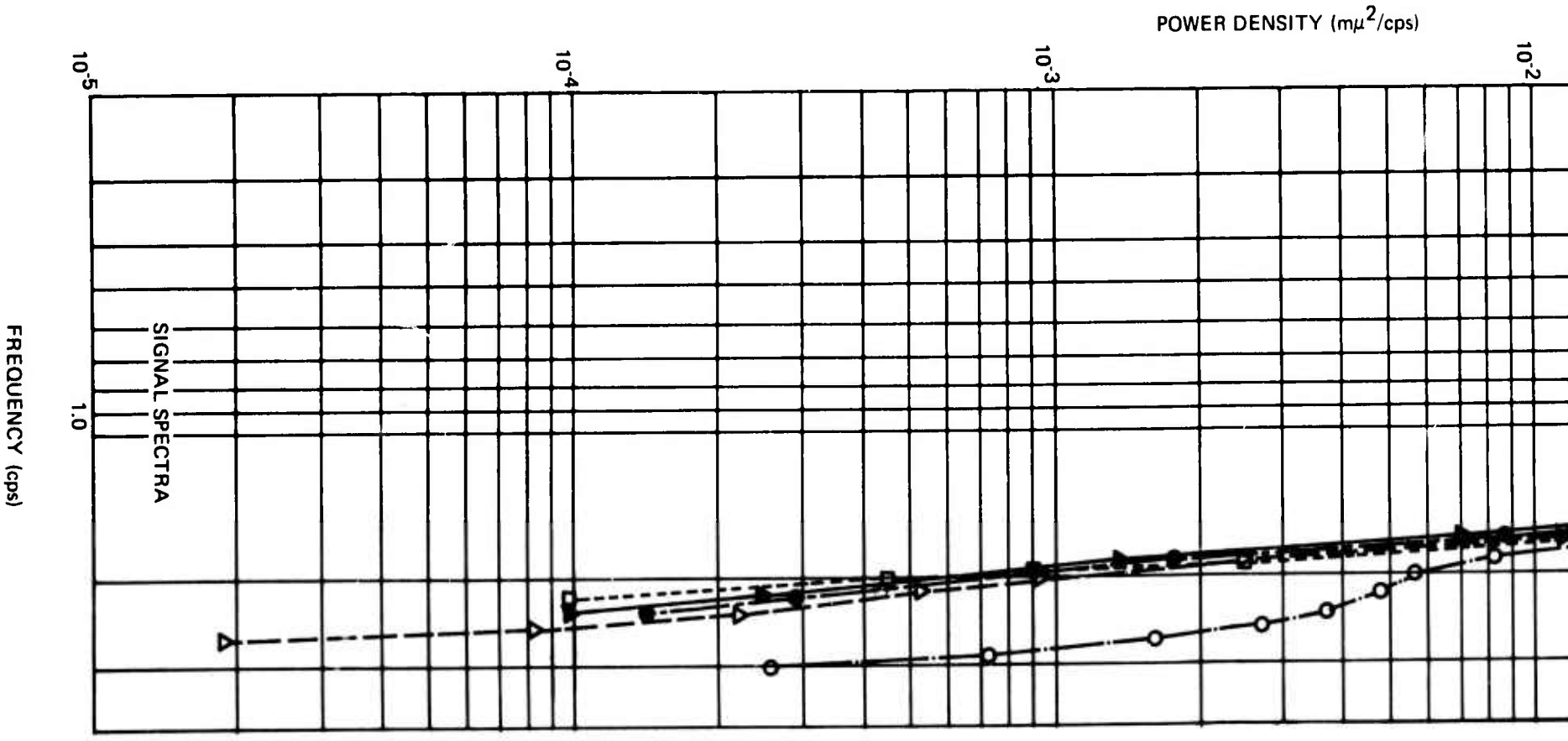
POWER DENSITY (mμ²/cps)
10⁻⁵
10⁻⁴
10⁻³
10⁻²
SIGNAL SPECTRA
1.0
FREQUENCY (cps)

A

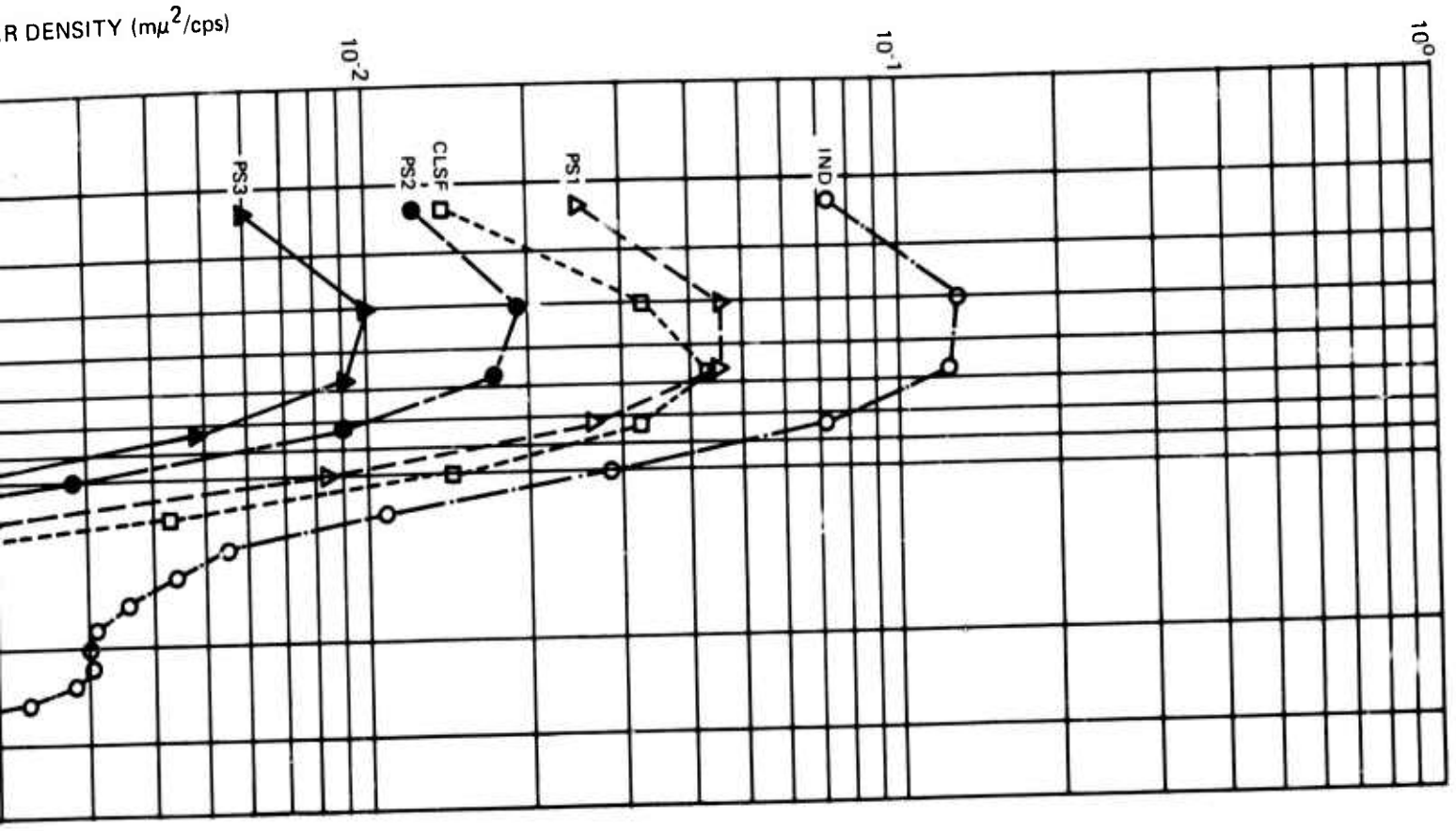

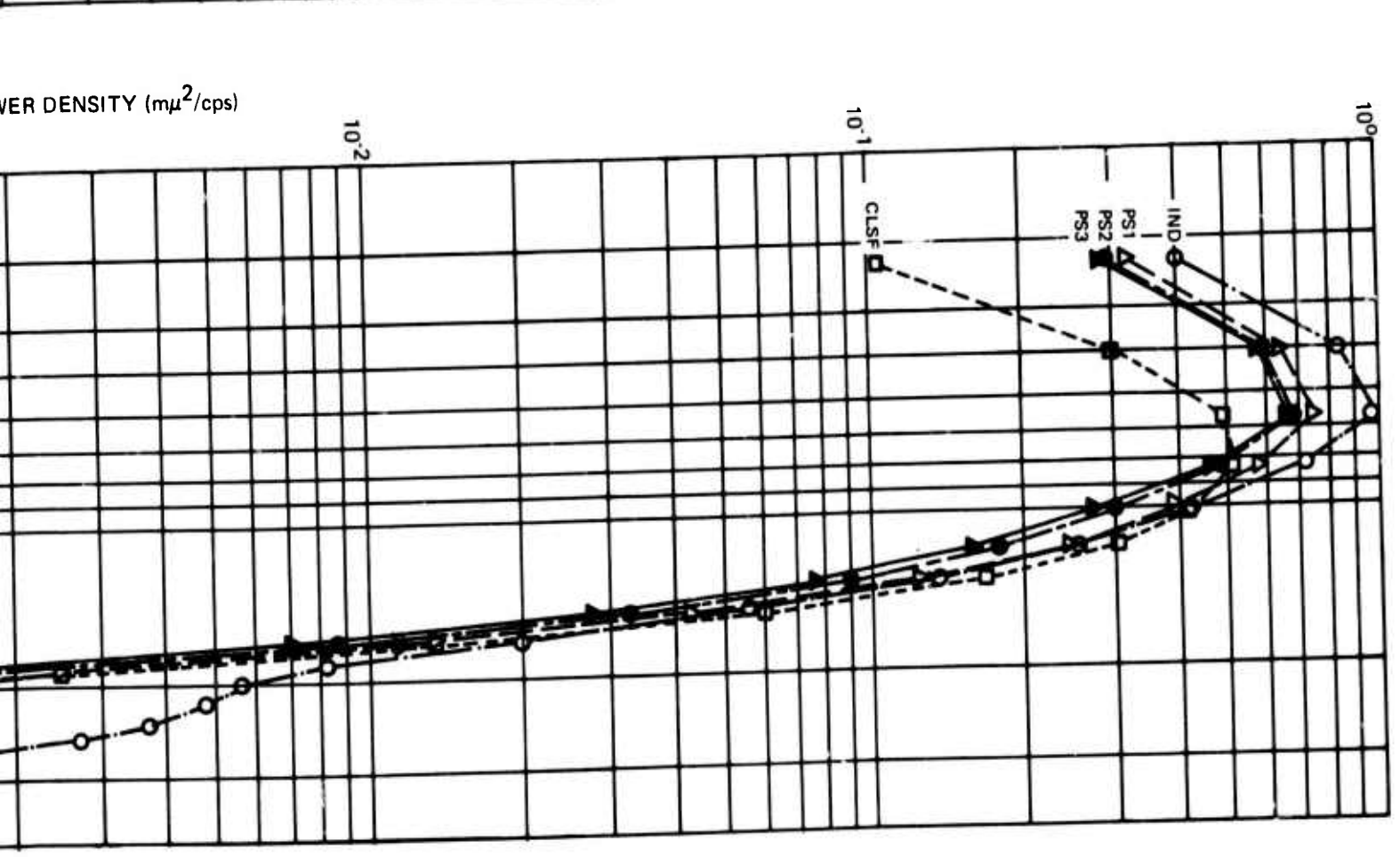

G 4531

Figure 2. Noise reduction ratios for data sample 2

B

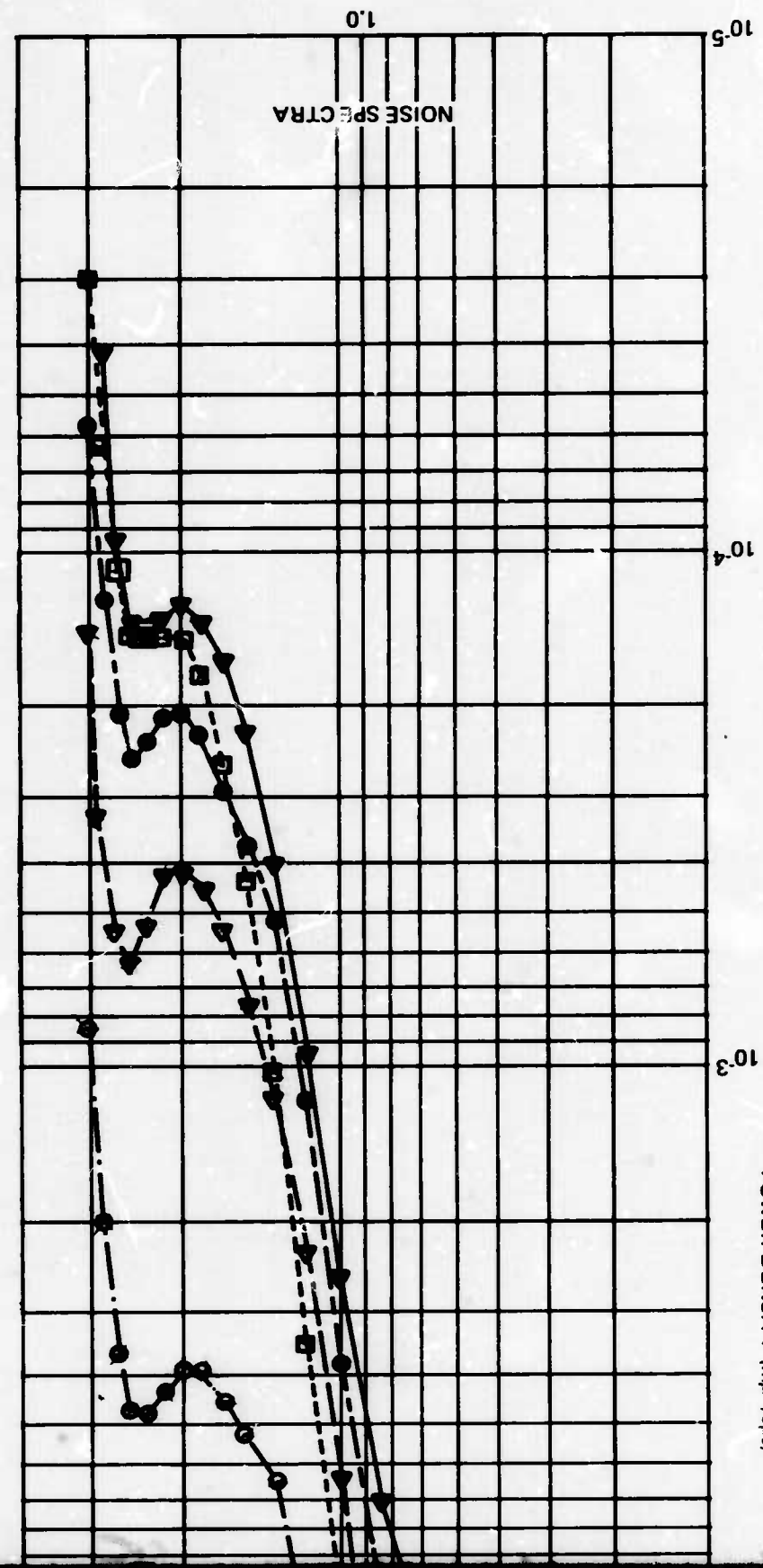
NOISE SPECTRA
FREQUENCY (cps)
1.0
10^{-5}
10^{-4}
10^{-3}
POWER DENSITY ($m\mu^2$/cps)

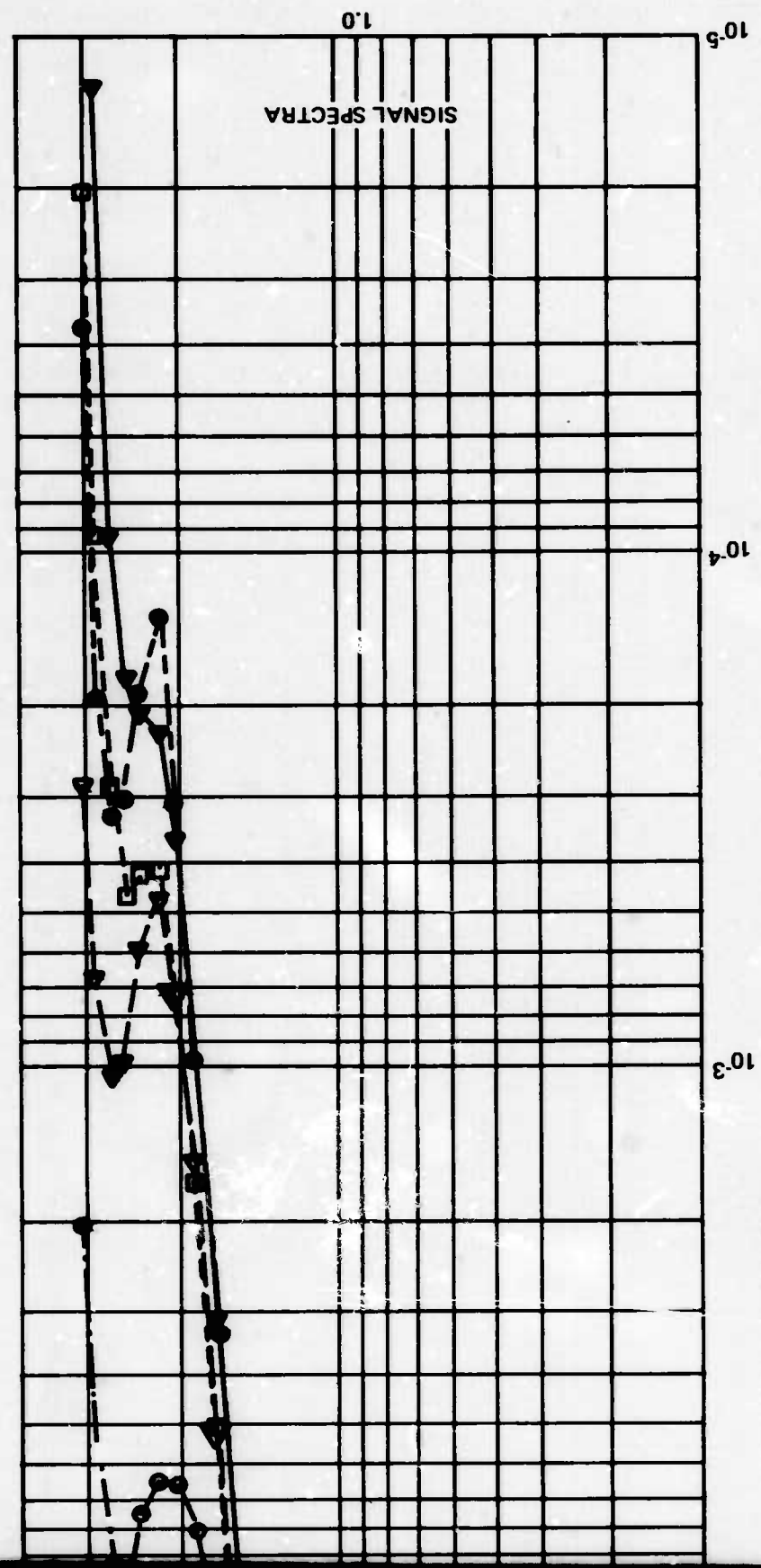
SIGNAL SPECTRA
FREQUENCY (cps)
1.0
10^{-5}
10^{-4}
10^{-3}
POWER DENSITY ($m\mu^2$/cps)

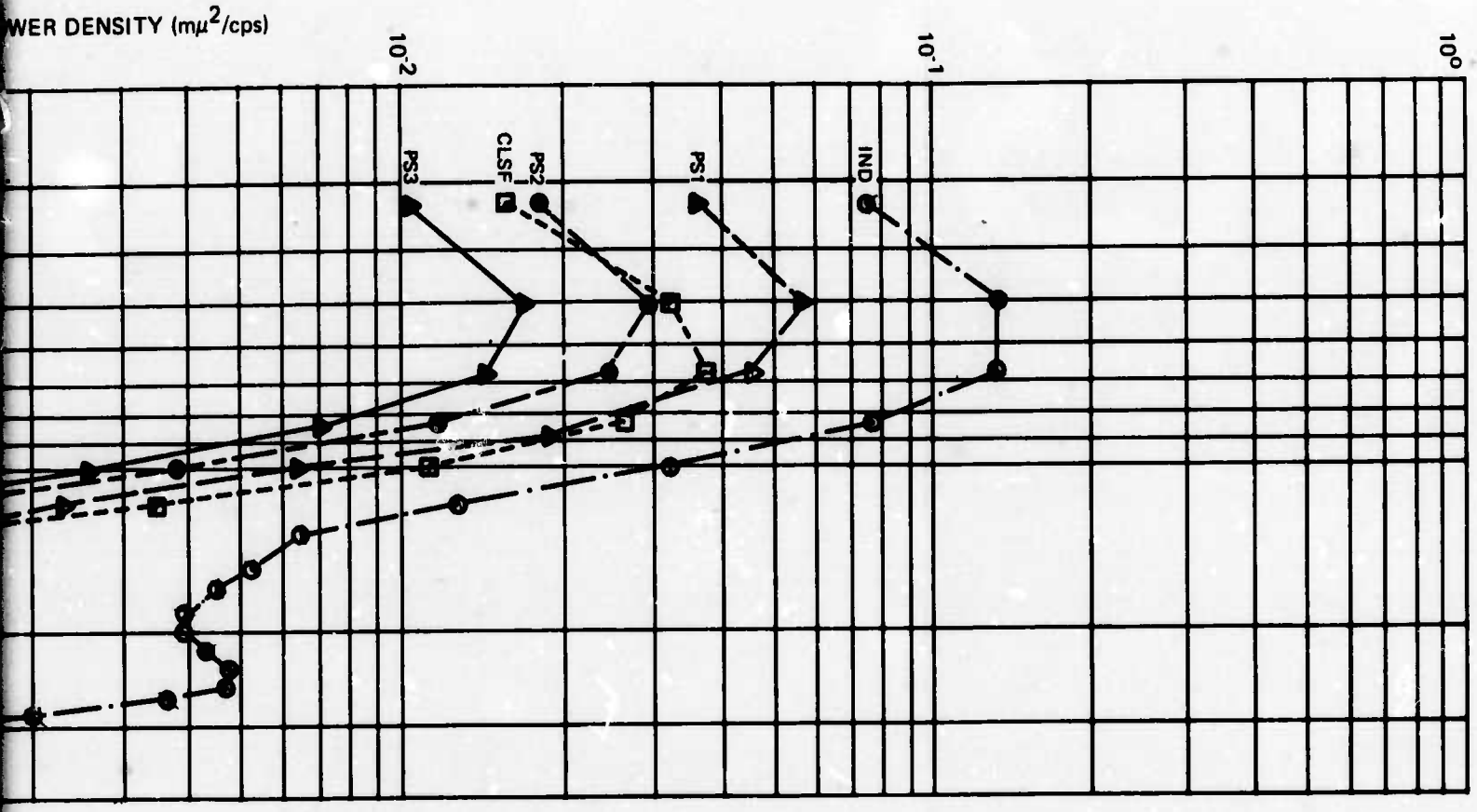

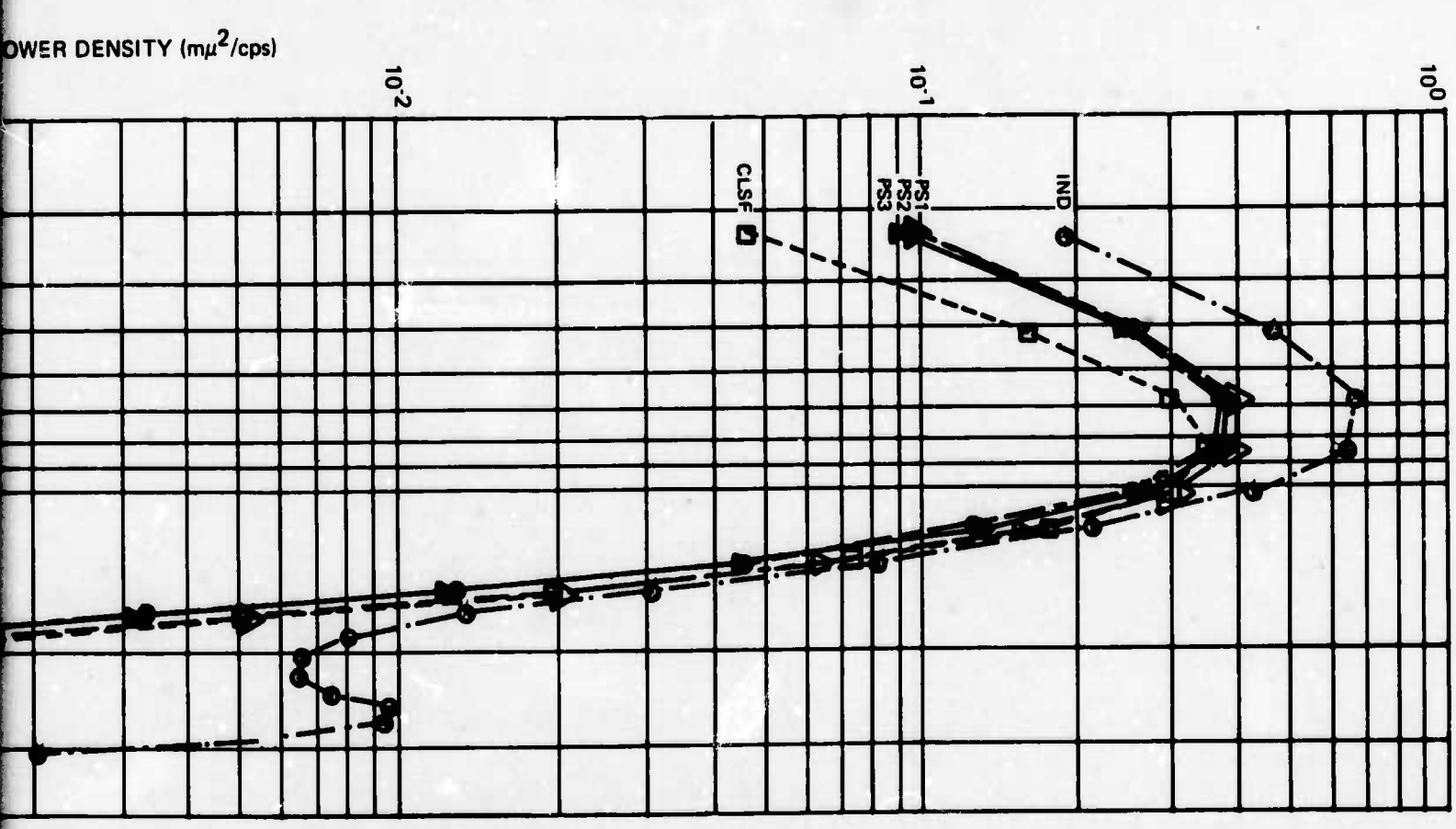

G 4532

Figure 3. Noise reduction ratios for data sample 3

B

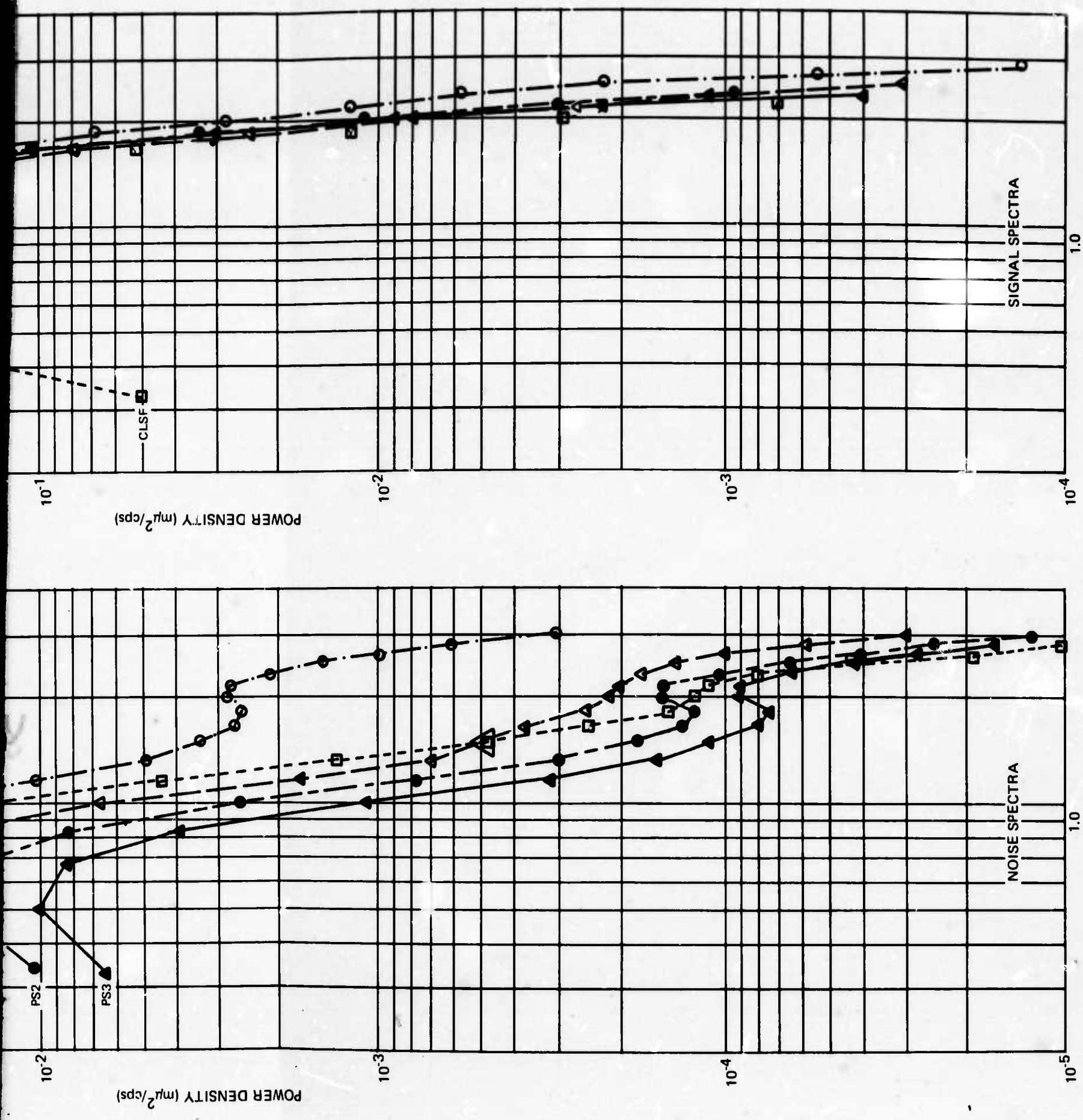
SIGNAL SPECTRA
FREQUENCY (cps)
POWER DENSITY (mμ²/cps)
10⁻¹
10⁻²
10⁻³
10⁻⁴
1.0
CLSF
NOISE SPECTRA
FREQUENCY (cps)
POWER DENSITY (mμ²/cps)
10⁻²
10⁻³
10⁻⁴
10⁻⁵
1.0
PS2
PS3

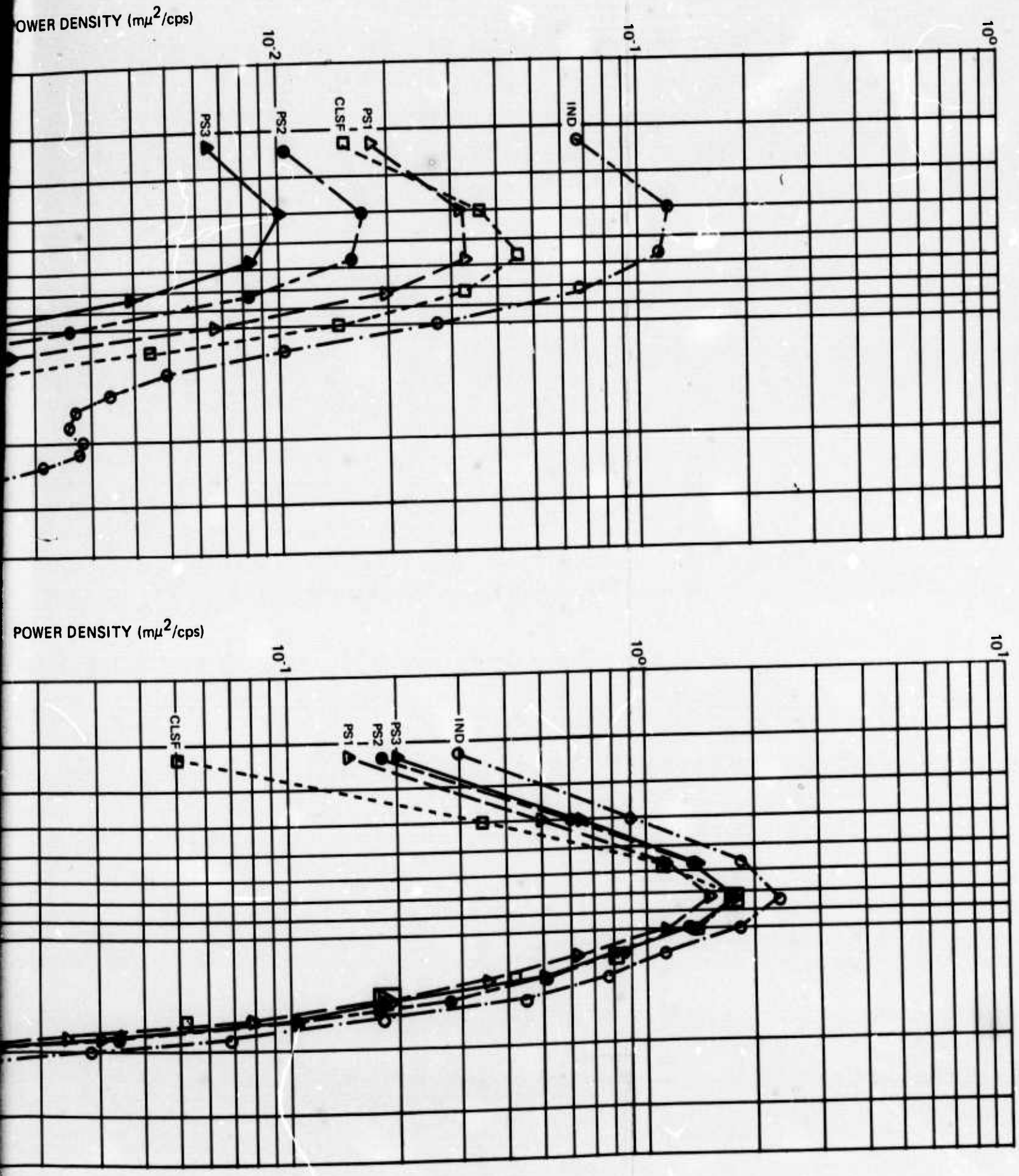

Figure 4. Noise reduction ratios for data sample 4

G 4533

B

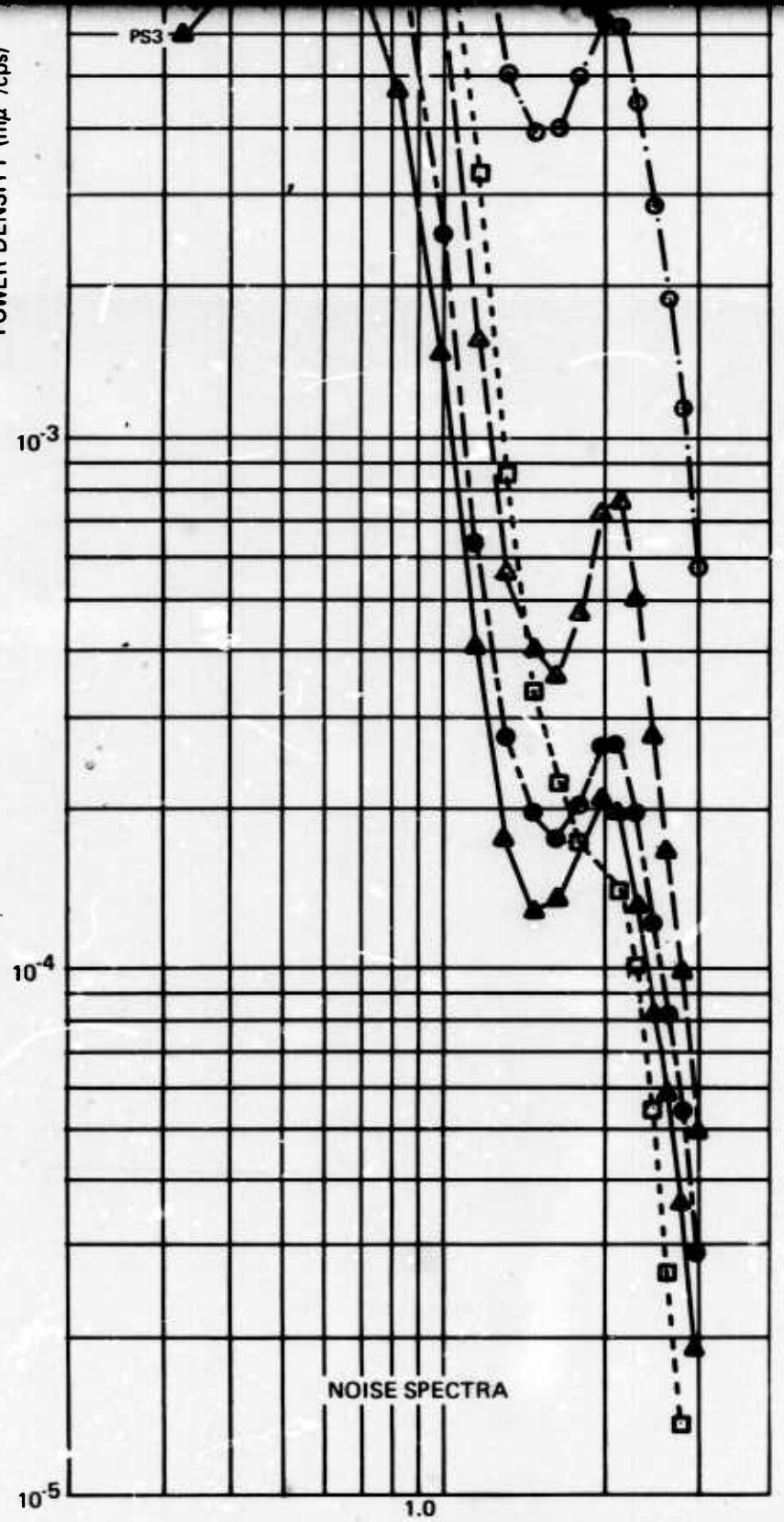
PS3
POWER DENSITY (mμ²/cps)
10⁻³
10⁻⁴
10⁻⁵
NOISE SPECTRA
1.0
FREQUENCY (cps)

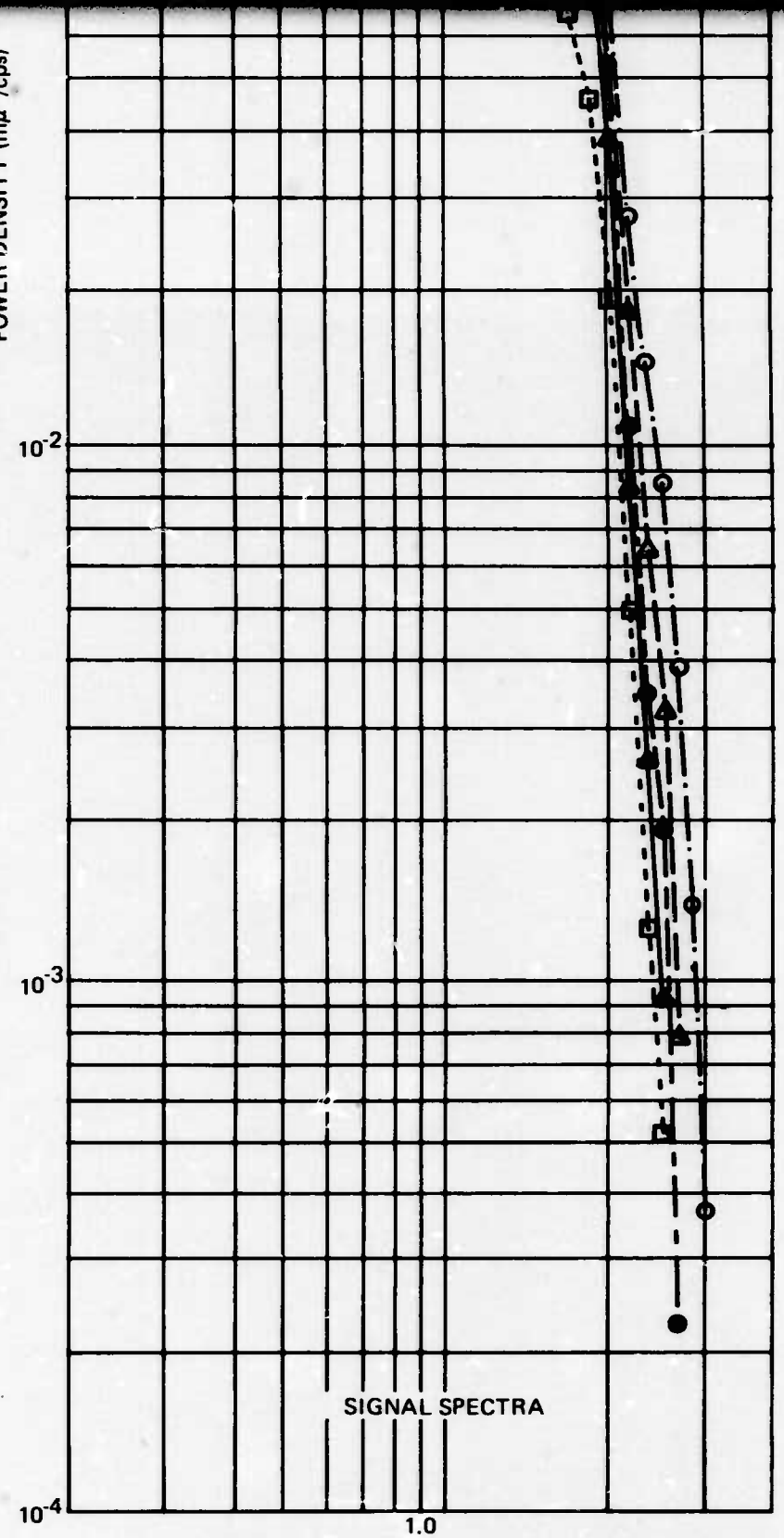
POWER DENSITY (mμ²/cps)
10⁻²
10⁻³
10⁻⁴
SIGNAL SPECTRA
1.0
FREQUENCY (cps)

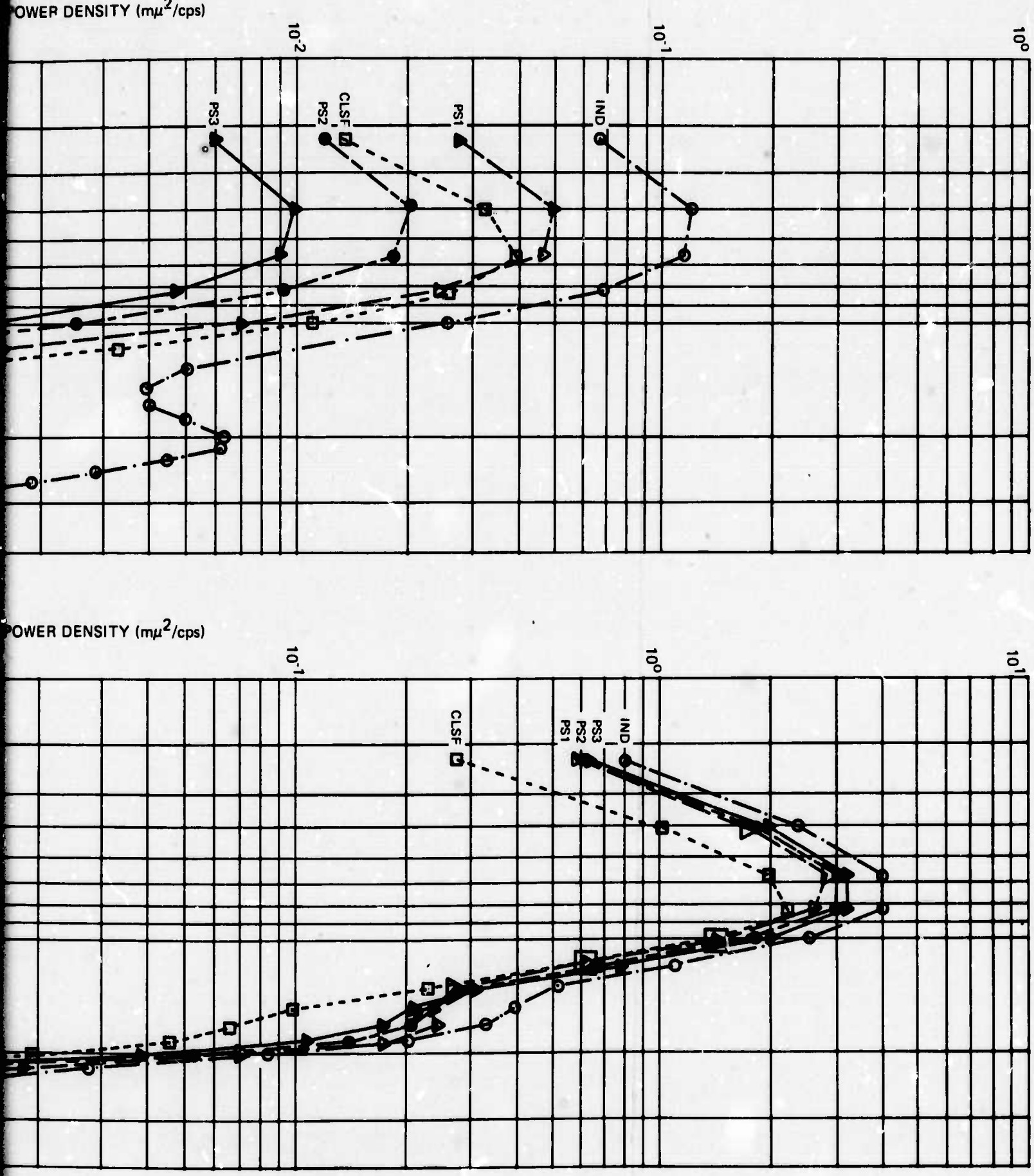

G 4534

Figure 5. Noise reduction ratios for data sample 5

B

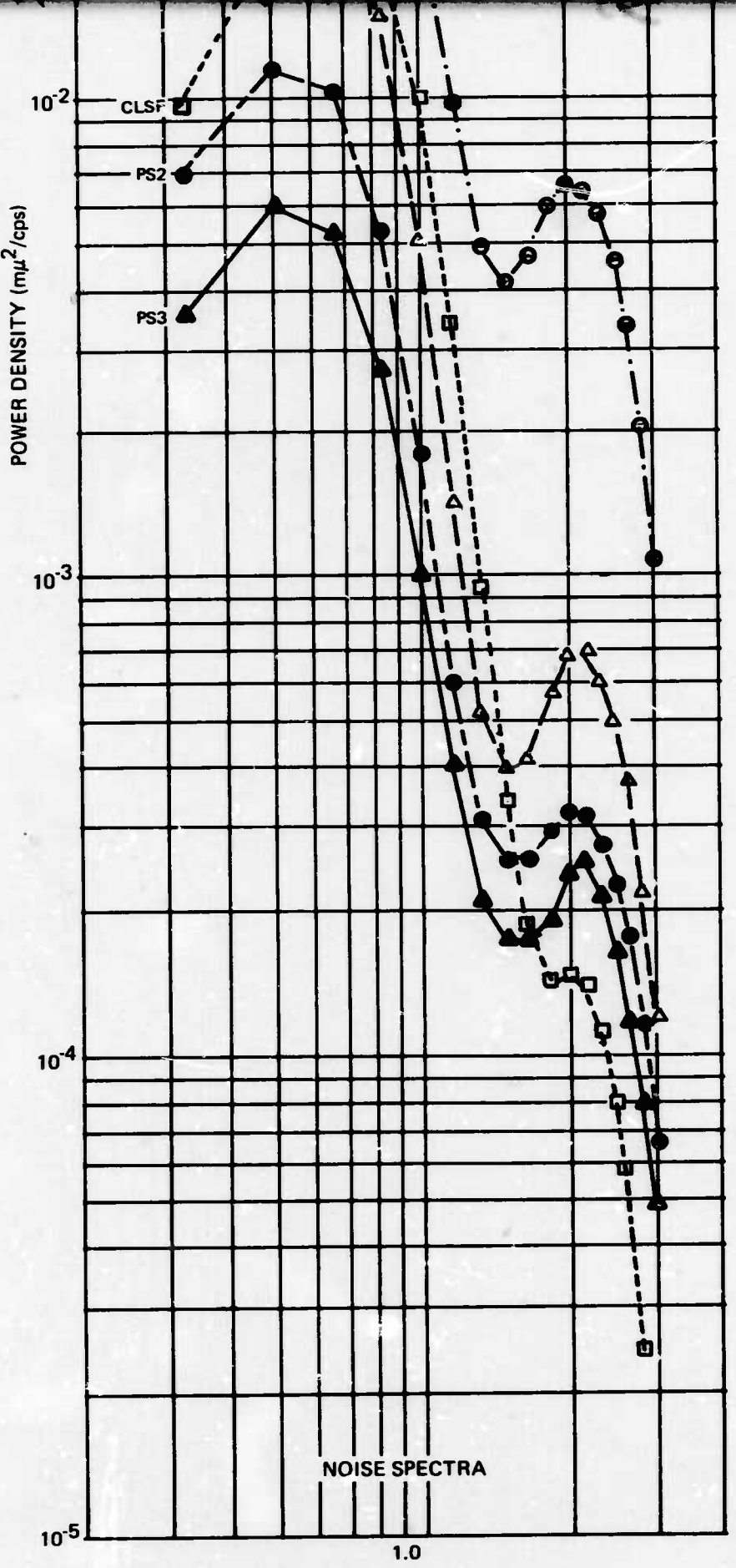
CLSF
PS2
PS3
10^{-2}
10^{-3}
10^{-4}
10^{-5}
POWER DENSITY ($m\mu^2$/cps)
NOISE SPECTRA
1.0
FREQUENCY (cps)

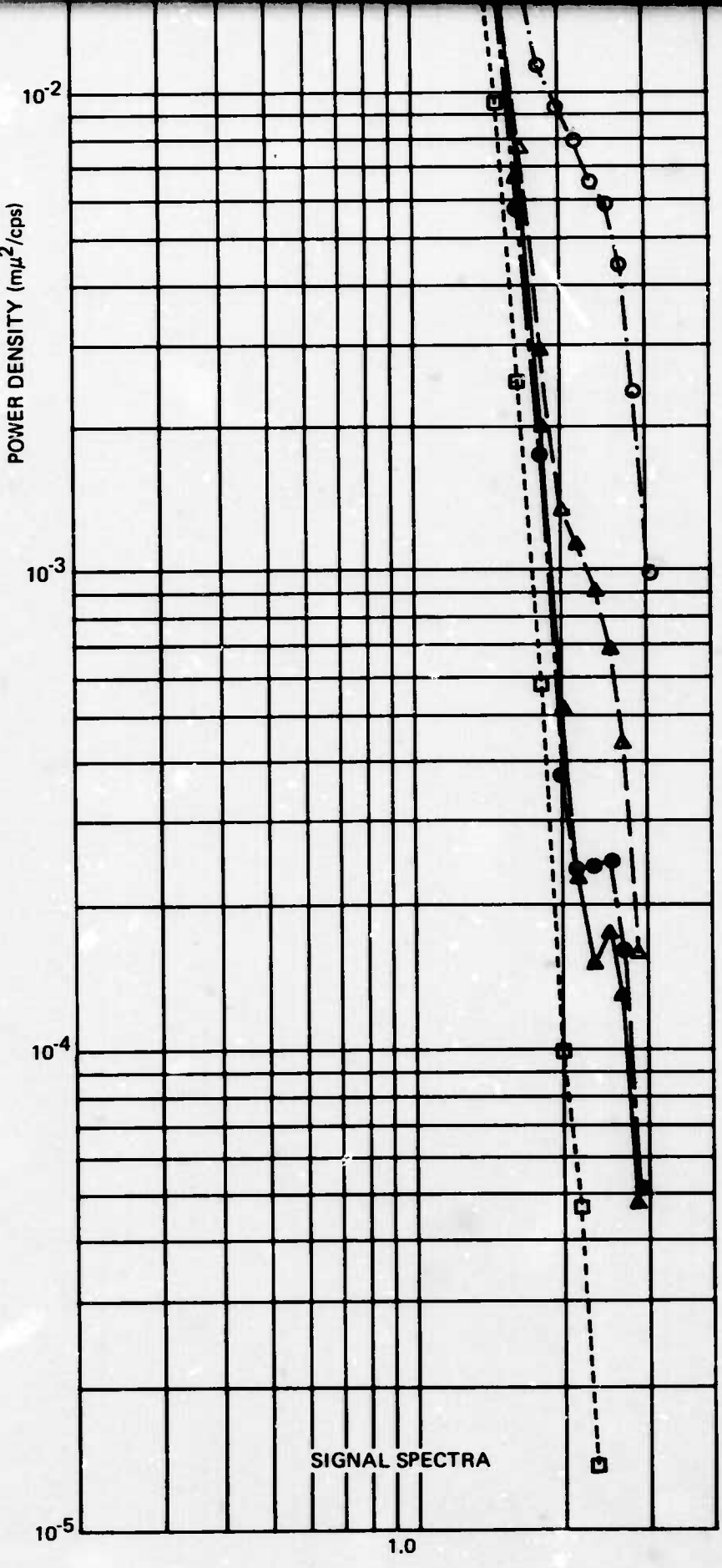
10^{-2}
10^{-3}
10^{-4}
10^{-5}
POWER DENSITY ($m\mu^2$/cps)
SIGNAL SPECTRA
1.0
FREQUENCY (cps)

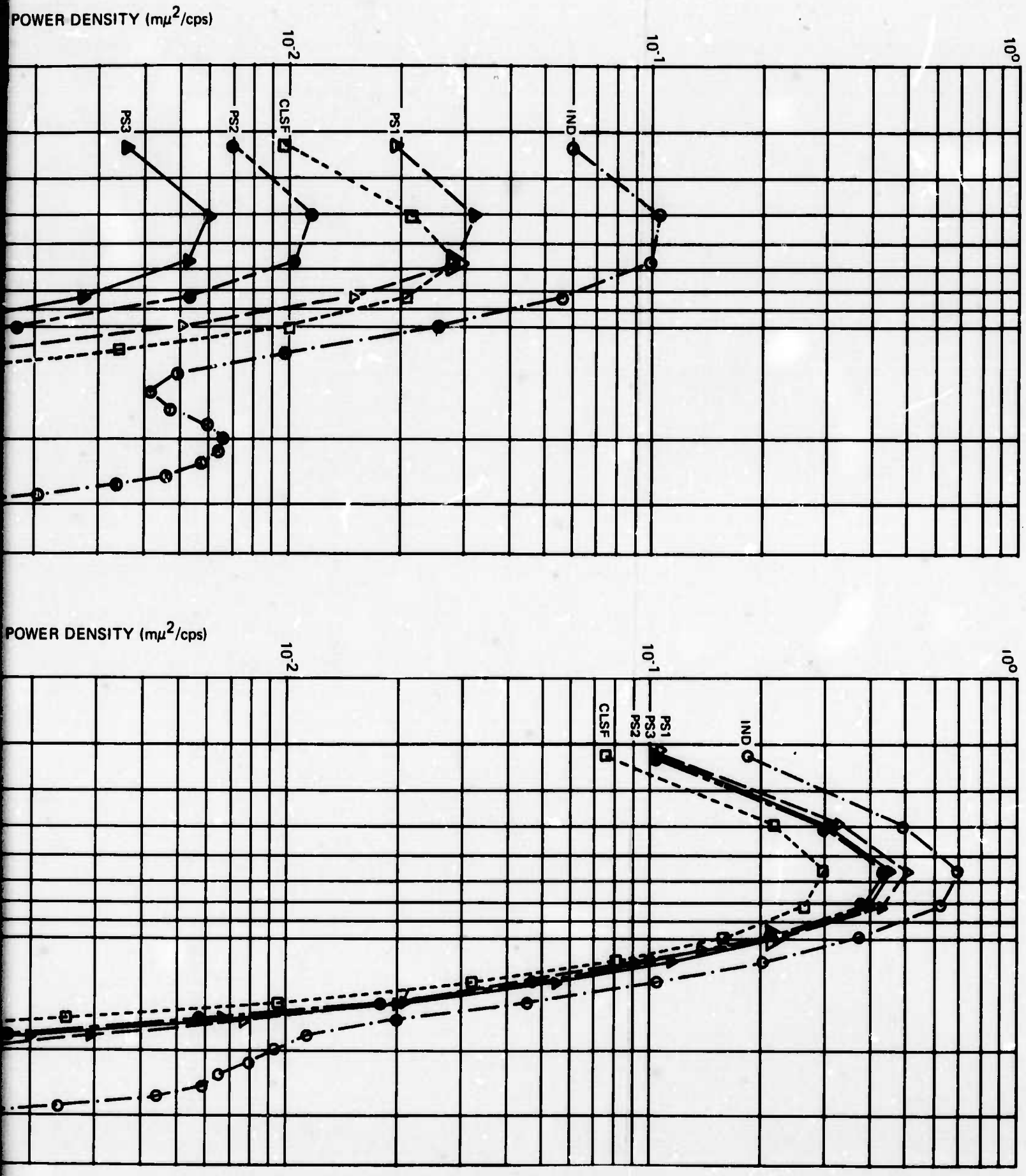

G 4535

Figure 6. Noise reduction ratios for data sample 6

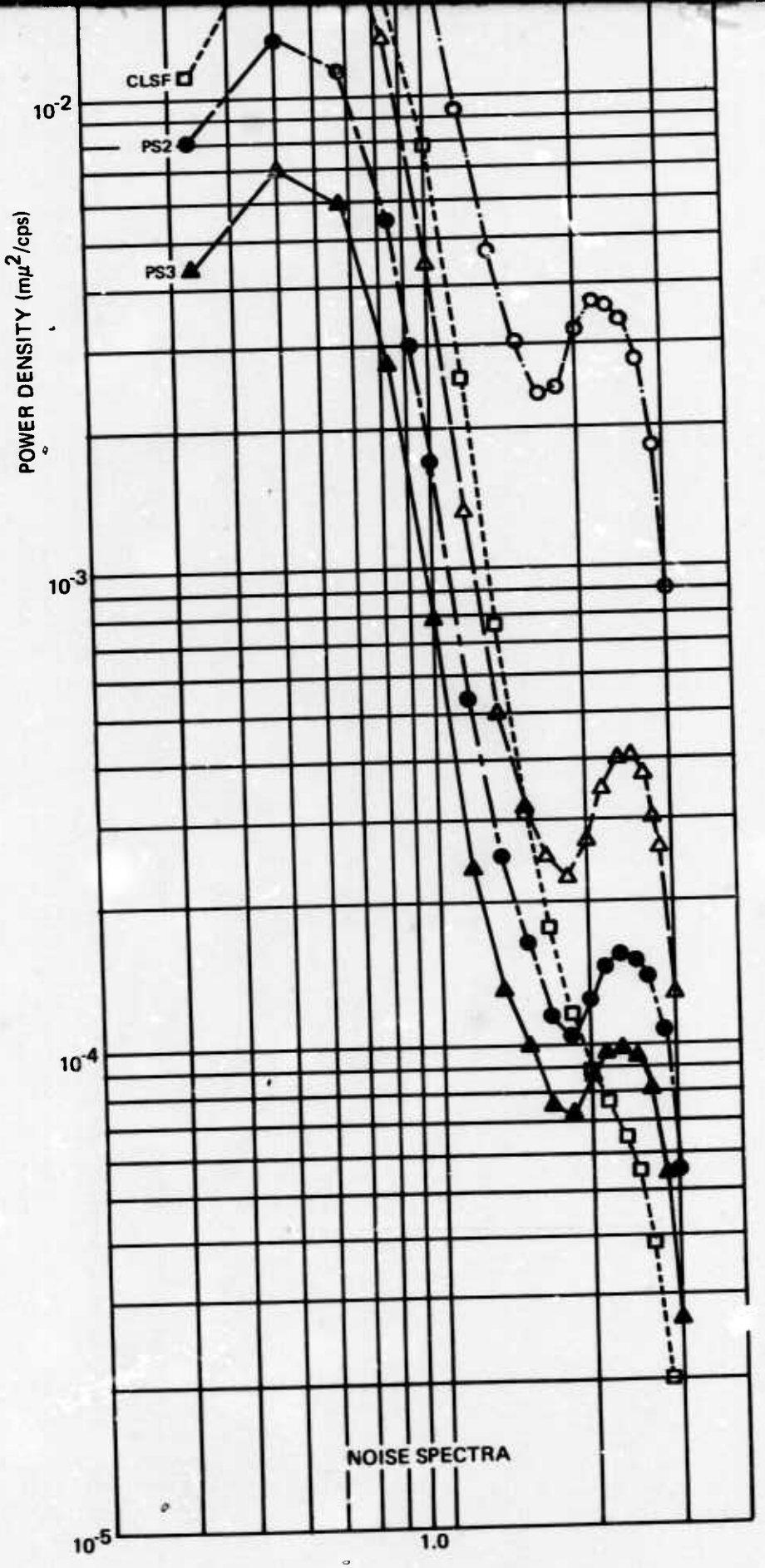
CLSF
PS2
PS3
10^{-2}
10^{-3}
10^{-4}
10^{-5}
POWER DENSITY ($m\mu^2$/cps)
1.0
NOISE SPECTRA
FREQUENCY (cps)

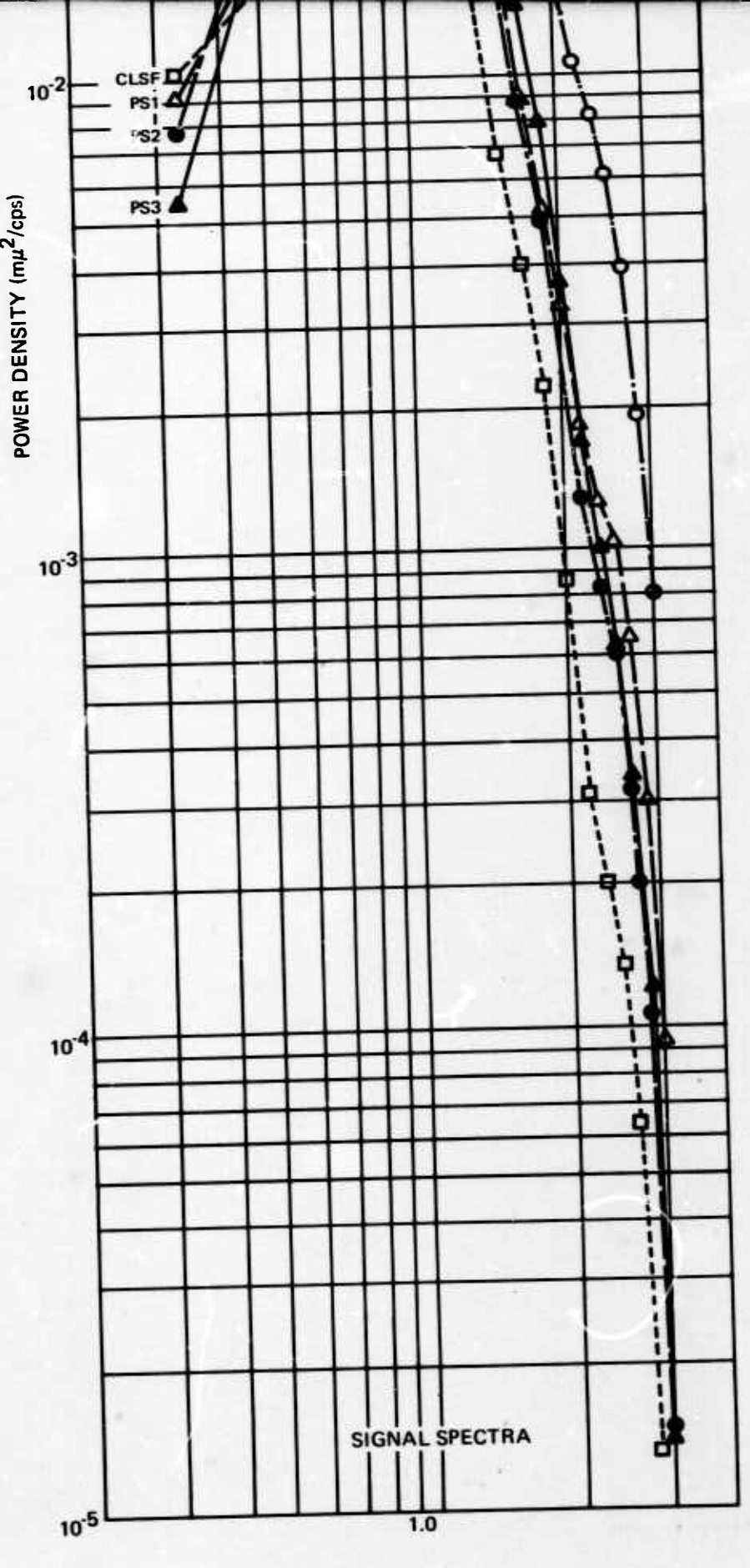
CLSF
PS1
PS2
PS3
10^{-2}
10^{-3}
10^{-4}
10^{-5}
POWER DENSITY ($m\mu^2$/cps)
1.0
SIGNAL SPECTRA
FREQUENCY (cps)

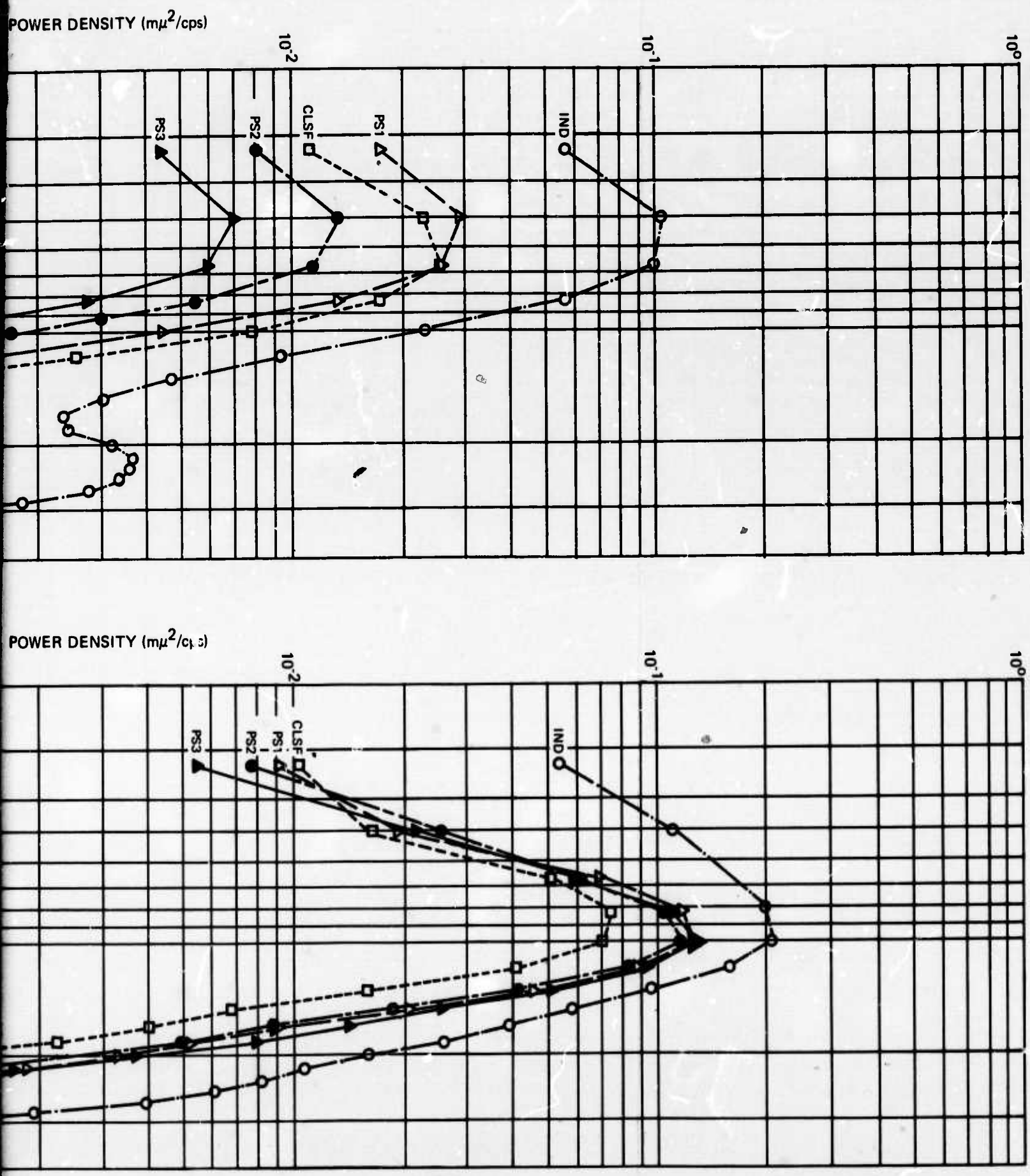

G 4536

Figure 7. Noise reduction ratios for data sample 7

B

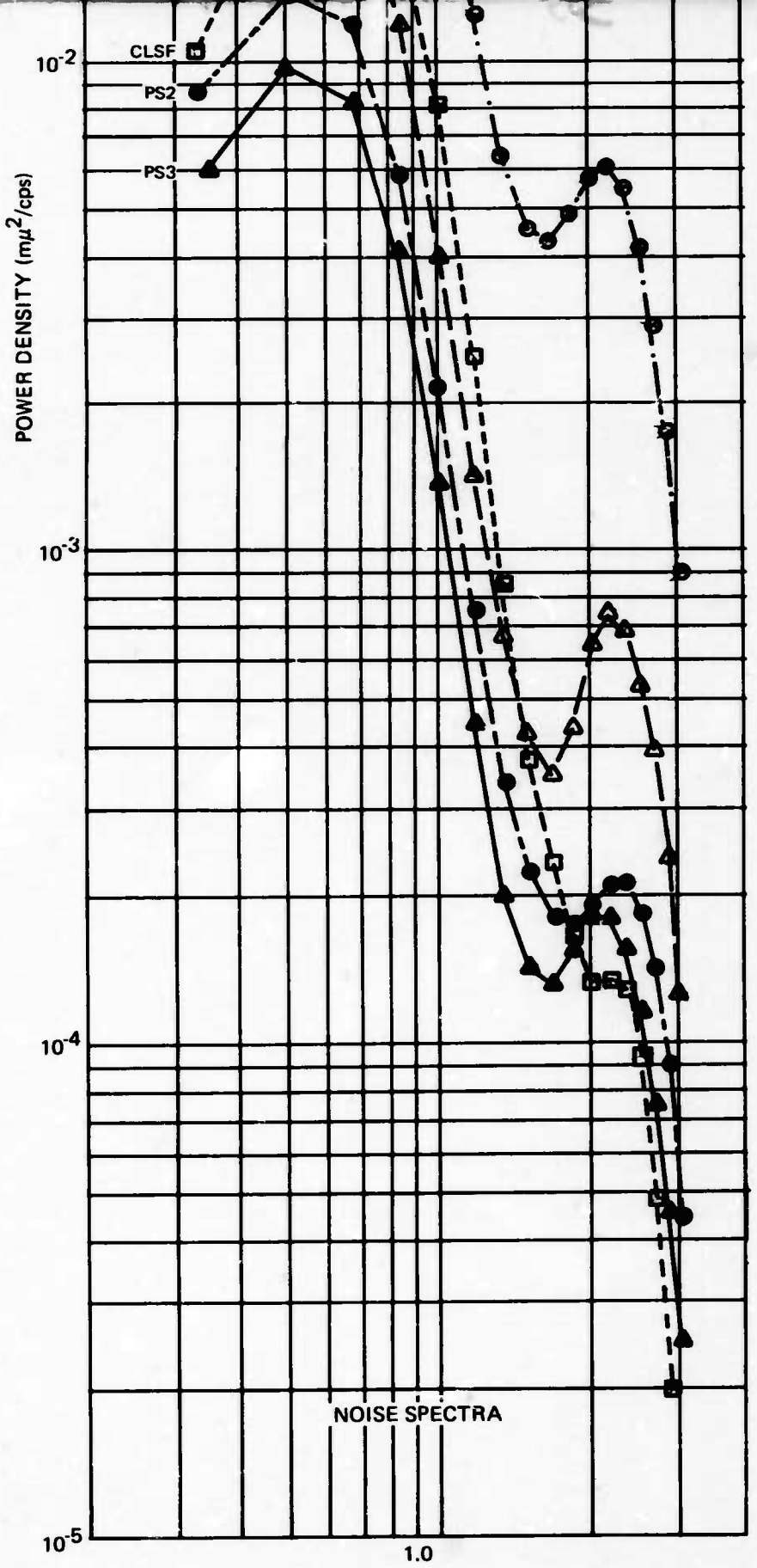
CLSF
PS2
PS3
10^{-2}
10^{-3}
10^{-4}
10^{-5}
POWER DENSITY (mμ²/cps)
1.0
NOISE SPECTRA
FREQUENCY (cps)

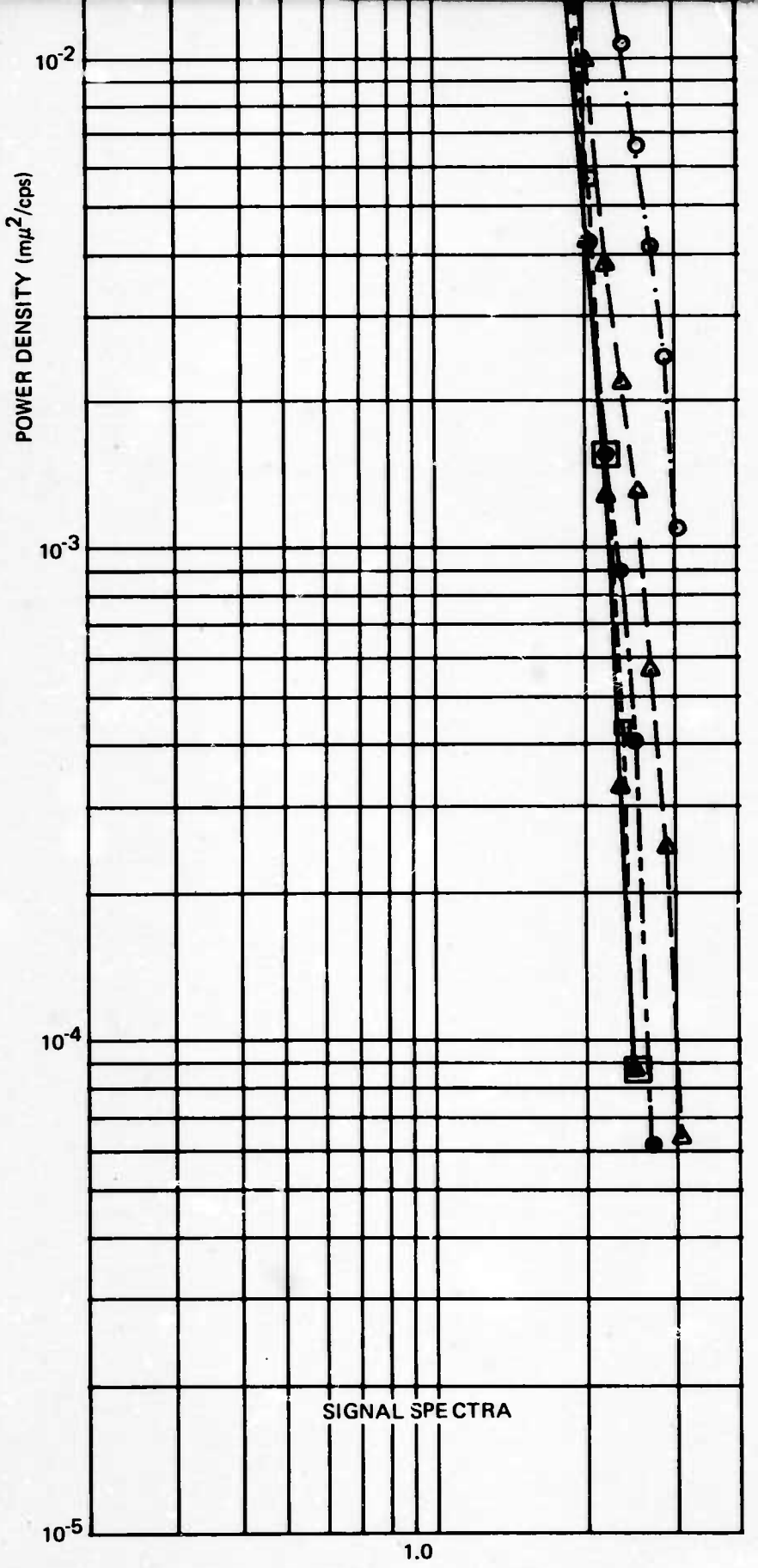
10^{-2}
10^{-3}
10^{-4}
10^{-5}
POWER DENSITY (mμ²/cps)
1.0
SIGNAL SPECTRA
FREQUENCY (cps)

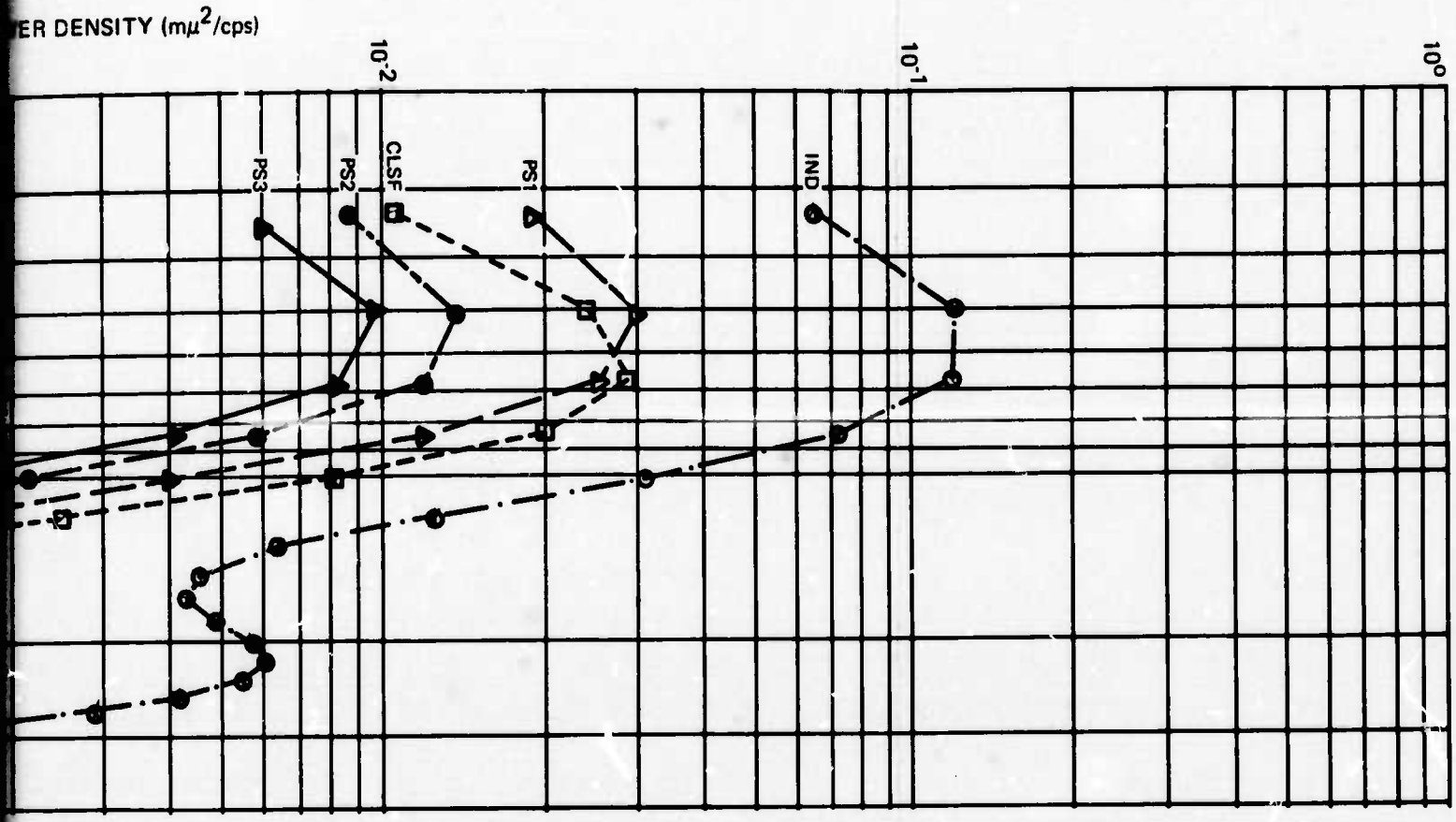

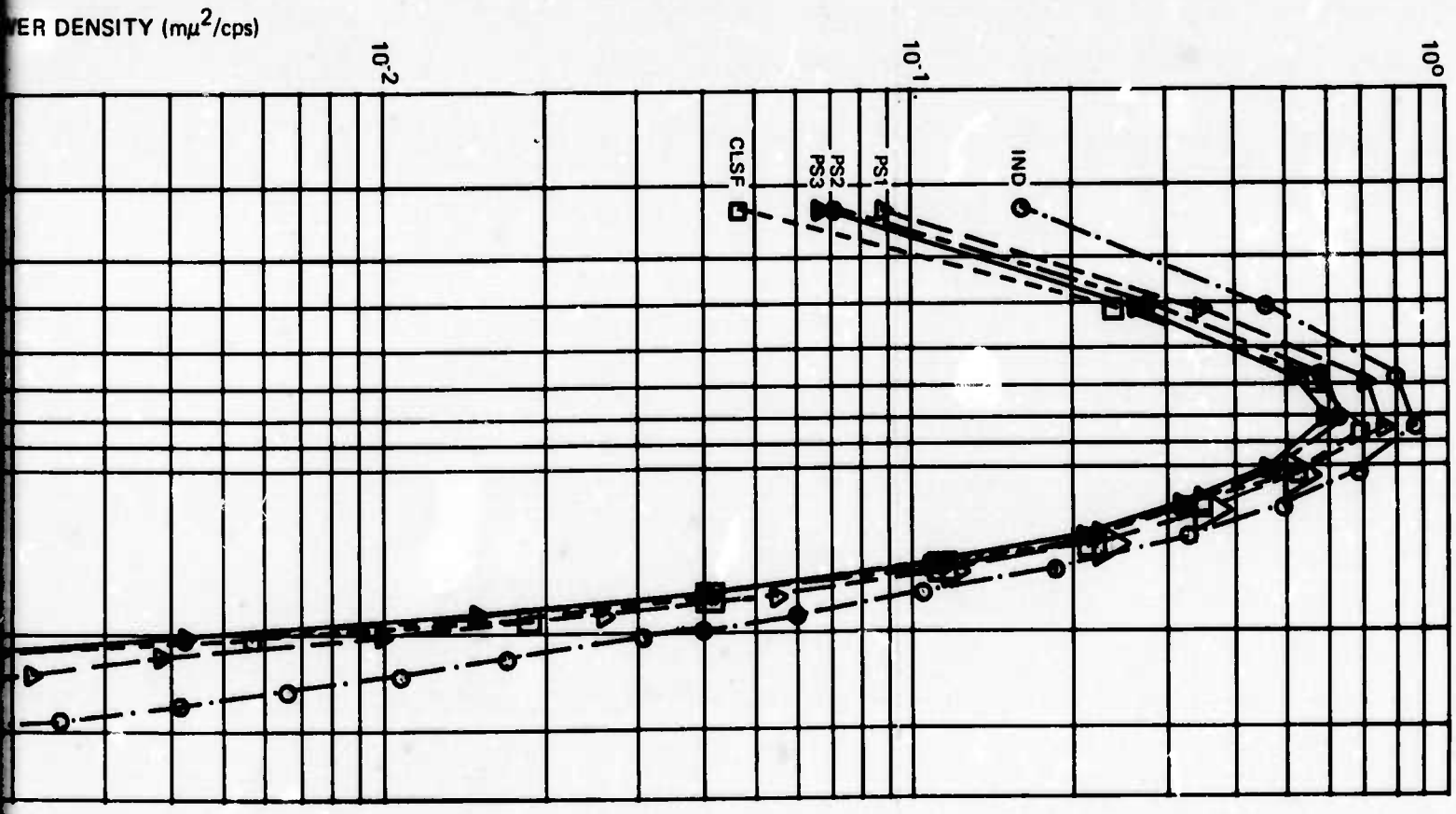

G 4537

Figure 8. Noise reduction ratios for data sample 8

B

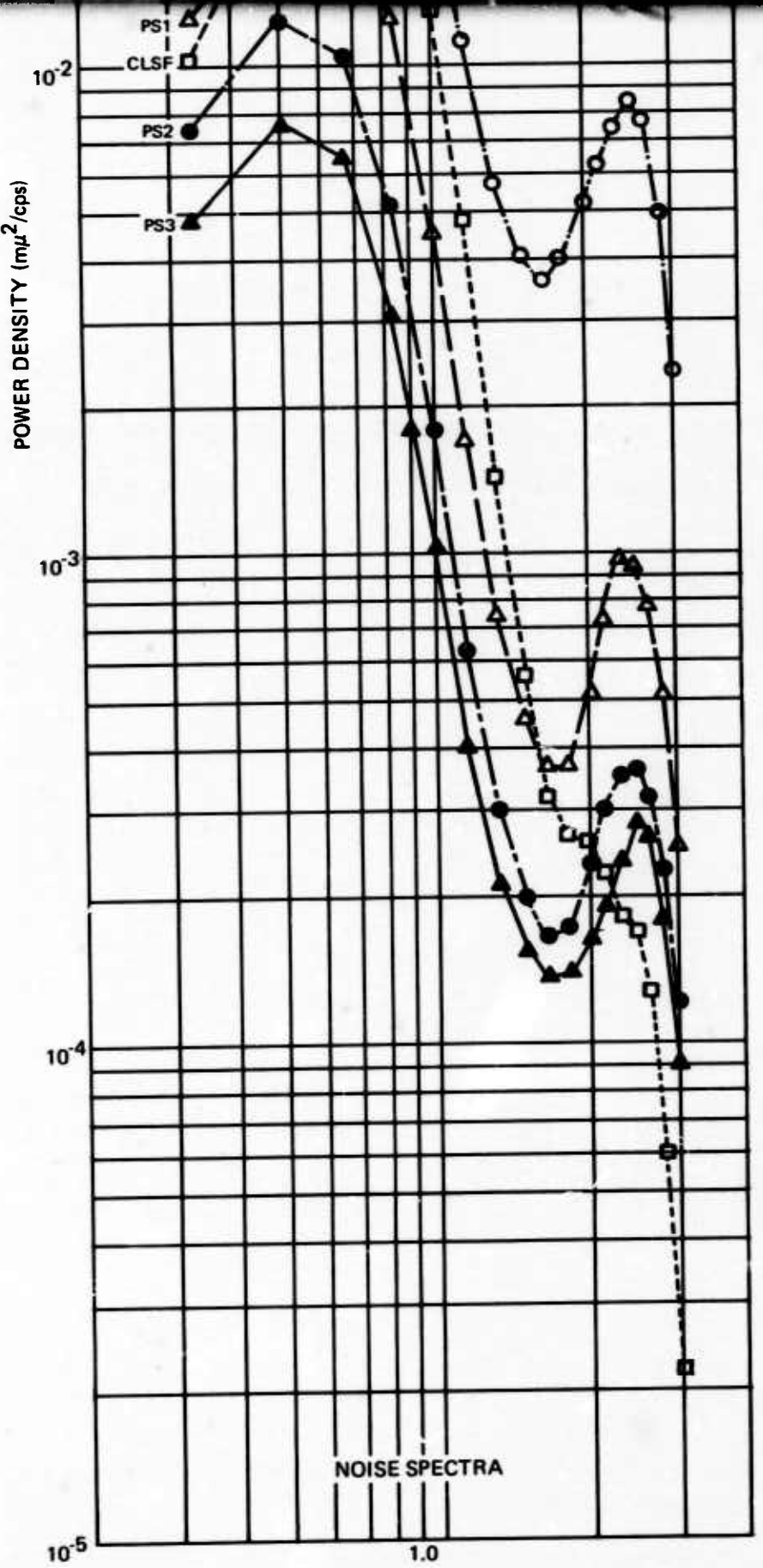
PS1
CLSF
PS2
PS3
10^{-2}
10^{-3}
10^{-4}
10^{-5}
POWER DENSITY ($m\mu^2$/cps)
NOISE SPECTRA
1.0
FREQUENCY (cps)

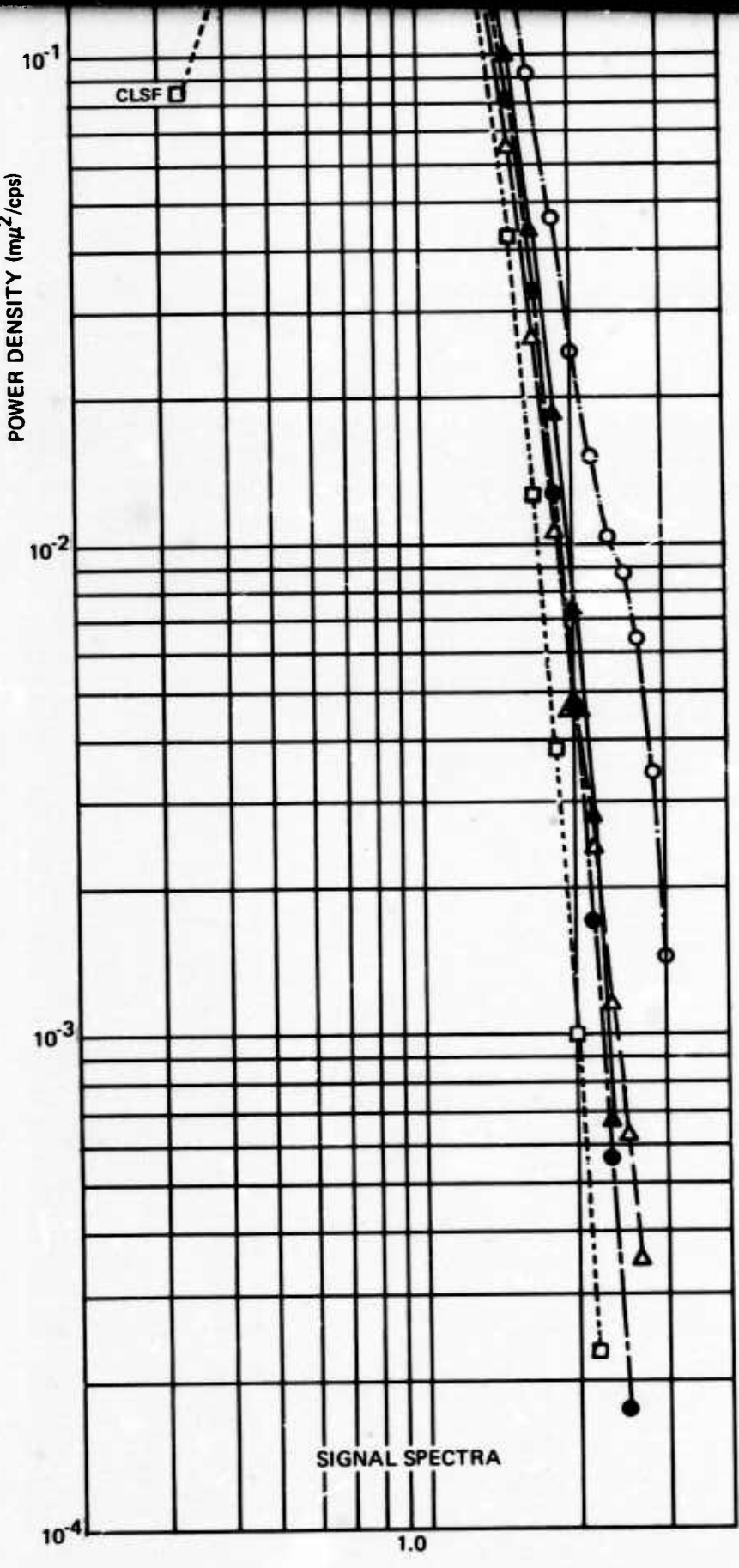
CLSF
10^{-1}
10^{-2}
10^{-3}
10^{-4}
POWER DENSITY ($m\mu^2$/cps)
SIGNAL SPECTRA
1.0
FREQUENCY (cps)

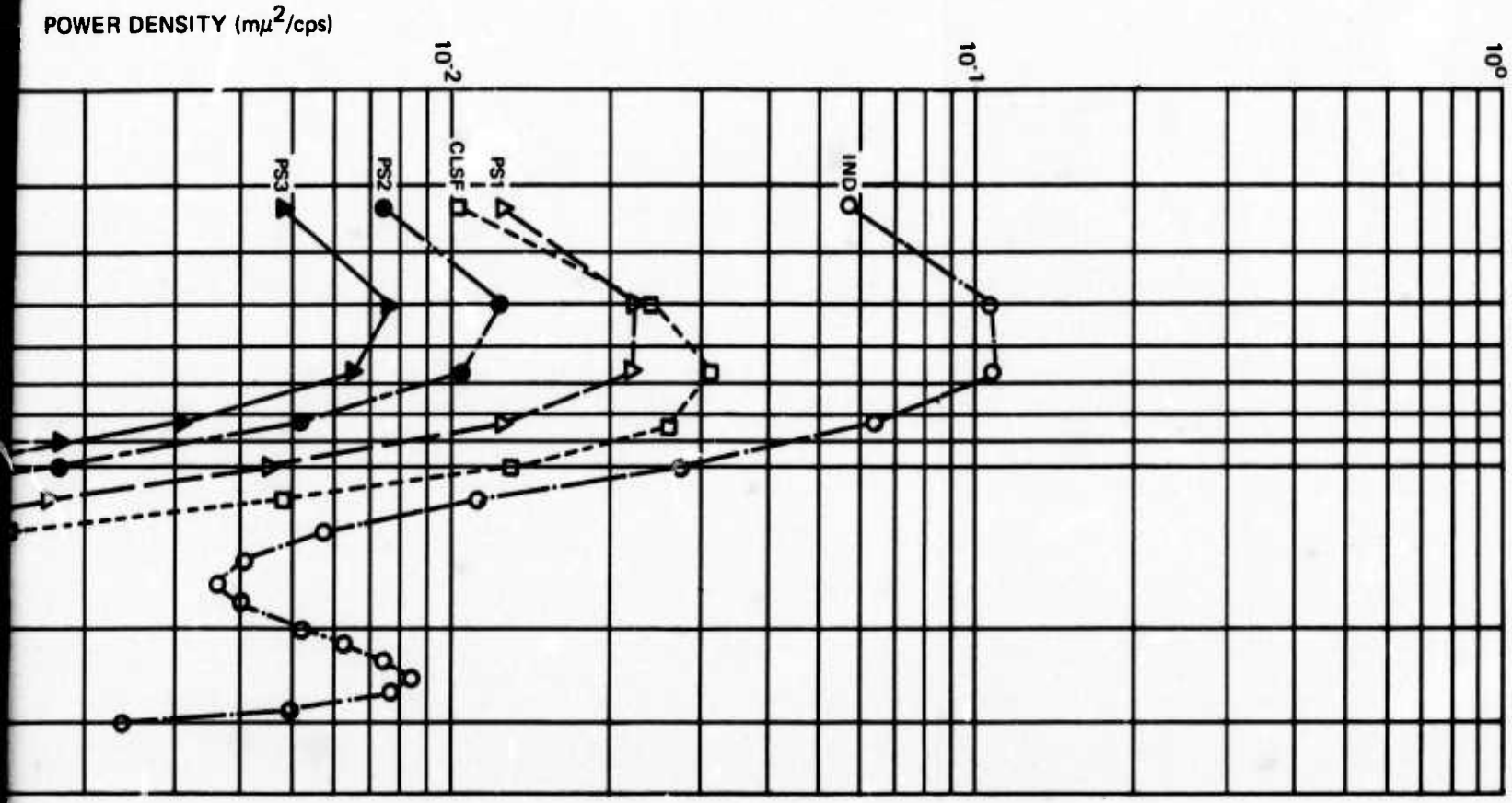

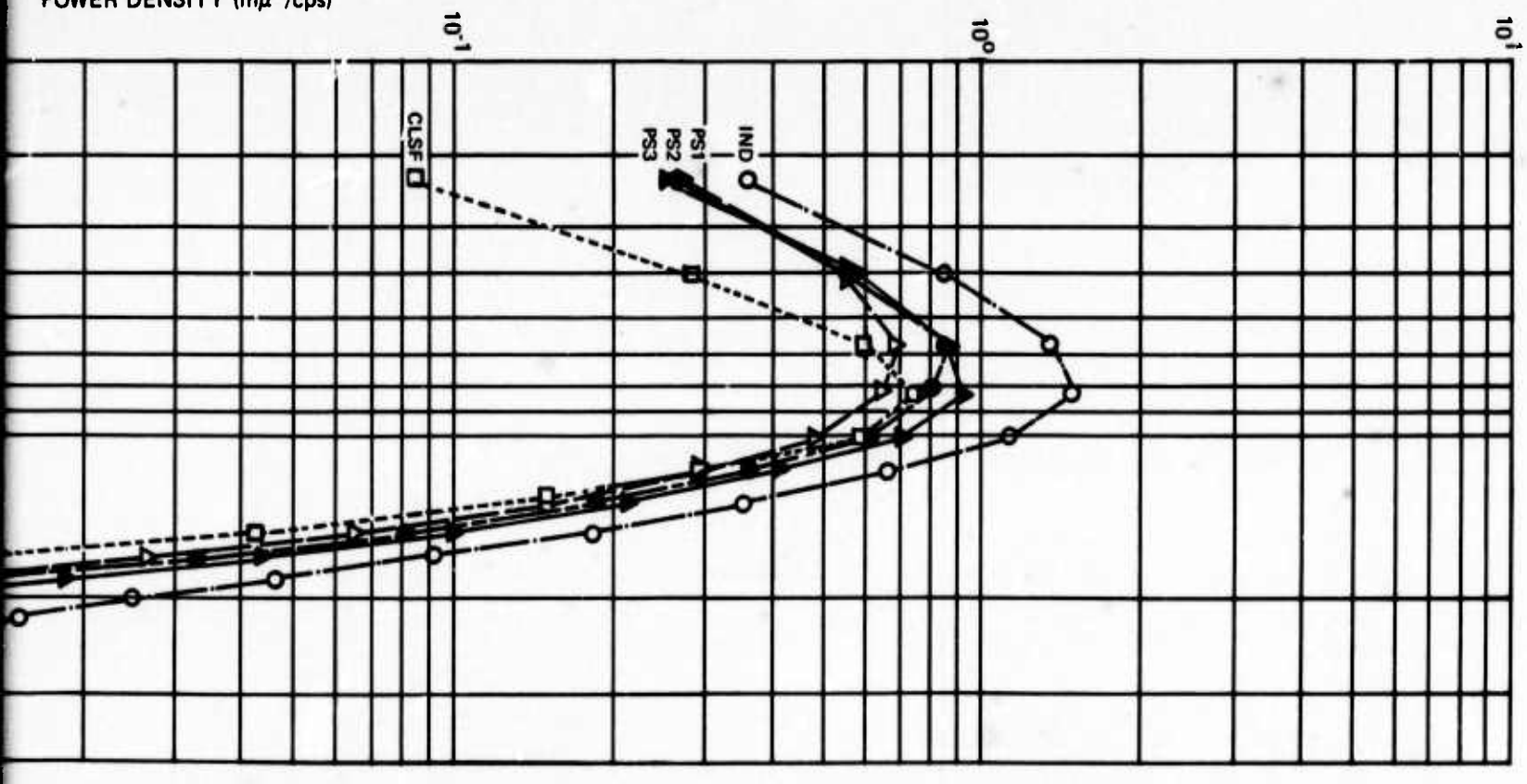

G 4538

Figure 9. Noise reduction ratios for data sample 9

B

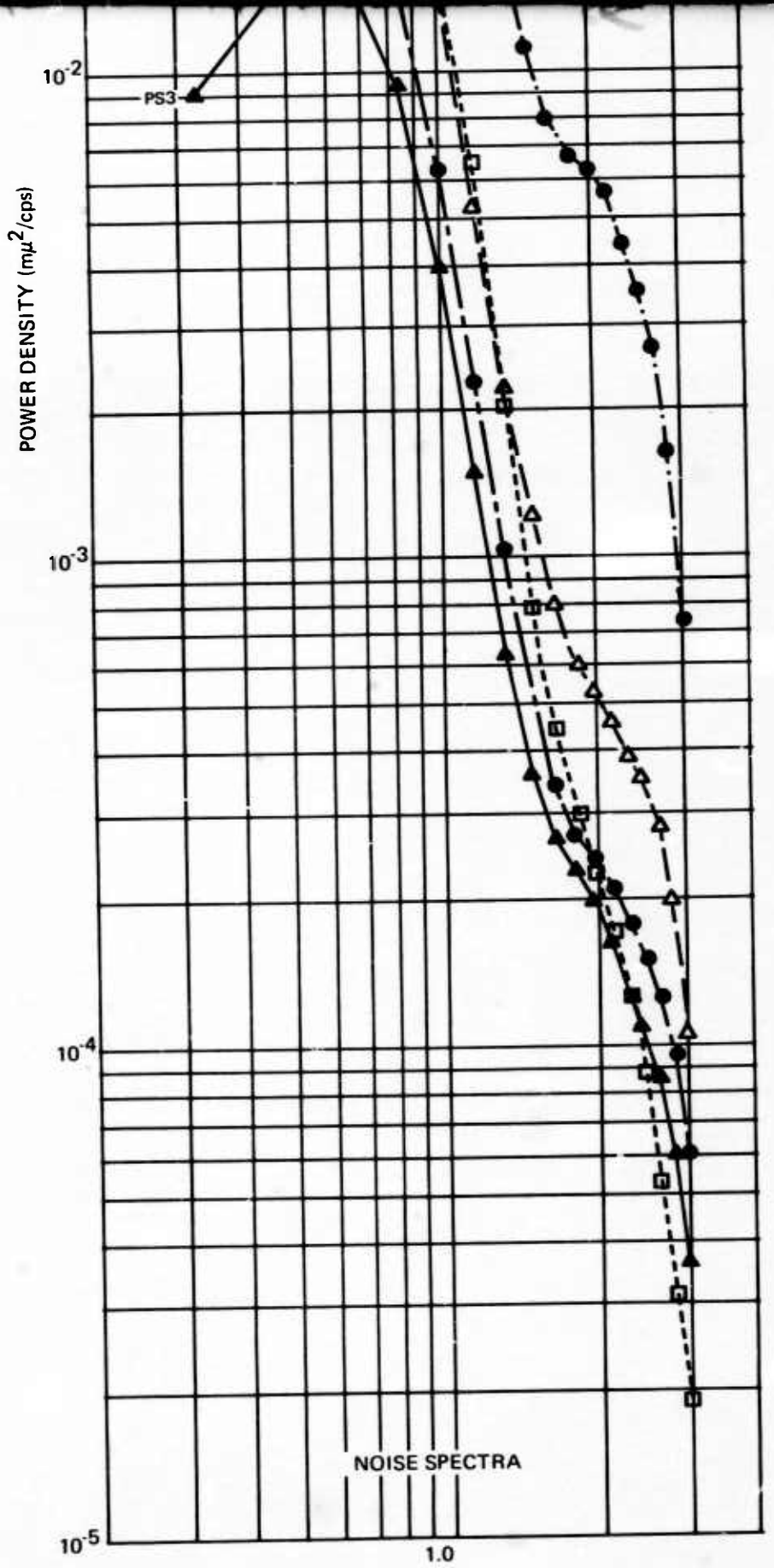
PS3
10^{-2}
10^{-3}
10^{-4}
10^{-5}
POWER DENSITY ($m\mu^2$/cps)
NOISE SPECTRA
1.0
FREQUENCY (cps)

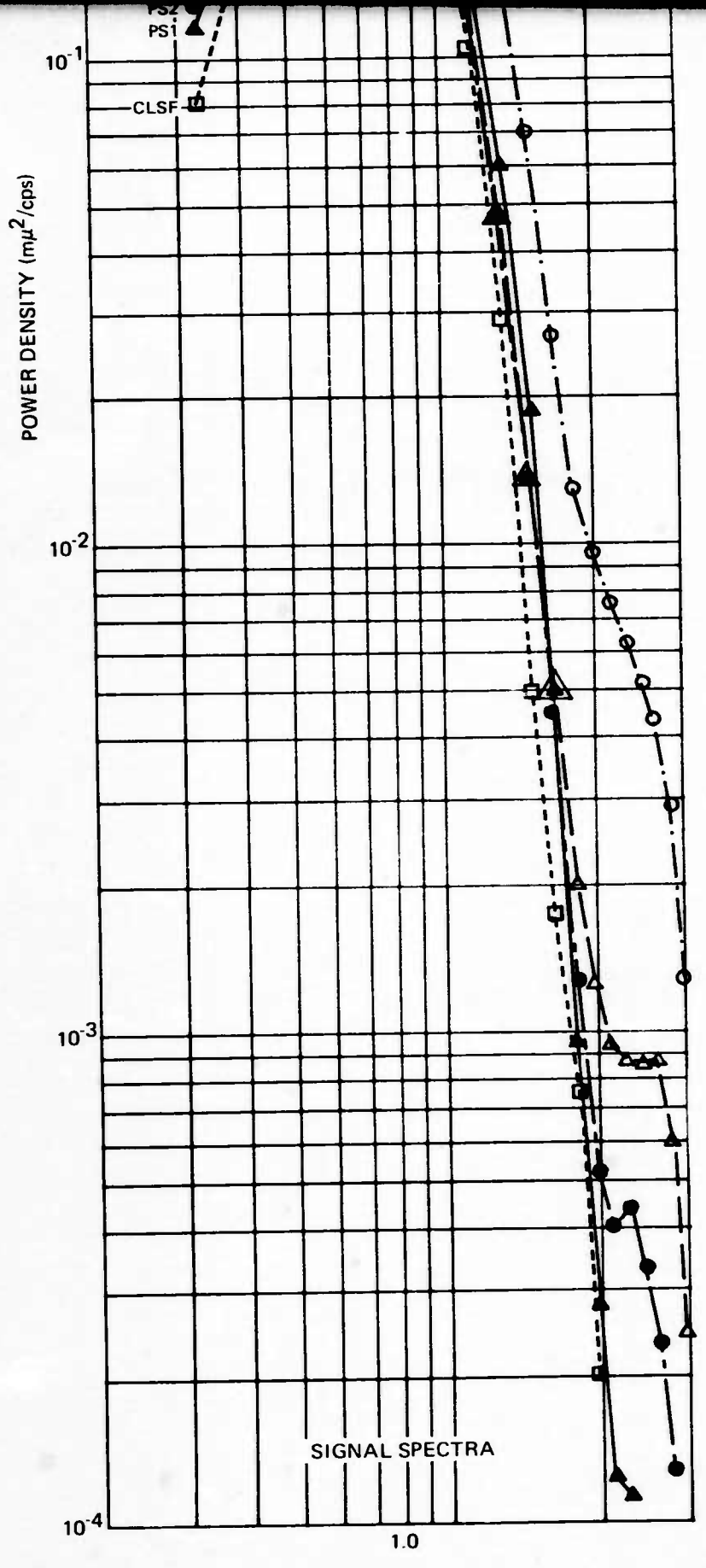
PS2
PS1
CLSF
10^{-1}
10^{-2}
10^{-3}
10^{-4}
POWER DENSITY ($m\mu^2$/cps)
SIGNAL SPECTRA
1.0
FREQUENCY (cps)

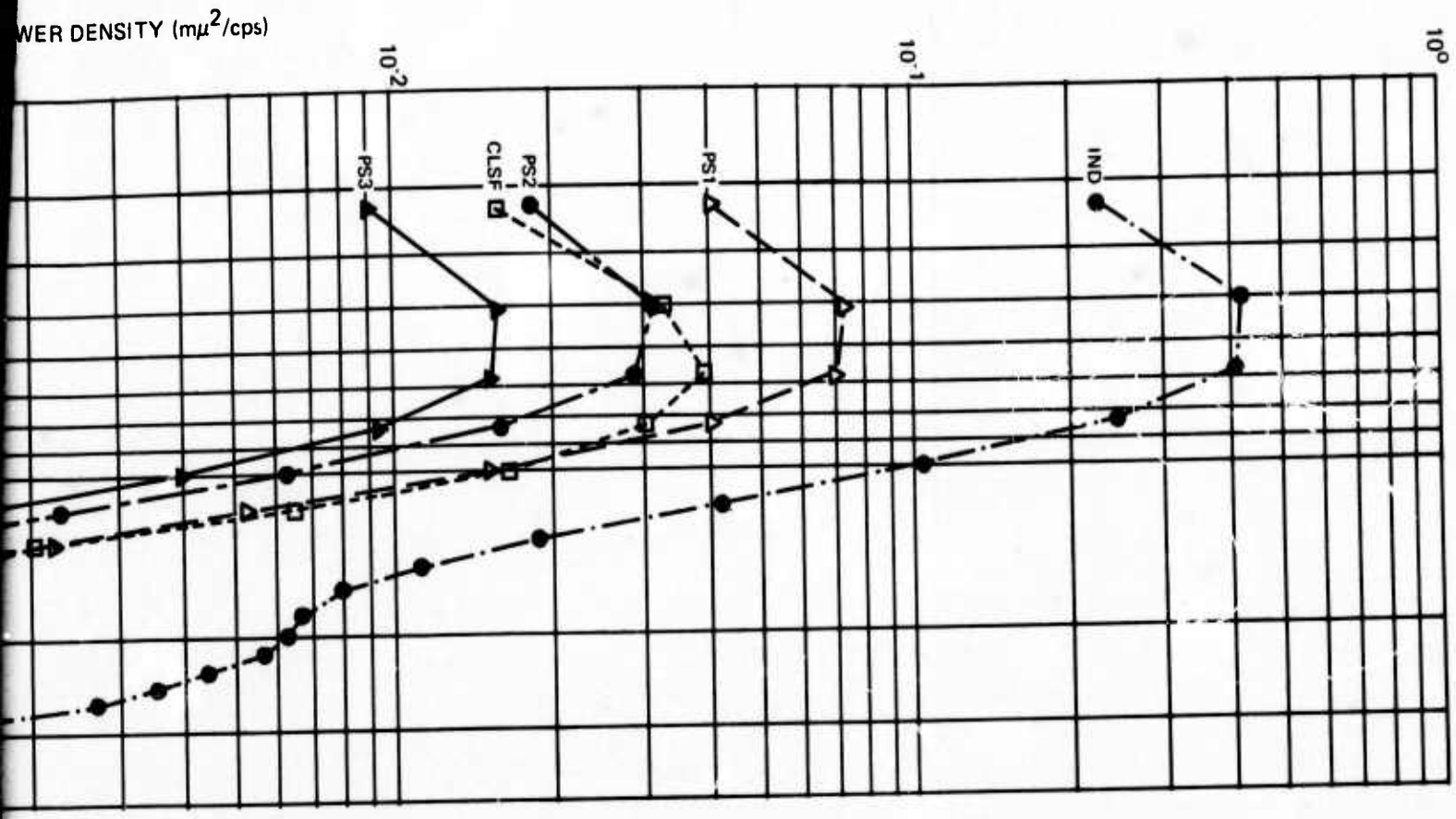

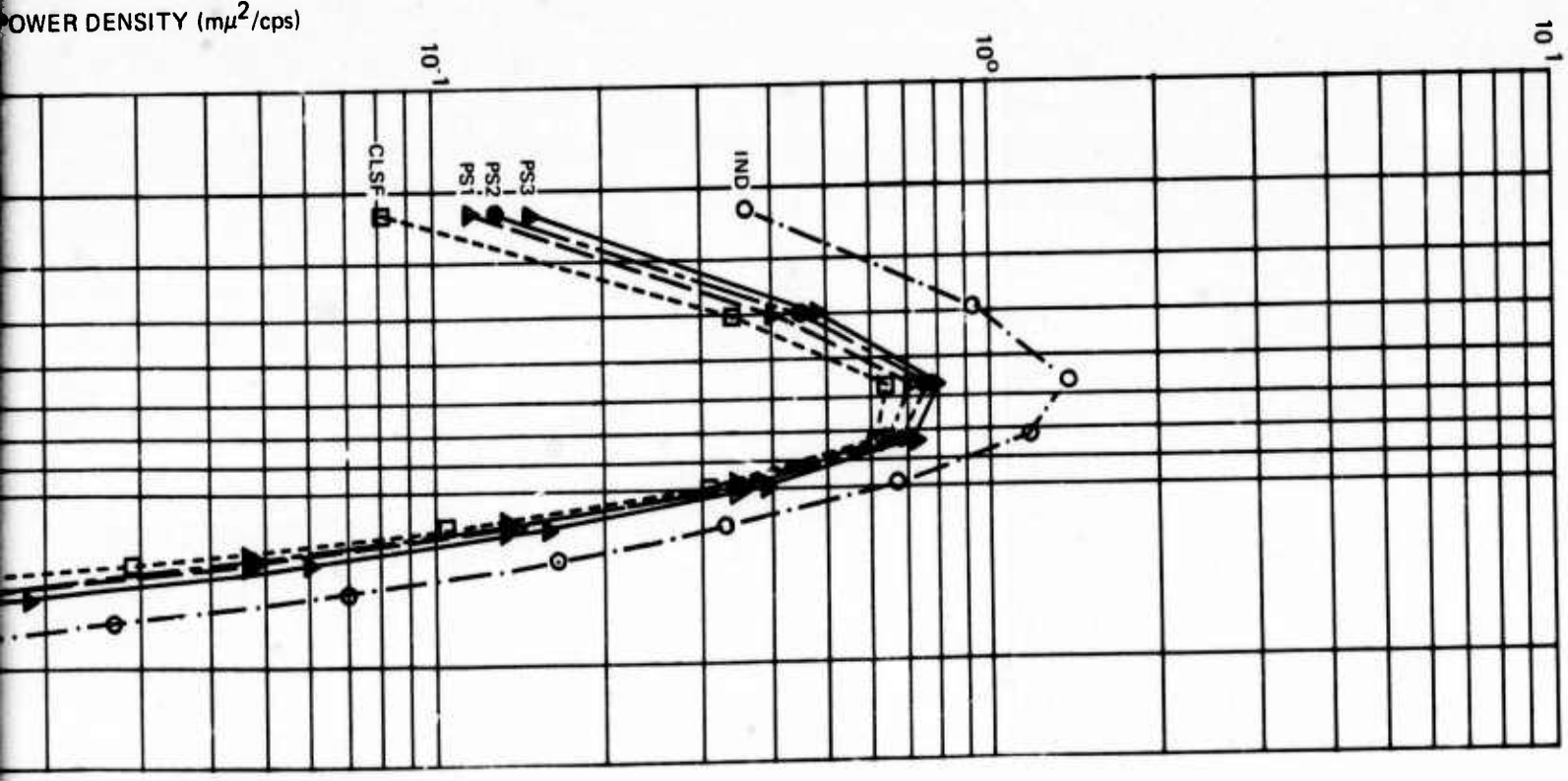

G 4539

Figure 10. Noise reduction ratios for data sample 10

B

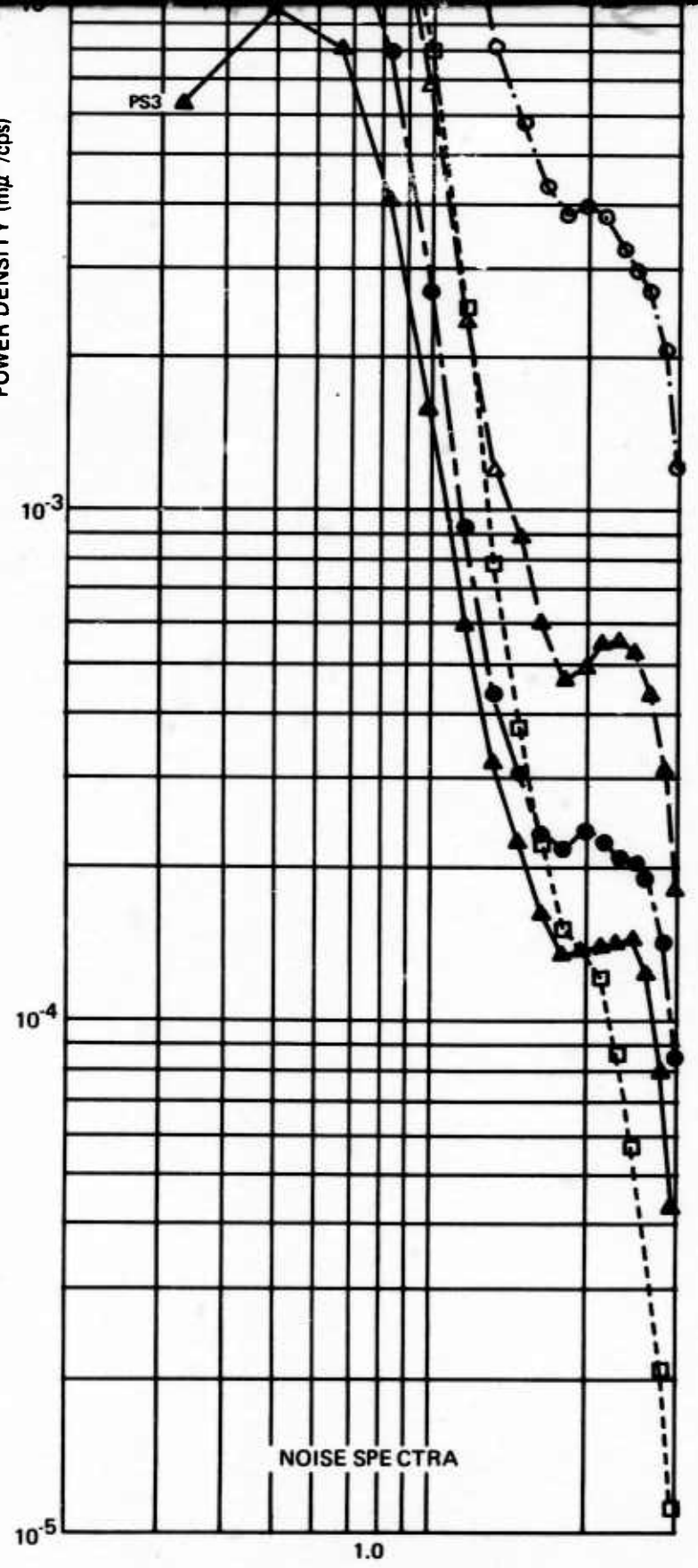
PS3
POWER DENSITY (mμ²/cps)
10⁻³
10⁻⁴
10⁻⁵
NOISE SPECTRA
1.0
FREQUENCY (cps)

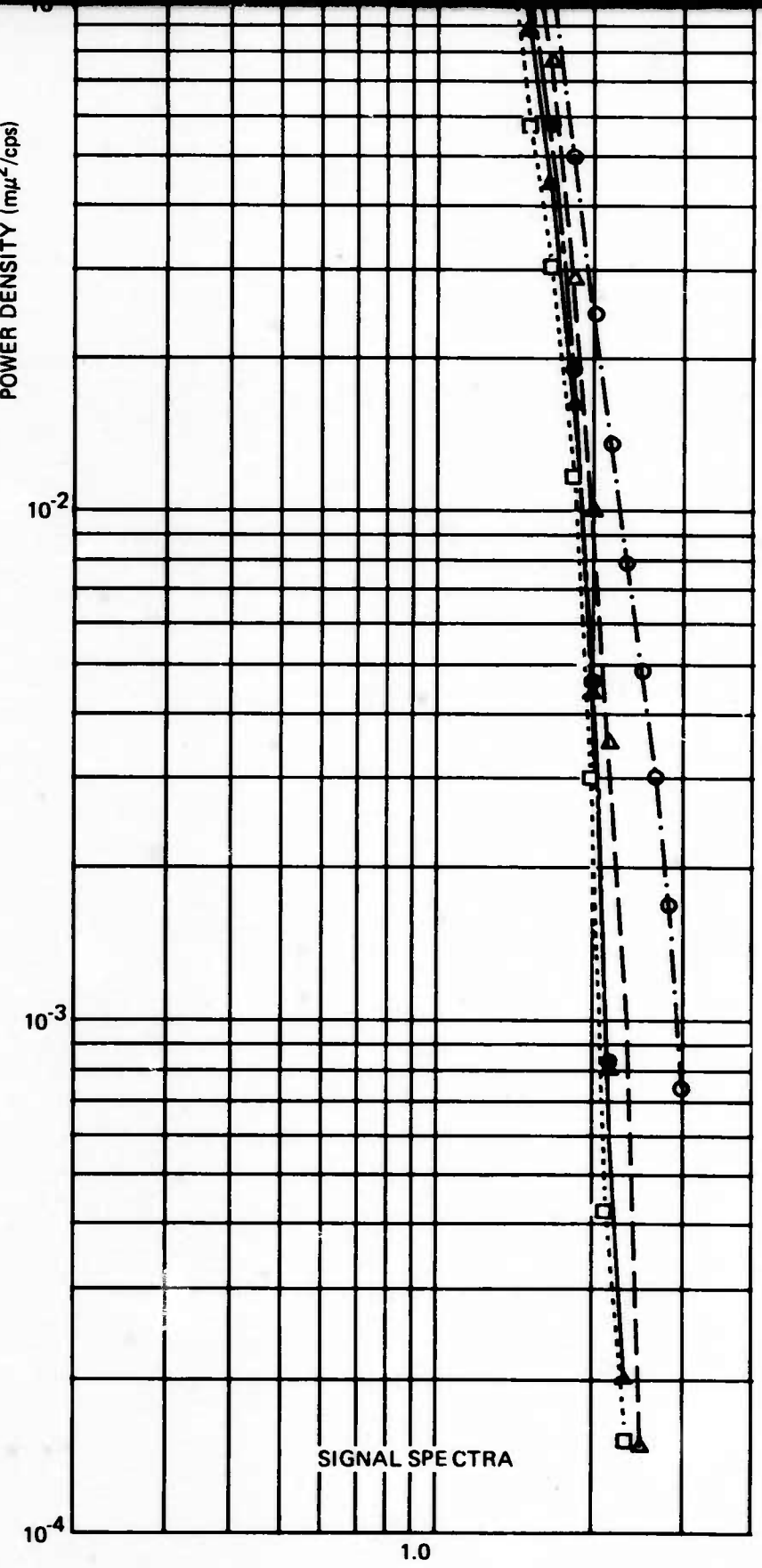
POWER DENSITY (mμ²/cps)
10⁻²
10⁻³
10⁻⁴
SIGNAL SPECTRA
1.0
FREQUENCY (cps)

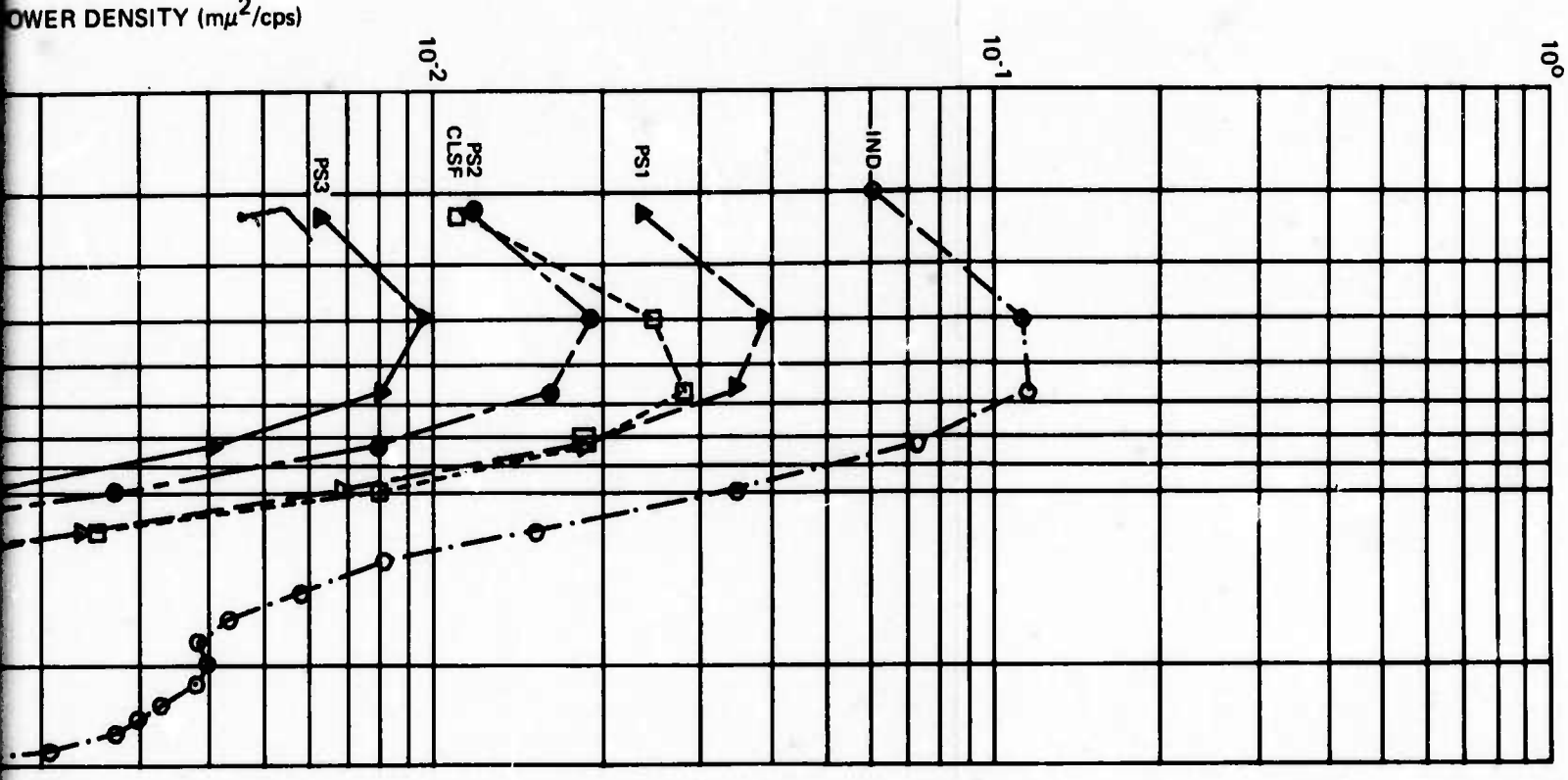

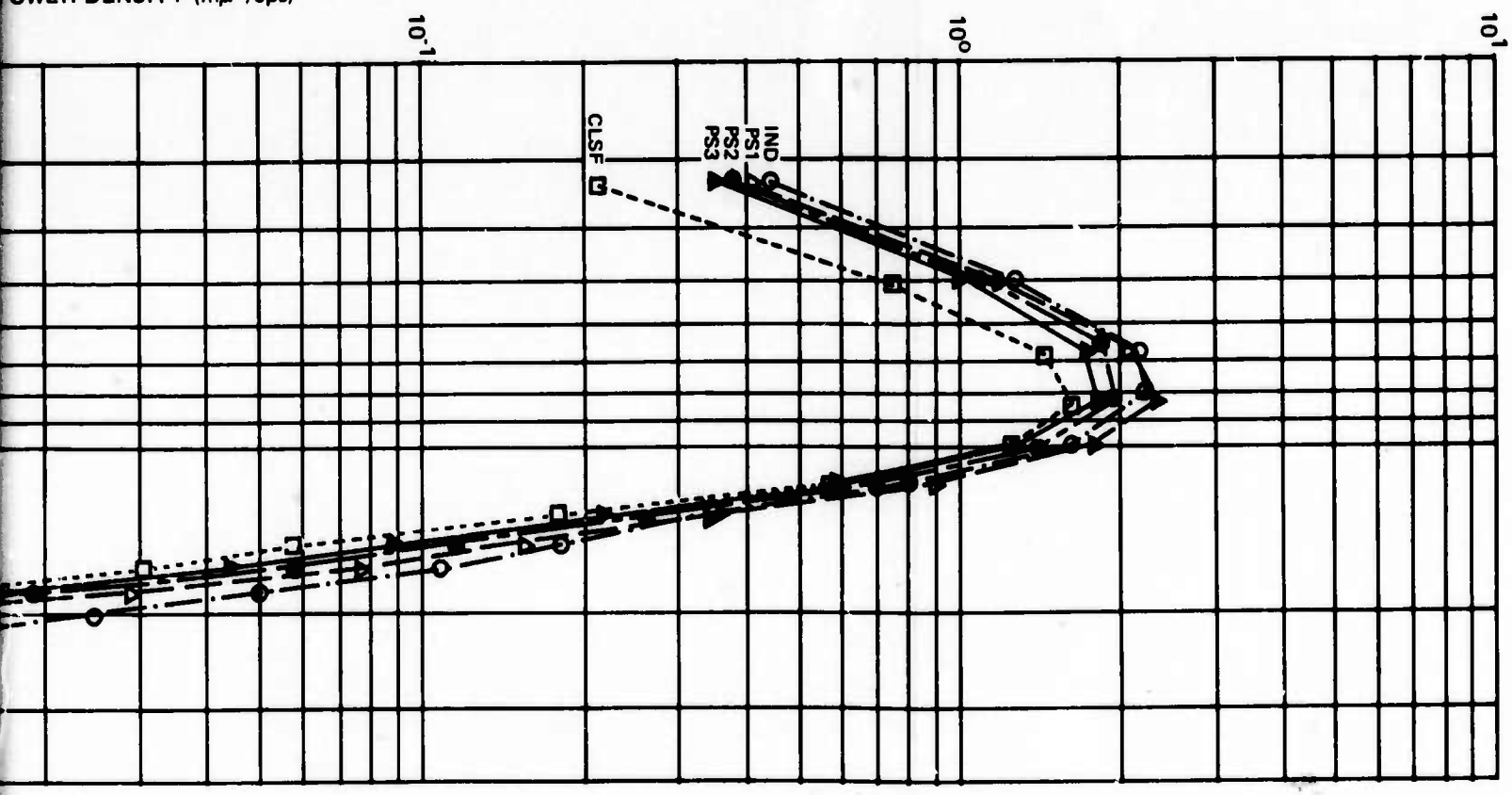

G 4540

Figure 11. Noise reduction ratios for data sample 11

B

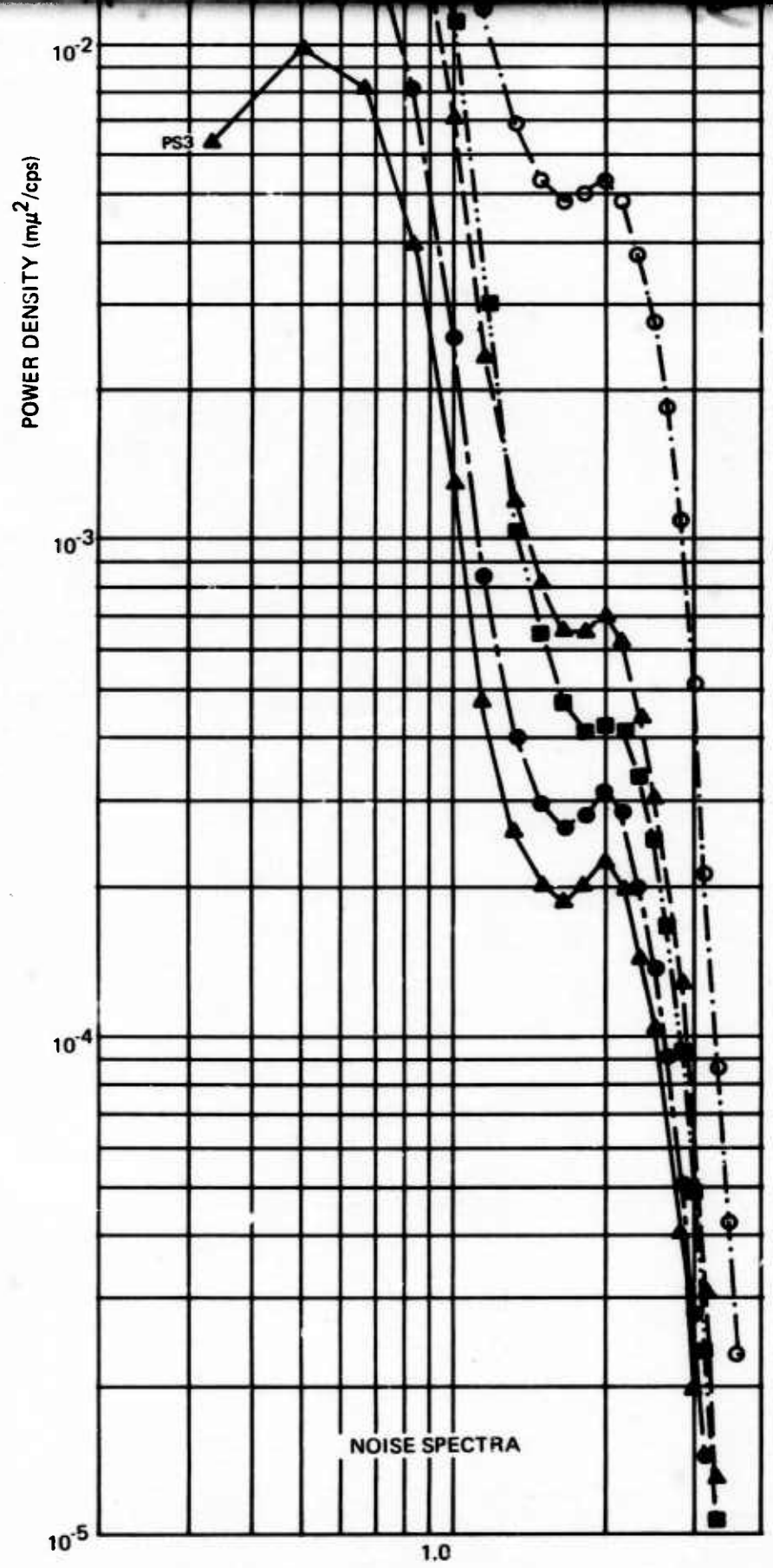
POWER DENSITY (mμ²/cps)
10⁻²
10⁻³
10⁻⁴
10⁻⁵
PS3
NOISE SPECTRA
1.0
FREQUENCY (cps)

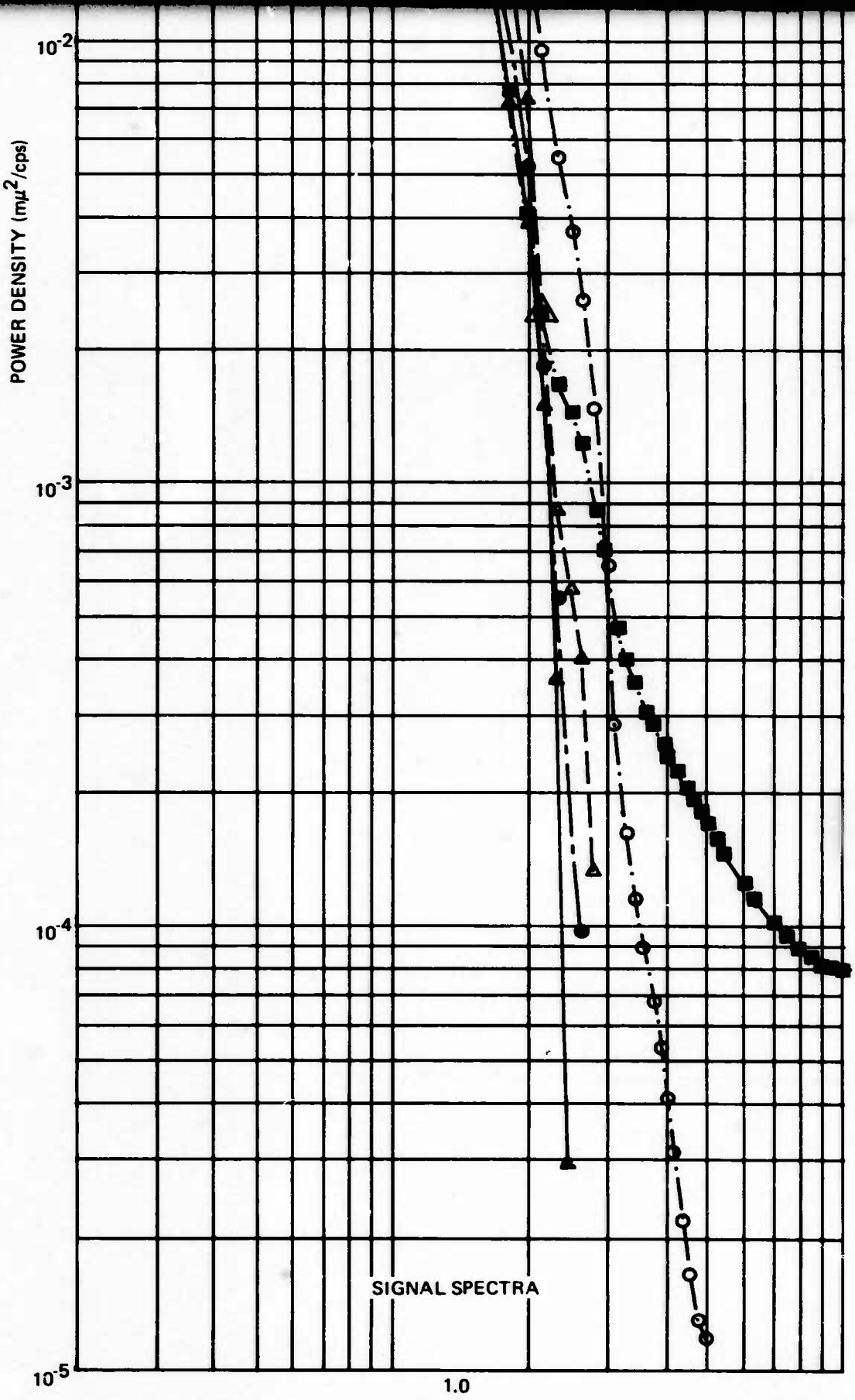
POWER DENSITY (mμ²/cps)
10⁻²
10⁻³
10⁻⁴
10⁻⁵
SIGNAL SPECTRA
1.0
FREQUENCY (cps)

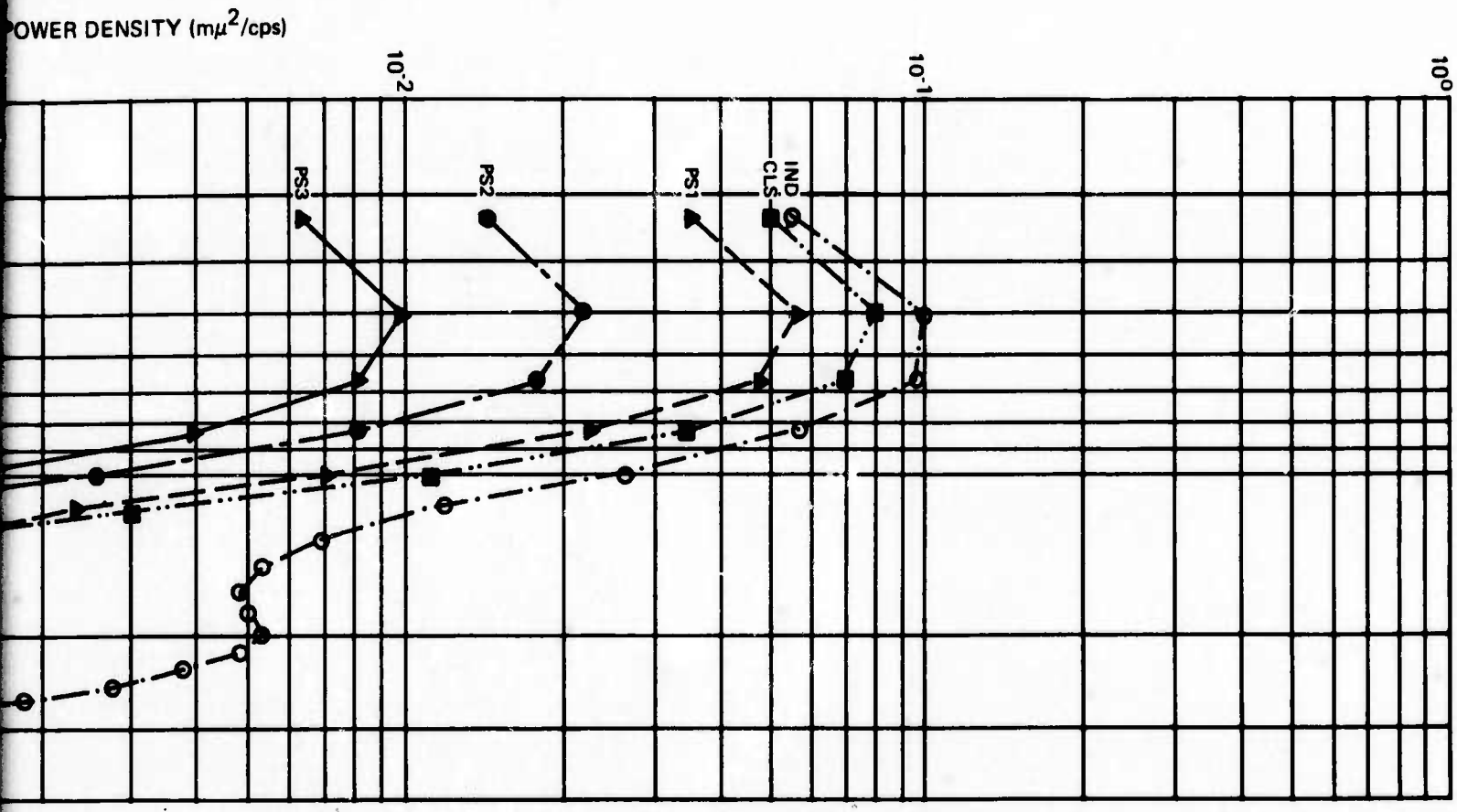

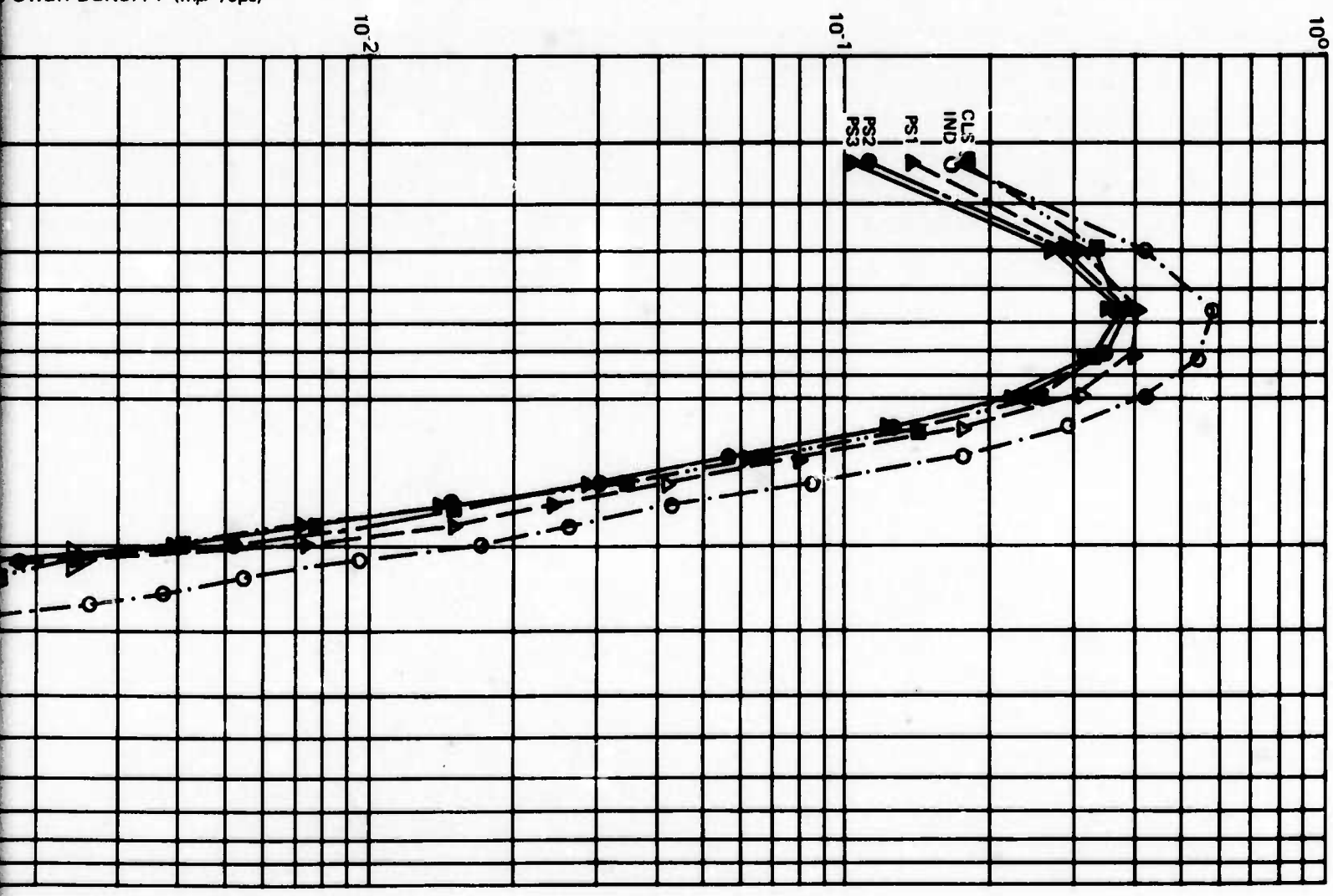

G 4541

Figure 12. Noise reduction ratios for data sample 12

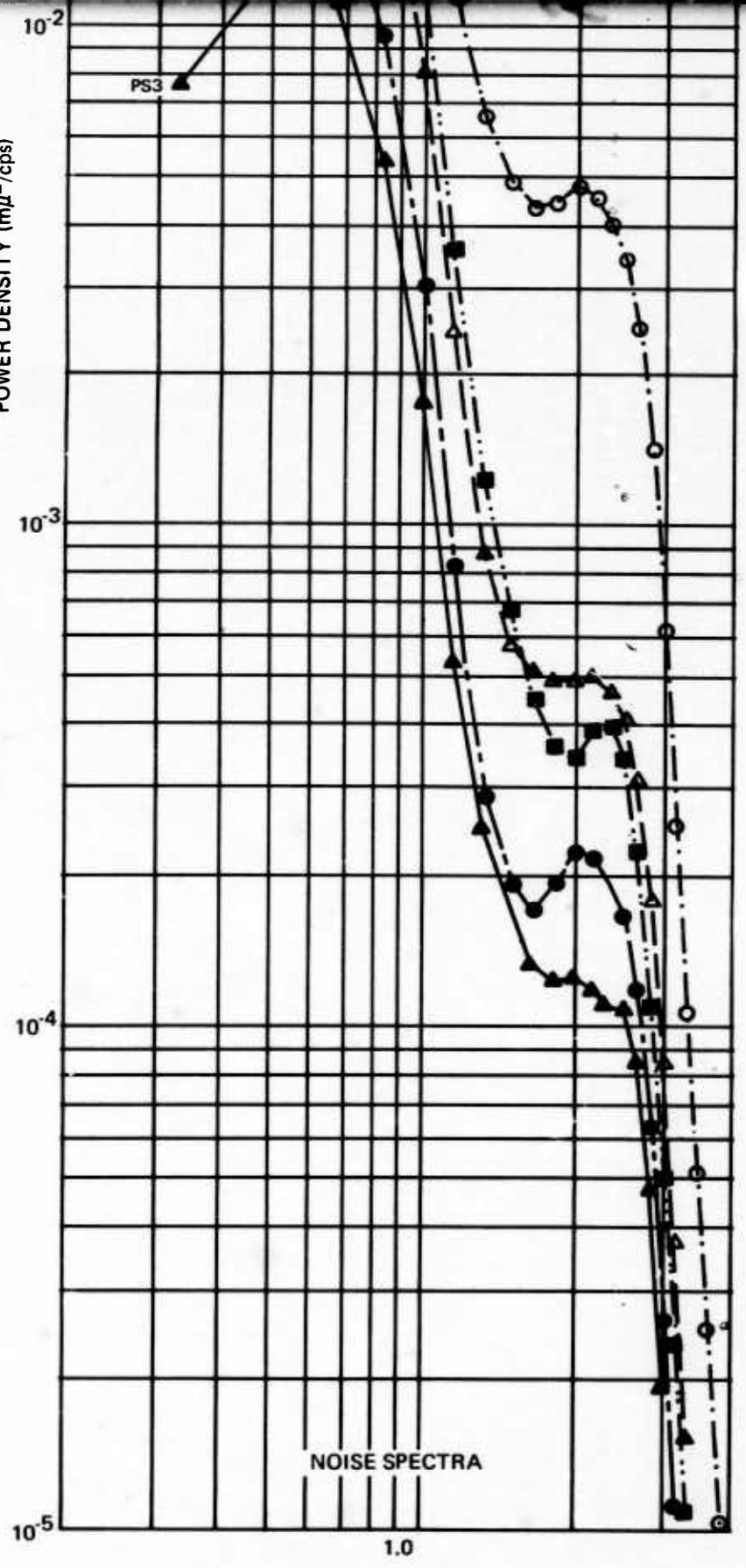
POWER DENSITY (mμ²/cps)
10⁻²
10⁻³
10⁻⁴
10⁻⁵
PS3
NOISE SPECTRA
1.0
FREQUENCY (cps)

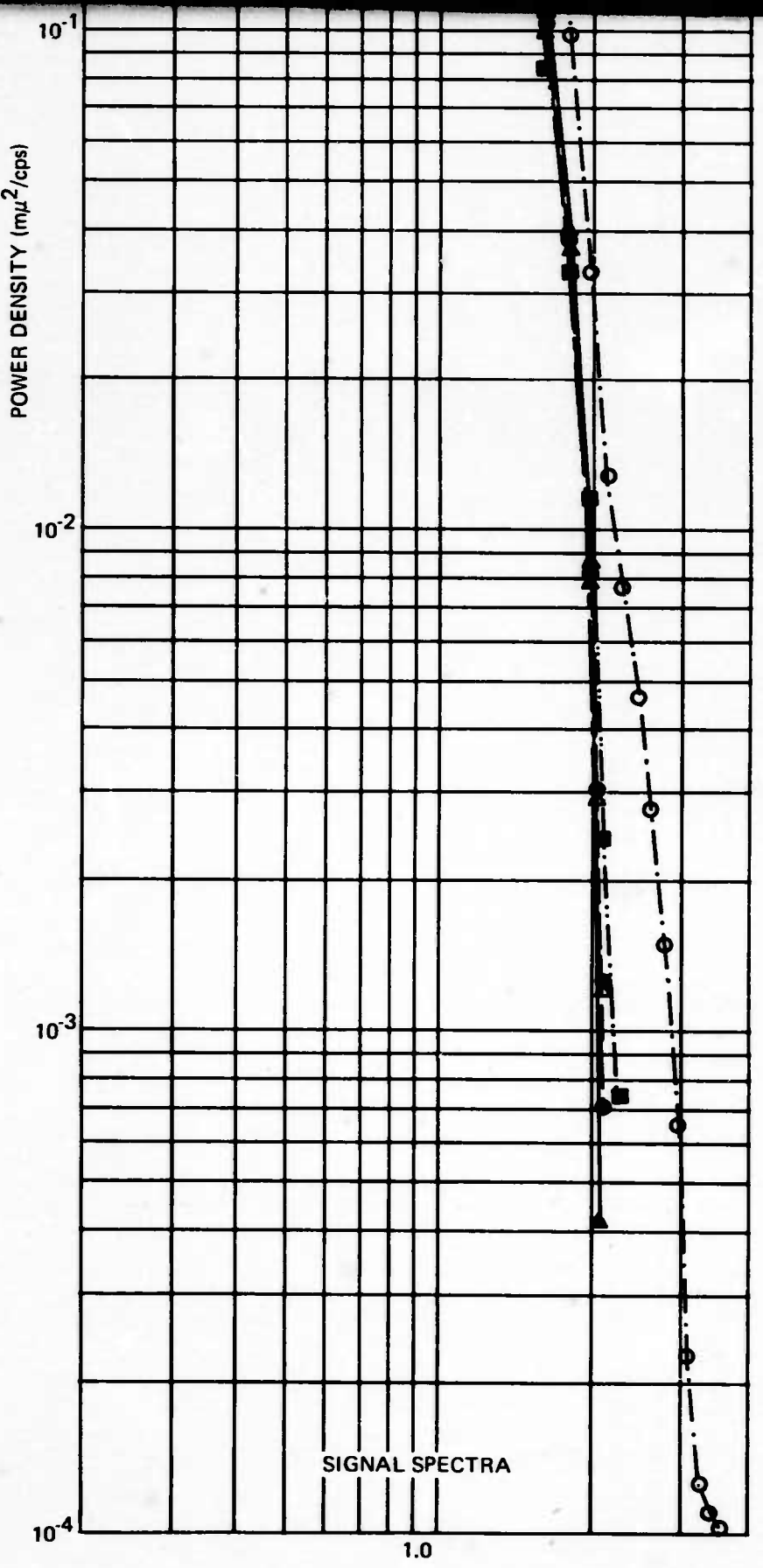
POWER DENSITY (mμ²/cps)
10⁻¹
10⁻²
10⁻³
10⁻⁴
SIGNAL SPECTRA
1.0
FREQUENCY (cps)

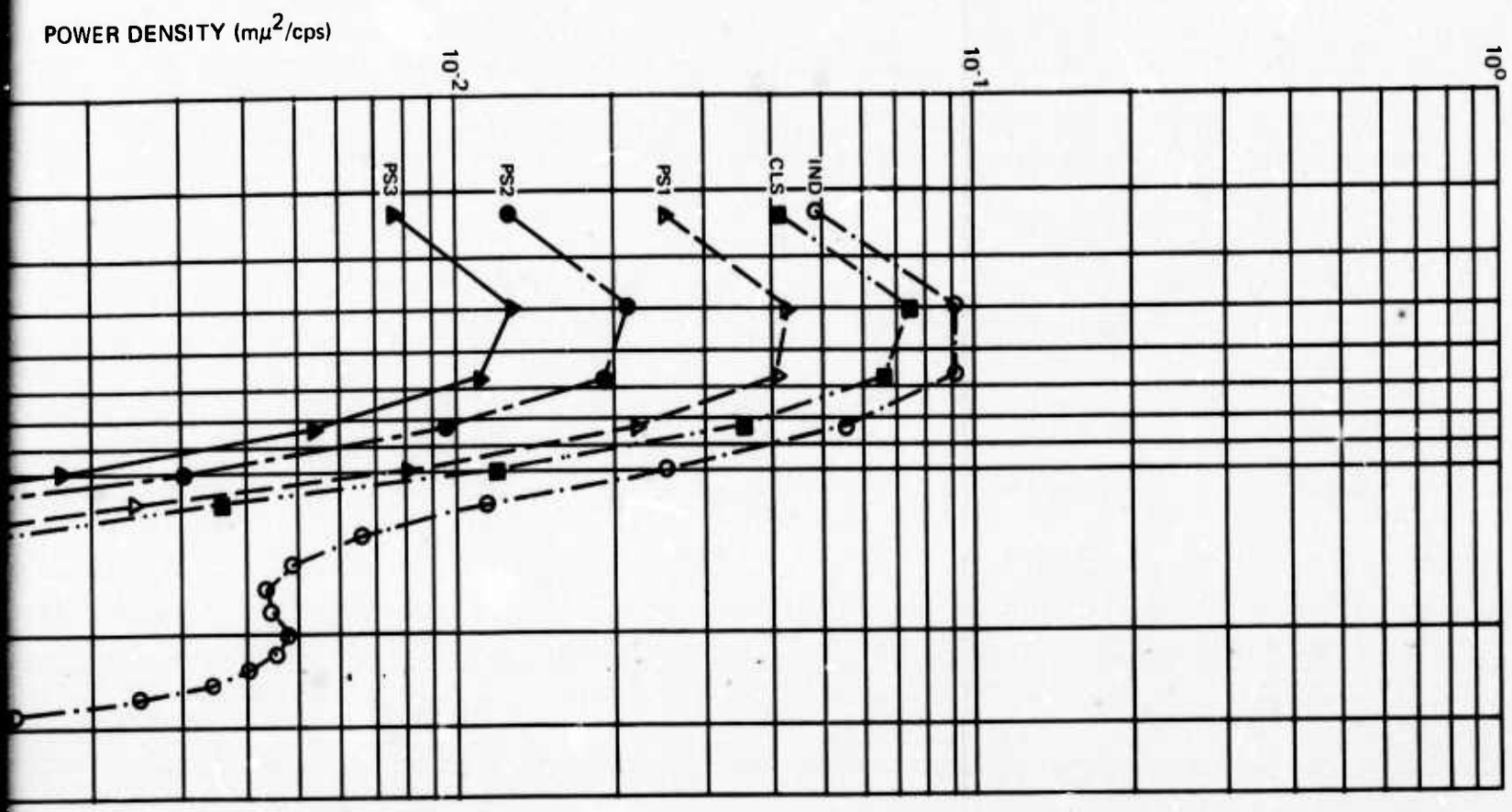

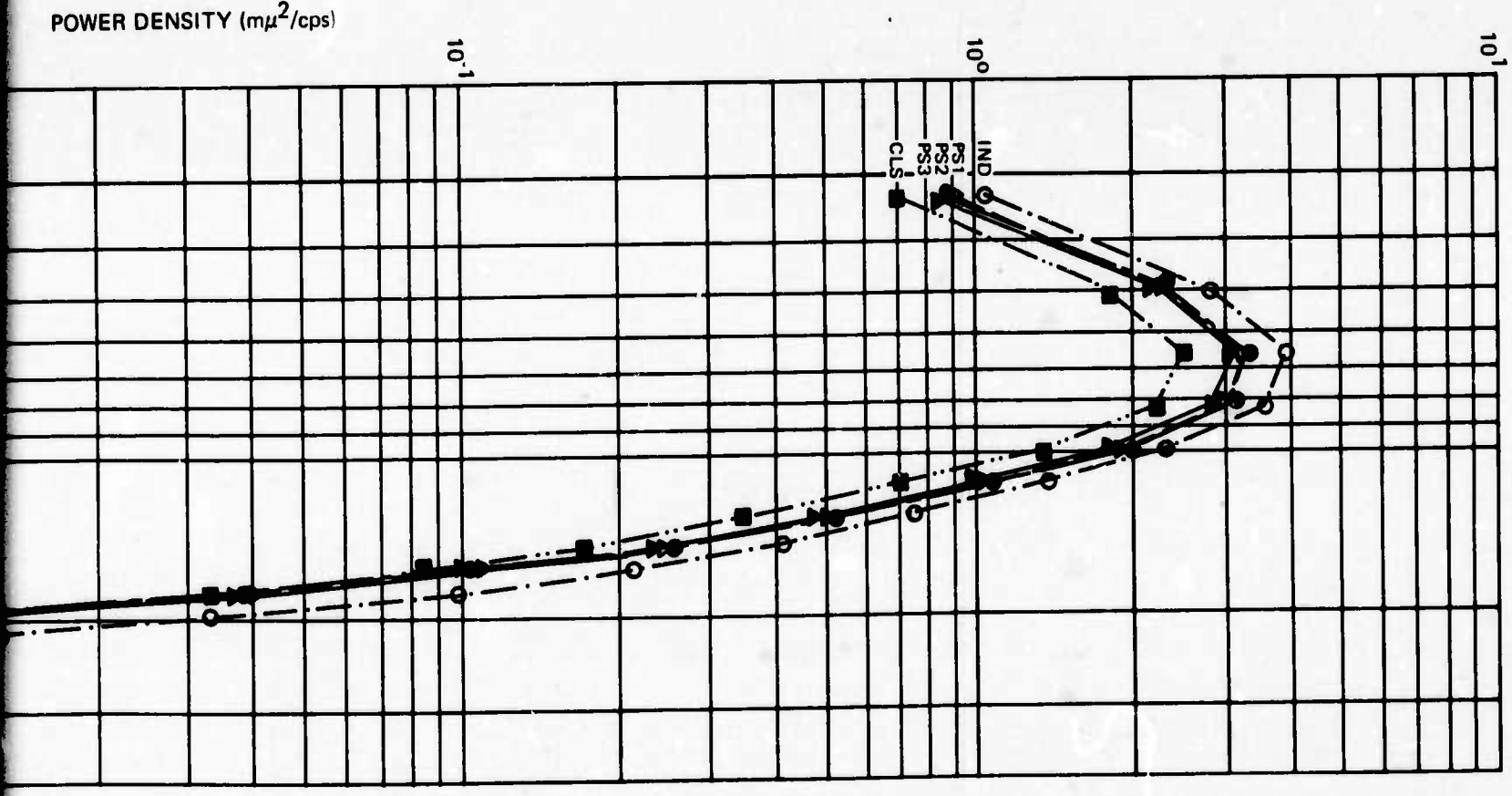

G 4542

Figure 13. Noise reduction ratios for data sample 13

B

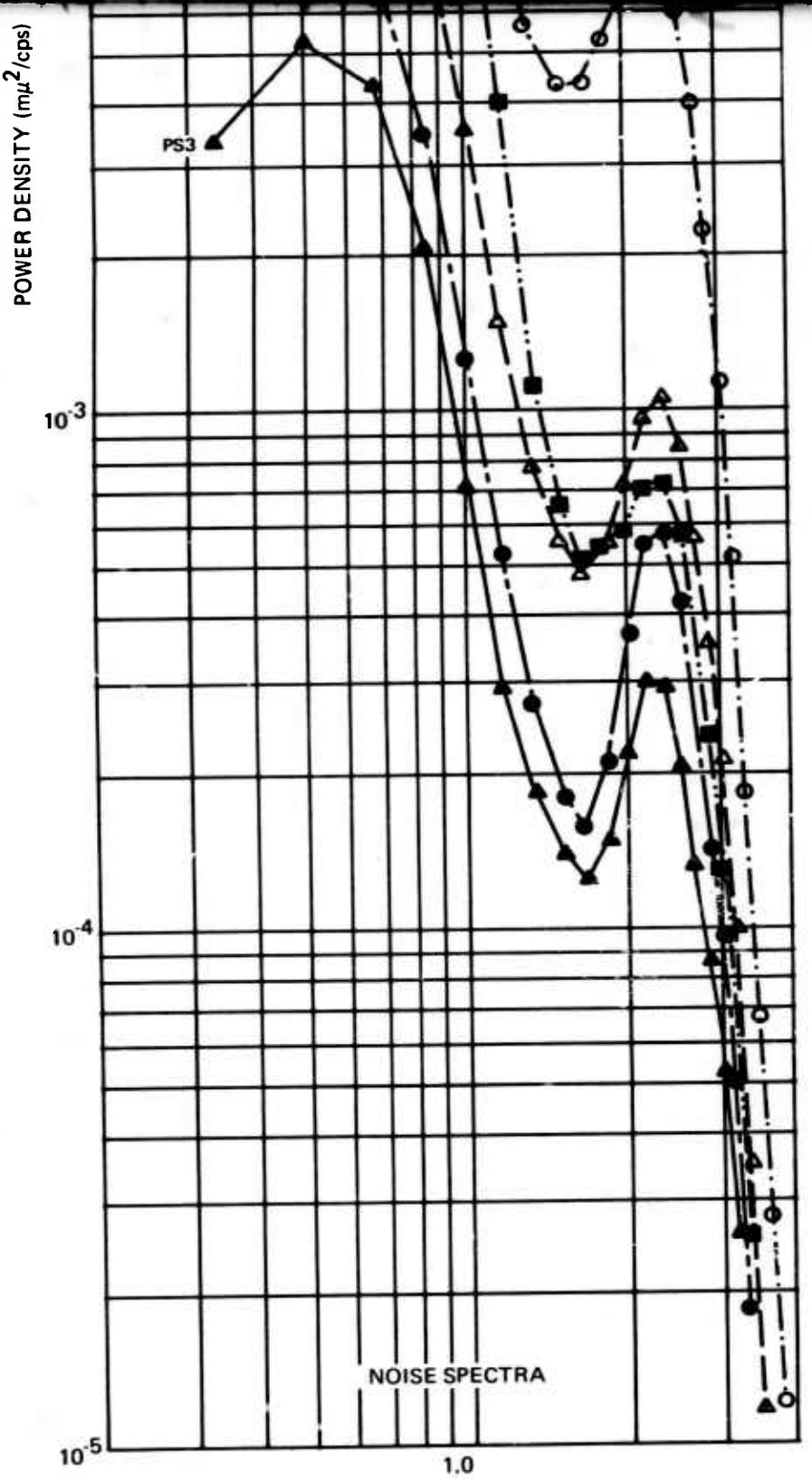
POWER DENSITY (mμ²/cps)
PS3
10⁻³
10⁻⁴
10⁻⁵
NOISE SPECTRA
1.0
FREQUENCY (cps)

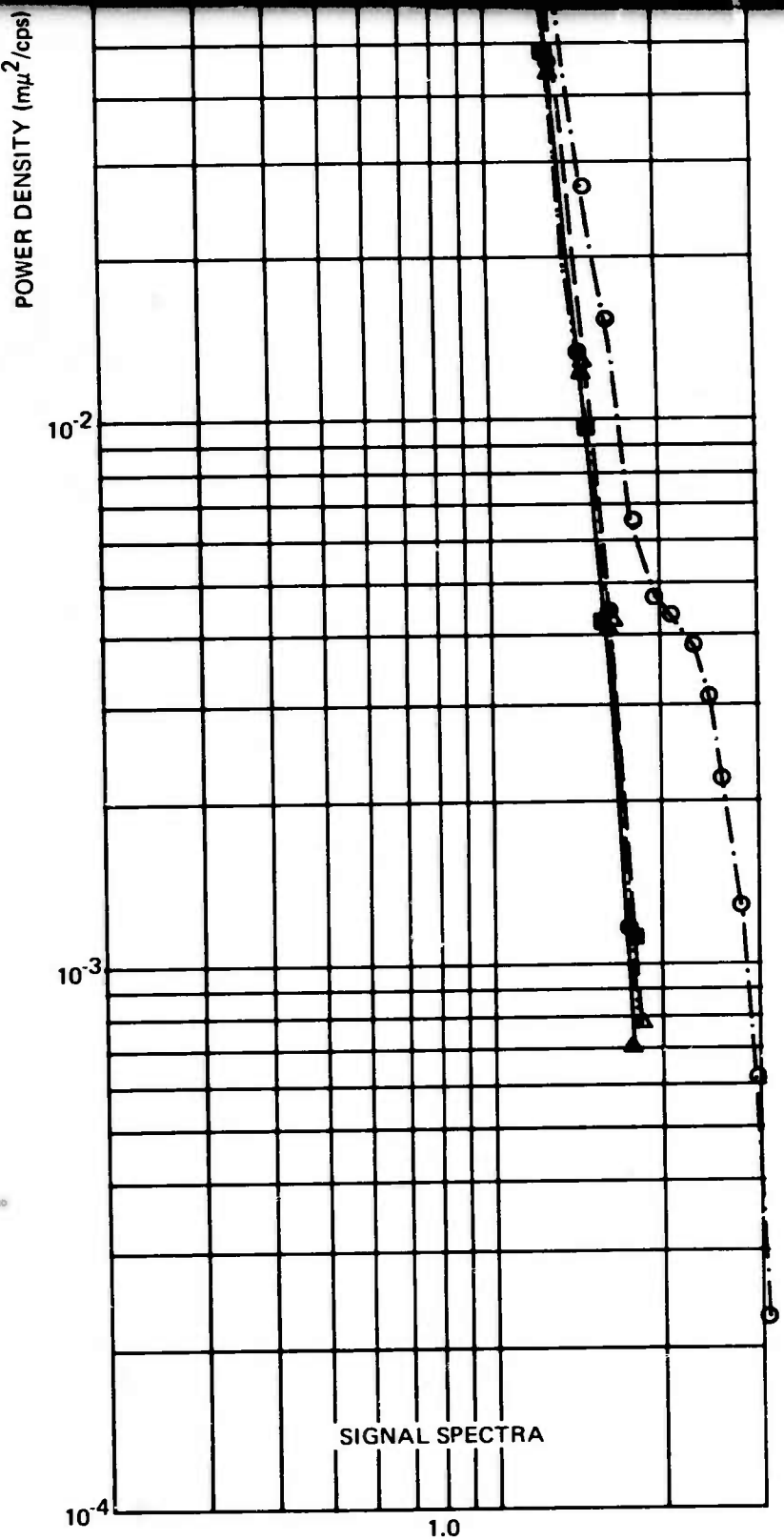
POWER DENSITY (mμ²/cps)
10⁻²
10⁻³
10⁻⁴
SIGNAL SPECTRA
1.0
FREQUENCY (cps)

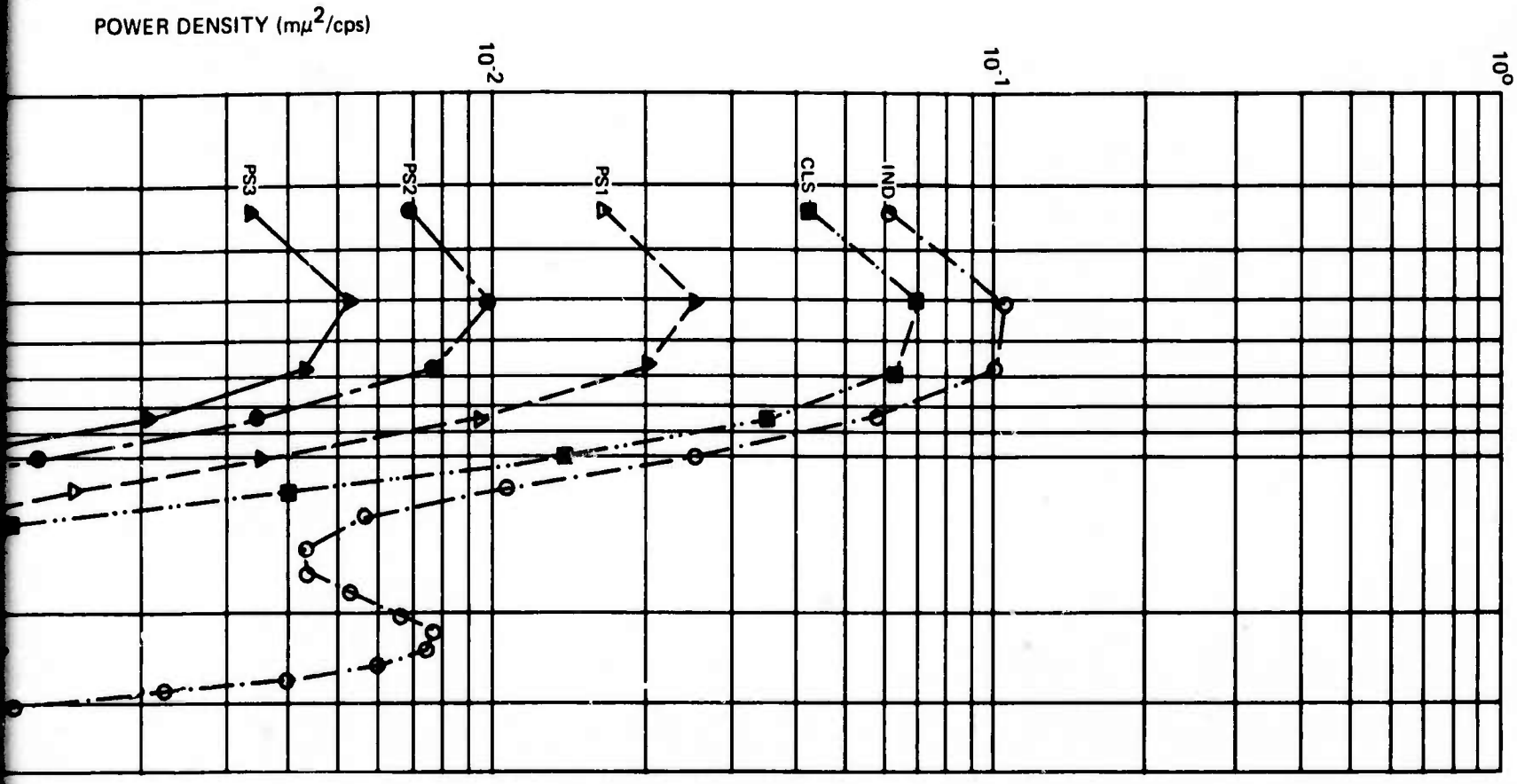

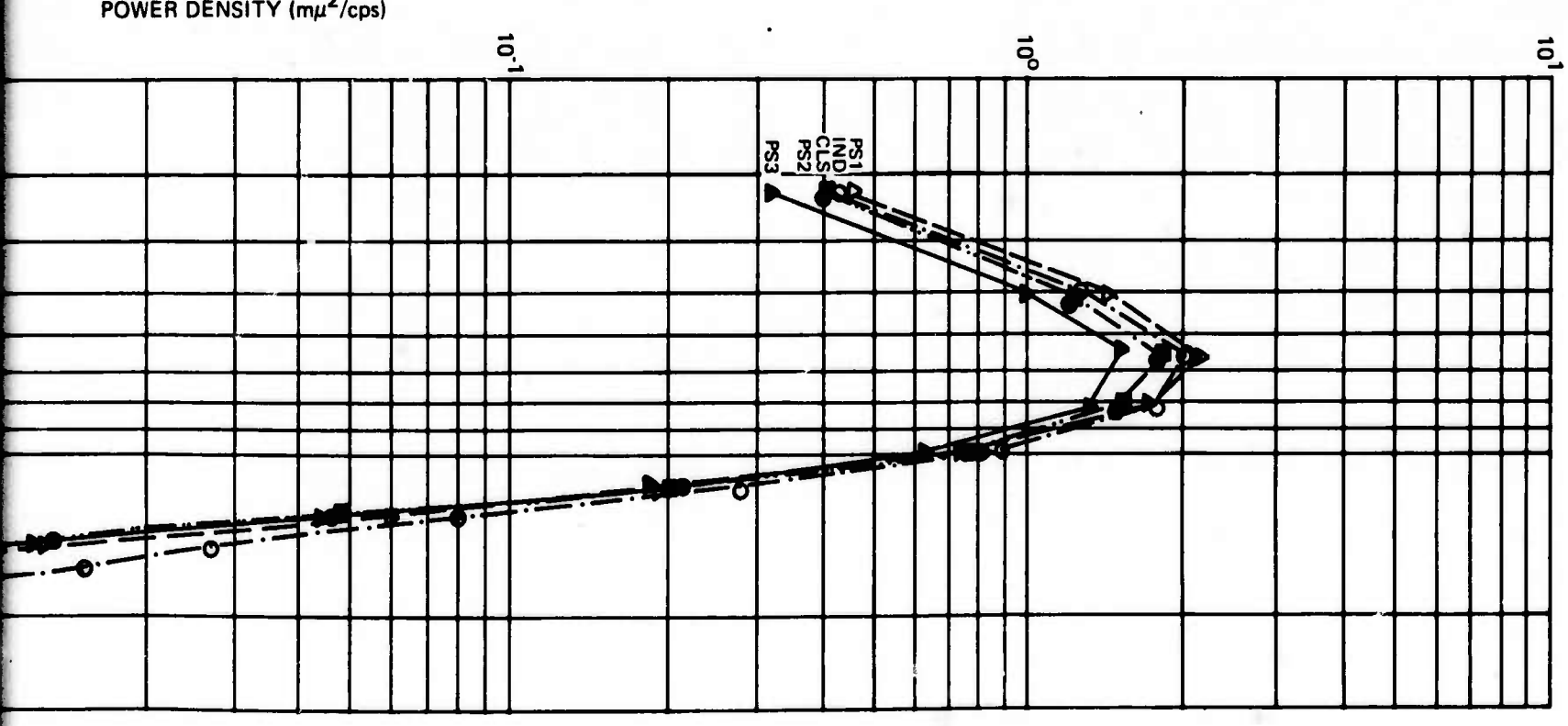

G 4543

Figure 14. Noise reduction ratios for data sample 14

B

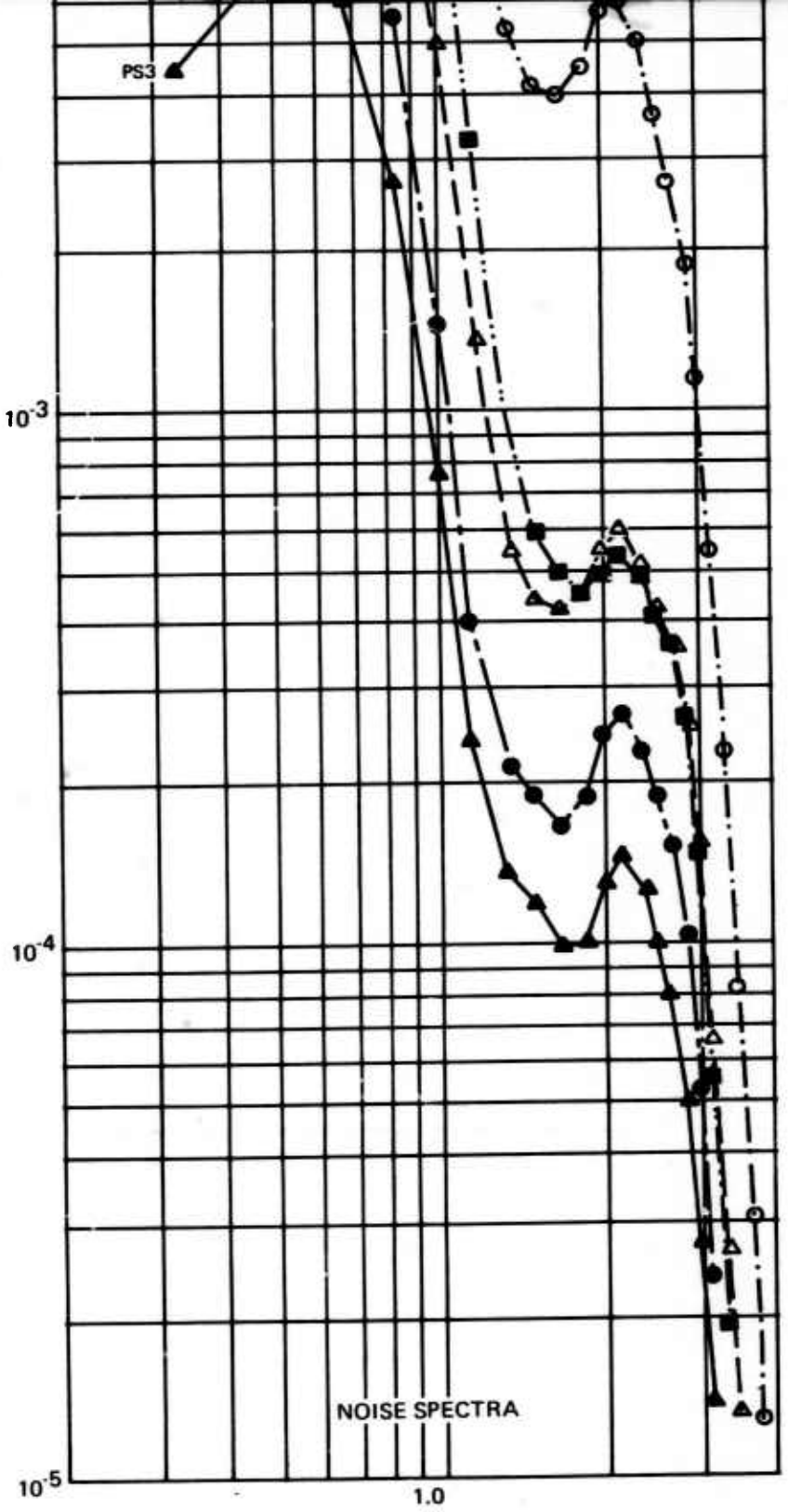
POWER DENSITY (mμ²/cps)
PS3
10⁻³
10⁻⁴
10⁻⁵
NOISE SPECTRA
1.0
FREQUENCY (cps)

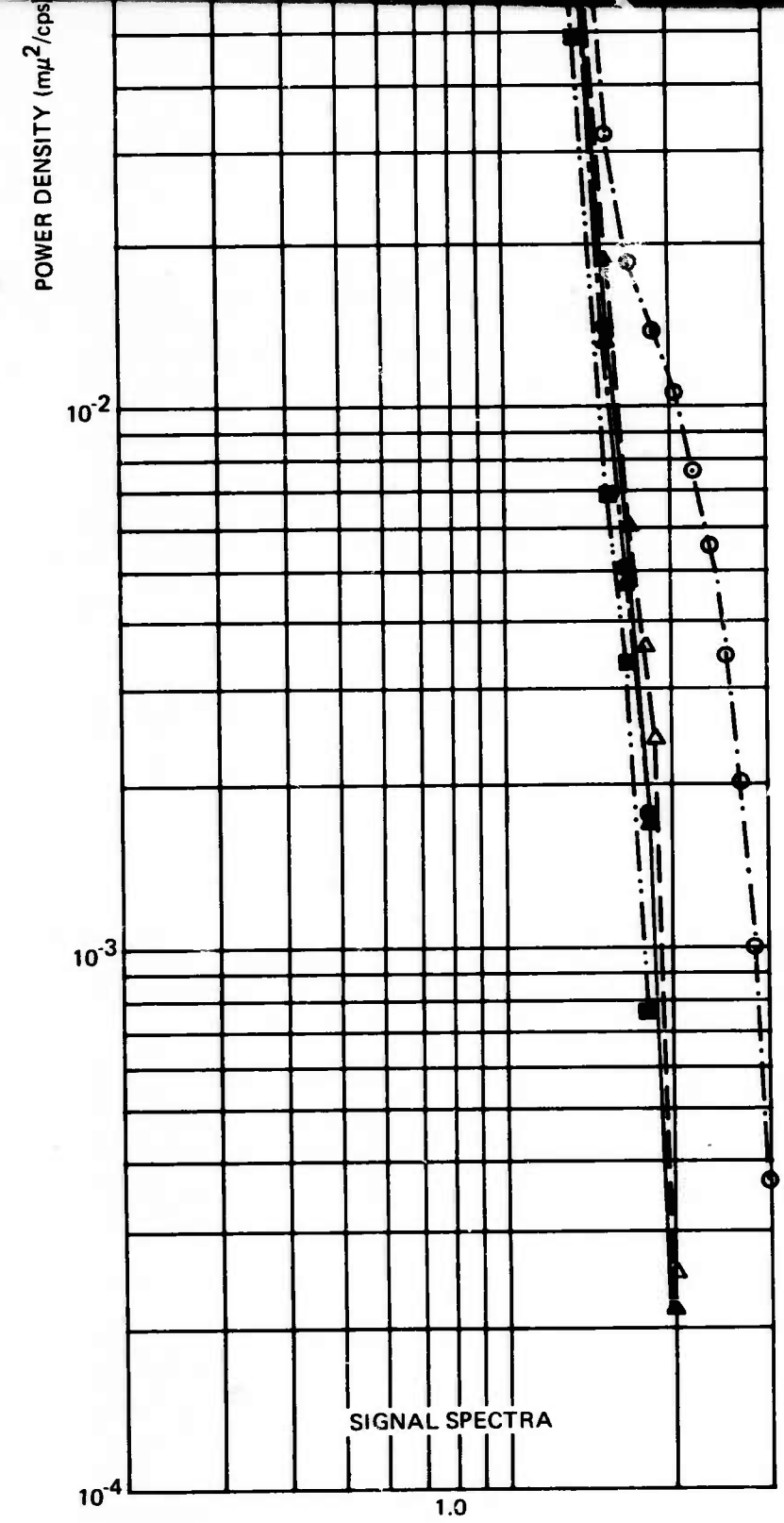
POWER DENSITY (mμ²/cps)
10⁻²
10⁻³
10⁻⁴
SIGNAL SPECTRA
1.0
FREQUENCY (cps)

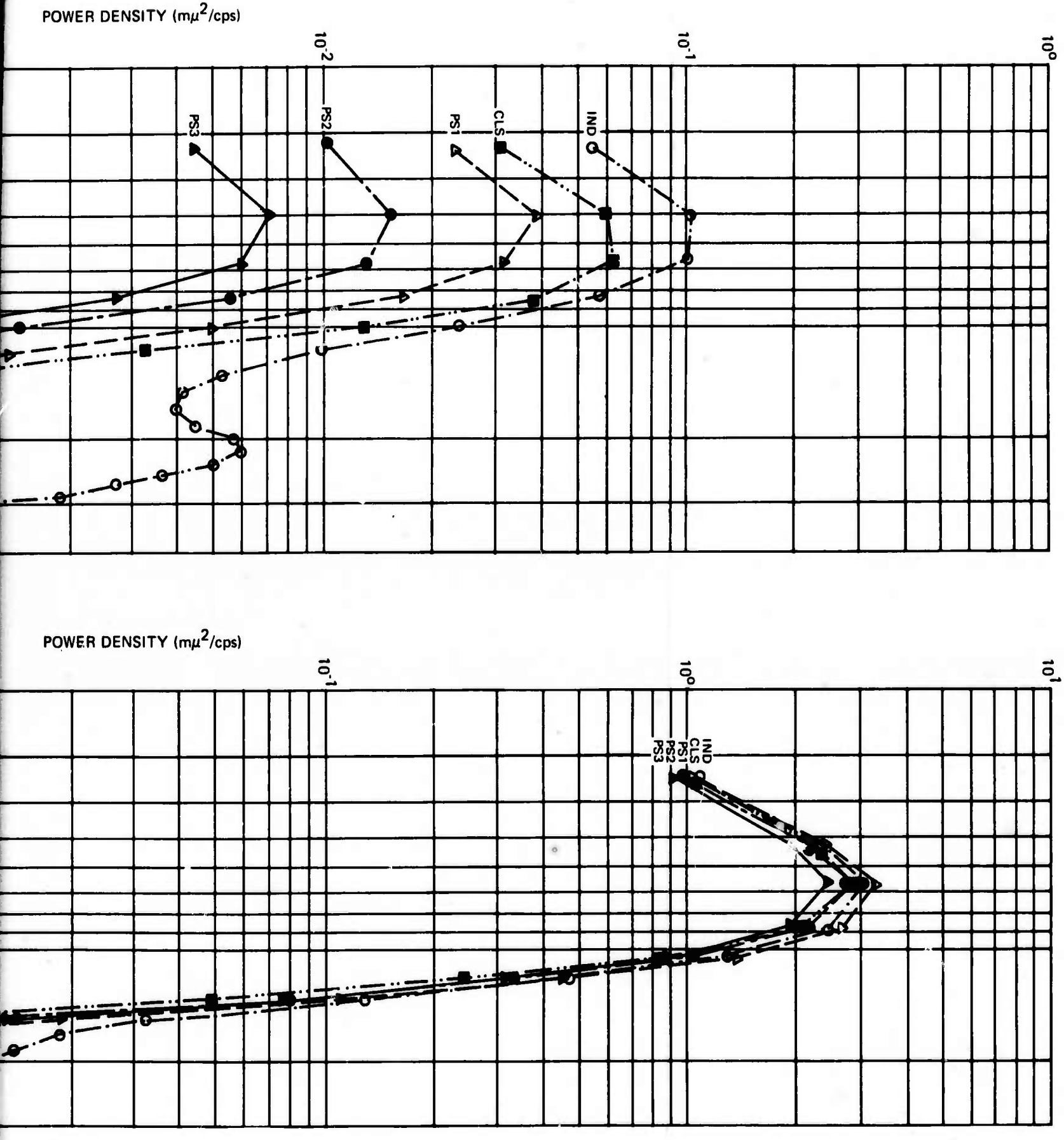

G 4544

Figure 15. Noise reduction ratios for data sample 15

B

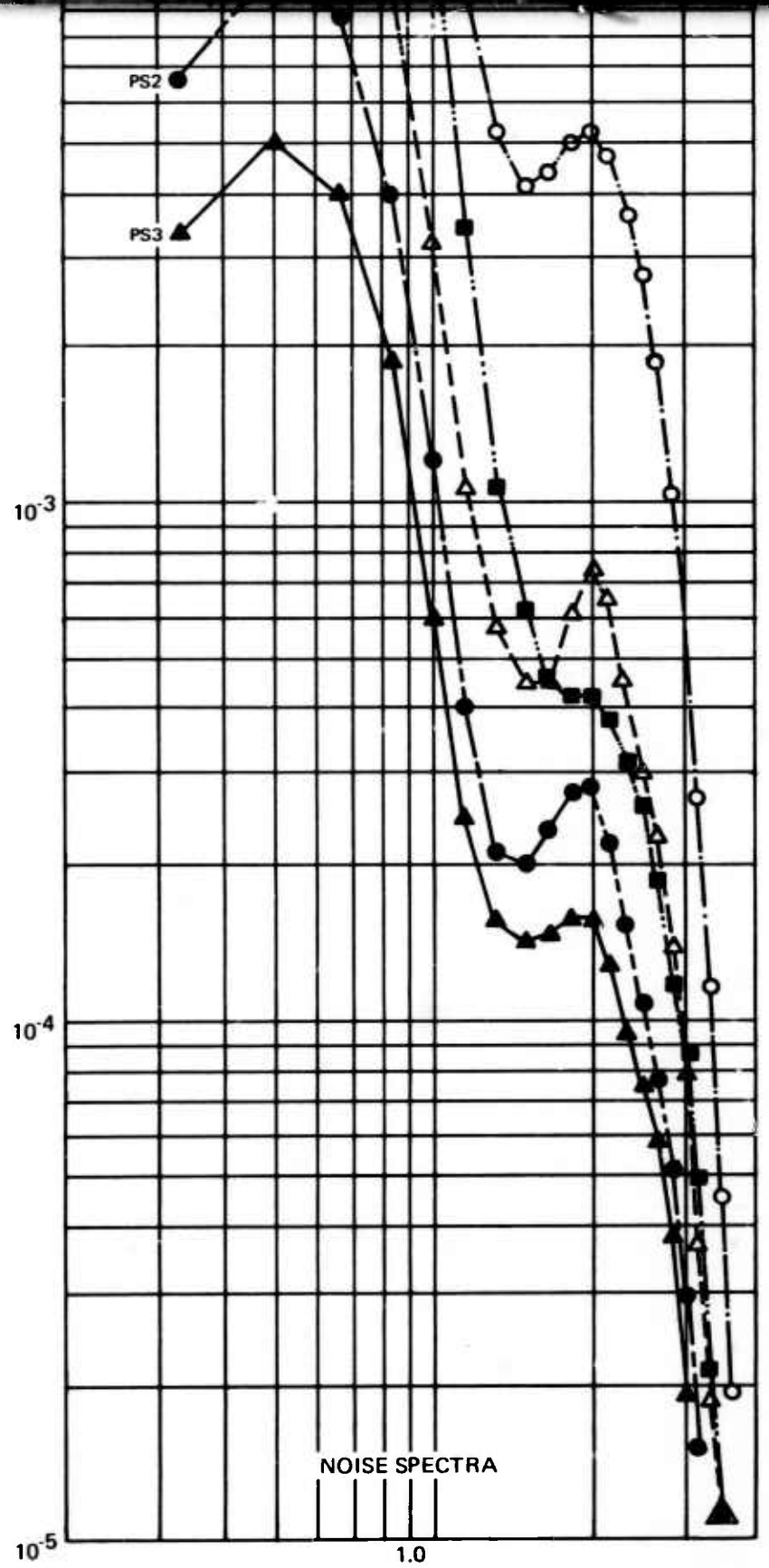
PS2
PS3
POWER DENSITY (mμ²/cps)
10⁻³
10⁻⁴
10⁻⁵
NOISE SPECTRA
1.0
FREQUENCY (cps)

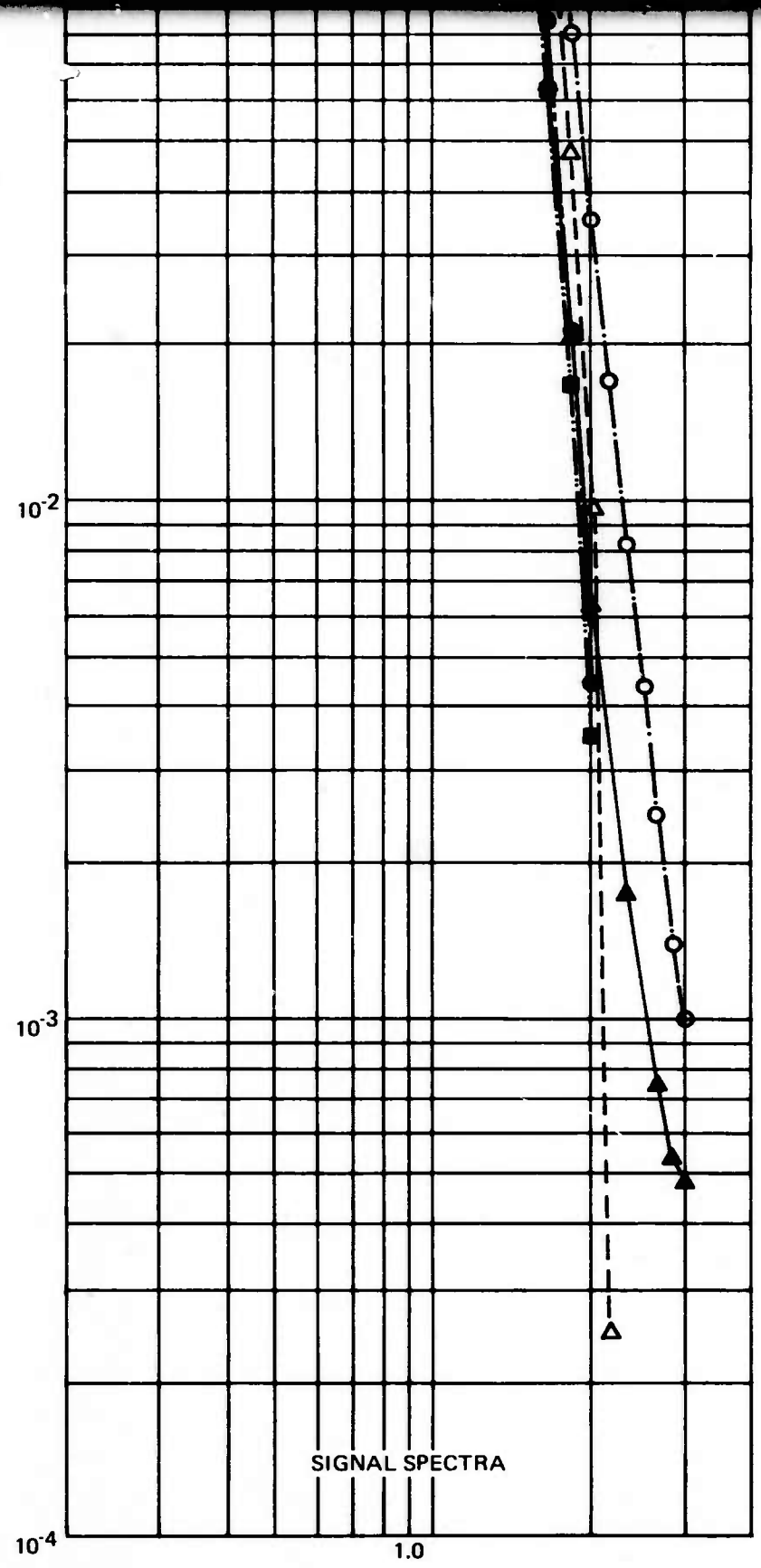
POWER DENSITY (mμ²/cps)
10⁻²
10⁻³
10⁻⁴
SIGNAL SPECTRA
1.0
FREQUENCY (cps)

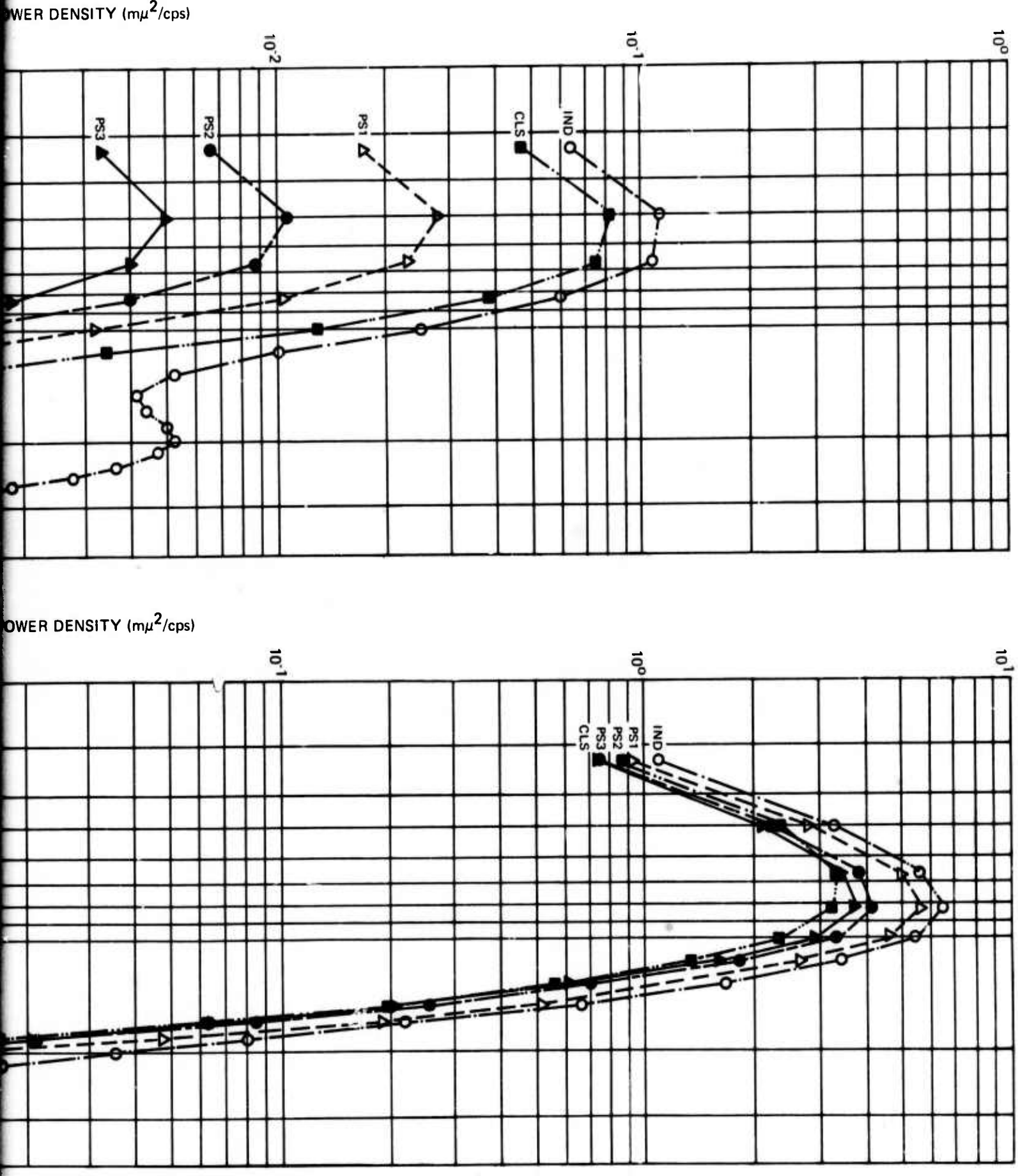

Figure 16. Noise reduction ratios for data sample 16

G 4545

B

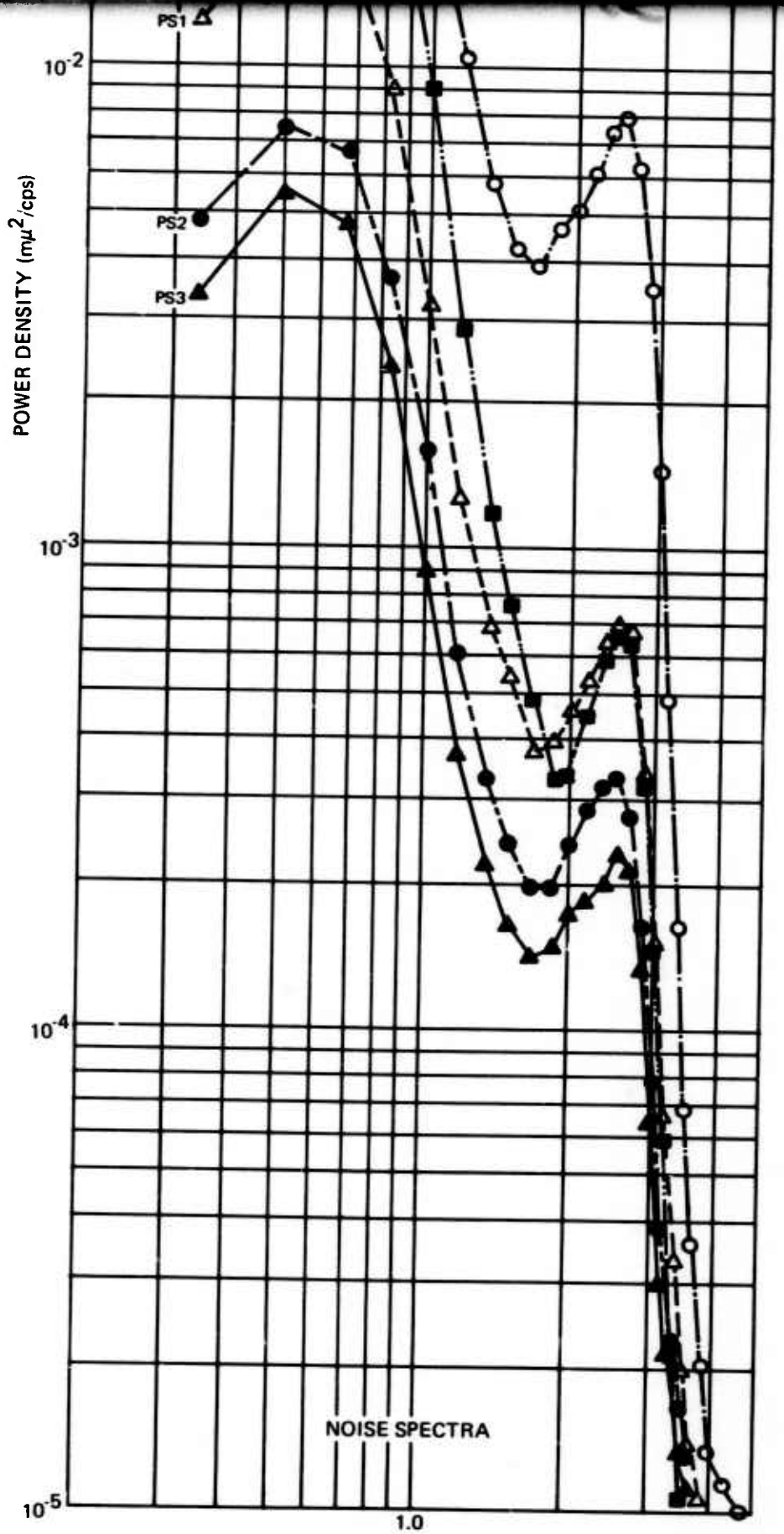
PS1
PS2
PS3
10^{-2}
10^{-3}
10^{-4}
10^{-5}
POWER DENSITY ($m\mu^2$/cps)
NOISE SPECTRA
1.0
FREQUENCY (cps)

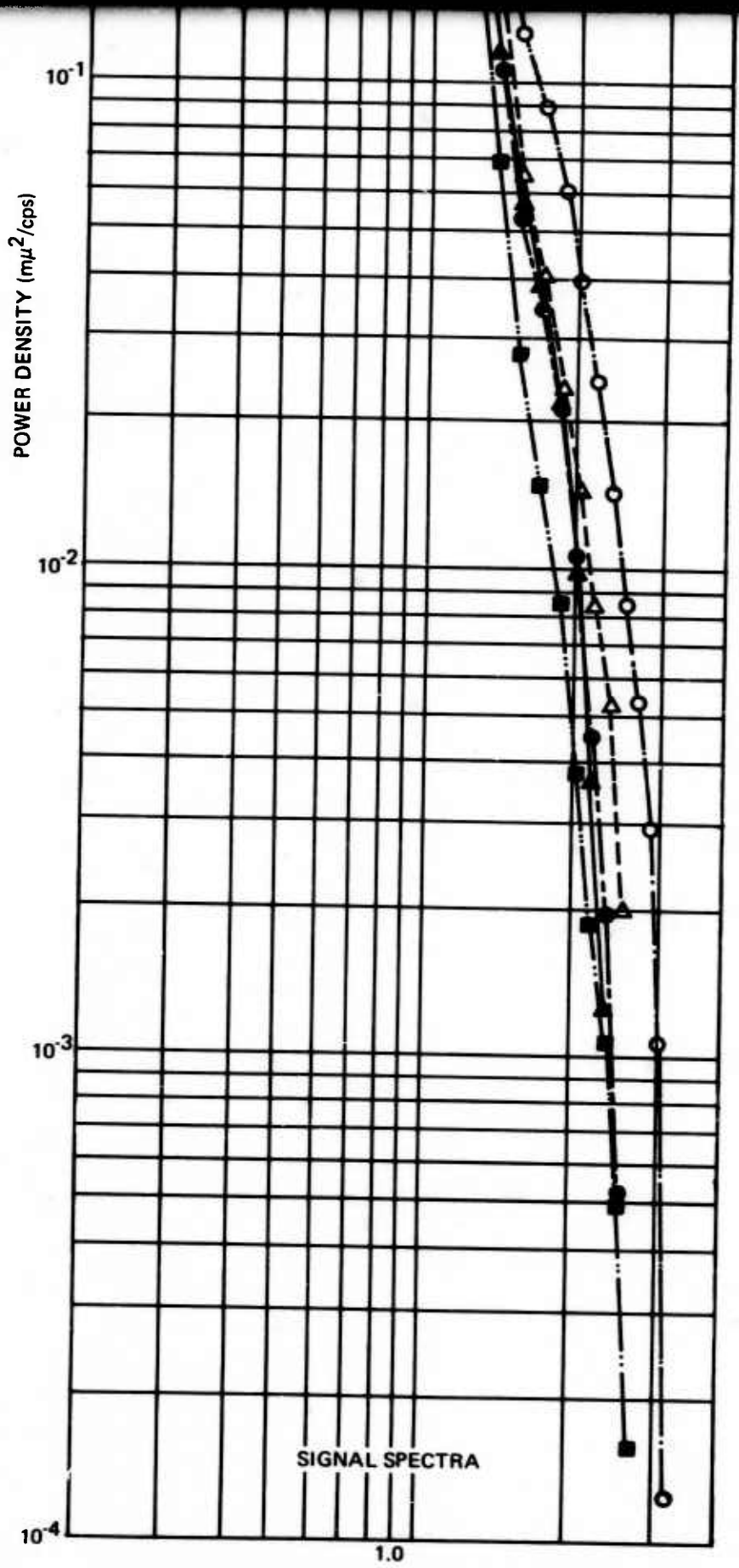
10^{-1}
10^{-2}
10^{-3}
10^{-4}
POWER DENSITY ($m\mu^2$/cps)
SIGNAL SPECTRA
1.0
FREQUENCY (cps)

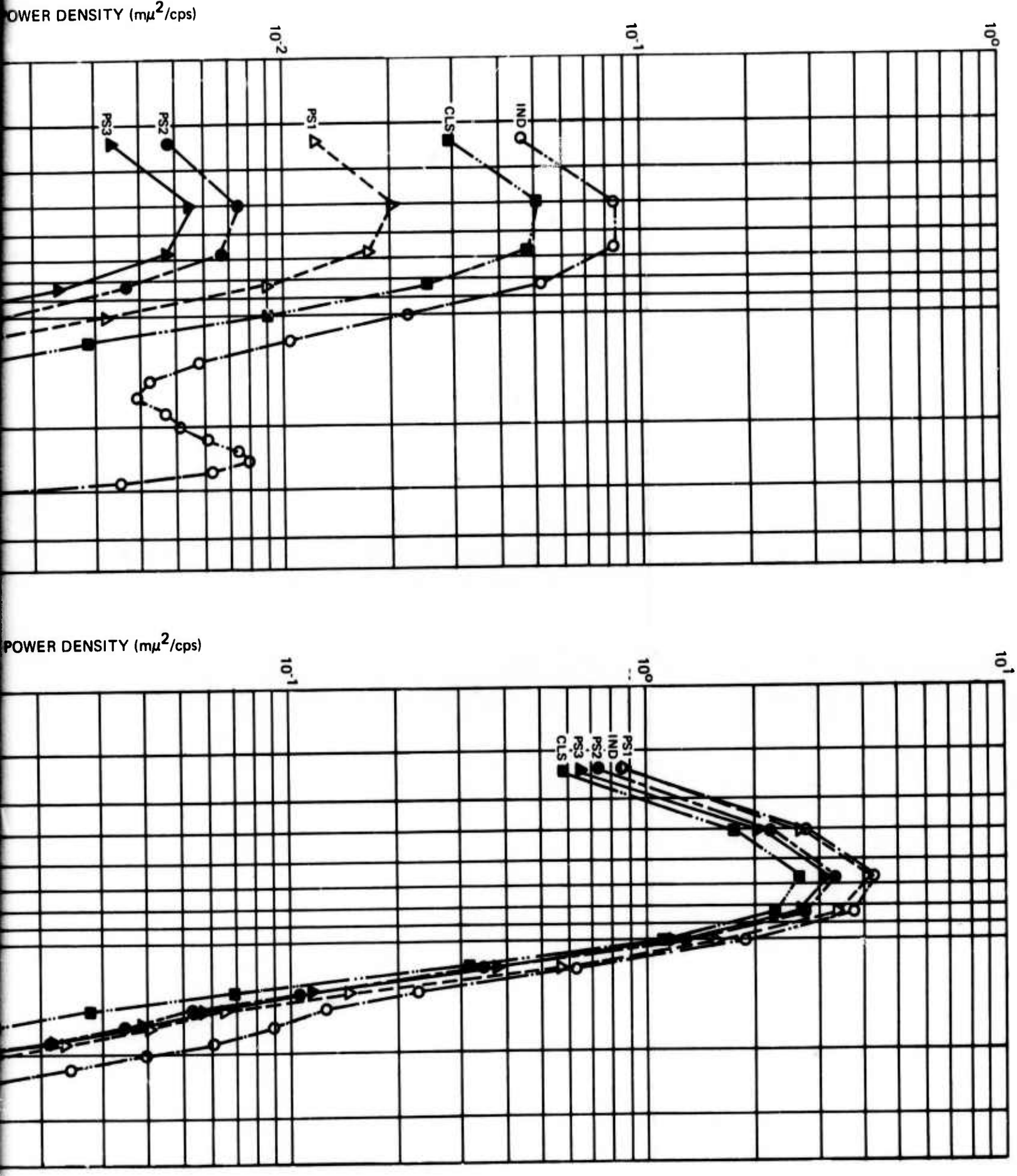

G 4546

Figure 17. Noise reduction ratios for data sample 17

B

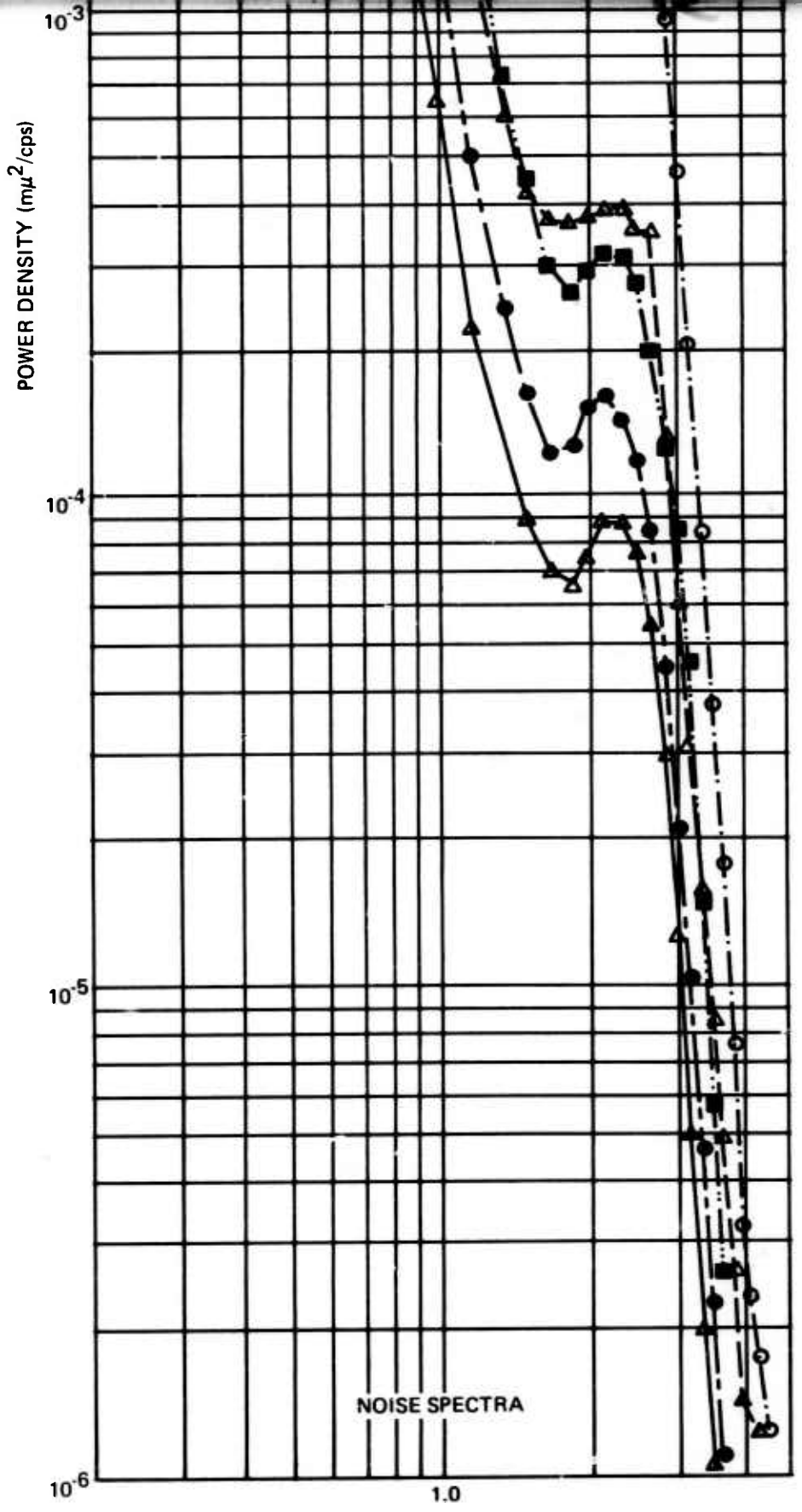
POWER DENSITY (mμ²/cps)
10⁻³
10⁻⁴
10⁻⁵
10⁻⁶
NOISE SPECTRA
1.0
FREQUENCY (cps)

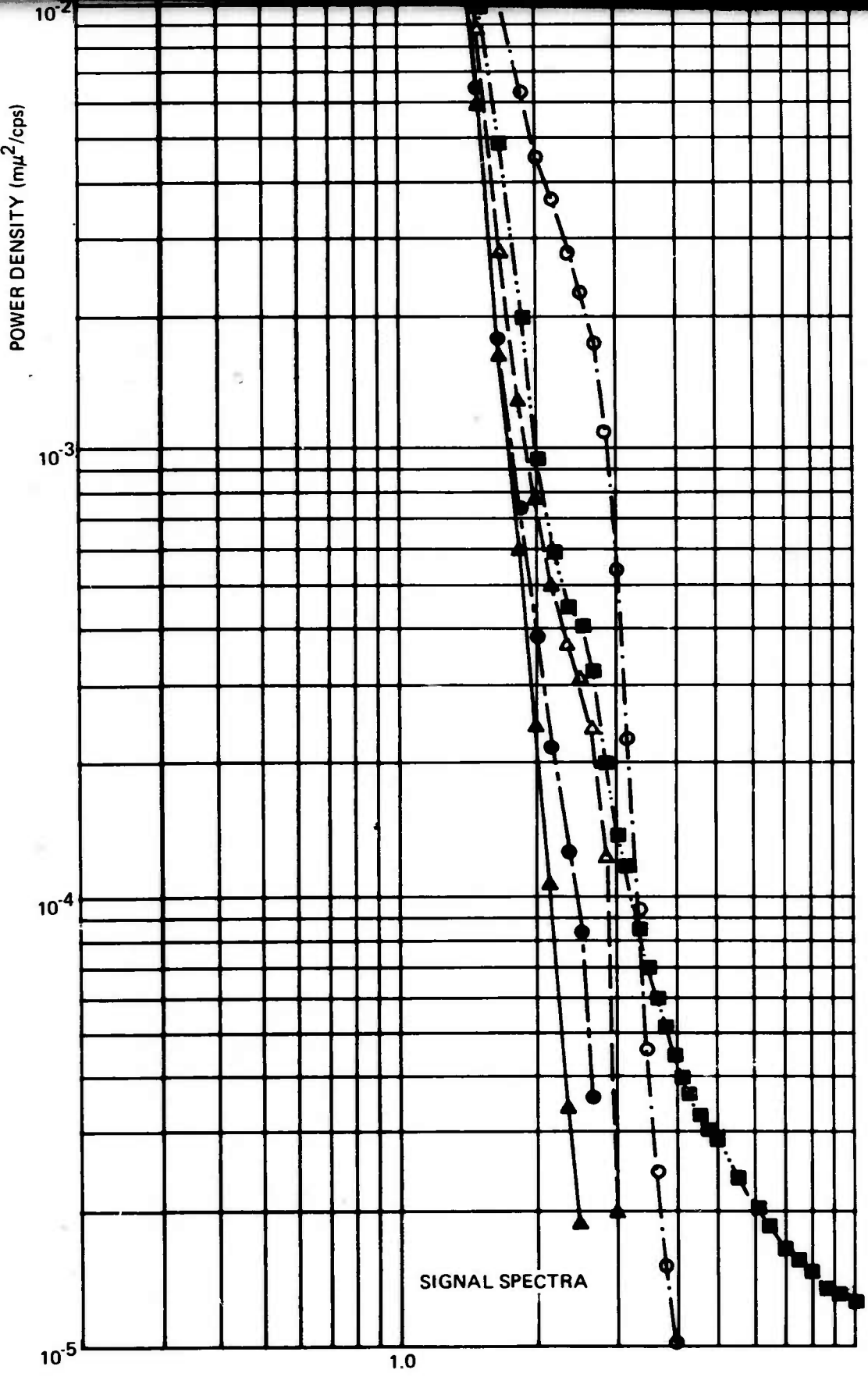
POWER DENSITY (mμ²/cps)
10⁻²
10⁻³
10⁻⁴
10⁻⁵
SIGNAL SPECTRA
1.0
FREQUENCY (cps)

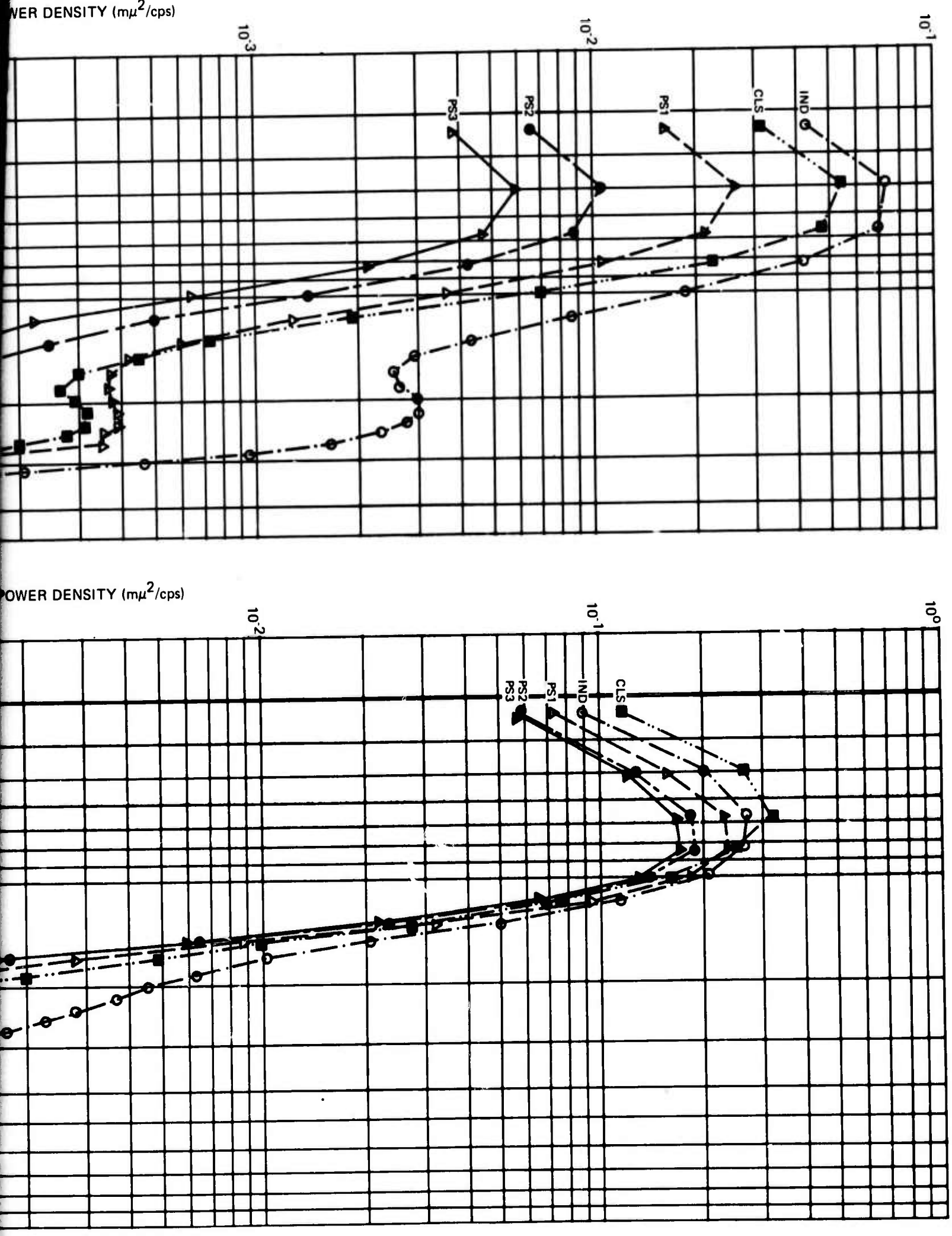

G 4547

Figure 18. Noise reduction ratios for data sample 18

B

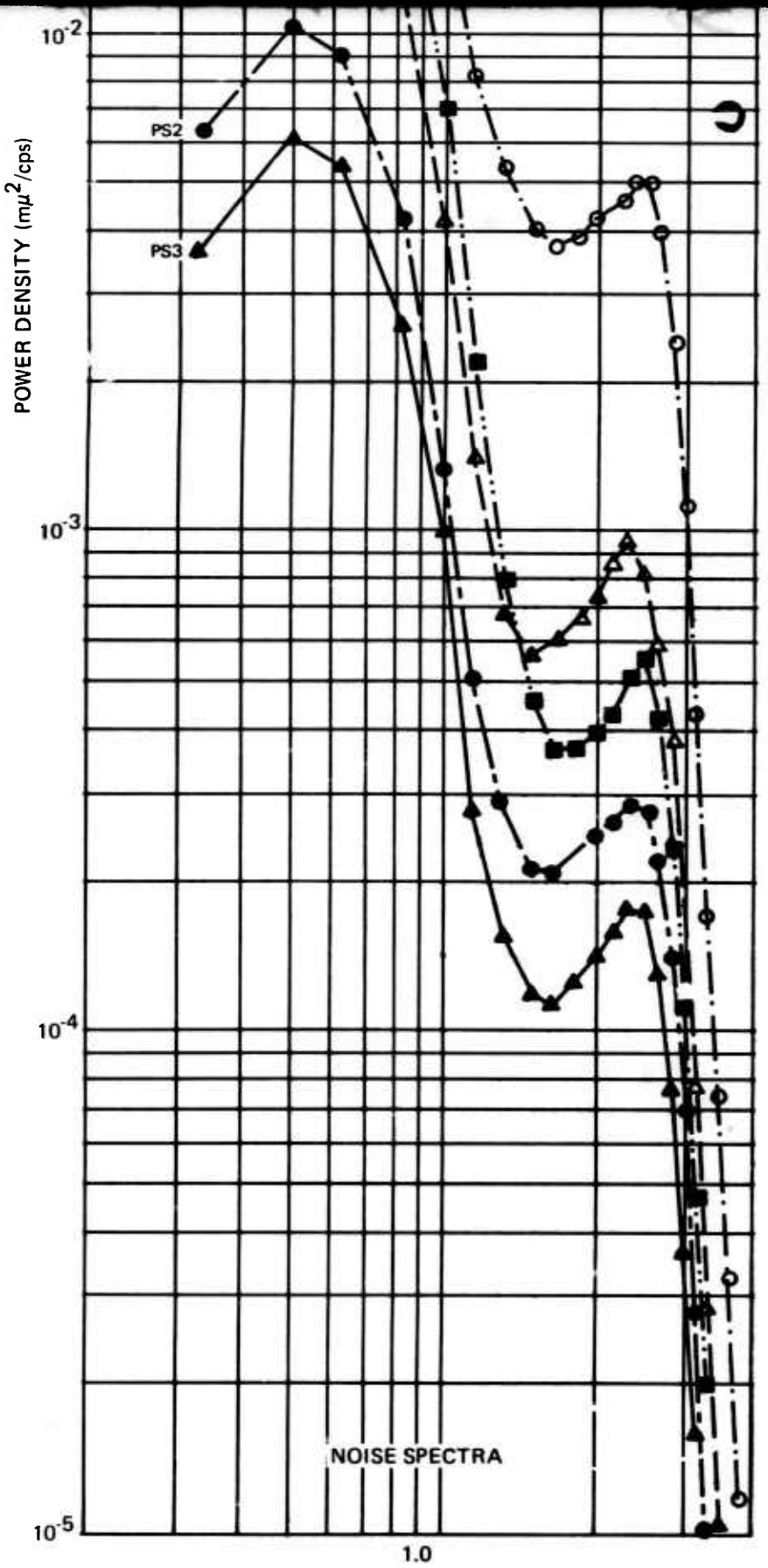
POWER DENSITY (mμ²/cps)
10⁻²
10⁻³
10⁻⁴
10⁻⁵
PS2
PS3
NOISE SPECTRA
1.0
FREQUENCY (cps)

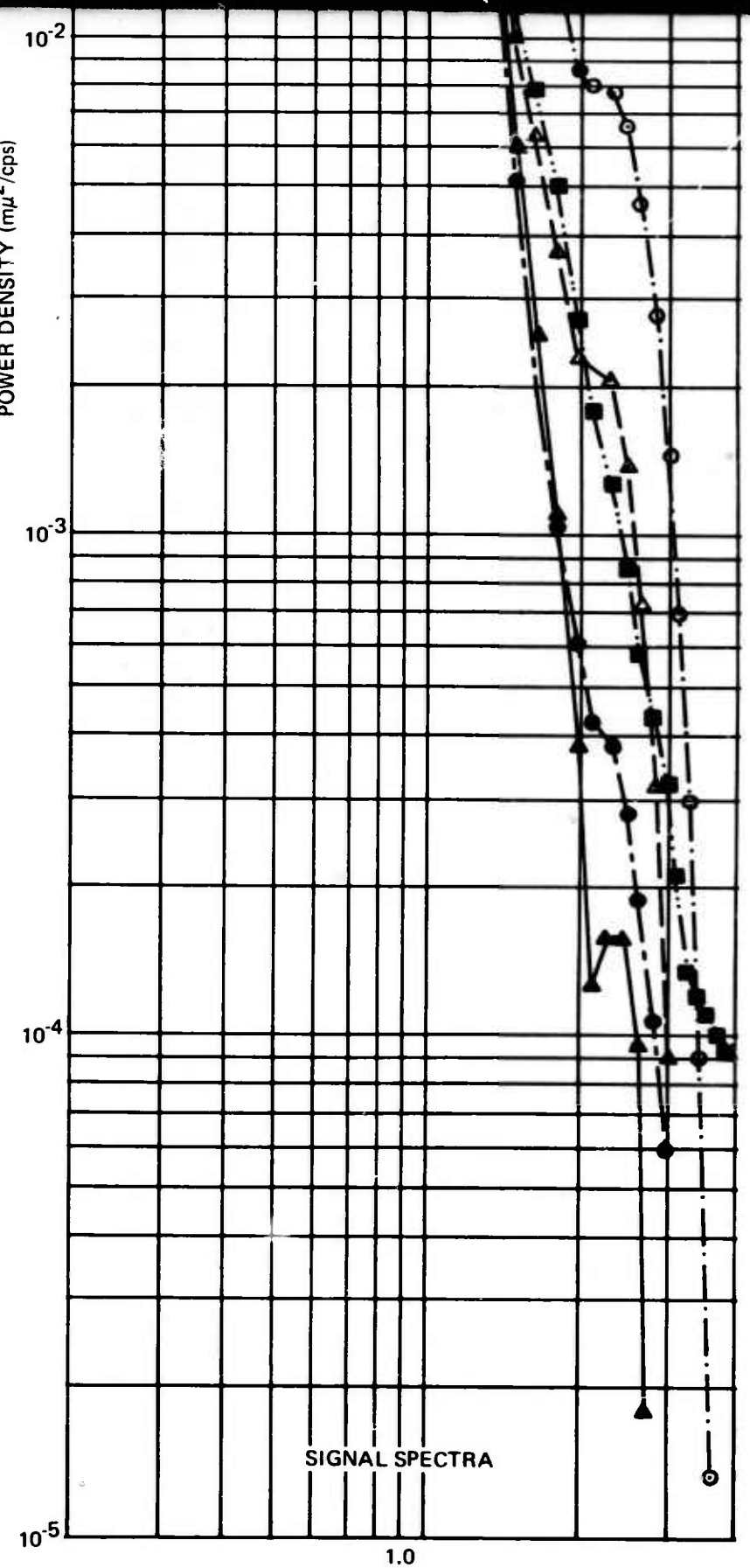
POWER DENSITY (mμ²/cps)
10⁻²
10⁻³
10⁻⁴
10⁻⁵
SIGNAL SPECTRA
1.0
FREQUENCY (cps)

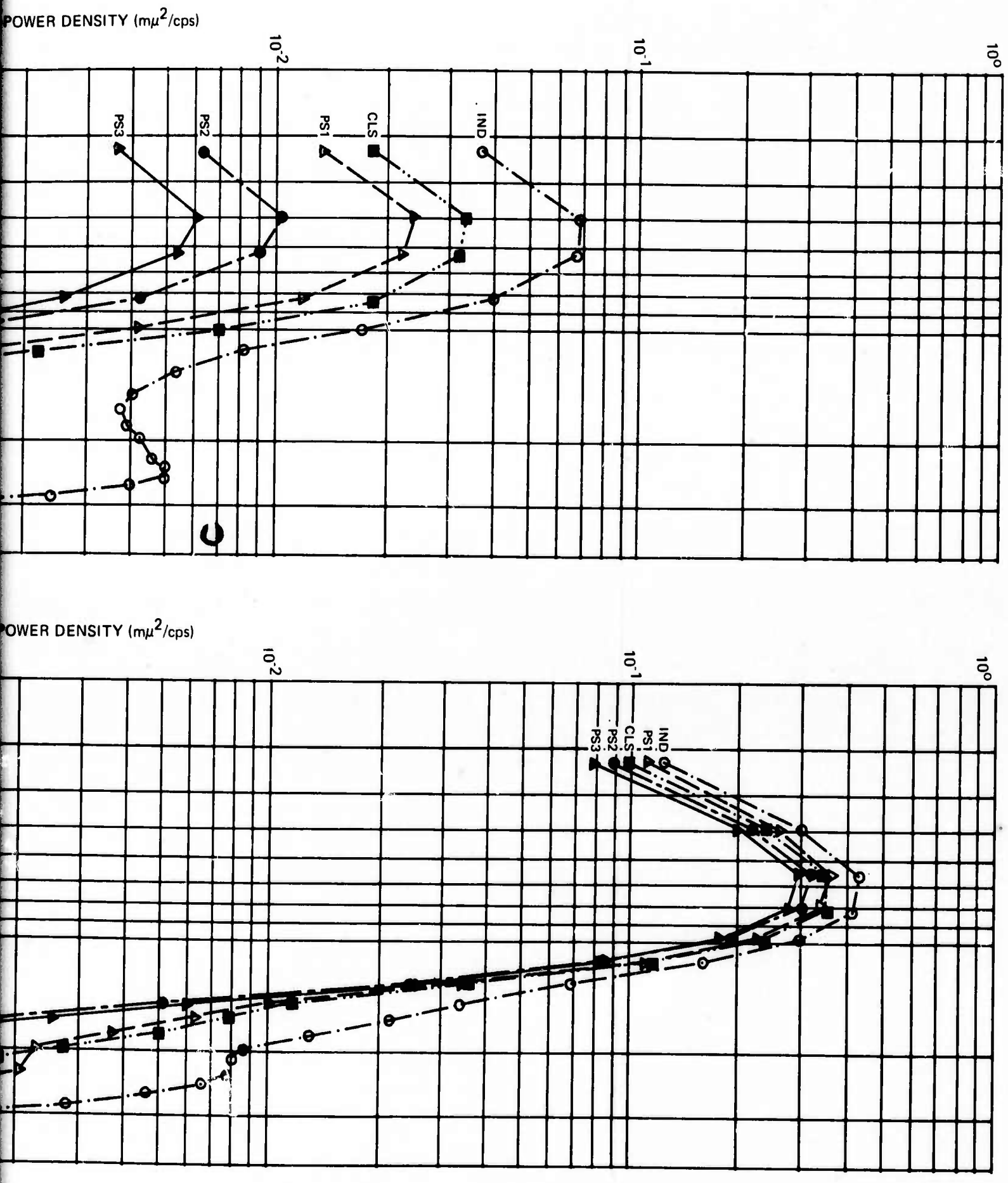

Figure 19. Noise reduction ratios for data sample 19

B

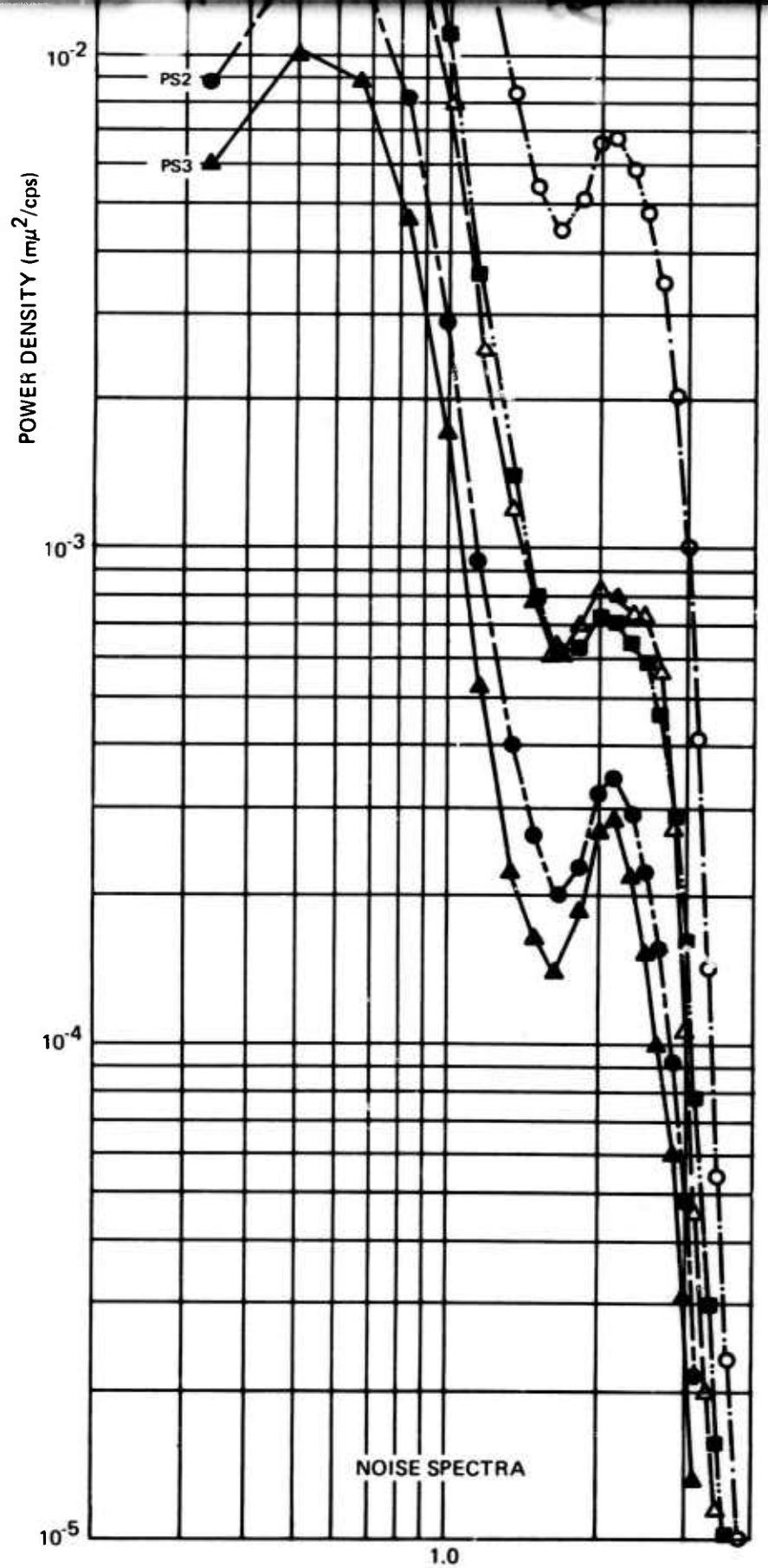
10^{-2}
PS2
PS3
POWER DENSITY ($m\mu^2$/cps)
10^{-3}
10^{-4}
10^{-5}
NOISE SPECTRA
1.0
FREQUENCY (cps)

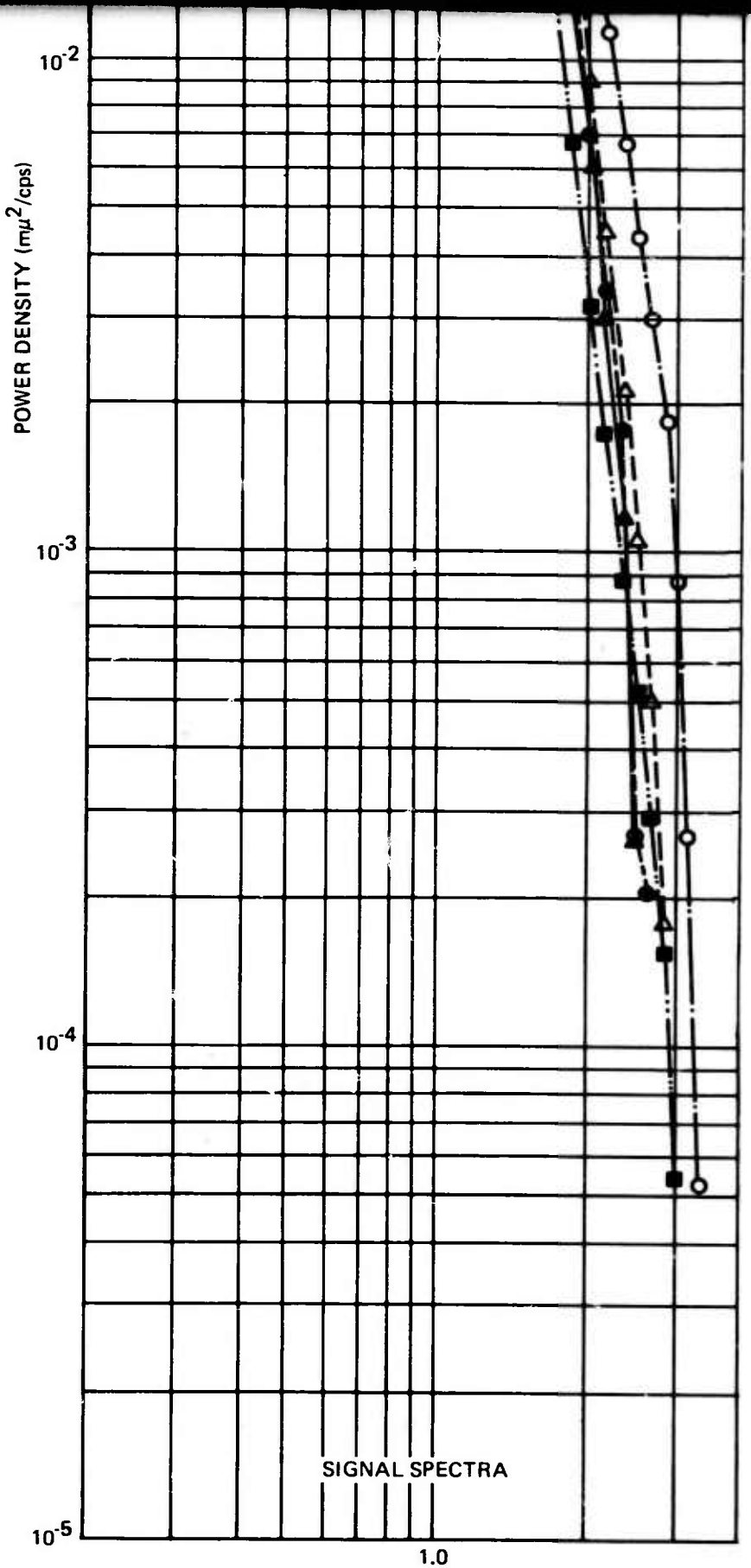
10^{-2}
POWER DENSITY ($m\mu^2$/cps)
10^{-3}
10^{-4}
10^{-5}
SIGNAL SPECTRA
1.0
FREQUENCY (cps)

A

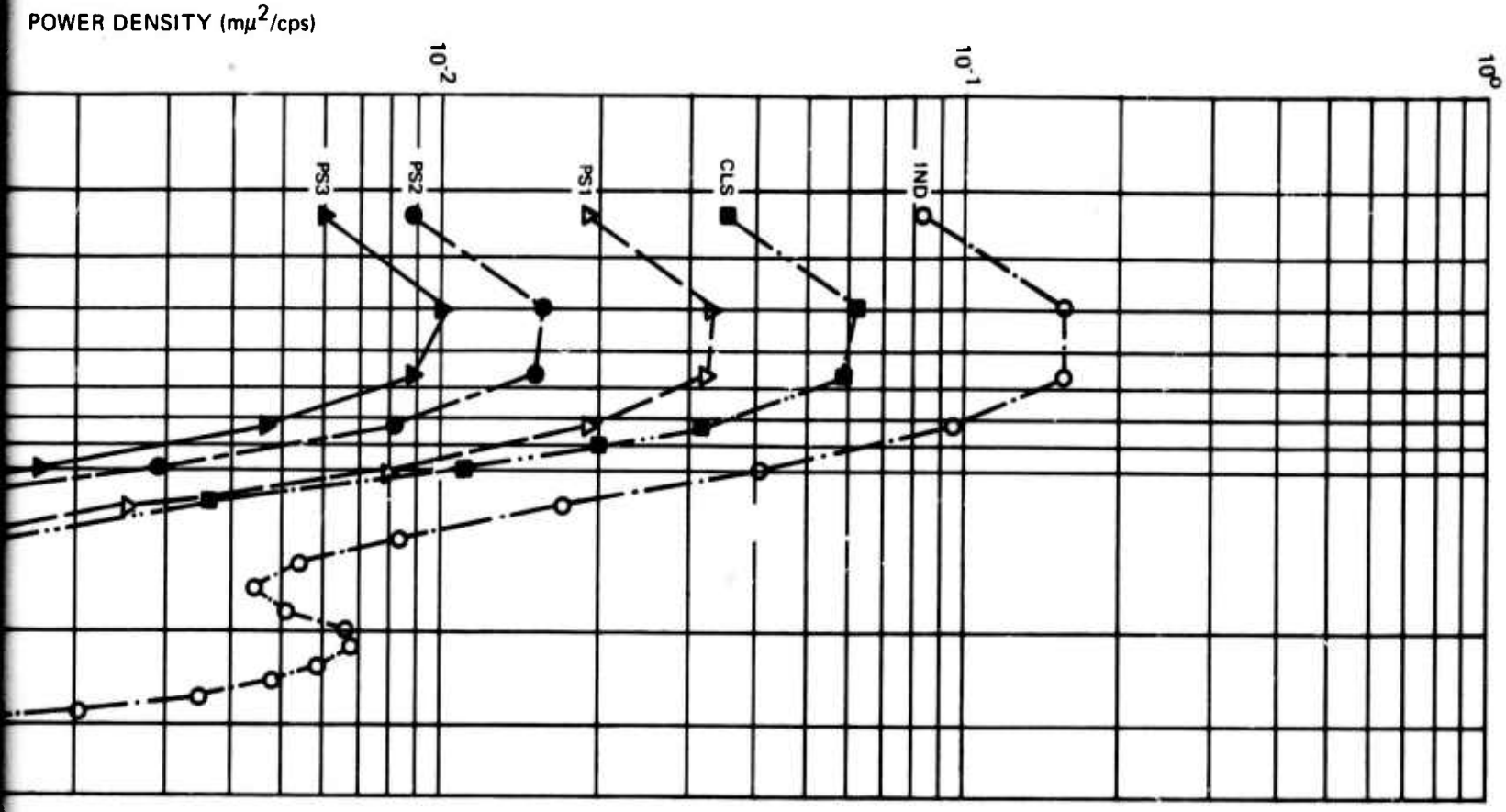

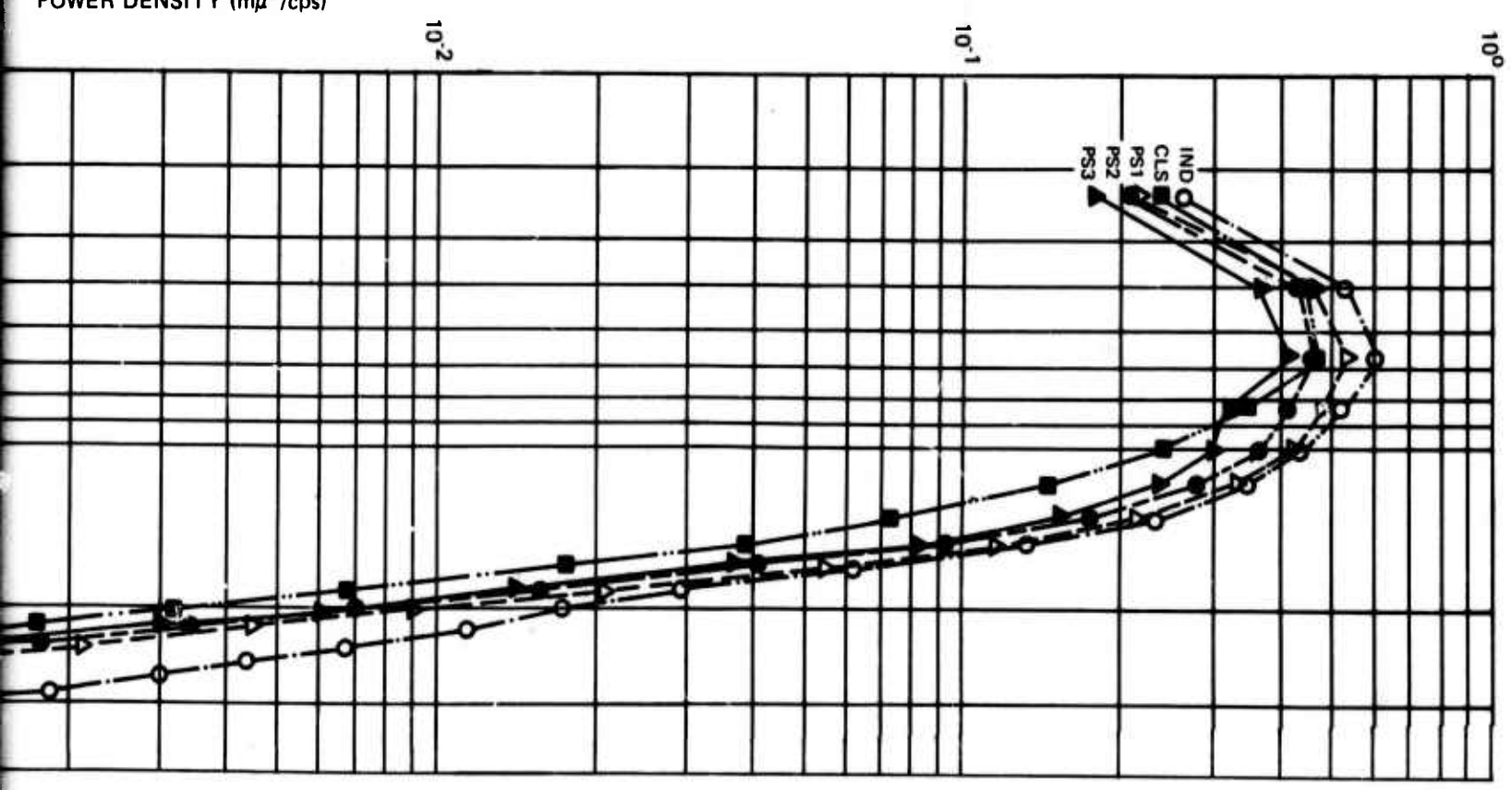

G 4549

Figure 20. Noise reduction ratios for data sample 20